It-Meng Low
Hatem R. Alamri
Abdullah M. S. Alhuthali

Advances in Polymeric Eco-Composites and Eco-Nanocomposites

Synthesis, Properties, and Applications

Springer

Advanced Ceramics and Composites

Volume 4

Series Editor

Longbiao Li ⓘ, College of Civil Aviation, Nanjing University of Aeronautics and Astronautics, Nanjing, Jiangsu, China

The book series "Advanced Ceramics and Composites" publishes insights and latest research results on advanced ceramics and composites, as well as the applications of these materials. The intent is to cover all the technical contents, applications, and multidisciplinary aspects of Advanced Ceramics and Composites.

The objective of the book series is to publish monographs, reference works, selected contributions from specialized conferences, and textbooks with high quality in the field advanced ceramics and composite materials. The series provides valuable references to a wide audience in research community in materials science, research and development personnel of ceramic and composite materials, industry practitioners and anyone else who are looking to expand their knowledge of ceramics and composites.

More information about this series at https://link.springer.com/bookseries/16543

It-Meng Low · Hatem R. Alamri ·
Abdullah M. S. Alhuthali

Advances in Polymeric Eco-Composites and Eco-Nanocomposites

Synthesis, Properties, and Applications

 Springer

It-Meng Low [ID]
School of Electrical Engineering
Computing and Mathematical Sciences
Curtin University
Perth, WA, Australia

Hatem R. Alamri [ID]
Physics Department
Aljamoum University College
Umm al-Qura University
Makkah, Saudi Arabia

Abdullah M. S. Alhuthali [ID]
Department of Physics
Taif University
Taif, Saudi Arabia

Foreword

Recently, polymer composites reinforced with natural fibres from different biorenewable resources have attracted the significant attraction of research community all around the globe owing to their exceptional intrinsic properties such as biodegradability, easy availability, environmental friendliness, flexibility, easy processing, and impressive physico-mechanical properties. Polymer composites using natural fibres provide the toll for the sustainable development for both bio-based resources and biorenewable-based economies because of their adaptability to a diverse array of dissimilar and widely variable resources and because of their potential allow materials engineers to add the most value and performance over a wide array of uses/products. Utilization research on bio-based composite materials can help to justify and provide a return for removal of the present biomass build-up, and it can contribute to rural health and jobs. Polymer composites assembled from bio-based materials provide technology that is more adaptable to a changing resource base. These products can incorporate a variety of natural fibres/wood fibres and wood-based raw materials in the form of fibres, particles, flakes, strands, and veneers. Polymer composites can also be made with raw materials that are recycled.In different countries, there is significant generation of amount of biomass, which consists of high-quality lignocellulosic fibres. Disposal of these agricultural by-products is so far still inefficient. Combining polymers with natural fibres to produce high-quality industrial products (e.g., extruded building material) provides a prospective solution for value-added utilization of the biomass resources.

One of the greatest challenges for scientists and engineers is to work together to achieve sustainable growth through bio-based renewable materials. The research in this direction is to find technologically feasible and economically acceptable solutions of using natural fibres and polymer matrices from different origins. The research should use the latest technologies in composite development and interface analysis to deal with phase incompatibility and composite brittleness, which are some of the predominant challenges in manufacturing natural fibre and their respective composites.

In this book, Dr. Low seeks to address the different issues related to the natural fibres reinforced polymers ecocomposites. This book covers the development of

advanced technologies for manufacturing of different types of polymer ecocomposites reinforced with natural fibres and nanomaterials such as nano-SiC and halloysite.This book is a milestone, which will facilitate the technologies leading to improved energy efficiency, significant rural economic development, and great environmental benefits.

Sincerely

Vijay Kumar

Vijay Kumar Thakur, Ph.D., AFHEA
Faculty in Manufacturing, School of Aerospace
Transport and Manufacturing, Cranfield University
Cranfield, Bedfordshire, UK

Preface

There has been increasing attention into the study of composite materials. Unlike the monolithic materials, these composite materials usually involve a matrix, such as a polymer, and filler such as a fibre. The addition of stiffer and stronger fibres can greatly improve the qualities of the polymer. To date, aramid, glass, and carbon are the most common synthetic fibres. Glass is a cheap fibre and with good mechanical properties. Fibre glass products are well known and are used in aerospace, leisure, sporting, automotive, and construction industries. Nonetheless, the shortcomings of synthetic fibres are fast being recognized due to increasing global concern over the depletion of petroleum resources, the emission of greenhouse gases, and a greater need to recycle and reuse. Flax, hemp, jute, pineapple, and sisal are natural fibres that can be used to produce eco-friendly materials that are light, affordable, successful in stiffness-critical designs, and sustainable. These so-called ecocomposites have attracted the attention of stakeholders worldwide because of greater compatibility of natural fibres with the environment. Already, natural fibres, with excellent acoustic damping properties, are preferable to glass or carbon for the purposes of noise attenuation, a requirement for automobile interior products. Notwithstanding the promising future of nature fibre composites, inherent incompatibility must be overcome between this category of fibres which are hydrophilic and the matrix components which are hydrophobic. To improve fibre–matrix adhesion and prevent loss of strength, treatment of the natural fibre surface is required. In addition, issues concerning moisture still compromise fibre–matrix interface integrity leading overall loss in mechanical properties. Addressing these limitations of natural fibre composites is critical to overcoming the existing barriers to research and development in this important field of materials.

This book outlines a novel approach of fabricating ecocomposites by enhancing the interfacial bonding between fibre and matrix. The book also investigates the fabrication of eco-nanocomposites by adding nano-fillers in these ecocomposites to achieve better mechanical and thermal properties. This approach not only enhances interfacial bonding in these eco-nanomaterials but also provides good barrier property and good resistance to water diffusion.

The scope of this book covers polymer ecocomposites that uses either epoxy or vinyl-ester as the matrix for three categories of composite materials. Firstly, ecocomposites were produced by reinforcing epoxy or vinyl-ester with very thin sheets of Recycled Cellulose Fibre (RCF). Secondly, nanocomposites were produced by reinforcing epoxy or vinyl-ester with Halloysite Nanotubes (HNT) and silicon carbide nanoparticles (n-SiC). Thirdly, eco-nanocomposites were produced by reinforcing epoxy or vinyl-ester with sheets of RCF sheets and nano-fillers (multi-scale reinforcement). The impetus of this work was to develop environmentally friendly composite materials with high performance using multi-scale reinforcement. This work is part of a larger movement towards designing for recycling, also referred to as eco-design. Manufacturer responsibility is increasingly understood as involving a commitment for materials to be used in products from "cradle to grave".

Firstly, the ecocomposites were prepared with RCF loadings of 20, 30, 40, and 50 wt%. A novel infiltration method was used in the preparation of the ecocomposites. Step one involved 10 μm sheets of RCF being fully soaked in the matrix. Step two required the saturated sheets to be laid-up on silicon moulds. Finally, the third step required saturated sheets of RCF be pressed together in vacuum under fixed pressure. During steps two and three, low pressure was applied frequently to remove trapped air bubbles. SEM micrographs confirmed that the novel infiltration method of preparation led to composites with good fibre/matrix adhesion, reduced void content, and increased fibre–volume fraction. The effect of fibre content on water absorption behaviour in the ecocomposites was also investigated. As the fibre content increases, the uptake of moisture was also found to increase. Increasing the fibre content was also found to lead to an increase in the elastic modulus, strength, and fracture toughness properties of the ecocomposites. Using typical mathematical models for prediction, the elastic modulus for the ecocomposites was modelled revealing experimental data consistent with Cox–Krenchel model obtained prediction data. Moisture exposure reduced the elastic modulus, strength, and toughness of the ecocomposites. This reduction was most noticeable at high fibre content and was attributed to compromise interfacial bonding because of water absorption.

Secondly, the nanocomposites, were prepared by reinforcing the matrix with different loadings of nano-SiC or HNTs using a high-speed mechanical mixer (30 minutes, 1200 rpm). The addition of HNT to epoxy or vinyl-ester is a field of material science with limited excurses. This work presents the first characterization of nanocomposites providing water absorption, fracture, mechanical, thermal properties, and flammability behaviours of this group of nanocomposites. HNT-reinforced composites were prepared at 1, 3, and 5 wt% using high-speed mechanical stirring. The intercalation of the HNT by the chains of epoxy or vinyl-ester is confirmed in XRD results. For example, the d-space of the peak (001) of pure HNT increased from 0.721 to 0.745 nm with 1.0 wt%. This intercalation confirms the formation of nanocomposites. TEM observations support that the extent of HNT particles dispersion is acceptable, notwithstanding the presence of micro-sized HNT clusters. The presence of only 5 wt% HNT imparted a significant the reduction in the water absorption behaviour.

The addition of HNT was also found to effectively enhance the toughness properties of epoxy or vinyl-ester. Crack bridging and plastic deformation mechanisms around clusters of HNT are believed to be three mechanisms of toughness that HNT provide as confirmed by SEM observations. A large aspect ratio, good interfacial adhesion, good degree of dispersion, and adequate inter-tubular interaction between HNT and VER are believed to be the factors underpinning enhanced strength properties. The experimental data was consistent with that of both Paul model and Guth model suggesting that the aspect ratios of fillers, their dispersion within the matrix, and the state of interfacial adhesion were all relevant to the prediction of elastic modulus for particulate reinforced composites. HNT's barriers for heat and mass transport, the presence of iron, and their hollow tubular structure are believed to be the factors enhancing thermal stability and decreasing in flammability in the nanocomposites.

Epoxy or vinyl-ester composites reinforced with nano-SiC were prepared at 1, 3, 5, and 10 wt% using high-speed mechanical stirring. Particularly, the project evaluated the influence of morphological structures such as particle dispersion and particle/matrix interaction on resulting mechanical and fracture properties of these nanocomposites. SEM micrographs revealed that at the fracture surfaces of composites there appeared to be no obvious voids at the particle/matrix interface. This is indicative of an absence of n-SiC pull-out from the polymer matrix supporting strong interaction between the n-SiC and the matrix. The absence of n-SiC agglomeration throughout the nanocomposite is also supportive of generally uniform dispersion of n-SiC throughout the matrix. The addition of n-SiC increased elastic modulus and strength but reduced the toughness of the nanocomposites. Good interfacial adhesion and a good degree of dispersion enhanced the strength of the nanocomposites, whereas agglomeration of nanoparticles at 10 wt% forming clusters of n-SiC decreased elastic modulus and strength.The experimental data was consistent with that of both the Guth and Kerner model suggesting that good dispersion within the matrix and good interfacial adhesion were both relevant to the prediction of elastic modulus of particulate reinforced composites.

Thirdly, the eco-nanocomposites were prepared using a two-step process. In the first step of preparation, three nano-mixtures were produced. The first of these was epoxy or vinyl-ester reinforced with nanoclay platelets. The second was epoxy or vinyl-ester reinforced with HNT. The third was epoxy or vinyl-ester reinforced with n-SiC.Each was prepared at 1, 3, and 5 wt%. The second step of the preparation required that sheets of RCF be used to reinforce the nano-mixtures. The eco-nanocomposites were then studied in terms of their water uptake, mechanical and thermal properties. Concerning water uptake, nano-filler addition was found to decrease water uptake with 5 wt% eco-nanocomposites giving more favourable results than the 1% and 3%. Concerning strength properties, nano-filler addition was also found to enhance these properties most optimally at 3 wt%.These results were attributed to the reinforcing effect of nano-filler with RCF sheets and the enhanced fibre–matrix adhesion observed in the eco-nanocomposites. Concerning toughness properties, when compared to pure epoxy or vinyl-ester, the composites reinforced with sheets of RCF featured a significantly higher toughness due to the toughness

mechanisms provided by cellulose fibre. However, nano-filler addition resulted in samples which were brittle due to the nano-fillers' effects on fibre-matrix adhesion limiting the mechanisms of fibre pull-out and fibre debonding. Therefore, the toughness properties of the eco-nanocomposites were lower than those of the ecocomposites. Concerning thermal stability and flammability, the eco-nanocomposites gave preferable results compared to those of the ecocomposites and pure samples. This observed improvement was believed to have occurred by virtue of improved mass and heat barriers and the enhanced fibre–matrix interfacial adhesion provided by the nano-fillers.

The influence of the reinforcement materials—sheets of RCF, nano-fillers, and multi-scale reinforcement (RCF/nano-fillers) were investigated. The physical, thermal, mechanical, and fracture properties of the resulting composites were studied in terms of the water absorption, flexural strength, flexural modulus, impact strength, fracture toughness, impact toughness, thermal stability, and flammability of each composite. The effect of water soaking on the mechanical properties of composites was also investigated. X-ray diffraction, synchrotron radiation diffraction, Fourier transform infrared spectroscopy, transmission electron microscopy, and scanning electron microscopy were used to examine the nano- and microstructures of these materials.

Conflict of Interest: None

Perth, Australia   It-Meng Low
Makkah, Saudi Arabia   Hatem R. Alamri
Taif, Saudi Arabia   Abdullah M. S. Alhuthali

Acknowledgements

Contents

Chapter 1
Introduction: Background and Literature Review

Abstract This chapter provides a background to the scope of this book and a comprehensive literature review of the latest advances in polymer ecocomposites reinforced with natural fibres and nano-fillers such as nanoclay platelets, halloysite nanotubes and nano-silicon carbide. The influence of adding various natural fibres on the mechanical properties of these composites is reviewed. The synthesis, structure, and properties of these reinforced composites are also described. Potential applications, challenges, and future directions of these composites are highlighted.

Keywords Cellulose fibres · Polymer ecocomposites · Natural fibres · Nanoclay platelets · Epoxy resin · Vinyl-ester resin · Water uptake · Diffusion · Aspect ratio · Microstructure · Mechanical properties · Flexural strength · Impact strength · Fracture toughness · Impact toughness

1.1 Background

The technology of traditional composites is a great one and was instrumental in advancing civilization in the twentieth century. However, as we move into the twenty-first century and beyond, we need to rely on natural reinforcements that are sustainable and renewable. This push for sustainability and renewability is quite like the push of battery technology to enable the transition from internal combustion engine to electric powertrain vehicles. In addition, the development of eco-friendly environmental and sustainable materials having high mechanical and fracture performances is imperative in the global quest for the minimization of greenhouse gas emission by substituting natural fibres for their synthetic counterparts.

Ecocomposites are eco-friendly materials which are produced by mixing cellulose fillers in a plastic matrix. Hitherto, most ecocomposites are based on thermoplastics while thermosets are rapidly emerging as alternatives. These materials are sometimes also referred to as biocomposites or "green composites". As such, these materials serve to reduce the harmful environmental impact and impart sustainability or cost-effectiveness. However, not all ecocomposites are fully biodegradable or recyclable, especially those based on thermosetting plastics. Recyclable themoplastic ecocomposites can be made from recycled plastics and agroresidues (Nassar et al.

2021). Similarly, biodegradable ecocomposites are made by dispersing natural fibres in a biopolymer matrix (AL-Oqla and Omari 2017) and these biocomposites are designed for "cradle-to-grave". Nevertheless, several ecocomposites have already been successfully developed and used in applications as non-load-bearing products. Examples of these products are as automotive interiors, household accessories, as well as decking and fences (Nassar et al. 2021; Gowda et al. 2019).

The structure of this introduction is organized as follows: Sect. (a) provides the details on the motivation and methodology for developing epoxy-based ecocomposites and eco-nanocomposites as well as brief reviews on similar work in the literature. In Sect. (b), the motivation and methodology for developing vinyl-ester ecocomposites and eco-nanocomposites are similarly described. A comprehensive literature review of topics relevant to natural reinforcements and ecocomposites is provided in Sect. 1.2.

(a)   Epoxy Ecocomposites and Eco-nanocomposites

Epoxy has unique properties such as comparatively high strength, high modulus, excellent heat and chemical resistance, and low shrinkage. For these reasons, it is increasingly being used as a matrix for fibre-reinforced polymer composites. Epoxy has found wide applications in the manufacture of adhesives, aerospace, and electronic structures as well as coatings. On the other hand, majority of the epoxy systems are characterized by low fracture toughness and low impact strength. The main disadvantages of the industrial use of epoxy resins include their brittleness and relatively high cost. Two different approaches have recently been reported in the literature to substantially enhance the properties and reduce the cost of the composite compared to that for the neat epoxy resin.

In the first approach, brittle polymers are modified using nano-sized inorganic particles. Nanoparticles embedded in polymer matrix have attracted increasing interest because of the unique mechanical, optical, electrical, and magnetic properties compared to neat polymers (Sinha Ray and Okamoto 2003). Polymer nanocomposites represent a new category of organic–inorganic hybrid material made up of nanometre-scale inorganic particles dispersed in a matrix of organic polymer (Chatterjee and Islam 2008). The nanometre size of nanoparticles is largely responsible for the unique properties of polymer nanocomposites because of their comparative large surface area per unit volume. Such properties are the results of the phase interactions that take place between the polymer matrix and the nanoparticles at the interfaces since many essential chemical and physical interactions are governed by surfaces (Pavlidou and Papaspyrides 2008; Yong and Hahn 2004). These properties include thermal (thermal stability, coefficient of thermal expansion, flammability, decomposition), mechanical (strength, toughness, modulus), and physical (optical, shrinkage, dielectric, permeability) properties (Sinha Ray and Okamoto 2003).

The interest in polymer nanocomposites comes from the fact that the addition of only a few percent (5 wt% or less) of the nano-additives into a polymeric matrix would have a great effect on the properties of the matrix (Zainuddin et al. 2010). Compared to conventional filled polymers with micron-sized particles, polymer nanocomposites possess superior specific strength and stiffness, good fire retardant, and enhanced

barrier properties (Liu et al. 2005a; Kiliaris and Papaspyrides 2010). Other superior properties include abrasive wear resistance, creep and fatigue performance, and functional properties. Owing to these enhanced mechanical, thermal, and physical properties, polymer nanocomposites find wide application in packages, automotive, adhesives, microelectronics, and the like (Yasmin et al. 2006). In 1990, the Toyota research group carried out the first study on the polymer nanocomposites. These researchers synthesized polymer nanocomposites based on nylon-6/montmorillonite clay via the in situ polymerization method. When 5 wt% clay was added to Nylon-6 polymer, the tensile modulus increased by 68% and the flexural modulus by 224% (Okada et al. 1990). This research was the fore-runner of the global trend researches in different types of polymer nanocomposites made of different combination of nano-fillers and matrix polymers (Pavlidou and Papaspyrides 2008; Chen and Evans 2006).

Kaynak and colleagues (2009) investigated mechanical and flammability properties of nanoclay (Na-montmorillonite)-based epoxy nanocomposites. The research findings revealed an enhancement in fracture toughness and flexural strength. The maximum value was attained at 0.5% nanoclay loading. The addition of nanoclay also enhanced thermal stability and reduced flammability of nanocomposites compared to neat epoxy. In another experiment, Ha and co-workers (2010a) investigated the effect of silane treated clay on the fracture toughness of clay/epoxy nanocomposites. It was reported that fracture toughness increased by 82% for nanocomposites with treated clay over untreated clay/epoxy nanocomposites. This improvement in fracture behaviours was due to the excellent dispersion of the treated clay into epoxy matrix and to the enhancement in interfacial adhesive strength between resin and clay layers. Zhao et al. (2005) investigated the mechanical, thermal, and flammability properties of polyethylene/clay nanocomposites. Results showed an increase in the tensile strength, flexural strength, and flexural modulus due to the presence of organoclay. Moreover, the enhanced thermal stability and flammability of nanocomposites was also attributed to the addition of nanoclay. Becker et al. (2004) reported that the moisture barrier properties of epoxy nanocomposites tended to improve as a result of the addition of nanoclay platelets. Ye et al. (2007) observed significant improvement in impact strength of halloysite (HNT)/epoxy nanocomposites at only 2.3 wt% HNT loading. The tremendous improvement in impact strength was as a result of particle (bridging, pull-out, and breaking) and micro-cracking. Tang et al. (2011) studied the mechanical properties of treated halloysite-reinforced epoxy nanocomposites. It was reported that the fracture toughness of epoxy significantly increased by 78.3% due to the presence of 10 wt% of intercalated HNTs. Additionally, Ismail et al. (2008) reported an enhancement in thermal and flammability properties of HNT-filled polymer nanocomposites. Chen et al. (2008) investigated the mechanical properties of silica-epoxy nanocomposites. They reported that the tensile modulus and fracture toughness increased by 25% and 30%, respectively, due to the addition of only 10 wt% nano-silica. Moreover, Wetzel et al. (2006) reported an increase in flexural strength (up to 15%), flexural modulus (up to 40%), and fracture toughness (up to 120%) for epoxy nanocomposites reinforced with aluminium oxide (Al_2O_3). Liao et al. (2011) reported an increase in thermal stability of polymer/n-SiC nanocomposites compared to unfilled polymer.

The second approach involves the use of cellulose fibres as reinforcements in the polymeric matrices for making low-cost engineering materials. Some of natural fibres used in this approach include flax, sisal, hemp, jute, kenaf, and wood. Cellulose fibres have a lot of desirable properties such as low cost, low density, recyclability, and renewability. In addition, they possess excellent mechanical properties like high toughness, flexibility high specific modulus, and specific strength (Nassar et al. 2021; Benallel et al. 2021; Marsh 2003). For these reasons, cellulose-fibre-reinforced polymer composites have become very popular in various engineering applications such as automobile, building, and furniture. Besides, there is much pressure on manufacturing industries especially packaging, construction, and automotive industries to utilize new materials in substituting the non-renewable reinforcing materials, for instance, glass fibre emerging from consumers and new environmental legislation due to increased sensitivity on environmental pollution (Benallel et al. 2021). Natural fibres are environmental-friendly materials (green composites). Thus, they have become a preferred compound as a replacement for the conventional petroleum-based fibre-reinforced composites like carbon, aramid fibres, and glass fibres (Nassar et al. 2021; Marsh 2003).

Recycled cellulose fibre (RCF) obtained from cellulosic waste products such as cardboard, printed paper as well as recycled newspaper and magazine has many advantages in comparison with natural cellulose fibres (Alamri and Low 2012). RCF is abundantly available throughout the world, very friendly to the environment, and cheap. Thus, RCF-based polymer composites can be classified as desirable performing composites based on their economic and environmental advantages (Wang et al. 2007a). Composites reinforced with RCF represent a new class of materials that are likely to replace wood and other plant composites in the future. This new class of composites may be used in manufacturing of furniture and automotive and in housing.

There is significant amount of work which can be found in the literature on the effect of the addition of cellulose fibres on mechanical, physical, and thermal properties of the polymer systems (Nassar et al. 2021; Benallel et al. 2021; Liu and Hughes 2008; Rosa et al. 2010; Mohan and Kanny 2011). For instance, Liu and Hughes (2008) carried out a research study to determine the fracture toughness of epoxy matrix reinforced with woven flax fibres. According to their research findings, there was a two—four-fold increase in the fracture toughness of the epoxy matrix due to the addition of flax fibres in comparison with pure epoxy samples. They concluded that this significant improvement in facture toughness was related to the increase in fibre volume fraction. Another study by Maleque et al. (2007) showed an increase in flexural strength and impact strength by 38 and 40%, respectively, when banana-woven fabric was added to the epoxy matrix. De Rosa et al. (2010) studied the mechanical and thermal properties of phormium tenax leaf fibre-reinforced epoxy composites. In that study, the epoxy matrix was reinforced using 20% loading of short and long fibres. The researchers observed that after the addition of long fibre, tensile and flexural strengths of pure epoxy increased by 25% and 32%, respectively. Moreover, tensile and flexural modulus was found to be two times higher than those measured

for neat epoxy. However, when short fibres were added, there was a significant reduction in tensile strength by approximately 40%, with very little impact on the flexural strength of the material. This reduction in strength was attributed to the poor distribution of the fibre, resulting in matrix-rich regions and fibre disorders. Also, the plant fibres were found to favourably enhance the thermal stability of the composites. Low et al. (2009) have reported a considerable increase in facture toughness, modulus, flexural strength, impact toughness, and impact strength of recycled cellulose-fibre-reinforced epoxy composites. Hitherto, considerable work has been successfully done on reinforced thermoplastics with natural fibres (Nassar et al. 2021), but not much work has been focused on thermosets with natural reinforcements.

However, cellulose fibres are hydrophilic in nature and hence have a poor resistance to water absorption. High moisture absorption is one of the major drawbacks of cellulose fibres, which restricts the use of cellulose-fibre-reinforced polymer composites in many outdoor applications. Water absorption can lead to swelling of the fibre forming voids and micro-cracks at the fibre–matrix interface region, which can result in a reduction of mechanical properties and dimensional stability of composites (Nassar et al. 2021; Benallel et al. 2021).

Therefore, in order to promote the wider use of these materials in high-performance applications, it is essential to consider the effect of moisture absorption and water uptake on their physical and mechanical properties. Many studies on epoxy-based composites have claimed that moisture and water absorption can strongly affect and reduce the mechanical and thermal properties of epoxy resins (Benallel et al. 2021; Athijayamani et al. 2009). Other studies reported that the rate of water absorption and moisture diffusion in polymer nanocomposites is significantly reduced by adding nanoclay, and the great reduction of water uptake was found by adding 5 wt% of nanoclay (Zhao and Li 2008; Lu and Mai 2005; Liu et al. 2008; Kim et al. 2005).

(b)   Vinyl-Ester Ecocomposites and Eco-Nanocomposites

Vinyl-ester resin (VER) has superior resistance to moisture and chemicals, providing greater hydrolytic stability compared to cheaper polymer resins and allowing greater control over cure rate and reaction conditions compared to epoxy resins (Sultania et al. 2010). VER also has excellent mechanical properties (Guo et al. 2007). The advanced polymer is produced by a reaction between an epoxy and carboxylic acid (Holbery and Houston 2006; Mallick 2007). As a thermoset, being produced by a curing process, VER is highly rigid. VERs are believed to combine the best properties of epoxies and unsaturated polyesters (Sultania et al. 2010). Though VERs are already used extensively in electrical components, automobile parts, coatings, adhesives, moulding compounds, structural laminates used in mining and chemical operations, and sporting goods, further research is required to better understand the potential of the material (Holbery and Houston 2006; Ku et al. 2007). The chemistry of VERs is complicated. The substance has carbon double bonds at the end of molecule providing a sole site for cross-linking. The means that the thermoset, i.e. cured, VER has less cross-links which makes it more flexible than other cured polyester resins. These intermolecular forces also give VERs higher facture toughness than other resins. VER

tends to have a low viscosity. The reason for this is that its substance is often dissolved in a styrene monomer. When polymerization is occurring, cross-links are formed between the unsaturation points. The two properties which are weaker in VERs compared to epoxy resins and polyester resins are firstly, the volumetric shrinkage is higher which is undesirable, and VERs have lower adhesive strength (Sultania et al. 2010; Mallick 2007; Marsh 2007).

In polymer science, a major challenge is broadening the window of application for such materials. This is generally achieved by preparation procedures, treatments, and other techniques that retain desirable features while enhancing features such as modulus, strength, fire performance, and heat resistance. As matrices, polymers have relatively poor mechanical, thermal, and electrical properties compared to metal or ceramic. Homopolymers, co-polymers, blended polymers, modified polymers, and other polymer types, alone, have insufficient property quality to meet the demands of industry. The inclusion of fibre (synthetic/natural), whisker, platelets, or particles is some of the alternative approaches that are used to improve the properties of polymers. Here, the inclusion of natural fibres and nanoparticles will be discussed.

The use of cellulose fibres to reinforce the polymeric matrices has been studied for at least a decade. Cellulose fibres, such as flax, sisal, oil palm, henequen, jute, banana, wood pulp, stinging nettle, coir, and hemp fibres, are natural fibres (Sreenivasan et al. 2011). Cellulose fibres are environmental friendly. They are biodegradable, so unlike many plastics, they will not stay on the earth's surface for millions of years. Moreover, the production of cellulose fibres requires less energy than the production of glass or carbon fibres (Venkateshwaran et al. 2011). They are less dense (1.25–1.5 g/cm^3) than for carbon fibre (1.8–2.1 g/cm^3) or E-glass (2.54 g/cm^3), and they are lighter than the synthetic fibres (Sgriccia et al. 2008; Anuar and Zuraida 2011). Cellulose fibres also have excellent modulus-weight ratio, which makes them successful in stiffness-critical designs. The acoustic damping property of cellulose fibres also makes them preferable to glass or carbon for noise attenuation purposes, an important requirement for automobile interior products (Mallick 2007). In addition, cellulose fibres possess excellent toughness, flexibility, specific modulus, and specific strength properties (Monteiro et al. 2009). Compared to most synthetic fibres, cellulose fibres are much more commercially viable.

Recycled cellulose fibre (RCF) refers to cellulose fibre that is extracted from newspapers, printed paper, and/or cardboard. Newspaper-fibre-reinforced composites, for example, have similar properties to wood-fibre-reinforced composites. Moreover, newspaper fibre-reinforced composites can be more easily produced due to cost advantage, renewability of the resource, greater flexibility, and lower wear of processing machinery. Load-bearing roof systems, sub-flooring, and framing components as well as residential applications such as doors, windows, and furniture are applications of RCF-reinforced materials. Composites reinforced with RCF represent a new class of materials with potential to replace wood and other plant composites soon.

However, drawbacks exist because cellulose-fibre-reinforced polymeric composites suffer from two inherent weaknesses. Firstly, cellulose fibres which are

hydrophilic and matrix components which are hydrophobic are inherently incompatible (Benallel et al. 2021; Athijayamani et al. 2009). This lack of chemical affinity due to the hydrophilic nature of cellulose fibres adversely affects composite strength. Thus, to improve fibre–matrix adhesion and prevent loss of strength, extensive physical and chemical treatment of the fibre surface is required (Herrera-Franco and Valadez-González 2005). Secondly, cellulose-fibre-reinforced polymeric composites suffer moisture-related problems (Chen et al. 2009). Fibre–matrix interface integrity is compromised on exposure to water which leads to poor stress transfer efficiencies and loss of overall mechanical properties. Issues relating to water absorption are, therefore, the predominant deterrent to cellulose-fibre-reinforced polymeric composites research and development.

The inclusion of nanoparticles is another one of the approaches used to improve the properties of polymers. The addition of nanoparticles to a polymer creates a multiphase material, known as a nanocomposite. In 1987, the first work on polymer/clay nanocomposites was conducted. In the early 1990s, researchers at the Toyota Company made a few breakthroughs with polymer-layered silicates. These researchers were the first to exfoliated clay with the polymer of nylon-6 (Chen and Evans 2006). Improvements in strength, modulus, and heat distortion temperature were all reported as due to addition of nanoclay (Pavlidou and Papaspyrides 2008; Wu et al. 2022). Since this time, polypropylene, polyethylene, polystyrene, polyvinylchloride, polylactide, polycaprolactone, phenolic resin, poly p-phenylene vinylene, polypyrrole, rubber, starch, polyurethane, polyvinylpyridine, and other more common polymers such as nylons have been included in studies with nanofillers (Okamoto 2006; Paul and Robeson 2008; Davtyan et al. 2012). Today the most commonly used polymers in nanocomposite science are the epoxies, polyurethanes, polyester, and vinyl ester.

Nanocomposite science has attracted interest due to the improvements that ~5 wt.% of nano-additive can have on the properties of the pre-existing material. Typically, moisture barrier, flammability resistance, thermal, and mechanical properties of polymeric composites are improved by virtue of ~5 wt.% nano-filler. The unique properties of polymer nanocomposites arise due to the nanometre size of nanoparticles. Having dimensions in the nanoscale, nanoparticles have a large surface area per unit volume. Since many essential chemical and physical interactions are governed by surfaces such a large surface area enables dense phase interactions to occur at the matrix/particle interfaces (Yong and Hahn 2009). Polymer nanocomposites possess superior specific strength and stiffness, good fire retardant, and enhanced barrier properties compared to most polymers filled with micron-sized particles (Wu et al. 2022). Abrasive wear resistance, creep and fatigue performance, and functional properties are other areas where polymer nanocomposites exhibit superior properties, and it is the enhanced mechanical, thermal, and physical properties overall that has enabled these materials to find wide application in the packaging, automotive, adhesive, and microelectronics industries (Pavlidou and Papaspyrides 2008; Zhao et al. 2008).

In this book, we describe the effect of recycled cellulose-fibre sheets and nanofillers (i.e. nanoclay platelets, halloysite nanotubes, and nano-silicon carbide) as well as both recycled cellulose fibre and nanoparticle dispersion on the microstructure,

mechanical, thermal, and barrier properties of epoxy resin and vinyl-ester composites. The properties of these composites were investigated and discussed in terms of wide-angle X-ray scattering (WAXS), synchrotron radiation diffraction (SRD), Fourier transforms infrared spectroscopy (FTIR), transmission electron microscopy (TEM), scanning electron microscopy (SEM), flexural strength, flexural modulus, impact strength, fracture toughness, impact toughness, thermo-gravimetric analysis (TGA), and water absorption. The effect of water absorption on the mechanical properties of these composites was also investigated and discussed.

1.2   Literature Review

(a)   Natural Fibres

Based on their sources, natural fibres are divided into mineral, animal, and plant fibres. The physical, thermal, and chemical properties of these fibres are also vastly different (Bismarck et al. 2005). Mineral fibres such as those derived from geological materials like quartz and asbestos are tough, highly temperature resistant, and their uses include ceiling tiles and high-temperature gaskets. Animal fibres such as animal hair protein of silk, wool, hair, angora, mohair, and alpaca find their main use in the textile industry. However, the high cost of these fibres and the inadequate quantities available to satisfy the demands have forced the textile manufacturers to switch to synthetic fibres (Cheung et al. 2009). Plant fibres are mainly made up of cellulose fibres as the main component and depending on the plant parts from where they are obtained, and they are further categorized into bast or stem fibres such as flax, hemp, ramie, jute and kenaf; leaf or hard fibres such as banana, sisal, and pineapple; seed fibres as in cotton and kapok; fruit fibres such as coir from coconut; wood fibres; stalk fibres; grass fibres; and so on (John and Thomas 2008; John et al. 2009).

Several methods that can be used to separate the fibres from the other plant parts include retting, scrapping, and pulping. Plant fibres are available all over the world. However, such countries like India, China, Bangladesh, Tanzania, Brazil, Mexico, and Philippines produce abundant quantities of plant fibres (Taj et al. 2007). Moreover, agrofibre-based products such as paper, cardboard, and waste wood can also be recycled to obtain large quantities of cellulose fibres. The easy availability in adequate quantities and the good mechanical properties of cellulose fibres have made them very desirable materials for reinforcing composites especially in the manufacture of reinforced polymers due to their breaking length mechanical properties (Riedel and Nickel 2005). Classification of the plant fibres according to their uses in various applications depends on their different properties such as stiffness, tensile strength, thermal stability, the adhesive quality between the fibre and the matrix, the cost factors relating to the materials as well as in their manufacture. These factors also determine their roles in different applications. These properties are further dependent on different factors like the nature of the plant, its age, its place of growth, and the method of fibre extraction. Table 1.1 displays the properties of some plant fibres.

Table 1.1 Properties of some nature fibres (Mallick 2007)

Properties	Hemp	Jute	Sisal	Flax
Density (g/cm^3)	1.48	1.46	1.33	1.4
Tensile strength (MPa)	550–900	400–800	600–700	800–1500
Tensile modulus (GPa)	70	10–30	38	60–80
Elongation to failure (%)	1.6	1.8	2–3	1.2–1.6

(b)   Structure and Chemical Constituents of Natural Fibres

Plant fibres are composite materials made by nature and their structure as well as their chemical composition is quite complex. They are essentially rigid, crystalline cellulose fibrils that are dispersed in a matrix made of lignin and/or hemicellulose (Mallick 2007; Bismarck et al. 2005). Apart from cotton, most plant fibres are composed of cellulose, hemicelluloses, lignin, pectin, waxes, and a few water-soluble compounds. The physical properties of the fibres are governed by the cellulose, hemicelluloses, and lignin that are its basic constituents (John and Thomas 2008). Depending on the type of plant fibres, cellulose forms about 30–90 wt% of the fibres and lignin about 3–40 wt%, while the moisture content is about 6–20 wt% (Rosa et al. 2010; Mallick 2007; Bismarck et al. 2005). Table 1.2 exhibits the chemical compositions of some important plant fibres.

   These plant fibres are made up of hollow cellulose fibrils held together by a matrix made up of lignin and hemicelluloses. The cells in these fibres do not have a homogenous membrane in their cell walls (Bismarck et al. 2005). Instead, the cell walls are complex and layered structures with the thin primary layer set during

Table 1.2 Chemical compositions of selected plant fibres (Rosa et al. 2010)

Type of fibre	Cellulose (wt%)	Hemicellulose (wt%)	Lignin (wt%)	Pectin (wt%)	Wax (wt%)
Bast fibre					
Hemp	70.2–74.4	17.9–22.4	3.7–5.7	0.9	0.8
Jute	61–71.5	12–20.4	11.8–13	0.2	0.5
Flax	64.1–71.9	16.7–20.6	2–2.2	1.8–2.3	1.7
Kenaf	31.57	21.5	8–19	3–5	
Leaf fibre					
Sisal	65.8–78	8–14	10–14	0.8–10	2
Pineapple	70–82		5–12.7		
Banana	63.64	10–19	5		
Seed fibre					
Cotton	82.7–90	5.7		0–1	0.6
Fruit fibre					
Coir	32–43	0.15–0.25	40–45	3–4	

the growth of the cell that encloses a secondary wall and is made of fibres that are not regularly arranged. The secondary wall is a three-layered structure, whose solid middle layer is the most important in determining the mechanical properties of the fibre (John et al. 2009). This middle layer consists of a series of cellular microfibrils that have a helically coiled structure that is made up of long chain cellulose molecules, with microfibrillar angles between the axis of the fibre and the microfibrils. This angle varies according to the type of fibre. Most microfibrils are made up of 30–100 cellulose molecules and have a diameter of about 10–30 nm These extended chain formations supply the mechanical strength to the fibre (Bismarck et al. 2005). The non-crystalline regions of the cell wall are complex structures made up of hemicelluloses, lignin, and sometimes pectin. Hydrogen bonds link the hemicelluloses to the cellulose microfibrils in a network of cross-linked molecules that are called the cellulose-hemicellulose network and form the backbone of the fibre cell (Bismarck et al. 2005; Stamboulis et al. 2001). The lignin network, on the other hand, is hydrophobic in nature and influences the properties by operating as a coupling agent and thus enhancing the strength of the cellulose-hemicellulose network. The properties of the fibres have many variable determinants such as the structure, the microfibrillar angle, dimensions of the cell, its defects, as well as the chemical composition of fibres (Bismarck et al. 2005; John and Thomas 2008).

It is usually found that there is a proportionate increase in the tensile strength and Young's modulus to the increase in the cellulose content and the microfibrillar angle has a direct influence on the stiffness of the fibres. Microfibrils oriented spiral to the fibre axis make the fibre flexible and those which are parallel oriented renders the fibres rigid with a high tensile strength (John and Thomas 2008).

(i)   Cellulose

Cellulose forms the main constituent of most of the natural plant fibres. It is hydrophilic nature polymer, comprising of D-anhydroglucose with the formula $C_6H_{11}O_5$ with repeating glucose units linked by 1,4-β-D glycosidic bonds, where each glucose molecule is bonded to the next one through 1 and 4 carbon atoms (John and Thomas 2008; Mohanty et al. 2005). Each of these repeated units comprises three hydroxyl groups. These hydroxyl groups and their ability to hydrogen bonds are the most influential in guiding the arrangement of the crystalline packing and in managing the physical properties of cellulose materials (Bismarck et al. 2005). The degree of polymerization (DP) in the cellulose molecules is about 10,000 and these cellulose molecules are disposed in the microfibrils with diameters ranging from 10 to 20 nm (Bismarck et al. 2005; John and Thomas 2008; Rösler et al. 2007). Solid cellulose has a microcrystalline structure with highly crystalline as well as amorphous regions with slender rod-like crystalline microfibrils. Natural cellulose also called cellulose I has a monoclinic sphenodic crystalline form. Although cellulose is highly resistant even to strong alkali up to 17.5 wt%, it dissolves easily in water-soluble sugars. The resistance of cellulose to oxidizing agents is also quite high. In the solid state, there are four main different allomorphic forms of cellulose (cellulose I, II, III, IV) (Mittal et al. 2011). Each type displays distinctive X-ray diffraction patterns. Cellulose I is the most abundant crystalline form, which occurs naturally with two structures,

cellulose I_α (triclinic) and cellulose I_β (monoclinic) (Wada et al. 2004). Cellulose II is modified cellulose. It is formed from cellulose I via mercerization (alkali treatment) or regeneration (recrystallization from a solution). These treatments change the chain structure of cellulose I from parallel to anti-parallel forming cellulose II (Ford et al. 2010). Cellulose III and IV can be both derived from either cellulose I or cellulose II by treatment with liquid ammonia and heating, respectively. Cellulose III_I and IV_I are obtained from cellulose I while cellulose III_{II} and IV_{II} are produced from cellulose II. Bledzki and Gassan (1999) stated that the cell geometry of each type of cellulose is the determinant factor of its mechanical properties and each type of cellulose has different cell geometry. The content of the cellulose matter in the raw material determines the pulp yield during chemical pulping. Thus, cellulose content is a vital factor in the fibre.

(ii)   Hemicellulose

Hemicelluloses are misnamed because they are not celluloses at all but polysaccharides with a blend of five-ring and six-ring carbon ring sugars. These sugars include glucose, and monomers like galactose, mannose, arabinose, and xylose (Saari et al. 2010). The polymer chains are non-crystalline in nature consisting of short and branched chains, with DP about 50 to 300 and pendant side groups that make it amorphous. The differences between hemicelluloses and cellulose are in three significant features: hemicelluloses are made up of different types of sugar units while celluloses are made up of only 1,4-β-D-glucopyranose units; the extensive chain branching and pendant side groups make hemicelluloses amorphous while the celluloses are strictly linear polymer. Although hemicelluloses have 50–300 DP or degree of polymerization, the DP of celluloses is 10–100 times higher. Another difference between them is that hemicelluloses form the matrix part of the composite whereas the cellulose microfibrils are dispersed in them (John and Thomas 2008). Moreover, hemicelluloses are easily hydrolysed in acids, are hydrophyllic in nature and dissolved by alkali (John and Thomas 2008). Stamboulis et al. (2001) found that the main structural constituents of fibre cells are the cellulose hemicelluloses networks that are made up of cross-linking molecules of hemicellulose bonding with cellulose microfibrils through hydrogen bonds.

(iii)   Lignin

After cellulose, lignin has the most importance in natural fibres. Rigidity and the length of plant fibres are provided by lignin. This complex hydrocarbon polymer is composed of aliphatic as well as aromatic components. Its properties include its completely non-crystalline and hydrophobic character, its resistance to most solvents and not easily fragmented into monomeric units. It is envisioned as a complex copolymer with high molecular weight, a three-dimensional structure and composed of aliphatic and aromatic compounds belonging to the hydroxyl, methoxyl, and carbonyl groups (Bismarck et al. 2005; John and Thomas 2008). Each building unit of lignin is made up of five hydroxyl and five methoxyl groups. The structural units are thought to be derived from 4-hydroxy-3-methoxy phenylpropane. Due to the non-availability of any conventional method to isolate lignin in a native state

from the fibre of which it is part, the study of its chemistry is difficult. There are more possible cross-linking sites available in lignin than in either cellulose or hemi-cellulose and that is considered the main chemical difference between them. These cross-linking sites are responsible for the non-crystalline structure of login and they are feasible on the propane chain, through the C4 oxygen and at the free aromatic ring carbons. Lignin that is extracted from fibres can be used as an alternative for phenol in the matrix material. Bledzki and Gassan (1999) also stated that isotropic lignin displayed significantly lower mechanical properties than those of cellulose.

Lignin is a thermoplastic polymer that starts to melt at about 170 °C and has glass transition temperature of about 90 °C. Lignin is resistant to hydrolysis by acids but dissolves in hot alkali, can be easily oxidized, and readily condenses with phenol. Lignin can only be removed through pulping methods that involve polluting bleaching process that are not environment friendly in procedures like in the manufacture of paper.

(iv)   Pectin

Hetero-polysaccharides are collectively known as pectins. These complex polysaccharide chains comprise of polymer form of glucuronic acid and residues of rhannose. Pectins provide flexibility to the plants (John and Thomas 2008). Pectin can dissolve in water only if they are partially neutralized with alkali like ammonium hydroxide (Bledzki and Gassan 1999).

(v)   Waxes

Waxes can be removed from the plant fibres by organic solutions. These materials form the last part of the plant fibre. They are mostly alcoholic in their structure and show resistance to water and acids such as palmitic, oleoginic, and stearic acids (John and Thomas 2008; Bledzki and Gassan 1999).

(c)   Natural-Fibre-Reinforced Polymer Composites

Natural fibres are used as fillers to reinforce the polymer matrix of the natural fibre-filled polymer composites. Generally, natural fibres such as bamboo, wood, kenaf, cotton, coconut husk, oil palm, jute, areca fruit, and so on. Right from Neolithic times, the usage of fibres and plant fibre composites has been widespread. Their history spreads back to the Neolithic era in the regions now known as Syria, Turkey, Iraq, and Iran. Carbon dating of hemp and linen remains found in these regions places them 8000–6000 B.C (Bismarck et al. 2005). They were mostly used in the production of energy, shelters, clothes, tools, and weapons. Fibres like straw were also used as strengthening materials in the construction of walls in Egypt about 3000 years ago (Zaman et al. 2011). The designs and shapes of these composites were simple and placed in layers to produce the required arrangement. Although more creative designs were introduced early in the last century, they still had limitations due to the shape and weight of the structural fibres. These were mostly in the form of two-dimensional sheets that were also fabricated into tubes and pipes. Their usage was mainly in the electrical arena with fibre materials like cotton or paper reinforcing sheets made of phenol- or melamine–formaldehyde resins.

Later, with the advent of durable materials like metals in construction, natural fibre composites became less popular. It was only in 1940 that the first engineering fibre composites were manufactured. These consisted of stronger materials like continuous filament glass fibre and tough and rigid unsaturated polyester resins and began to be manufactured on extensively (Bader 2001). These fibres still have their uses in the reinforcing thermosetting and thermoplastic composites that are needed by industries such as automotive, aeronautics, and aerospace. Since then, such cellulose-fibre materials are mostly used in the manufacture of rope, clothing, carpets, and other decorative products (Haghighat et al. 2005).

In the environment conscious present times, natural fibre dispersed polymer composites are being given a lot of importance for research, not only because they are no harm to the environment but also because they can be easily reproduced as replacements for the non-renewable reinforcing materials like glass fibre, carbon fibre, Kevlar fibre, and so on. More stringent environmental safety regulations and consumer demands in the automotive, construction, and packaging industries have made research on natural fibre composites more significant (Moeini et al. 2009; Bachtiar et al. 2008; Wambua et al. 2003). Inorganic fibres such as glass fibres cannot be renewed or recycled and use large amounts of energy to manufacture, pose serious health risks due to their harmful gas emissions, and negative biodegradability although they can be produced at low cost and offer moderate strength properties useful in structural materials (Wambua et al. 2003; Harish et al. 2009). At the same time, the natural fibre composites offer exceptional mechanical properties, low density, low cost, and good chemical resistance. The more conventional glass and other reinforcing materials can be replaced or substituted by natural fibres such as hemp, jute, wood, and even waste cellulose products in the automotive, construction, or packaging industries due to their desirable qualities such as stiffness, impact resistance, flexibility, and modulus (Hodzic and Shanks 2014). Also, their ready availability in large quantities, their biodegradability, and renewable nature are much appreciated in these industries. Additional properties like low density, low cost, less equipment abrasion, less irritation of skin and respiration, damping of vibrations, and recovery of more energy have made these composites more welcome in various industries as good alternatives to the traditional synthetic fibre composites.

The global automotive industry that is being pressurized by stringent legislation and strong consumer demands for more environment-friendly cars is looking to the natural fibre composites as good alternatives. Stamboulis et al. (2001) argue that the price-performance ratio and low weight materials that have the added advantage of being environmentally friendly has made the natural fibre composites being used in large volume engineering markets like the construction and automotive industries. The statistics for natural fibres in the automotive industry in 1999 stood at 75% for flax, 10% jute, 8% hemp, 5% kenaf, and 2.5% sisal (Lotfi et al. 2019).

With the 2006 European Union legislation, that 80% of a vehicle must be reusable or recyclable rising to 85% by 2015, the European car manufacturers have started using thermoplastic and thermoset natural fibre composites in the door panels, seat backs, head-liners, package trays, dashboards, and other interior components (Holbery and Houston 2006). The same is the case with the Japanese automotive

industry where the requirements are even higher at 88% of vehicle components to be recovered including by incineration by 2005 and 95% by 2015. The impact of the vehicles on the environment throughout their life cycle right from the raw materials, manufacture, and usage of the vehicle to its ultimate disposal is being studied very carefully and research is being carried out for alternative and more desirable materials that are not harmful to the environment (Holbery and Houston 2006). It is here that natural fibre composites score high because apart from being biodegradable, they also possess the desired reinforcement properties to improve the mechanical properties of the components. Other industries that use natural fibre composites are in the manufacture of panels, furniture, and denser beams used in outdoor railings and decking (Marsh 2003; Baroulaki et al. 2006; Sanadi et al. 1994).

Polymers such as unsaturated polyesters, epoxides, and polyurethanes are beginning to be used as matrices for the cellulose fibres. Out of these, epoxy resins have shown better adhesive properties to the natural fibres. The resulting materials have noteworthy mechanical properties for use in the manufacture of structural materials because of their higher grades of strength, stiffness, and low distortion properties (Buehler and Seferis 2000).

(d)   Properties of Cellulose-Fibre-Reinforced Polymer Ecocomposites

An enormous attention has been focused on cellulose-fibre-reinforced polymer due to the desirable properties of cellulose fibres over traditional fibres. Therefore, several investigations have been carried out on several types of cellulose fibres such as kenaf, hemp, flax, bamboo, jute, and waste cellulose products to study the effect of these fibres on the properties of composites materials. This section outlines the mechanical, thermal, and moisture properties of cellulose-fibre-reinforced polymers.

(i)   *Mechanical properties*

Maleque et al. (2007) have investigated the mechanical properties of pseudo-stem banana fibre-epoxy composite. The hand lay-up method was used to fabricate the pseudo-stem banana-woven fabric-reinforced epoxy composite. It was reported that there was an increase in flexural strength from 53.38 to 73.58 MPa when banana-woven fabric was added to the epoxy matrix. The impact strength of the pseudo-stem banana-woven fabric-reinforced epoxy composite was found to be approximately 40% higher than that of pure epoxy. The results also showed that the tensile strength of the banana fibre significantly enhances the tensile strength of the material by 90% when compared to pure epoxy.

Liu and Hughes (2008) investigated the fracture toughness of epoxy matrix composites reinforced with woven flax fibre. Woven flax fibre-epoxy composites were prepared by a vacuum infusion process. It was found that the fracture toughness of the composites was increased by two—four times due to the presence of flax fibre compared to pure epoxy samples. The authors concluded that this significant improvement in facture toughness was related to the fibre volume fraction.

De Rosa et al. (2010) carried out the mechanical properties of phormium tenax leaf fibre-reinforced epoxy composites. Quasi-unidirectional long fibres and short fibres were used to reinforce epoxy matrix with a 20% loading of natural fibre. It was

observed that the long fibres increased tensile strength and flexural strength of pure epoxy by 25% and 32%, respectively. Moreover, tensile and flexural modulus was found to be two times higher than those measured for pure epoxy samples. However, the addition of short fibres dramatically decreased tensile strength by around 40% and had a significant effect on the flexural strength. The authors explained that in the case of short fibre composites, the stress was not uniform along the fibre, which resulted in the lack of stress transmission between the matrix and fibre causing reduction in mechanical properties. However, long fibre-reinforced polymer exhibited better stress transmission along the composites, which provided better mechanical properties.

Fibre–matrix adhesion is an essential factor that influences the mechanical properties of cellulose fibre/polymer composites. To overcome this problem, many types of fibre surface treatments have been carried out to modify the surface tension and polarity of cellulose fibres for better fibre–matrix adhesion (AL-Oqla and Omari 2017; Wang et al. 2007b; Rong 2001; Tejyan 2021).

Wang et al. (2007b) have investigated the effects of fibre treatment on the mechanical properties for flax-thermoplastic composites. They used four types of chemical treatments on flax fibres, namely, mercerization, silane treatment, benzoylation, and peroxide treatment. Improvement in tensile strength was observed in the samples with silane and peroxide treatment over the samples with untreated fibres.

Rong (2001) studied the mechanical properties of treated sisal fibre-reinforced epoxy composites. Three types of fibre treatments were used: alkalization, acetylation, and cyanoethylation. An overall improvement of flexural strength and modulus properties was reported for all treated fibre-epoxy samples. The authors pointed out that fibre treatment can improve the mechanical properties of cellulose fibre/polymer composites by improving matrix–fibre interface adhesion. Fibre volume fraction is another critical factor that influences the mechanical properties of cellulose fibre/polymer composites. Hughes et al. (2002) investigated the variation of fracture toughness with fibre volume fraction of hemp and jute fibre-reinforced polyester composites. Their results showed that fracture toughness increases as fibre volume fraction increases. The fracture toughness of polyester matrix composites reinforced with glass, hemp, and jute fibre (at fibre volume fraction = 0.2) was found to be 9.01, 3.51, and 2.56 ($MNm^{-3/2}$), respectively, while the fracture toughness of the virgin polyester was 0.62 ($MNm^{-3/2}$). Moreover, the critical strain energy release rate (G_{IC}) was measured and found to be increased from 0.1 (kJm^{-2}) for polymer to 0.97 and 1.84 (kJm^{-2}) for polymer reinforced with jute and hemp, respectively.

(ii)   *Thermal properties*

Albano et al. (1999) studied the thermal stability of thermoplastic polymers reinforced with plant fibres. Polypropylene (PP) systems were reinforced with treated and untreated sisal fibres. Results of initial and maximum degradation temperatures are summarized in Table 1.3. Treated fibres appeared to display better thermal properties than untreated fibre. In all cases, the present of sisal fibres increased the thermal stability of PP matrix by shifting the maximum decomposition temperature (T_{max})

Table 1.3 Initial and maximum degradation temperatures of raw materials and composites (Albano et al. 1999)

Sample	T_i (K)	T_{max} (K)
Untreated sisal	503	638
Treated sisal	523	658
PP	603	713
PP/untreated sisal	563	724
PP/treated sisal	583	733

to higher values. In the other hand, the addition of sisal fibres accelerated the initial decomposition process of PP matrix.

In another interesting study, Al-Oqla and Omari (2017) carried out the influence of different chemical treatments of the fibres on the thermal behaviour of epoxy matrix reinforced with 30% sisal fibres. Thermogravimetric analysis indicated that chemical treatments enhanced the thermal stability of sisal fibre by increasing the maximum degradation peak temperatures of sisal fibre from 335 to 390 °C. This improvement was related to the modification of the chemical structure of the fibres. The study also revealed that the addition of treated fibres to the epoxy matrix was found to enhance the epoxy degradation slightly compared to untreated fibre composites. Finally, author stated that natural fibres governor the thermal stability of polymer composites.

The thermal properties of composites of poly (L-lactide) reinforced with different contents (1, 5, 10, 20, and 30%) of hemp fibres were investigated by Masirek et al. (2007). The thermo-gravimetric analysis of the composites, carried out in nitrogen atmosphere, showed that the addition of cellulose fibre accelerated the starting degradation of the hemp/PLA composites. The maximum degradation rate for neat PLA was at about 375 °C, while it was shifted to lower temperatures in the range of 320–338 °C for PLA/hemp composites, which is close to the typical degradation peak temperature of plain hemp. This result showed agreement with the previous study about the condition of cellulose fibre on polymer composites thermal stability. Table 1.4 displays onset (T_{onset}) and derivative peak (T_D) temperatures of PLA and hemp fibre/PLA composites.

De Rosa et al. (2010) investigated the thermal behaviour of epoxy composites reinforced with untreated phormium tenax lead fibres. Their results showed that the

Table 1.4 TGA data of PLA and PLA/hemp fibre composites in nitrogen atmosphere (Masirek et al. 2007)

Composites	T_{onset} in N_2 (°C)	T_D in N_2 (°C)
PLA	342	375
99/1 PLA/hemp	322	338
95/5 PLA/hemp	295	323
90/10 PLA/hemp	301	322
80/20 PLA/hemp	289	322
70/30 PLA/hemp	305	331

incorporation of plant fibres increased the thermal stability of epoxy matrix whereby the most mass of cellulose fibres and neat epoxy decomposed at temperatures of 337 °C and 335 °C, respectively, while cellulose fibre/epoxy composites decomposed at 347 °C. They concluded that this enhancement in thermal properties was due to the improvement of fibre/matrix interface.

(iii)   *Water absorption behaviour of cellulose-fibre-polymer composites*

The use of nature plant fibres as reinforcements in polymer composites to replace traditional fibres like glass has currently generated much attention because of the advantages, including cost-effectiveness, low density, high specific strength, as well as their availability as renewable resources. However, one of the major drawbacks that have limited the use of plant fibre as reinforcement in polymer composites is their susceptibility to moisture absorption, which in turn can lead to swelling of the fibre forming voids and micro-cracks at the fibre–matrix interface region, which results in a reduction of mechanical properties and dimensional stability of composites. Cellulose fibres are hydrophilic in nature and they tend to absorb or attract much of water depending on the environmental condition. The chemical reason for this is due to the presence of hydroxyl groups in the cellulose structure which attracts water molecules and bind with them through hydrogen bonding (Han and Drzal 2003; Fraga et al. 2006; Kim and Seo 2006; Doan et al. 2007). A study on moisture behaviour of plant fibre/polymer composites was done by Benallel et al. (2021). Unsaturated polyester was reinforced with 2, 3, 4, and 5 layers of hemp fibre. It was found that moisture absorption increased as fibre content increased. Composite reinforced with five layers showed higher moisture absorption with higher maximum water uptake due to the higher cellulose content among other composites. Authors explained that hemp fibre swells after exposed to moisture creating micro-crack within the matrix–fibre interface. These micro-cracks make water molecules diffuse easily inside the composites which result in high moisture absorption.

Similar result was reported by Athijayamani et al. (2009) where they studied the effect of fibre content on the moisture absorption behaviour of cellulose fibre/polyester composites. Their results indicated that water uptake increased as fibre load increased, and that water absorption of composites increased as exposure time to moisture increased.

Because of the hydrophilic nature of cellulose fibres, composites reinforced with cellulose fibres always tend to absorb much water than other types of composites. Rashdi et al. (2009) also indicated in their study on kenaf fibre-reinforced unsaturated polyester composites that as fibre load increased moisture absorption increased due to the high content of cellulose.

(d)   Polymer–Clay Nanocomposites

Polymer nanocomposite materials possess two phases consisting of inorganic particles of nanometre scale in the range between 1 and 100 nm that are dispersed in a matrix of polymeric material. These nanoparticles demonstrate remarkable properties because of their comparative large surface area per unit volume. Such properties are the results of the phase interactions that take place between the polymer matrix

Table 1.5 Examples of layered host crystals used in polymer nanocomposites (Wypych and Satyanarayana 2005)

Chemical nature	Examples
Element	Graphite
Metal chalcogenides	$(PbS)_{1.18}$ $(TiS_2)_2$, MoS_2
Carbon oxides	Graphite oxide
Metal phosphates	$Zr(HPO_4)_2$
Clay and layered silicates	Montmorillonite, hectroite, saponite, fluoromica, fluorohectorite, vermiculite, kaolinite, magadiite
Layered double hydroxides	$Mg_6Al_2(OH)_{16}CO_3$ nH_2O; M=Mg. Zn

and the nanoparticles at the interfaces (Pavlidou and Papaspyrides 2008; Yong and Hahn 2009; Choudalakis and Gotsis 2009). The interest in polymer nanocomposites comes from the fact that the addition of nano-sized fillers into a polymeric matrix would have a great effect on the properties of the matrix. Therefore, in the last couple decades, polymer nanocomposite materials have attracted increasing research and development attention because of their unique characteristics in terms of mechanical properties, thermal stability, barrier properties, and flame retardancy (Pavlidou and Papaspyrides 2008; Kiliaris and Papaspyrides 2010; Mallick 2007). Many nanofillers are available for combination with the polymers in the formation of nanocomposites. Table 1.5 displays six such materials that can be utilized for this purpose (Wypych and Satyanarayana 2005).

Polymer–clay nanocomposites have been unique among composites and they have been preferred in many applications for their unique mechanical, thermal, electrical, and barrier properties (Wu et al. 2022). In these nanocomposites, the polymers are reinforced with high aspect ratio layered silicate sheets having about 1 nm thickness and a range of lengths between 100 and 300 nm. As the high aspect ratio provides a larger contact surface area, small concentrations of clay are enough to provide the necessary physical interactions between the polymer and the filler silicate sheets. This makes them extremely compatible as filler materials (Pavlidou and Papaspyrides 2008; Kiliaris and Papaspyrides 2010; Mallick 2007). In 1990, the Toyota research group carried out the first study on the polymer nanocomposites. These researchers synthesized polymer nanocomposites based on nylon-6/montmorillonite clay via the in situ polymerization method. When 4.7 wt% clay was added to nylon-6 polymer, the tensile modulus increased by 68% and the flexural modulus by 124% (Okada et al. 1990; Kojima et al. 1993). This research was the fore-runner of the global trend in polymer–clay research. Many types of polymers including engineering polymers such as polypropylene, polyethylene, polystyrene, polyvinylchloride, polylactide, polycaprolactone, phenolic resin, poly p-phenylene vinylene, polypyrrole, rubber, starch, polyurethane, polyvinylpyridine as well as common polymers like nylons and the focus of this research epoxy resins are developed for producing such nanocomposites (Gao 2004).

(i)   *Clay structure*

Nanoclay can be found in nature as a common material and is made up of minerals with a fine grain structure that demonstrates a varied array of plasticity according to the amount of water it contains and becomes hardened when dried or fired. Clays are chemically known as hydrous aluminium silicate with the formula $Al_2O_3 \cdot SiO_2 \cdot H_2O$. They are usually found contaminated with small amounts of potassium, sodium, calcium, magnesium, or iron. The clay mineral has a basic crystal structure consisting of layers, a sandwich of an aluminium oxide or magnesium oxide sheet with one or two silicon dioxide sheets. The thickness of the sheets is usually on the older of 1 nm whereas the lateral aspect can range from 30 to 200 nm or even more. Both tetrahedral and octahedral types of sheets can be found in all clay minerals that unite in sharing the apical oxygen atoms from the tetrahedral sheets (Choudalakis and Gotsis 2009). The classification of the clay minerals is based on the way the tetrahedral and octahedral sheets are arranged into layers. When a single tetrahedral sheet is linked to a single octahedral sheet, a 1:1 layered structure is produced such as in kaolinite. When a single octahedral sheet is attached to tetrahedral sheets on both sides a 2:1 layered structure result such as in 2:1 phyllosilicates. The silicate layers in the 2:1 layered structure are drawn towards each other by the van der Waals forces.

Montmorillonite (MMT) is one of the most popular layered silicates being studied for its properties. This silicate has a 2:1 layer crystal structure that consists of a sandwich with an aluminium octahedron layer between two of silicon tetrahedron layers. The physical aspects of the MMT provide unique properties that render them highly suitable for inclusion as fillers in composites. The high aspect ratio sheets that are produced by the 2:1 layer structure have a thickness of 1 nm and lengths ranging from 30 nm to several microns. When a clay platelet is diffused properly into the polymeric matrix without breaking, the aspect ratio of MMT increases to around 1000 with surface area is about $750\,m^2/g$ (Wu et al. 2022). Therefore, small quantities of silicates possess large surface areas that can be effectively utilized for interaction and thus are considered effective as fillers. The efficiency of the polymer chains in transferring stress into the filler particles increases dramatically due to the large surface area available for the interaction. Moreover, these high aspect ratio particles can also find use in the enhancement of barrier properties of polymer membranes by increasing the tortuosity of the material (Pavlidou and Papaspyrides 2008; Kiliaris and Papaspyrides 2010). Major clay mineral groups and the ideal structural chemical compositions of these minerals can be seen in Table 1.6.

(e)   Structure of Polymer–Clay Nanocomposites

There are three categories of polymer–clay composites: conventional composites, intercalated nanocomposites, and exfoliated nanocomposites (Chatterjee and Islam 2008).

Conventional composites are those composites in which the polymer matrix is not introduced into the conventional clay filler that has the structure of combined layers and perform as micro-scale fillers. The properties of these composites and those of the traditional microcomposites are comparable (Beyer 2002).

Table 1.6 Common clay minerals used in polymer nanocomposites (Wu et al. 2022)

Structure type	Group	Mineral examples	Ideal composition	Basal spacing (Å)
2:1(TOT)	Smectite	Montmorillonite	$[(Al_{3.5-2.8}Mg_{0.5-0.2})(Si_8)O_{20}(OH)_4] Ex_{0.5-1.2}$	12.4–17
		Hectorite	$[(Mg_{5.5-4.8}Li_{0.5-1.2}) (Si_8)O_{20}(OH)_4] Ex_{0.5-1.2}$	
		Saponite	$[(Mg_6)(Si_{7.5-6.8}Al_{0.5-1.2}) O_{20}(OH)_4] Ex_{0.5-1.2}$	
2:1(TOT)	Illite	Illite	$[(Al_4)(Si_{7.5-6.5}Al_{0.5-1.5})O_{20}(OH)_4]K_{0.5-1.5}$	10
2:1(TOT)	Vermiculite	Vermiculite	$[(Al_4)(Si_{6.8-6.2}Al_{1.2-1.8})O_{20}(OH)_4]Ex_{1.2-1.8}$	9.3–14
1:1(TO)	Kaolin-serpenite	Kaolinite, dickite, nacrite	$Al_4Si_4O_{10}(OH)_8$	7.14

Intercalated nanocomposites: In this composite, the polymer chains are inserted into the gallery gaps of the silicate layers in a diffuse and regularly repeating fashion (Auad et al. 2007). As a result of this, there is a complete loss of the registry in the clay layers that are well diffused in a continuous polymer matrix. Intercalated structures are not found suitable in applications that have strength as a requirement.

Exfoliated nanocomposites: The silicate layers in this type of nanocomposites are dispersed in the polymer matrix individually in an exfoliated microstructure. They have larger inter-spaces than in the intercalated nanocomposites and the amount of clay necessary for such composites is also comparatively less (Krishnamoorti and Yurekli 2001; Sinha and Okamoto 2003). They are also known as delaminated polymer–clay nanocomposites and are the most desirable as they provide better strength, stiffness, and barrier characteristics while using less mineral content than the conventional polymer composites. The enhancement of these properties is due to the larger surface area and aspect ratio that provide for greater contact between the polymer and the clay components. It is seen that the degree of exfoliation is directly proportional to the improvement in these properties.

(f)   Synthesis of Polymer–Clay Nanocomposites

Many different methods are available for the synthesis of polymer/clay nanocomposites. But for the hydrophobic clay must first be organically modified to allow the organic polymer to be integrated between the silicate layers so that it changes into organoclay or polymer-compatible clay. This pre-treatment is achieved through the ion exchange method in which the clay reacts with organic cations like alkyl ammonium or phosphonium ions. For the actual synthesis of the nanocomposite, three methods are popularly used: in situ polymerization, solution-induced intercalation, and melt processing or melt blending. Each of these methods has its own positive as well as negative aspects which are being well researched in recent times (Gao 2004; Zanetti and Costa 2004).

(i)   In situ *polymerization*

This type of polymerization technique was the very first used in the synthesis of polymer/clay nanocomposite-based polyamide-6 (Okada et al. 1990). This method involves the swelling of the treated organoclay using monomers in liquid or solution form. The polymerization reaction occurs when the monomer migrates into the galleries within the intercalated sheets of the silicate (Sabaa et al. 2020). In this type of reaction, the initiators such as curing agents or high temperature must be supplied before the swelling process to initiate the polymerization process. This method was first carried out by the Toyota research group in the production of clay/nylon-6 nanocomposites.

The advantages of in situ polymerization are that it can be used in the production of well-exfoliated nanocomposites and has been used in a wide range of polymeric systems (Yan et al. 2020). But processing through this method is time-consuming and some types of polymers need a solvent when synthesized through this method. These problems must be tackled successfully to make use of this method at a large-scale industrial level.

Alexandre et al. (2002) used this method in the synthesis of polyethylene/hectorite nanocomposites. They found that there was an increase of up to 259% in Young's modulus for an 11.4 wt% clay sample when compared to an unfilled sample. The exfoliation structure of layered silicates was confirmed by the XRD analysis and TEM observation. Imai et al. (2002) used in situ polymerization to prepare poly(ethylene terephthalate) (PET)-based polymer/layered silicate nanocomposites (PLSNs). The results showed that the intercalations of the PLSNs prepared by this method were poorly diffused. Compared to neat PET, the PLSNs displayed an 85% enhancement in their flexural modulus.

(ii)   *Solution-induced intercalation*

Although this process is somewhat like the in situ polymerization method, it differs in the use of polar solvents in the synthesis of intercalated polymer/clay nanocomposites. The swelling process of the organoclay is carried out using the polar solvents like chloroform, toluene, or water (Beyer 2002; Rai and Singh 2004). After that, a dissolved polymer is added to the solution that intercalates into the layers of the silicate galleries. Methods like vaporization under vacuum or precipitation are used to eliminate the solvent from the finished material.

The driving force of this method is the compensation of the decrease in the conformational entropy of the resultant intercalated polymer chain by desorption of the solvent molecules. On the positive side, polymers with low or no polarity can be synthesized using this method, but commercial production on a large scale is difficult because of the need for solvents that are expensive and the removal of those solvents from the finished products. Health and safety issues are also another negative aspect of this method.

Krishnamoorti et al. (2001) prepared polystyrene-polyisoprene block copolymer through solution mixing method and toluene that was used as a solvent could only be separated by extensive drying in a vacuum oven at 100 °C. X-ray diffraction analysis of the resultant PLSN structure showed it to be a mixture of intercalated and exfoliated silicate layers.

(iii)   *Melt processing*

Melt processing involves the mechanical blending of the molten polymer and the organoclay to enhance the interactions between them and then annealing the mixture at a temperature that is placed at or above the melting point of the polymer to form the intercalated nanocomposite (Beyer 2002).

The thrust of this method is in the significant enthalpic involvement between the organoclay and the polymer throughout the blending and the annealing processes. Although this method is not as highly efficient in the intercalation as the in situ process (shown by the presence of partially exfoliated layered structures in the finished product), it is useful in the production of nanocomposites at the industry level by the traditional polymer processing methods like extrusion, injection moulding, and so on. In fact, this technology serves to accelerate the commercial manufacture of clay/polymer nanocomposites (Gao 2004). The main positive aspects of the melt intercalation process over the in situ and the solution-induced methods are that it

does not involve environmentally harmful chemical solvents or reagents and quite compatible with the conventional extrusion or injection moulding methods, thus rendering it economical to the polymer industries as it reduces capital expenditure. Cho and Paul (2001) made a study of nylon-6 organoclay nanocomposites that they processed through direct melt compounding making use of a conventional twin-screw extruder. Their results proved that when the twin-screw extruder is used, there is a good exfoliated dispersion of the organoclay into the nylon-6 matrix but when a single-screw extruder is used for the preparation, there was poor exfoliation. Shakil et al. (2021) investigated the influence of the rotational screw speed on polypropylene-based organically modified silicate (montmorillonite). They employed a twin-screw extruder at three different speeds: 200, 500, and 1000 rpm. The authors found a proportional increase in intercalation and some increase in exfoliation to the increase in the screw speed.

Although more fabrication techniques are being developed such as solid intercalation, co-vulcanization, and the sol–gel method, these are still in the early stage and still to be widely accepted.

(g)   Properties of Polymer–Clay Nanocomposites

As compared to the conventional composite materials, nanocomposites are more advantageous due to their enhanced properties of mechanical, thermal, solvent resistance, and fire resistance. Because of this, a lot of research is being conducted in the creation of polymer–clay composites that utilize a variety of polymers. In this section, several studies on polymer nanocomposites are investigated from the available literature. These studies showed improvements in the mechanical, thermal, and barrier properties of polymer nanocomposites when small amounts (≤ 10 wt %) of nanoclay are added to them.

(i)   *Mechanical properties*

One of the most important advantages of using nanoclay platelet for reinforcement polymers is that nanoclay platelet has high aspect ratios, high modulus, high surface area, and high strengths which result in the enhancement of polymer mechanical properties when nanoclay is dispersed well into polymer system (Pavlidou and Papaspyrides 2008; Kiliaris and Papaspyrides 2010). In fact, the combination of well-dispersed nanoclay layers with good interfacial interactions between matrix and filler is the major reason for the superior properties of nanocomposites (Manfredi et al. 2008). The first major report in the improving of the mechanical properties of polymers/clay nanocomposites was done by Toyota researchers in 1990. They studied the properties of nylon-6 clay nanocomposites through in situ polymerization. It was reported that with the addition of only 4.7 wt% of exfoliated clay, the tensile strength, tensile modulus, flexural strength, and flexural modulus increased by 41%, 68%, 60%, and 124%, respectively, over neat polymer (Okada et al. 1990; Kojima et al. 1993).

Qi et al. (2006) studied the effect of different nanoclay additives on the mechanical properties of a series of clay/epoxy nanocomposites. In situ polymerization method was used to prepare the nanocomposites with four types of nanoclays, namely,

Table 1.7 Tensile properties of epoxy nanocomposites with different nanoclay loads and types (Qi et al. 2006)

Nanocomposites	Elastic modulus (GPa)	Ultimate failure strength (MPa)	Ultimate failure strains (%)
Neat DGEBA	2.71 ± 0.11	72.06 ± 1.37	4.21 ± 0.36
2%MMT-Na$^+$/DGEBA	2.79 ± 0.07	68.04 ± 4	3.83 ± 0.39
5%MMT-Na$^+$/DGEBA	2.92 ± 0.17	57.2 ± 2.22	2.9 ± 0.3
10%MMT-Na$^+$/DGEBA	3.44 ± 0.29	57.68 ± 3.69	2.61 ± 0.35
2%MMT-30B/DGEBA	3.11 ± 0.09	62.19 ± 2.56	2.94 ± 0.19
5%MMT-30B/DGEBA	3.10 ± 0.08	58.35 ± 5.87	2.6 ± 0.47
10%MMT-30B/DGEBA	3.12 ± 0.23	57.31 ± 6.97	2.4 ± 0.2
2%MMT-I.30E/DGEBA	2.68 ± 0.26	64.58 ± 6.56	4.02 ± 0.33
5%MMT-I.30E/DGEBA	2.82 ± 0.12	59.94 ± 9.01	2.67 ± 0.64
10%MMT-I.30E/DGEBA	3.04 ± 0.11	58.23 ± 4.39	2.51 ± 0.38
2%MMT-CPC/DGEBA	2.57 ± 0.15	49.03 ± 2.72	2.52 ± 0.21
5%MMT-CPC/DGEBA	2.79 ± 0.08	50.14 ± 2.80	2.51 ± 0.26

montmorillonite (MMT-Na$^+$), Cloisite 30B, Nanomer I.30E, and CPC. Table 1.7 summarizes the tensile properties.

It was found that an increase in nanoclay content led to an increase in the tensile modules. At the maximum addition of nanoclay 10%, the maximum improvement in the tensile modules of the nanocomposites was found to be 26.9% for MMT-Na+/epoxy, 15.1% for MMT-30B/epoxy, and 12.2% for MMT-I.30E/epoxy. The improved modulus was explained by the strong stiffening effect of the clay fillers which themselves have a higher modulus than epoxy. However, it was observed that the addition of nanoclay significantly reduced the failure strength and failure strain. This was explained by the poor dispersion of the nanoclay particles in the resin due to the increased viscosity of the system after adding nanoclay.

It was also reported that fracture toughness increased with increased nanoclay content as seen in Table 1.8. The addition of 10% nanoclay increased the fracture toughness by 58.3% for MMT-Na+/epoxy, 25% for MMT-30B/epoxy, and 41.6% for MMT-I.30E/epoxy. The reason for this increase in fracture toughness was due to the intercalation structure of the resulting nanocomposites.

It was concluded that poor mechanical properties could possibly be linked to the existed voids within the samples and formation of clay agglomerates due to the viscosity of the system and to the poor dispersion of nanoclay particles, respectively.

Kaynak et al. (2009) investigated the flexural strength and fracture toughness of nanoclay (Na-montmorillonite)-based epoxy nanocomposites. Nanocomposites were prepared via in situ intercalative polymerization. Three different chemical treatments were used to modify the nanoclay. The results showed significant improvements in flexural strength and fracture toughness with maximum value at 0.5% nanoclay load, after which the values decreased as the nanoclay content increased.

Table 1.8 Fracture toughness of nanocomposites as a function of clay content (Qi et al. 2006)

Epoxy	Nanoclay	Clay content (wt%)	Fracture toughness (K_{IC}) (MPa m$^{1/2}$)
DGEBA	–	0	0.60
DGEBA	MMT-Na$^+$	2	0.63
DGEBA	MMT-Na$^+$	5	0.91
DGEBA	MMT-Na$^+$	10	0.95
DGEBA	MMT-30B	2	0.71
DGEBA	MMT-30B	5	0.72
DGEBA	MMT-30B	10	0.75
DGEBA	MMT-I.30B	2	0.64
DGEBA	MMT-I.30B	5	0.92
DGEBA	MMT-I.30B	10	0.85
DGEBA	MMT-CPC	2	0.83
DGEBA	MMT-CPC	5	0.99

Ha et al. (2008) investigated the dependence of fracture toughness of surface-modified MMT/epoxy nanocomposite with various clay contents (0%wt, 2%wt, 4%wt, 6%wt, and 10%wt). The authors used a clay modified (3-aminopropyltriethoxysilane) to produce nanocomposites with well-dispersed nanoclay. The addition of nanoclay decreased the fracture toughness for all the samples. However, the sample with 6%wt of clay content showed better toughness. It was reported that this reduction was due to the presence of voids within nanocomposites as well as increased debonding between the nanoclay and polymer.

In another study, Ha and co-workers (2010b) investigated the effects of clay silane treatment on the fracture toughness of clay/epoxy nanocomposites. Unlike the previous study, it was reported that fracture toughness increased by 82% for nanocomposites with clay silane treatment over untreated clay/epoxy nanocomposites. This improvement in fracture behaviours was due to the excellent dispersion of the treated clay into epoxy matrix and enhancement in interfacial adhesive strength between resin and clay layers.

Le Pluart et al. (2005) reported an increase in fracture toughness by 50% when 10 wt% of nanoclay was added to the epoxy matrix. In similar study, Brunner et al. (2006) investigated the fracture toughness of modified nanoclay-based epoxy nanocomposites. The results showed that 10 wt% of nanoclay improved fracture toughness and energy release rate by 50% and 20%, respectively, over neat epoxy. Daud et al. (2009) investigated the effects of the addition of nanoclay on the mechanical properties of three-phase glass fibre-reinforced composites (GFRP) consisting of traditional woven glass fibre and polyamide-6 (PA6) matrix. Nanocomposites were prepared via melt mixing method. The authors found an increase up to 30% in both flexural strength and compressive strength for the GFRP sample with 5 wt% nanoclay.

Zainuddin et al. (2010) investigated the flexural properties of clay–epoxy nanocomposites. Nanocomposites were fabricated with 1–3 wt% loading of

montmorillonite-layered silicate via magnetic stirring mixing for 5 h. The results showed that mixed intercalation and exfoliation structure was achieved by a 2% wt load of nanoclay. Their results showed that the flexural strength and modulus could be increased to a maximum of up to 8.7% and 17.4%, respectively, for samples reinforced by only 2% wt of nanoclay over neat epoxy. The authors stated that the poor dispersion of nanoclay led to poor mechanical properties.

Manfredi et al. (2008) found that flexural strength, flexural modulus, and impact strength were increased by 20%, 29%, and 23%, respectively, for composites made with the addition of 5 wt% of nanoclay. Ratna and co-worker (2003) proved that the impact strength of nanocomposites was increased by about 57% with a clay content of 5% over neat polymer.

Yasmin et al. (2006) investigated the influence of nanoclay content on the mechanical properties of clay/epoxy nanocomposites. The team used shear mixing to fabricate nanocomposites with 1–10 wt% of nanoclay. The results showed that the addition of nanoclay significantly improved the elastic modulus of neat epoxy. It was also found that as the clay content increased, the elastic modulus also increased gradually for both types of clay (Nanomer I.28E and Cloisite 30B). Authors concluded that the improvement in mechanical properties was due to the better dispersion of the nanoparticles as well as effective interfacial adhesion.

(ii)   *Thermal properties*

One of the highly interesting properties of polymer-layered silicate nanocomposites is their increased thermal stability. Thermogravimetric analysis (TGA) is the general method used to study the thermal stability of polymeric materials. The mass lost by the polymer when it undergoes degradation at high temperatures is ascribed to the creation of volatile products and is considered as a function of temperature. Non-oxidative decomposition occurs when the material is heated under a flow of an inert gas like helium or nitrogen, while the use of air or oxygen allows analysis of oxidative decomposition reactions. It is seen that, as a rule, the integration of nanoclay in the polymer matrix was found to enhance the thermal stability of the samples, because the nanoclay platelets act as insulators to the heat as well as a barrier to the production of volatile products (Pavlidou and Papaspyrides 2008; Yeh et al. 2006). In the early 90 s, Toyota researchers reported a remarkable improvement in thermal and flammability properties in polymers on the addition of nanoclay. The Toyota team found that the heat distortion temperature of nylon-6 increased from 65 to 152 °C for nylon-6 nanoclay composites by the addition of only 4.7 wt% of nanoclay contents (Okada et al. 1990; Kojima et al. 1993). Later, several studies have reported similar improvements in thermal stability for nanocomposites prepared with various types of polymer matrices and nanoclay.

Phang and his team (2005) studied the thermal properties of PA12/organoclay nanocomposites. They reported a slight improvement in the thermal stability with additions of less than 2 wt% of nanoclay, while a significant enhancement was observed for nanocomposites with only 5 wt% nanoclay.

Wang et al. (2006) reported that the addition of nanoclay improved the thermal stability of nanocomposites by increasing the onset temperature of degradation

(T_{onset}) and the temperatures at maximum mass loss rate (T_{peak}). T_{onset} and T_{peak} of neat polymer increased by 22 and 23 °C, respectively, at a 3 wt% silicate loading. The authors indicated that the dispersion quality of organoclay and its content can influence the thermal properties.

In the same year, Yeh et al. (2006) investigated the thermal stability by TGA under nitrogen atmosphere of epoxy modified with different percentages (1, 3, 5, 7%) of MMT clay. The TGA curves showed that the decomposed temperature at weight loss 5 wt% (T_d) of epoxy increases gradually with increase of nanoclay content. By adding only 7 wt% of clay into epoxy system, T_d increased from 304 to 343 °C. This significant enhancement on thermal properties was attributed to the presence of silicate layers acting as barriers to reduce the permeability of volatile degradation products out of the polymer/clay nanocomposites samples.

Hwang et al. (2010) investigated the thermal properties of polybutylene terephthalate (PBT)/clay nanocomposites. Different amounts of nanoclay and two speeds of twin-screw extruders were used to prepare the nanocomposites. The results demonstrated that the presence of 0.5 and 1.0 wt% nanoclay slightly increased the temperature of thermal decomposition and the melting temperature of the nanocomposites samples over the neat PBT.

Despite the general improvement of thermal stability for nanocomposites, several studies reported decrease in the thermal stability for some cases of higher nanoclay loading. Paul et al. (2003) studied the thermal stability of poly (L-lactide) (PLA)-based nanocomposites. The authors reported that thermal stability increased with increased clay content, with the maximum thermal stability achieved by 5 wt% of nanoclay. However, a reduction in the thermal stability was observed for polymers filled with 10 wt% nanoclay.

This concurs with another study done by Valera-Zaragoza et al. (2006) where they investigated the thermal and flammability properties of ethylene vinyl acetate (EVA) copolymer/organoclay nanocomposites. It was reported that thermal stability increased as clay contents increased up to 6 wt% of nanoclay loading, then thermal stability decreased when nanoclay load increased to more than 6 wt%.

Another conforming conclusion was made by Araújo et al. (2009) in their study of polyamide 66 (PA66)/clay nanocomposites. The results demonstrated that the addition of nanoclay improved the thermal stability of nanocomposites over the neat PA66. The authors concluded that the thermal stability of the nanocomposites was influenced by the two opposing functions of the nanoclay in it. The first one is the barrier properties to the oxygen, which results in the improvement in the thermal stability. The other is the catalytic effect of the nanoclay in the degradation of the polymer, which decreases the resistance to degradation and resulting in reduction in thermal stability. At a low addition of nanoclay, the first effect is most likely to accrue. But when the load of clay increases, thermal stability of the nanocomposite decreases due to the increase in the dominance of the catalysing effect.

Another thermal property of polymers is the glass transition temperature (T_g). The effect of clay addition on T_g of the system has been widely investigated by many researchers, results have shown a variety of behaviours, depending on different

conditions. An increase in T_g has been observed by some of them, while others showed a reduction or no change.

Liu et al. (2005a) investigated the thermal properties of epoxy/clay nanocomposites made by either direct-mixing method (DMM) or a high-pressure mixing method (HPMM). Nanocomposites synthesized by both methods showed to be slightly decreasing in T_g as the clay contents increased. However, samples made by HPMM showed higher T_g than those made by DMM. The reduction in T_g could be explained by the fact that clay can change the network of the epoxy system by catalysing the homo-polymerization of the resin during the mixing stage.

Auad et al. (2007) studied the T_g of epoxy-phenolic clay nanocomposites. In general, it was found that T_g decreased with increasing nanoclay contents. This reduction in T_g was related to the effect of the cross-linking density on the interference between clay and matrix.

Ye et al. (2011) also used epoxy/HNT (halloysite nanotubes) to measure T_g. They found that the addition of HNT decreased T_g in nanocomposites. However, the presence of HNT improved their thermal stability. Addition of 1.6 wt% of HNT increased the maximum thermal of the nanocomposites from about 393 °C to 416 °C. In similar study, Nassar et al. (2021) investigated the T_g of epoxy filled HNT. Result showed that clay has no significant effect on the value of T_g.

Yasmin et al. (2006) studied the thermal behaviour of epoxy/clay nanocomposites. Nanocomposites with two types of nanoclay (Cloisite 30B and Nanomer I.28E) at different clay concentrations (1–10 wt %) were prepared by shear mixing. The results indicated that the T_g in nanocomposites decreased with increasing clay contents for both types of nanoclay. The authors argued that the drop in T_g may be related to various reasons such as clay aggregates, interphase regions, and adhesion problems at the clay–matrix interface at elevated temperatures.

Zainuddin et al. (2010) investigated the thermal properties of nanoclay–epoxy nanocomposites. The results showed an increase in T_g with increased clay content as seen in Table 1.9. T_g increased from 99 to 115 °C for nanocomposites with addition of only 2 wt% clay. The authors elucidated their results as the incorporation of nanoclay into epoxy led to increase in the cross-link density of the nanocomposites. This increase in cross-linking slowed down the segmental motion of the polymer chains which require higher temperatures to initiate segmental motion and resulted in increased T_g.

This explanation concurs with a previous study done by Yeh et al. (2006). They had reported an increase in both T_g and storage modulus for nanocomposites over

Table 1.9 Glass transition temperature (T_g) results of neat and 1–3 wt% epoxy nanocomposite (Zainuddin et al. 2010)

Sample	Glass transition temperature, T_g (°C)	% Change over neat
neat	99 ± 3.2	–
1 wt.%	105 ± 4.7	+6.06
2 wt.%	115 ± 2.5	+16.16
3 wt.%	110 ± 4.1	+11.11

neat epoxy as the clay concentration increased. The incorporation of 7 wt% nanoclay into the epoxy matrix enhanced its T_g by about 35% from 73.19 to 96.77 °C.

(iii)   *Water absorption and barrier properties*

Another highly interesting aspect revealed by polymer/clay nanocomposites is their excellent barrier properties. The integration of layered silicate usually increases the barrier properties of nanocomposites against oxygen, nitrogen, carbon dioxide, water vapour, gasoline and reduces the water uptake. This improvement of the barrier properties is attributed to the large aspect ratio of the nanoclay layers, which increases the tortuous path of the gas and water molecules that permeate into the material as they diffuse into the nanocomposite.

It was reported by the Toyota researchers in 1990 that the addition of nanoclay reduced the rate of water absorption of their polyamide-6 clay hybrid by about 40% over pure polymer (Liu et al. 2008). Later, they were followed by Messersmith and Giannelis in 1995 who observed a remarkable decrease of water permeability reach up to 80% with about 5 wt% of clay into poly (ε-caprolactone) matrix (Liu et al. 2008; Shahinur and Hasan 2020). After that, many researchers have carried out the water absorption and barrier properties of polymer/clay nanocomposites.

Becker et al. (2004) studied the water uptake of high-performance epoxy-layered silicate nanocomposites. It was found that the addition of nanoclay reduced the maximum water uptake for all nanocomposites compared to pure epoxy systems. However, the diffusion rate of water uptake was observed to be unaffected by the incorporation of nanoclay.

Liu et al. (2005b) investigated the water absorption of epoxy/clay nanocomposites. The results revealed significant reductions in both diffusivity and maximum water uptake for nanocomposites over neat epoxy. Water uptake and diffusivity decreased gradually with increasing nanoclay content as shown in Table 1.10.

Alexandre et al. (2009) studied the water barrier properties of polyamide-12/C30B nanocomposite. Their study demonstrated that water permeability and the diffusivity of nanocomposites decrease with increasing clay volume fraction up to 2.5% of clay content. However, with more increase in clay content barrier properties were reduced for both intercalated and exfoliated structures. In general, the exfoliated structure displayed better properties than the intercalated structure. The authors concluded that

Table 1.10 Maximum water uptakes (M_∞) and diffusion coefficients (D) of nanocomposites as function of nanoclay loading at 23 °C (Liu et al. 2005b)

Clay loading (phr)	M_∞ (%)	$D \times 10^{-8}$ (mm^2/s)
0	7.76	8.80
3	7.50	8.74
6	7.26	8.33
9	7.07	7.90
12	6.92	7.51
15	6.69	7.34

the water diffusion properties depend on several factors such as nanocomposite structures, polymer crystallinity, plasticization phenomenon, solubility, and free volume variations.

Other studies have focused on nanocomposite barrier properties against gases and vapours. Ke and Yongping (2005) investigated the O_2 permeability of film made by PET/clay nanocomposites with different clay contents varying from 1 to 3 wt%. Their results showed that the presence of clay dramatically reduced the permeability of O_2 for nanocomposites with maximum reduction reach of up to 50% at 3 wt% of nanoclay load over pure PET film.

Ogasawara et al. (2006) measured the helium gas permeability of epoxy/MMT nanocomposites. The authors reported that the incorporation of nanoclay improved the barrier properties of epoxy by reducing the helium gas permeability. It was also found that the gas diffusivity decreased as the clay contents increased.

Reddy et al. (2007) studied the oxygen permeation properties of low-density polyethylene (LDPE) nanocomposites prepared by melt intercalating method. Their results showed that oxygen permeation of LDPE system decreased after the addition of nanoclay. The authors reported that the exfoliation structure of clay dispersion was the reason for the good barrier properties. Such dispersion with high aspect ratio of clay layers can create more tortuous paths for the gas as it diffuses into the nanocomposite.

Zhang et al. (2010) investigated the gas permeability of a series of kaolin/natural rubber composites prepared by melt blending. It was found that the addition of nanoclay significantly decreased the nitrogen permeability with the increase in clay content. The authors explained that this improvement in barrier properties was due to two factors. Firstly, the high aspect ratio of the impenetrable nanoclay layers forced gas molecules to diffuse in a tortuous path. Secondly, the presence of the nanoclay increased the polymer crystallinity, which resulted in decrease of free volume for the penetrating gas molecules.

(h)   Halloysite/Epoxy Nanocomposites

In enhancing the thermal and mechanical properties of polymers, halloysite nanotubes (HNTs) as new types of additives have recently received much attention (Nassar et al. 2021; Tang et al. 2011; Prashantha et al. 2011). These are a type of naturally occurring aluminosilicate clays, chemically like kaolinite with chemical composition $(Al_2Si_2O_5(OH)_4\text{-}2H_2O)$. Halloysite is a 1:1 layered clay mineral, containing one alumina octahedron sheet and one silica tetrahedron sheet (Tang et al. 2011). HNTs have a structure of hollow nanotubular with a multi-layered wall structure like that of carbon nanotubes (CNTs) (Nassar et al. 2021; Tang et al. 2011; Prashantha et al. 2011). The length of HNTs ranges from 500 nm to 1.6 μm and the thickness is smaller than 100 nm (Ye et al. 2011; Hedicke-Höchstötter et al. 2009). The resemblance of HTNs to CNTs in aspect ratio resulting from their unique crystal structure lowered cost of HNTs as compared to CNTs, ability of HTNs to disperse easily in a polymer matrix and the fact that halloysites are rigid materials have resulted to halloysite nanotubes being considered as ideal materials in polymer

nanocomposites preparation (Nassar et al. 2021; Ye et al. 2011; Prashantha et al. 2011).

The use of HNTs in reinforcing epoxy matrices is still new in the field of polymer nanocomposites. Previous researchers have found that the mechanical performance of epoxy resins materials including toughness, modulus, and strength was increased through the addition of a small amount of halloysite particles without necessarily sacrificing other properties such as thermal stability and glass transition temperature (T_g). Ye et al. (2011) investigated the mechanical and thermal properties of HNTs/epoxy nanocomposites. It was reported an improvement in impact strength of halloysite–epoxy nanocomposites without sacrificing strength and thermal properties. Impact strength gradually increased with maximum enhancement of 400% at 2.3 wt% HNT load. Authors stated that massive micro-cracking, and particle breaking, bridging, and pull-out were responsible for the significant enhancement in impact toughness. It was also found that the incorporation of HNTs in epoxy matrix increased the thermal stability by increasing the maximum thermal decomposition temperature and char yield at 700 °C of nanocomposites.

Nassar et al. (2021) reported a great increase in impact and fracture toughness without a reduction in strength and thermal properties of HNT-epoxy composites. Results showed that fracture toughness and impact toughness increased as HNTs content increased. Maximum enhancement in fracture toughness (50%) and impact toughness (127%) was achieved at 10 wt% HNT load. The presence of HNTs increased the tensile strength of epoxy filled with HNTs when compared to unfilled counterparts.

In another study, Deng and co-workers (2009) reported an enhancement in facture toughness of halloysite tube–epoxy nanocomposites without sacrificing thermal properties after improving HNTs particles dispersion into epoxy matrix though chemical treatments and ball mill homogenization.

Tang et al. (2011) studied the mechanical properties of treated halloysite-reinforced epoxy nanocomposites. Intercalated structure was achieved due to the treatment by phenylphosphonic acid (PPA). It was reported that the fracture toughness of epoxy significantly increased by 78.3% due to the presence of 10 wt% of intercalated HNTs. This enhancement as authors claimed was due to the facture mechanism such as fibre (breakage, debonding, and pull-out), crack bridging, and plastic deformation. It was also found that tensile strength, tensile modulus, and glass transition temperatures (T_g) slightly increased after the addition of treated HNTs.

There have been other studies on using HNT as a modifier for other polymer matrixes. For example, Ismail et al. (2008) investigated the mechanical and thermal properties of halloysite nanotube-filled ethylene propylene diene monomer (EPDM) nanocomposites. Results showed that tensile strength and modulus increased dramatically as HNT content increased. Thermal stability and flammability properties also increased as a result of HNT addition. Authors reported that this enhancement in tensile and thermal properties was due to the well dispersion of HNTs inside EPDM matrix and to the formation of zig-zag structure by HNTs interaction. Pasbakhsh et al.

(2010) studied the tensile properties of a modified HNTs-reinforced ethylene propylene diene monomer (EPDM) nanocomposites. γ-methacryloxypropyl trimethoxysilane (MPS) was used to treat HNTs and improves their dispersion inside EPDM matrix. It was reported that samples filled with modified HNTs displayed better tensile strength and modulus than those filled with unmodified HNTs. SEM and TEM micrographs revealed that the dispersion of modified HNTs was better than unmodified HNTs due to the treatment by MPS. Hedicke-Höchstötter et al. (2009) investigated the tensile properties of HNT/polyamide-6 nanocomposites prepared by melt extrusion and an adjacent injection moulding method. Tensile strength and modulus were found to increase due to the presence of HNTs. However, authors compared between polyamide-6 reinforced with HNTs and same matrix reinforced with organically modified montmorillonite. Results showed that samples filled with organoclay exhibited higher tensile strength and modulus than those filled with HNTs. Prashantha et al. (2010) studied the effect of unmodified HNTs and quaternary ammonium salt-treated halloysite nanotubes (QM-HNTs) on the mechanical and thermal properties of HNT/polypropylene (PP) nanocomposites. Results indicated that tensile strength and modulus, flexural strength and modulus, impact strength, and glass transition temperature (T_g) increased due to the addition of HNTs. However, samples reinforced with modified HNTs showed better mechanical and thermal properties than those filled with unmodified HNTs. Authors explained that by the enhancement in matrix/particles interface and particles dispersion in the matrix due to the quaternary ammonium salt treatment.

(i)   *Silicon Carbide/Epoxy Nanocomposites*

Silicon carbide particles are very attractive ceramic material that can be used as filler in different polymer matrices due to the unique properties including high thermal conductivity, low thermal expansion coupled with high strength, high hardness, and high elastic modulus (Satapathy et al. 2009). Silicon carbide (SiC) is rigid crystalline material that is compound of silicon and carbon and has been used in grinding abrasive products including wheels for over a period of 100 years. Currently, the material has been developed to a point that it has very good mechanical properties as a high-quality grade ceramic used in numerous high-performance applications. Therefore, ceramic-filled polymer composites have been the subject of extensive research in the last two decades (Wetzel et al. 2006; Liao et al. 2011; Zhao and Li 2008; Rodgers et al. 2005). Rodgers et al. (2005) investigated SC-15 epoxy-based nanocomposites reinforced with three different loading (0.5, 1, and 1.5 wt%) of β-SiC nanoparticles, which were prepared by high-intensity ultrasonic liquid processor. Results showed that SiC dispersion was homogenous into epoxy system. In general, the presence of SiC particles into epoxy increased thermal and mechanical properties. The addition of only 1 wt% of SiC displayed better mechanical and thermal properties over neat epoxy and nanocomposites reinforced with 0.5 and 1.5 wt%. Tables 1.11 and 1.12 show thermal and mechanical properties of neat epoxy and epoxy/SiC nanocomposites. For example, the insertion of 1 wt% SiC increased T_g and flexural strength by 16% and 21.4%, respectively.

Table 1.11 Thermal properties of neat epoxy and epoxy/β-SiC nanocomposites (Rodgers et al. 2005)

Material	DSC glass transition temperature (T_g) (°C)	TGA decomposition temperature (°C)
SC-15 epoxy, neat	73	356
+0.5 wt% SiC	80	378
+1.0 wt% SiC	85	385
+1.5 wt% SiC	65	358

Table 1.12 Flexural properties of neat epoxy and epoxy/β-SiC nanocomposites (Rodgers et al. 2005)

Material	Flexural modulus (GPa)	Gain/loss in modulus (%)	Flexural strength (MPa)	Gain/loss in strength (%)
SC-15 epoxy, neat	2.45 ± 0.09		91.87 ± 5.13	
+0.5 wt% SiC	3.26 ± 0.21	33.06	111.73 ± 9.35	21.62
+1.0 wt% SiC	3.33 ± 0.21	35.92	111.53 ± 6.97	21.40
+1.5 wt% SiC	3.32 ± 0.10	35.51	95.86 ± 4.01	4.34

Wetzel et al. (2006) studied the mechanical properties of epoxy nanocomposites reinforced with either aluminium oxide (Al_2O_3) or titanium dioxide (TiO_2) nanoparticles. It was seen that both flexural modulus and strength increased as nano-fillers content increased. They also reported that fracture toughness increased significantly as nano-filler content increased. Interestingly, the addition of Al_2O_3 particles showed better mechanical properties than TiO_2. Authors concluded that several toughness mechanisms were responsible for the toughness enhancements.

Zhao et al. (2005), on the other hand, used nano-alumina particles to toughen epoxy resin. However, no improvement was reported in fracture toughness due to the addition of nano-alumina. Chen et al. (2008) investigated the mechanical properties of silica-epoxy nanocomposites. It was reported that the addition of only 10 wt% nano-silica increased fracture toughness and tensile modulus by 30% and 25%, respectively. Sinha Ray and Okamoto (2003) carried out the mechanical and thermal properties of TiO_2/epoxy nanocomposites prepared by ultrasonic mixing process. Authors reported homogenous dispersion for nanoparticles into the epoxy matrix with enhancement in thermal stability, glass transition temperature, tensile, and flexural modulus due to the presence of nano-silica particles. However, no improvement was reported in tensile and flexural strength. Ma et al. (2008) investigated the effect of silica nanoparticles on the mechanical property of two types of epoxy systems. It was found that the presence of nano-silica increased Young's modulus, tensile strength, fracture toughness, and critical energy release rate for both epoxy systems.

Liao et al. (2011) studied the mechanical properties of maleated high-density polyethylene (mPE) reinforced with SiC nanoparticles. Injection moulding method was used to prepare nanocomposites with four different SiC loading (2, 4, 6, and 8) wt%. Results showed that Young's modulus and yield strength increased for nanocomposites as SiC content increased. However, the addition of SiC particles decreased impact strength of mPE nanocomposites when compared to unfilled mPE. Authors reported that the absence of particle cavitation and matrix fibrillation was the reason of the reduction in impact strength of mPE/SiC nanocomposites.

(j)   Fibre-Reinforced Polymer Nanocomposites

The use of nanocomposites filled with nanoparticles (clays, silica, carbon nanotubes, silicon carbide, etc.) as a matrix for fibre-reinforced composites has been recently carried out by number of researchers (Auad et al. 2007; Bozkurt et al. 2007; Xu and Hoa 2008; Khan et al. 2011). Previously published research on the use of nanoclay matrix for fibre composites showed that the addition of nanoclay enhances the mechanical properties of fibre-reinforced epoxy composites (Mohan and Kanny 2011; Bozkurt et al. 2007; Xu and Hoa 2008; He et al. 2020; Faruk and Matuan 2008). For example, Bozkurt et al. (2007) investigated the effect of nanoclay dispersion on the mechanical properties of non-crimp glass fibre-reinforced epoxy nanocomposites. It was found that flexural properties increased with the addition of unmodified clay (MMT) and modified clay (OMMT), up to 6 wt% of clay loading due the enhancement in the interface between the glass fibre and epoxy matrix. Their results showed that samples filled with OMMT displayed better flexural strength and modulus than those filled with unmodified clay.

In a similar study, He et al. (2020) reported an improvement in flexural strength and modulus of glass fibre-reinforced epoxy/clay nanocomposites due to the addition of organo-treated nanoclay. The interface between the glass fibre and epoxy matrix was increased due to the presence of nanoclay.

Xu and Hoa (2008) investigated the mechanical properties of carbon fibre-reinforced epoxy/clay nanocomposites. An increase in fracture toughness and flexural strength after the addition of a small content of nanoclay was observed.

An interesting study on wood/clay/epoxy nanocomposites was obtained by Faruk and Matuan (2008). They investigated the effect of five different types of nanoclay on the mechanical properties of wood/epoxy composites. Two different methods (melt blending process and direct dry blending process) were used to fabricate wood/epoxy nanocomposites. Melt blending process involved using the clay-reinforced epoxy as a matrix for wood/epoxy nanocomposites while direct dry blending process involved adding the nanoclay directly into the wood/epoxy composites. Results are summarized in Tables 1.13 and 1.14. Table 1.13 shows the effect of nanoclay types on the mechanical properties of clay/epoxy nanocomposites made by melt blending method. The addition of nanoclay increased flexural properties and tensile properties of epoxy-based nanocomposites compared to unfilled epoxy composites. The addition of Cloisite 10A displayed better mechanical properties than other types of clay. This was attributed to the better intercalation of Cloisite 10A among other nanoclays.

Table 1.13 The effect of nanoclay types on mechanical properties of epoxy/clay nanocomposites (Faruk and Matuan 2008)

Types of nanoclay in HDPE matrix	Flexural properties		Tensile properties	
	Strength (MPa)	Modulus (MPa)	Strength (MPa)	Modulus (MPa)
None (control)	25.3 ± 1.4	667 ± 61	24.8 ± 0.3	1050 ± 16
Cloisite 10A	31.7 ± 1.8	947 ± 76	27.6 ± 1.1	1353 ± 50
Cloisite 15A	24.7 ± 0.8	693 ± 40	25.0 ± 0.5	1333 ± 36
Cloisite 20A	26.4 ± 0.5	757 ± 35	25.1 ± 0.3	1334 ± 24
Cloisite 25A	26.8 ± 0.6	759 ± 21	25.1 ± 0.1	1341 ± 23
Cloisite 30B	25.7 ± 0.3	744 ± 19	25.3 ± 0.2	1335 ± 10

Table 1.14 The effect of blending method on flexural properties of wood/Cloisite 10A/epoxy nanocomposites (Faruk and Matuan 2008)

Blending process	Flexural properties	
	Strength (MPa)	Modulus (MPa)
Control (no nanoclay)	28.9 ± 1.4	1919.7 ± 112
Direct dry blending (direct mix)	27.1 ± 1.4	2233.8 ± 144
Melt blending (HDPE/nanoclay as matrix)	33.5 ± 0.4	2726.9 ± 196

Table 1.14 shows the effect of mixing methods on the flexural properties of wood/Cloisite 10A/epoxy nanocomposites. As it can be seen, the addition of nanoclay by melt blending method increased flexural strength and modulus compared to unfilled wood/epoxy composites. However, using direct dry blending method led to reduction in flexural strength. Authors recommended using clay/epoxy as a matrix to wood/polymer nanocomposites to achieve better mechanical properties for wood/clay/polymer nanocomposites.

Mohan and Kanny (2011) investigated the water absorption behaviour of sisal fibre-reinforced epoxy/clay nanocomposites. Results indicated that the presence of nanoclay improved the water barrier properties by reducing water mass uptake of sisal fibre/epoxy nanocomposites. Water mass uptake decreased as clay content increased with maximum reduction occurred at 5 wt% nanoclay. Composites filled with 5 wt% nanoclay showed better barrier properties than those filled with 5 wt% microclay.

Ye et al. (2011) studied the effect of halloysite nanotubes (HNTs) on the mechanical and thermal properties of epoxy/carbon fibre (CF) composites. It was reported that the addition of HNTs generally increased flexural strength, flexural modulus, impact strength, and glass transmission temperature (T_g) of CF/epoxy nanocomposites compared to unfilled CF/epoxy composites. Adding only 2 wt% of HNTs increased impact strength by 25% compared to unfilled CF/epoxy composites. Their results showed that the combination of HNT/CF/epoxy displayed the best impact properties among other composites. This enhancement in impact strength

was attributed to the toughness mechanisms due to the addition of HNTs as rigid particles as well as due to the presence of carbon fibres.

Satapathy et al. (2009) added nano-silicon carbide (SiC) to jute fibre-reinforced epoxy composites and investigated the physical and mechanical properties of the resulted composites. In their studied, they prepared two different types of composites. The first type was about epoxy reinforced with three different loading of jute fibre (20, 30, and 40) wt%. The second type was about epoxy/40 wt% jute fibre composites filled with either 10 wt% SiC or 20 wt% SiC. Results showed that volume fraction of voids increased slightly due to the presence of jute fibre. However, voids significantly increased in composites after the addition of SiC. Tensile and flexural strength of unfilled composites increased as jute fibre content increased. However, the addition of SiC into composites led to a reduction in both tensile and flexural strength. Authors claimed that the incorporation of SiC particles could reduce the stress transfer at the matrix/fibres interface which resulted in low tensile strength.

References

Alamri H, Low IM (2012) Microstructural, mechanical and thermal characteristics of recycled cellulose fiber-halloysite-epoxy hybrid nanocomposites. Polym Compos 33:589–600

Albano C, González J, Ichazo M et al (1999) Thermal stability of blends of polyolefins and sisal fiber. Polym Degrad Stab 66(2):179–190

Alexandre M, Dubois P, Sun T et al (2002) Polyethylene-layered silicate nanocomposites prepared by the polymerization-filling technique: synthesis and mechanical properties. Polymer 43(8):2123–2132

Alexandre B, Langevin D, Médéric P et al (2009) Water barrier properties of polyamide 12/montmorillonite nanocomposite membranes: Structure and volume fraction effects. J Membr Sci 328(1–2):186–204

AL-Oqla FM, Omari MA (2017) Sustainable biocomposites: challenges, potential and barriers for development. In: Jawaid M, Sapuan S, Alothman O (eds) Green biocomposites. Green energy and technology. Springer, Cham. https://doi.org/10.1007/978-3-319-46610-1_2

Anuar H, Zuraida A (2011) Improvement in mechanical properties of reinforced thermoplastic elastomer composite with kenaf bast fibre. Composites B 42:462–465

Araújo EM, Araujo KD, Paz RA et al (2009) Polyamide 66/Brazilian clay nanocomposites. J Nanomater 136856

Athijayamani A, Thiruchitrambalam M, Natarajan U et al (2009) Effect of moisture absorption on the mechanical properties of randomly oriented natural fibers/polyester hybrid composite. Mater Sci Eng A 517(1–2):344–353

Auad ML, Nutt SR, Pettarin V et al (2007) Synthesis and properties of epoxy-phenolic clay nanocomposites. eXPRESS Polym Lett 1(9):629–639

Bachtiar D, Sapuan SM, Hamdan MM (2008) The effect of alkaline treatment on tensile properties of sugar palm fibre reinforced epoxy composites. Mater Des 29(7):1285–1290

Bader MG (2001) Polymer composites in 2000: structure, performance, cost and compromise. J Microsc 201(2):110–121

Baroulaki I, Karakasi O, Pappa G et al (2006) Preparation and study of plastic compounds containing polyolefins and post used newspaper fibers. Composites A 37(10):1613–1625

Becker O, Varley RJ, Simon GP (2004) Thermal stability and water uptake of high performance epoxy layered silicate nanocomposites. Eur Polymer J 40(1):187–195

Benallel A, Tilioua A, Ettakni M et al (2021) Design and thermophysical characterization of new thermal insulation panels based on cardboard waste and vegetable fibers. Sustain Energy Technol Assess 48:101639

Beyer G (2002) Nanocomposites: a new class of flame retardants for polymers. Plast Addit Compd 4(10):22–28

Bismarck A, Mishra S, Lampke T (2005) Plant fibers as reinforcement for green composites. In: Mohanty AK, Misra M, Drzal LT (eds) Natural fibers, biopolymers, and biocomposites. CRC Press, Boca Raton, FL, pp 37–108

Bledzki AK, Gassan J (1999) Composites reinforced with cellulose based fibres. Prog Polym Sci 24(2):221–274

Bozkurt E, Kaya E, Tanoğlu M (2007) Mechanical and thermal behavior of non-crimp glass fiber reinforced layered clay/epoxy nanocomposites. Compos Sci Technol 67(15–16):3394–3403

Brunner A, Necola A, Rees M et al (2006) The influence of silicate-based nano-filler on the fracture toughness of epoxy resin. Eng Fract Mech 73(16):2336–2345

Buehler FU, Seferis JC (2000) Effect of reinforcement and solvent content on moisture absorption in epoxy composite materials. Composites A 31(7):741–748

Chatterjee A, Islam MS (2008) Fabrication and characterization of TiO_2–epoxy nanocomposite. Mater Sci Eng A 487(1–2):574–585

Chen B, Evans JRG (2006) Elastic moduli of clay platelets. Scripta Mater 54:1581–1585

Chen C, Justice RS, Schaefer DW et al (2008) Highly dispersed nanosilica–epoxy resins with enhanced mechanical properties. Polymer 49(17):3805–3815

Chen H, Miao M, Ding X (2009) Influence of moisture absorption on the interfacial strength of bamboo/vinyl ester composites. Composites A 40:2013–2019

Cheung HY, Ho MP, Lau KT et al (2009) Natural fibre-reinforced composites for bioengineering and environmental engineering. Composites B 40(7):655–663

Cho JW, Paul DR (2001) Nylon 6 nanocomposites by melt compounding. Polymer 42(3):1083–1094

Choudalakis G, Gotsis AD (2009) Permeability of polymer/clay nanocomposites: a review. Eur Polymer J 45(4):967–984

Daud W, Bersee HEN, Picken SJ et al (2009) Layered silicates nanocomposite matrix for improved fiber reinforced composites properties. Compos Sci Technol 69(14):2285–2292

Davtyan SP, Berlin A, Agabekov V et al (2012) Synthesis, properties, and applications of polymeric nanocomposites. J Nanomater 2012:215094

De Rosa IM, Santulli C, Sarasini F (2010) Mechanical and thermal characterization of epoxy composites reinforced with random and quasi-unidirectional untreated Phormium tenax leaf fibers. Mater Des 31(5):2397–2405

Deng S, Zhang J, Ye L (2009) Halloysite–epoxy nanocomposites with improved particle dispersion through ball mill homogenisation and chemical treatments. Compos Sci Technol 69(14):2497–2505

Doan T, Brodowsky H, Mader E (2007) Jute fibre/polypropylene composites II. Thermal, hydrothermal and dynamic mechanical behaviour. Compos Sci Technol 67:2707–2714

Faruk O, Matuan LM (2008) Nanoclay reinforced HDPE as a matrix for wood-plastic composites. Compos Sci Technol 68(9):2073–2077

Ford ENJ, Mendon SK, Rawlins JW et al (2010) X-ray diffraction of cotton treated with neutralized vegetable oil-based macromolecular crosslinkers. J Eng Fibres Fabrics 5(1):10–20

Fraga AN, Frullloni E, de la Osa O et al (2006) Relationship between water absorption and dielectric behaviour of natural fibre composite materials. Polym Testing 25(2):181–187

Gao F (2004) Clay/polymer composites: the story. Mater Today 7(11):50–55

Gowda TGY, Sanjay MR, Jyotishkumar P et al (2019) Natural fibers as sustainable and renewable resource for development of eco-friendly composites: a comprehensive review. Front Mater 6:226

Guo Z, Liang X, Pereira T et al (2007) CuO nanoparticle filled vinyl-ester resin nanocomposites: fabrication, characterization and property analysis. Compos Sci Technol 67:2036–2044

Ha SR, Rhee KY, Kim HC et al (2008) Fracture performance of clay/epoxy nanocomposites with clay surface-modified using 3-aminopropyltriethoxysilane. Colloids Surf A 313–314:112–115

Ha SR, Rhee KY, Park SJ et al (2010a) Temperature effects on the fracture behavior and tensile properties of silane-treated clay/epoxy nanocomposites. Compos B Eng 41(8):602–607

Ha SR, Rhee KY, Park SJ et al (2010b) Temperature effects on the fracture behavior and tensile properties of silane-treated clay/epoxy nanocomposites. Composites B 41(8):602–607

Haghighat M, Zadhoush A, Khorasani SN (2005) Physicomechanical properties of α-cellulose–filled styrene–butadiene rubber composites. J Appl Polym Sci 96(6):2203–2211

Han SO, Drzal LT (2003) Water absorption effects on hydrophilic polymer matrix of carboxyl functionalized glucose resin and epoxy resin. Eur Polymer J 39(9):1791–1799

Harish S, Michael DP, Bensely A et al (2009) Mechanical property evaluation of natural fiber coir composite. Mater Charact 60(1):44–49

He W, Song P, Yu B et al (2020) Flame retardant polymeric nanocomposites through the combination of nanomaterials and conventional flame retardants. Prog Mater Sci 114:1006687

Hedicke-Höchstötter K, Lim GT, Altstädt V (2009) Novel polyamide nanocomposites based on silicate nanotubes of the mineral halloysite. Compos Sci Technol 69(3–4):330–334

Herrera-Franco PJ, Valadez-González A (2005) A study of the mechanical properties of short natural-fiber reinforced composites. Composites B 36:597–608

Hodzic A, Shanks R (2014) Natural fiber composites: materials, processes and properties, 1st edn. Woodhead Publishing

Holbery J, Houston D (2006) Natural-fiber-reinforced polymer composites in automotive applications. JOM 58(11):80–86

Hughes M, Hill CAS, Hague JRB (2002) The fracture toughness of bast fibre reinforced polyester composites. Part 1 evaluation and analysis. J Mater Sci 37(21):4669–4676

Hwang SS, Liu SP, Hsu PP et al (2010) Effect of organoclay on the mechanical-thermal properties of microcellular injection molded PBT–clay nanocomposites. Int Commun Heat Mass Transfer 37(8):1036–1043

Imai Y, Nishimura S, Abe E et al (2002) High-modulus poly(ethylene terephthalate)/expandable fluorine mica nanocomposites with a novel reactive compatibilizer. Chem Mater 14(2):477–479

Ismail H, Pasbakhsh P, Fauzi MNA et al (2008) Morphological, thermal and tensile properties of halloysite nanotubes filled ethylene propylene diene monomer (EPDM) nanocomposites. Polym Test 27(7):841–850

John MJ, Anandjiwala RD, Thomas S (2009) Lignocellulosic fiber reinforced rubber composites. In: Thomas S, Pothan LA (eds) Natural fibre reinforced polymer composites: macro to nanoscale. Old City Publishing, Philadelphia, pp 252–269

John MJ, Thomas S (2008) Biofibres and biocomposites. Carbohyd Polym 71(3):343–364

Kaynak C, Nakas GI, Isitman NA (2009) Mechanical properties, flammability and char morphology of epoxy resin/montmorillonite nanocomposites. Appl Clay Sci 46(3):319–324

Ke Z, Yongping B (2005) Improve the gas barrier property of PET film with montmorillonite by in situ interlayer polymerization. Mater Lett 59(27):3348–3351

Khan SU, Iqbal K, Munir A et al (2011) Quasi-static and impact fracture behaviors of CFRPs with nanoclay-filled epoxy matrix. Composites A 42:253–264

Kiliaris P, Papaspyrides CD (2010) Polymer/layered silicate (clay) nanocomposites: an overview of flame retardancy. Prog Polym Sci 35(7):902–958

Kim HJ, Seo DW (2006) Effect of water absorption fatigue on mechanical properties of sisal textile-reinforced composites. Int J Fatigue 28:1307–1314

Kim JK, Hu C, Woo RSC et al (2005) Moisture barrier characteristics of organoclay–epoxy nanocomposites. Compos Sci Technol 65(5):805–813

Kojima Y, Usuki A, Kawasami M et al (1993) Mechanical properties of nylon 6-clay hybrid. J Mater Res 8:1185

Krishnamoorti R, Yurekli K (2001) Rheology of polymer layered silicate nanocomposites. Curr Opin Colloid Interface Sci 6(5–6):464–470

Krishnamoorti R, Ren J, Silva AS (2001) Shear response of layered silicate nanocomposites. J Chem Phys 114(11):4968–4973

Ku H, Chan WL, Trada M et al (2007) An evaluation of fracture toughness of vinyl ester composites cured under microwave conditions. J Mater Eng Perform 16:741–745

Le Pluart L, Duchet J, Sautereau H (2005) Epoxy/montmorillonite nanocomposites: influence of organophilic treatment on reactivity, morphology and fracture properties. Polymer 46:12267–12278

Liao CZ, Bao SP, Tjong SC (2011) Effect of silicon carbide nanoparticle additions on microstructure and mechanical behavior of maleic anhydride compatibilized high density polyethylene composites. Compos Interfaces 18(2):107–120

Liu Q, Hughes M (2008) The fracture behaviour and toughness of woven flax fibre reinforced epoxy composites. Compos A Appl Sci Manuf 39(10):1644–1652

Liu W, Hoa SV, Pugh M (2005a) Organoclay-modified high performance epoxy nanocomposites. Compos Sci Technol 65(2):307–316

Liu W, Hoa SV, Pugh M (2005b) Fracture toughness and water uptake of high-performance epoxy/nanoclay nanocomposites. Compos Sci Technol 65(15–16):2364–2373

Liu W, Hoa SV, Pugh M (2008) Water uptake of epoxy–clay nanocomposites: model development. Compos Sci Technol 68(1):156–163

Lotfi A, Li H, Dao DV et al (2019) Natural fiber–reinforced composites: a review on material, manufacturing, and machinability. J Thermoplast Compos Mater 34(2):238–284

Low IM, Somers J, Kho HS et al (2009) Fabrication and properties of recycled cellulose fibre-reinforced epoxy composites. Compos Interfaces 16:659–669

Lu C, Mai YW (2005) Influence of aspect ratio on barrier properties of polymer-clay nanocomposites. Phys Rev Lett 95:088303

Ma J, Mo MS, Du XS et al (2008) Effect of inorganic nanoparticles on mechanical property, fracture toughness and toughening mechanism of two epoxy systems. Polymer 49(16):3510–3523

Maleque MA, Belal FY, Sapuan SM (2007) Mechanical properties study of pseudo-stem banana fiber reinforced epoxy composite. Arabian J Sci Eng 32(2B):359–364

Mallick PK (2007) Fiber-reinforced composites: materials, manufacturing, and design, 3rd edn. CRC Taylor & Francis, Boca Raton, FL

Manfredi LB, De Santis H, Vázquez A (2008) Influence of the addition of montmorillonite to the matrix of unidirectional glass fibre/epoxy composites on their mechanical and water absorption properties. Composites A 39(11):1726–1731

Marsh G (2003) Next step for automotive materials. Mater Today 6(4):36–43

Marsh G (2007) Vinyl ester: the midway boat building resin. Reinf Plast 51:20–23

Masirek R, Kulinski Z, Chionna D et al (2007) Composites of poly(L-lactide) with hemp fibers: morphology and thermal and mechanical properties. J Appl Polym Sci 105(1):255–268

Mittal A, Katahira R, Himmel ME et al (2011) Effects of alkaline or liquidammonia treatment on crystalline cellulose: changes in crystalline structure and effects on enzymatic digestibility. Biotechnol Biofuels 4:41–57

Moeini MH, Heidary SH, Amiri I et al (2009) Wood: polyvinyl chloride composite for insulation of electrical wires: fabrication and investigation of properties. J Reinf Plast Compos 29(6):899–908

Mohan TP, Kanny K (2011) Water barrier properties of nanoclay filled sisal fibre reinforced epoxy composites. Compos A Appl Sci Manuf 42(4):385–393

Mohanty AK, Misra M, Drzal LT et al (2005) Natural fibers, biopolymers, and biocomposites: an introduction. In: Mohanty AK, Misra M, Drzal LT (eds) Natural fibers, biopolymers, and biocomposites. CRC Press, Boca Raton, FL, pp 1–30

Monteiro S, Lopes F, Ferreira A et al (2009) Natural-fiber polymer-matrix composites: cheaper, tougher, and environmentally friendly. JOM 61:17–22

Nassar MMA, Alzebdeh KI, Pervez T et al (2021) Progress and challenges in sustainability, compatibility, and production of eco-composites: a state-of-art review. J Appl Polym Sci 138:e51284. https://doi.org/10.1002/app.51284

Ogasawara T, Ishida Y, Ishikawa T et al (2006) Helium gas permeability of montmorillonite/epoxy nanocomposites. Composites A 37(12):2236–2240

Okada A, Kawasumi M, Usuki A et al (1990) Nylon 6-clay hybrid. Mater Res Soc Proc 171:45–50

Okamoto M (2006) Recent advances in polymer/layered silicate nanocomposites: an overview from science to technology. Mater Sci Technol 22:756–779

Pasbakhsh P, Ismail H, Fauzi MNA et al (2010) EPDM/modified halloysite nanocomposites. Appl Clay Sci 48(3):405–413

Paul MA, Alexandre M, Degée P et al (2003) New nanocomposite materials based on plasticized poly(L-lactide) and organo-modified montmorillonites: thermal and morphological study. Polymer 44:443–450

Paul DR, Robeson LM (2008) Polymer nanotechnology: nanocomposites. Polymer 49:3187–3204

Pavlidou S, Papaspyrides CD (2008) A review on polymer–layered silicate nanocomposites. Prog Polym Sci 33(12):1119–1198

Phang IY, Liu T, Mohamed A et al (2005) Morphology, thermal and mechanical properties of nylon 12/organoclay nanocomposites prepared by melt compounding. Polym Int 54(2):456–464

Prashantha K, Lacrampe MF, Krawczak P (2011) Processing and characterization of halloysite nanotubes filled polypropylene nanocomposites based on a masterbatch route: effect of halloysites treatment on structural and mechanical properties. eXPRESS Polym Lett 5(4):295–307

Qi B, Zhang QX, Bannister M et al (2006) Investigation of the mechanical properties of DGEBA-based epoxy resin with nanoclay additives. Compos Struct 75(1–4):514–519

Rai US, Singh RK (2004) Synthesis and mechanical characterization of polymer-matrix composites containing calcium carbonate/white cement filler. Mater Lett 58(1–2):235–240

Rashdi A, Sapuan S, Ahmad M et al (2009) Water absorption and tensile properties of soil buried kenaf fibre reinforced unsaturated polyester composites (KFRUPC). J Food Agric Environ 7(3–4):908–911

Ratna D, Manoj NR, Varley R et al (2003) Clay-reinforced epoxy nanocomposites. Polym Int 52(9):1403–1407

Reddy M, Gupta R, Bhattacharya S et al (2007) Structure-property relationship of melt intercalated maleated polyethylene nanocomposites. Korea-Australia Rheol J 19(3):133–139

Riedel U, Nickel J (2005) Applications of natural fiber composites for constructive parts in aerospace, automobiles, and other areas. In: Biopolymers online, Wiley-VCH Verlag GmbH & Co. KGaA

Rodgers RM, Mahfuz H, Rangari VK et al (2005) Infusion of SiC nanoparticles into SC-15 epoxy: an investigation of thermal and mechanical response. Macromol Mater Eng 290(5):423–429

Rong M (2001) The effect of fiber treatment on the mechanical properties of unidirectional sisal-reinforced epoxy composites. Compos Sci Technol 61(10):1437–1447

Rösler J, Harders H, Bäker M (2007) Mechanical behaviour of engineering materials metals, ceramics, polymers, and composites. Springer, Berlin Heidelberg

Saari P, Heikkilä H, Hurme M (2010) Adsorption equilibria of arabinose, fructose, galactose, glucose, mannose, rhamnose, sucrose, and xylose on ion-exchange resins. J Chem Eng Data 55(9):3462–3467

Sabaa MW, Abdelhakim M, Soliman SMA (2020) Characterization and application of cured epoxy resin reinforced with montmorillonite. Bull Mater Sci 43:126

Sanadi AR, Young RA, Clemons C et al (1994) Recycled newspaper fibers as reinforcing fillers in thermoplastics: part I—analysis of tensile and impact properties in polypropylene. J Reinf Plast Compos 13(1):54–67

Satapathy A, Alok Kumar J, Mantry S et al (2009) Processing and characterization of jute-epoxy composites reinforced with Sic derived from rice husk. J Reinf Plast Compos 29(18):2869–2878

Sgriccia N, Hawley MC, Misra M (2008) Characterization of natural fiber surfaces and natural fiber composites. Compos A Appl Sci Manuf 39:1632–1637

Shahinur S, Hasan M (2020) Jute/coir/banana fiber reinforced bio-composites: critical review of design, fabrication, properties and applications. In: Hashmi S, Choudhury IA (eds) Encyclopedia of renewable and sustainable materials, Elsevier, pp 751–756

Shakil UA, Abu Hassan S, Yahya MY et al (2021) A review of properties and fabrication techniques of fiber reinforced polymer nanocomposites subjected to simulated accidental ballistic impact. Thin-Walled Struct 158:107150

Sinha SR, Okamoto M (2003) Polymer/layered silicate nanocomposites: a review from preparation to processing. Prog Polym Sci 28:1539–1641

Sinha Ray S, Okamoto M (2003) Polymer/layered silicate nanocomposites: a review from preparation to processing. Prog Polym Sci 28(11):1539–1641

Sreenivasan VS, Ravindran D, Manikandan V et al (2011) Mechanical properties of randomly oriented short Sansevieria cylindrica fibre/polyester composites. Mater Des 32:2444–2455

Stamboulis A, Baillie CA, Peijs T (2001) Effects of environmental conditions on mechanical and physical properties of flax fibers. Composites A 32(8):1105–1115

Sultania M, Yadaw SB, Rai JSP et al (2010) Laminates based on vinyl ester resin and glass fabric: a study on the thermal, mechanical and morphological characteristics. Mater Sci Eng A 527:4560–4570

Taj S, Munawar MA, Khan S (2007) Review natural fiber-reinforced polymer composites. Proc Pakistan Acad Sci 44(2):129–144

Tang Y, Deng S, Ye L et al (2011) Effects of unfolded and intercalated halloysites on mechanical properties of halloysite–epoxy nanocomposites. Compos A Appl Sci Manuf 42(4):345–354

Tejyan S (2021) Effect of erosive parameters on solid particle erosion of cotton fiber–based nonwoven mat/wooden dust reinforced hybrid polymer composites. J Ind Text. https://doi.org/10.1177/15280837211064241

Valera-Zaragoza M, Ramírez-Vargas E, Medellín-Rodríguez FJ et al (2006) Thermal stability and flammability properties of heterophasic PP–EP/EVA/organoclay nanocomposites. Polym Degrad Stab 91(6):1319–1325

Venkateshwaran N, Elayaperumal A, Alavudeen A et al (2011) Mechanical and water absorption behaviour of banana/sisal reinforced hybrid composites. Mater Des 32:4017–4021

Wada M, Heux L, Sugiyama J (2004) Polymorphism of cellulose I family: reinvestigation of cellulose IVI. Biomacromol 5:1385–1391

Wambua P, Ivens J, Verpoest I (2003) Natural fibres: can they replace glass in fibre reinforced plastics? Compos Sci Technol 63(9):1259–1264

Wang Y, Gao J, Ma Y et al (2006) Study on mechanical properties, thermal stability and crystallization behavior of PET/MMT nanocomposites. Composites B 37(6):399–407

Wang B, Panigrahi S, Tabil L et al (2007a) Pre-treatment of flax fibers for use in rotationally molded biocomposites. J Reinf Plast Compos 26(5):447–463

Wang B, Panigrahi S, Tabil L et al (2007b) Pre-treatment of flax fibres for use in rotationally molded biocomposites. J Reinf Plast Compos 26(5):447–463

Wetzel B, Rosso P, Haupert F et al (2006) Epoxy nanocomposites—fracture and toughening mechanisms. Eng Fract Mech 73(16):2375–2398

Wu Y, Liang Y, Mei C et al (2022) Advanced nanocellulose-based gas barrier materials: present status and prospects. Chemosphere 286:131891

Wypych F, Satyanarayana KG (2005) Functionalization of single layers and nanofibers: a new strategy to produce polymer nanocomposites with optimized properties. J Colloid Interface Sci 285(2):532–543

Xu Y, Hoa SV (2008) Mechanical properties of carbon fiber reinforced epoxy/clay nanocomposites. Compos Sci Technol 68(3–4):854–861

Yan L, Xu Z, Jia H et al (2020) Combination effect of organically modified montmorillonite and nano-silica on reducing the fire hazards of intumescent flame-retarded epoxy resins. J Vinyl Add Tech 26(4):490–501

Yasmin A, Luo JJ, Abot JL et al (2006) Mechanical and thermal behavior of clay/epoxy nanocomposites. Compos Sci Technol 66(14):2415–2422

Ye Y, Chen H, Wu J et al (2007) High impact strength epoxy nanocomposites with natural nanotubes. Polymer 48(21):6426–6433

Ye Y, Chen H, Wu J et al (2011) Evaluation on the thermal and mechanical properties of HNT-toughened epoxy/carbon fibre composites. Composites B 42(8):2145–2150

Yeh JM, Huang HY, Chen CL et al (2006) Siloxane-modified epoxy resin–clay nanocomposite coatings with advanced anticorrosive properties prepared by a solution dispersion approach. Surf Coat Technol 200(8):2753–2763

Yong V, Hahn HT (2004) Processing and properties of SiC/vinyl ester nanocomposites. Nanotechnology 15:1338–1343

Yong V, Hahn HT (2009) Monodisperse SiC/vinyl ester nanocomposites: dispersant formulation, synthesis, and characterization. J Mater Res 24(4):1553–1558

Zainuddin S, Hosur MV, Zhou Y et al (2010) Experimental and numerical investigations on flexural and thermal properties of nanoclay–epoxy nanocomposites. Mater Sci Eng A 527(29–30):7920–7926

Zaman HU, Khan MA, Khan RA (2011) A comparative study on the mechanical and degradation properties of plant fibers reinforced polyethylene composites. Polym Compos 32(10):1552–1560

Zanetti M, Costa L (2004) Preparation and combustion behaviour of polymer/layered silicate nanocomposites based upon PE and EVA. Polymer 45(13):4367–4373

Zhang Y, Liu Q, Zhang Q et al (2010) Gas barrier properties of natural rubber/kaolin composites prepared by melt blending. Appl Clay Sci 50(2):255–259

Zhao H, Li RKY (2008) Effect of water absorption on the mechanical and dielectric properties of nano-alumina filled epoxy nanocomposites. Compos A Appl Sci Manuf 39(4):602–611

Zhao C, Qin H, Gong F et al (2005) Mechanical, thermal and flammability properties of polyethylene/clay nanocomposites. Polym Degrad Stab 87:183–189

Zhao S, Schadler L, Hillborg H et al (2008) Improvements and mechanisms of fracture and fatigue properties of well-dispersed alumina/epoxy nanocomposites. Compos Sci Technol 68(14):2976–2982

Chapter 2
Processing and Testing of Ecocomposites: Materials and Methodology

Check for updates

Abstract The materials and methodologies used to fabricate and characterize the cellulose-fibre-reinforced epoxy and vinyl-ester ecocomposites are described in this chapter. The characteristics of cellulose-fibre sheets and nano-fillers (i.e. nanoclay platelets, halloysite nanotubes, and nano-silicon carbide) used for the fabrication of ecocomposites are described. The structure and properties of these composites were investigated using a wide range of techniques which include wide-angle X-ray scattering (WAXS), synchrotron radiation diffraction (SRD), Fourier transforms infrared spectroscopy (FTIR), transmission electron microscopy (TEM), scanning electron microscopy (SEM), and thermo-gravimetric analysis (TGA). Methodologies for evaluating flexural strength, flexural modulus, impact strength, fracture toughness, impact toughness, and water absorption are also described.

Keywords Cellulose fibres · Nanoclay platelets · Epoxy resin · Vinyl-ester resin · Water uptake · Diffusion · SEM · TEM · SRD · XRD · TGA · FTIR · Aspect ratio · Microstructure · Mechanical properties · Flexural strength · Impact strength · Fracture toughness · Impact toughness

2.1 Epoxy Ecocomposites

(a) Cellulose-Fibre-Reinforced Epoxy Ecocomposites

Recycled cellulose fibre (RCF)/epoxy samples were prepared by initially pre-drying the paper sheets for 60 min at 70 °C, and then fully soaked into the epoxy system until they became entirely wetted by the resin. After that, the epoxy soaked RCF sheets were carefully laid down in a closed silicone mould under 8.2 kPa compressive pressure and left 24 h for curing at room temperature as seen in Fig. 2.1. CF/epoxy composites were fabricated with different weight percentage of fibres (10, 20, 30, and 40) wt% to investigate the effect of fibre weight percentage on the physical and mechanical properties of the resulted composites.

(b) Epoxy-Based Nanocomposites

Nanoparticles including nanoclay (30B), halloysite nanotubes (HNTs), and nano-sized SiC (n-SiC) were first dried for 60 min at 70 °C before they mixed individually
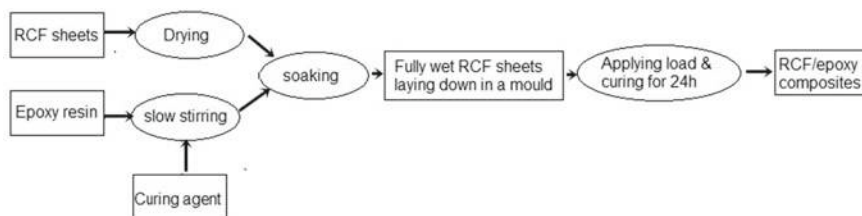
Fig. 2.1 Schematic illustration of the fabrication of RCF/epoxy composites
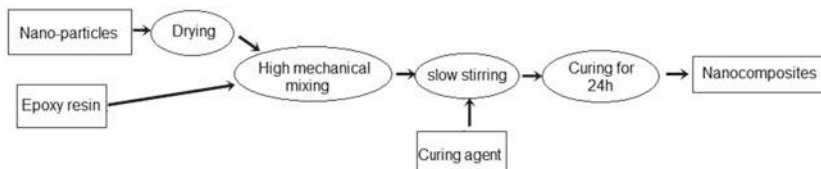

Fig. 2.2 Schematic illustration of the fabrication of epoxy-based nanocomposites

with epoxy resin. Nanocomposites were prepared by mixing the epoxy resin with three different weight percentages (1, 3, and 5%) of each type of nanoparticles using high-speed mechanical mixer for 10 min with a rotation speed of 1200 rpm. After that, a hardener was added to the mixture and then stirred slowly to minimize the formation of air bubbles within the sample. The final mixture was poured into silicon moulds and left for 24 h at room temperature for curing purpose as seen in Fig. 2.2. Pure epoxy sample was made as a control.

(c)   Cellulose Fibre-Reinforced Epoxy/Organoclay Eco-nanocomposites

The nanoclay/epoxy nanocomposites were prepared by mixing the epoxy resin with three different wt% (1, 3, and 5%) of nanoclay (Cloiste 30B) using a high-speed mechanical mixer for 10 min. After that, a hardener was added to the mixture and then stirred slowly to minimize the formation of air bubbles within the sample. The final mixture was poured into silicon moulds and left for 24 h at room temperature for curing purpose. Pure epoxy sample was also made as a control.

In the fabrication of RCF-reinforced eco-nanocomposites, the epoxy system and the nanocomposites dispersed with organoclay were used as the matrix material. RCF sheets were first dried for 60 min at 70 °C. After that, RCF sheets were fully soaked into a mixture of epoxy/30B organoclay until they became entirely wetted by the mixture, before they were laid down in a closed silicone mould under 8.2 kPa compressive pressure and left 24 h for curing at room temperature. The same processing procedure was used to prepare RCF/epoxy ecocomposites without the addition of nanoclay. The amount of RCF in the final products was about 52 wt%. All the samples made are summarized in Table 2.1.

Table 2.1 Compositions of synthesized 30B/epoxy nanocomposites and RCF-epoxy/30B eco-nanocomposites

30B/epoxy samples	Organoclay (wt%)	RCF/organoclay/epoxy samples	Organoclay (wt%)
Pure epoxy (PE)	0	PE/RCF	0
PE/30B1	1%	PE/RCF/30B1	1%
PE/30B3	3%	PE/RCF/30B3	3%
PE/30B5	5%	PE/RCF/30B5	5%
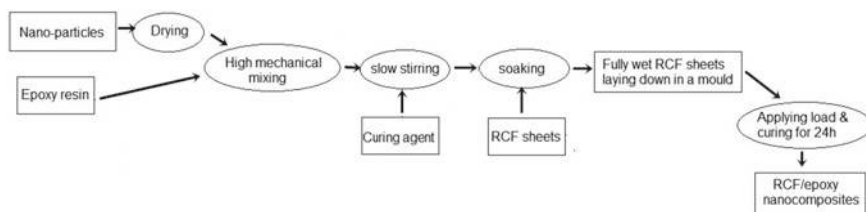
Fig. 2.3   Schematic illustration of the fabrication of RCF/epoxy eco-nanocomposites

(d)   RCF-Reinforced Epoxy Eco-nanocomposites

In this section, the epoxy nanocomposites dispersed with either nanoclay (30B), HNTs, or n-SiC particles as previously described in Sect. 2.2 were used as the matrix material. RCF sheets were first dried for 60 min at 70 °C. After that, RCF sheets were fully soaked into a mixture of epoxy-based nanocomposites until they became entirely wetted by the mixture, before they were laid down in a closed silicone mould under 8.2 kPa compressive pressure and left 24 h for curing at room temperature as seen in Fig. 2.3. The amount of RCF in the final products was in the range 48–52 wt%.

(e)   Nano-SiC-filled Cellulose Fibre-Reinforced Epoxy Eco-nanocomposites

Recycled cellulose-fibre (RCF) paper and nano-silicon carbide (n-SiC) particles were used as reinforcements for the fabrication of n-SiC/RCF/epoxy nano-ecocomposites. General-purpose low-viscosity epoxy resin (FR-251) was used as a matrix. For fabrication procedure, n-SiC particles were pre-dried at 50 °C for 30 min, then a mixture of n-SiC and epoxy was prepared by mixing the epoxy resin with three different weight percentages (1, 3, and 5%) of n-SiC particles using a high-speed mechanical mixer for 10 min with a rotation speed of 1200 rpm. After that, a hardener (isophorone-diamine) was added to the mixture and then stirred slowly to minimize the formation of air bubbles within the sample. The RCF sheets were first heated at 70 °C for 60 min in order to get rid of the absorbent moisture. Then, RCF sheets were fully soaked into the mixture of n-SiC/epoxy until they became entirely wetted by the mixture, then laid down in a closed silicone mould under 8.2 kPa compressive pressure and left 24 h for curing at room temperature. The amount of RCF in the final products was about 48 wt%.

2.2 Vinyl-Ester Ecocomposites

(a)   RCF-Reinforced Vinyl-Ester Ecocomposites

To provide the baseline data, pure vinyl-ester resin (VER) samples were made as controls. Preparation of these samples required the VER to be mixed with a 1.0 wt% catalyst (MEKP). To ensure that no air bubbles were formed within the matrix, the system was slowly and thoroughly mixed. The resultant mixture was then poured into silicon moulds and left under low vacuum (20 kPa) for 2 h, then left at room temperature for 24 h to cure. To prepare the VER/RCF composites, it was necessary to remove stored moisture in RCF. To do this, the RCF sheets were dried at 150 °C in a fan-assisted oven for 60 min. Storage moisture was recorded to be approximately 10%. The RCF sheets were then fully soaked in the vinyl-ester system and laid up in the mould. During the laying-up of the RCF sheets, low pressure was applied frequently to remove trapped air bubbles. The moulds were placed under compressive pressure and in a vacuum of 60 kPa for 2 h. The composites were then left at room temperature to cure for 24 h. To investigate the effect of the fibre content on the physical and mechanical properties of the VER/RCF composites, samples with 20, 30, 40, and 50 wt% fibre were fabricated. These composites were then labelled VER/20% RCF, VER/30% RCF, VER/40% RCF, and VER/50% RCF, respectively.

(b)   Halloysite Nanotube-Reinforced Vinyl-Ester Nanocomposites

As a control to provide the baseline data of the properties of pure vinyl-ester resin, pure vinyl-ester samples (VER) were first made. 1.0 wt% catalyst (MEKP) was mixed into the vinyl-ester resin to prepare the control samples. The resultant mixture was poured into silicon moulds and kept for 2 h under low vacuum (20 kPa) and later for 24 h at room temperature to cure. The nanocomposite samples were prepared with a dispersion of HNTs at concentrations of 1, 3, and 5%. To remove the moisture, HNTs were dried for 60 min at 150 °C, followed by mixing with a high-speed electrical mixer (1200 rpm) for 30 min. Then a catalyst (MEKP) was added slowly to the mixture. The resultant mixtures were poured into silicone moulds, de-gassed in vacuum of 60 kPa for 2 h and cured at room temperature for 24 h. The samples were labelled as VER/1%HNTs, VER/3%HNTs, and VER/5%HNTs.

(c)   Halloysite-Filled   Cellulose   Fibre-Reinforced   Vinyl-Ester   Eco-
       Nanocomposites

Vinyl-ester samples (VER) were first made as a control to provide the baseline data of the properties of pure vinyl-ester resin. The vinyl-ester resin was mixed with 1.0 wt% methyl ethyl ketone peroxide (MEKP) in order to prepare the samples. The mixture was slowly and thoroughly mixed to ensure that no air bubbles formed within the matrix. The resultant mixture was poured into silicon moulds and left under low vacuum (20 kPa) for 2 h and later left at room temperature for 24 h to cure.

Recycled cellulose-fibre sheets (RCF) were dried for 60 min at 150 °C. RCF sheets were then fully soaked in the vinyl-ester system. Next, the sheets were laid

up in a silicon mould under compressive pressure (10.2 kPa) and then placed under vacuum (60 kPa) for 2 h. Then samples left to cure for 24 h at room temperature. The weight percentage of fibres in these ecocomposites was 40%.

Nanocomposites containing different concentrations, namely, 1, 3, and 5 wt% HNTs were prepared. HNTs was first dried for 60 min at 150 °C, and then mixed with vinyl-ester resin for 30 min using high-speed electrical mixer. The mixtures were then left under vacuum of (60 kPa) to remove air bubbles. After that, catalyst was added and mixed manually to avoid creating air bubbles inside the composites. Next, the mixtures were then reinforced with the same percentage of RCF sheets (40 wt%). The sheets were also dried for 60 min at 150 °C. The sheets were then fully soaked in the mixtures and pressed together under 20 kg and under vacuum of (60 kPa) for 2 h. Finally, the samples were left to cure at room temperature for 24 h. The resultant eco-nanocomposites were labelled as VER/RCF/1%HNTs, VER/RCF/3%HNTs, and VER/RCF/5%HNTs, respectively.

(d)   Hybrid Eco-Nanocomposites

Three groups of samples were prepared, namely, pure vinyl-ester (VER), ecocomposites (VER/RCF), and eco-nanocomposites (VER/RCF/n-SiC). First, pure vinyl-ester samples were prepared as controls. The vinyl-ester resin was mixed with 1.0 wt% catalyst (MEKP) slowly and thoroughly to ensure that no air bubbles formed within the matrix. The mixture was left under low vacuum (20 kPa) for 2 h and then left at room temperature for 24 h for curing. To prepare ecocomposite samples, recycled cellulose-fibre sheets (RCF) were dried for 60 min at 150 °C, prior to soaking in vinyl-ester resin and then laid up in closed silicon mould under 20 kg load and vacuum of (60 kPa) for 2 h. Then samples left to cure for 24 h at room temperature. To prepare eco-nanocomposites, first, mixtures containing different concentrations (1, 3, and 5 wt%) of n-SiC were prepared. N-SiC was first dried for 60 min at 150 °C, and then mixed with vinyl-ester resin for 30 min using high-speed electrical mixer. The mixtures were then left under 60 kPa to remove air bubbles. After that, catalyst was added and mixed manually to minimize creating air bubbles inside the composites. Next, the mixtures were then reinforced with the same percentage of RCFs sheets. Sheets were also dried for 60 min at 150 °C and then fully soaked in the mixtures and pressed together under 20 kg and under vacuum of (60 kPa) for 2 h. Finally, the samples were left to cure at room temperature for 24 h.

2.3 Morphological Analyses

(a)   Wide Angle X-ray Scattering (WAXS)

Wide-angle X-ray scattering measurement was carried out at the SAXS/WAXS beamline of the Australian Synchrotron in Melbourne, Australia. A beam energy of 20 keV (wavelength of 0.62 Å) was used in the 2θ range of ~0.29–30.00°.

(b)   Synchrotron Radiation Diffraction (SRD)

Synchrotron radiation diffraction measurement was carried out on the powder diffraction beamline at the Australian synchrotron. The diffraction patterns of each sample were collected using a beam of wavelength 1.377 Å in the two-theta range of 2°–82°.

(c)   Fourier Transform Infrared (FTIR) Spectra

The Fourier transform infrared spectroscopy (FTIR) was performed on Perkin Elmer Spectrum 100 FTIR spectrometer in the transmission mode at room temperature. FTIR spectra were recorded in the range 4000–500 cm^{-1} at a resolution of 2 cm^{-1} with 10 scans. Background spectra were taken in the empty chamber before measurements to eliminate the influence of water moisture and CO_2 in air.

(d)   Transmission Electron Microscopy (TEM)

Ultra-thin sections (~80 nm) of samples were prepared using an ultramicrotome (Leica microsystem) and were recovered on a copper grid. Transmission electron microscopy imaging was done using a Titan Cryotwin (FEI Company) operating at 300 kV equipped with a 4 k × 4 k CCD camera (Gatan). TEM was carried out at King Abdullah University of Science and Technology (KAUST), Saudi Arabia.

(e)   Scanning Electron Microscopy (SEM)

Scanning electron microscope (Zeiss Evo 40XVP) was used to investigate the microstructures and the fracture surfaces of composites. The samples were mounted on aluminium stubs using carbon tape. The samples were then coated with a thin layer of gold to prevent charging before the observation by SEM.

(f)   Thermogravimetric Analysis

The thermal stability of samples was studied by thermogravimetry analysis (TGA) and differential thermogravimetry (DTG). It is a useful technique to evaluate the thermal stability of composites by measuring the weight changes in a material as a function of temperature or time under a controlled atmosphere. Therefore, the thermal stability properties of samples were investigated using A Mettler Toledo TGA/DSC star system analyzer. Samples with ~10 mg were placed in a platinum can and tests were carried out in nitrogen atmosphere with a heating rate of 10 °C/min from 35 to 800 °C.

2.4   Mechanical Property Measurements

(a)   Flexural Strength

Rectangular bars with dimensions 60 mm × 10 mm × 6 mm were cut for three-point bend tests to measure flexural strength and flexural modulus. The three-point

bend tests were performed using a LLOYD Material Testing Machines-Twin Column Bench Mounted (5–50 kN). The support span used was 40 mm with a displacement rate of 1.0 mm/min. Five specimens of each composition were tested to evaluate the mechanical tests. The flexural strength (σ_F) in the units of MPa was evaluated using the following equation:

$$\sigma_F = \frac{3}{2}\frac{P_m S}{W D^2} \tag{2.1}$$

where P_m is the maximum load at crack extension, S is the span of the sample, D is the specimen thickness, and W is the specimen width. Values of the flexural modulus (E_F) in GPa units were computed using the initial slope of the load–displacement curve, $\Delta P/\Delta X$, using the following formula:

$$E_F = \frac{S^3}{4W D^3}\left(\frac{\Delta P}{\Delta X}\right) \tag{2.2}$$

(b)   Fracture Toughness

Single edge notch bending (SENB) specimens were used to evaluate the fracture toughness in a three-point bending mode. A sharp notch was introduced at the central of the specimen bar using a diamond blade saw. The ratio of notch length to width (a/w) was about (0.4). A sharp pre-crack was initiated into the notched specimens by tapping a sharp razor blade. Fracture toughness test was performed on a LLOYD Material Testing Machines-Twin Column Bench Mounted (5–50 kN) with the same conditions of the flexural strength test. The values of fracture toughness (K_{IC}) were calculated in the units of MPa m$^{1/2}$ using equation (Low et al. 1992) as given below:

$$K_{IC} = \frac{p_m S}{W D^{2/3}} f\left(\frac{a}{w}\right) \tag{2.3}$$

where a is the crack length and $f(a/w)$ is the polynomial geometrical correction factor given as

$$f\left(\frac{a}{W}\right) = \frac{3(a/W)^{1/2}[1.99 - (a/W)(1 - a/W) \times (2.15 - 3.93a/W + 2.7a^2/W^2)]}{2(1 + 2a/W)(1 - a/W)^{2/3}} \tag{2.4}$$

(c)   Charpy Impact

A Zwick Charpy impact testing with 1.0 J pendulum hammer was used to evaluate the impact strength and impact toughness. Un-notched samples were used to compute the impact strength in the units of kJ/m^2 using the following formula:

$$\sigma_I = \frac{E}{A} \tag{2.5}$$

where E is the impact energy to break a sample with a ligament of area A.

Samples of various notch lengths were used to determine the impact toughness of composites. The configuration of the specimen was the same as that for the facture toughness but with different notch lengths. In order to measure the impact toughness, the value of the critical strain energy release rate (G_{IC}) was evaluated as the slope of the fracture energy (U) versus the energy calibration factor (ϕ) as shown in equation (Low et al. 2007) given below:

$$U = G_{IC} B D \phi + U_o \tag{2.6}$$

where U_o is the kinetic energy, D is the specimen width, and B is the specimen thickness.

2.5 Characterization of Physical and Thermal Properties

(a)   Porosity

The apparent porosity P_a of the samples was studied to measure the ratio of open pores in the material to its bulk volume. The Australia Standard 1774.5, 2001 was used to determine the apparent porosity of samples using the following equation:

$$P_a = \left(\frac{m_s - m_d}{m_s - m_i} \right) \times 100 \tag{2.7}$$

where m_d is dry mass, m_i is mass of sample immersed in water, and m_s is the mass of soaked sample. Three specimens of each composition were used for porosity measurements.

(b)   Density and Void Content

The fibre volume fraction, the density, and void content of the composites were determined according to ASTM D2734-94 standard by using the following equations:

$$V_v = [(p_{ct} - p_{ce})/p_{ct}] * 100 \tag{2.8a}$$

$$p_{ct} = 1/[W_f/p_f + W_m/p_m] \tag{2.8b}$$

$$p_{ce} = M(gm)/V(cm^3) \tag{2.8c}$$

$$V_f = (W_f/p_f)/[W_f/p_f + W_m/p_m] \tag{2.8d}$$

where V_v is the void fraction percentage; p_{ct} *and* p_{ce} are the theoretical density and the experimental density of the composites, respectively; W_f and W_m are the weight

fractions; p_f and p_m are the densities of the fibre and matrix, respectively; and V_f is the fibre volume fraction (where there are no voids).

(c)   Water Uptake

The water absorption of the composites was determined as a percentage by using the difference in weight between dry samples and samples immersed in water. This is shown in the following equation:

$$M_A = \frac{M_T - M_D}{M_D} \times 100 \tag{2.9}$$

where M_A is water uptake, M_D is dry mass, and M_T is mass of the sample soaked, within time, t.

Different models to describe the moisture absorption behaviour of materials have been developed over time. For moisture absorption that is one dimensional, each sample is exposed on two sides to the same environment. The following equation can be used to express total moisture content (G) (Espert et al. 2004):

$$G = \frac{m - m_i}{m_s - m_i} = 1 - \frac{8}{\pi^2} \sum_{j=0}^{\infty} \frac{1}{(2j+1)^2} \exp\left[-\frac{(2j+1)^2 \pi^2 D_x t}{h^2}\right] \tag{2.10}$$

where m_i is the initial weight of moisture in the material; m_s is the weight of moisture in the fully saturated material in equilibrium with its environment; D is the mass diffusivity in the composite, which represents effective diffusivity as heterogeneities of the composites have been neglected; t is time; h is thickness of the specimen; and j represents the summation index. The diffusion coefficient is an important constraint of Fick's law. The following Eq. 2.14 shows how the diffusion equation for the weight of moisture can be determined and then rearranged in terms of moisture content (M):

$$M = \frac{4M_m}{h}\left(\frac{t}{\pi}\right)^{0.5} D_x^{0.5} \tag{2.11}$$

where M_m is the moisture content of the sample at equilibrium. A graph of weight gain versus time can be plotted by using the weight gain data of the material with respect to time. Using the following equation, by considering the slope of the first part of the weight gain curve versus the square root of time, the diffusion properties of the composites described by Fick's laws were evaluated by using the weight gain measurements of the pre-dried specimens immersed in water. The diffusion coefficient (D) can be defined as the slope of the normalized mass uptake set against the square of time. This takes the form (Liu et al. 2008):

$$D = \pi\left(\frac{kh}{4M_m}\right)^2 \tag{2.12}$$

where k is the initial slope of the plot of $M(t)$ versus $t^{1/2}$, M_m is the weight gain maximum, and h is composite thickness.

2.6   Moisture Absorption

Water absorption test was carried out by immersing samples with dimensions 10 mm $\times$ 10 mm $\times$ 3.5 mm in a water bath at room temperature. The weight gain of the samples was measured periodically. Each sample was dried using a tissue before weighing to remove excess water form sample's surfaces, immediately weighed, and then immersed again in the water bath for next measurement. The percentage of the moisture content (M_t) is determined using the following equation:

$$M_t(\%) = \left(\frac{W_t - W_o}{W_o} \right) \times 100 \tag{2.13}$$

where W_t is the weight of the sample at time t and W_o is the initial weight of the sample.

The water absorption behaviour in the samples can be studied as Fickian behaviour. Therefore, for short immersion times the following formula has been used (Mohan and Kanny 2011; Reddy et al. 2007):

$$\frac{M_t}{M_\infty} = 4 \left(\frac{Dt}{\pi h^2} \right)^{1/2} \tag{2.14}$$

The following equation can be used to calculate relevant diffusion coefficients for each of the samples (Dhakal et al. 2007):

$$D = \frac{\pi}{16} \left(\frac{M_t/M_\infty}{\sqrt{t}/h} \right)^2 \tag{2.15}$$

where M_∞ is maximum water uptake, M_t is water uptake at time t, h is sample thickness, and D is diffusion coefficient.

2.7   Characterization of Thermal Stability and Flammability

The thermal stability of samples was studied by thermogravimetry analysis (TGA) and differential thermogravimetry (DTG). It is a useful technique to evaluate the thermal stability of composites by measuring the weight changes in a material as a function of temperature or time under a controlled atmosphere. Therefore, the thermal

stability properties of samples were investigated using A Mettler Toledo TGA/DSC star system analyzer. Samples with ~10 mg were placed in a platinum can and tests were carried out in nitrogen atmosphere with a heating rate of 10 °C/min from 35 to 800 °C. Thermal decomposition temperatures of the composites were examined under 20 ml/min of nitrogen using platinum pans. Flammability was determined through horizontal burning testing using three measures, ignition time, burning out time, and fire velocity.

2.8   Modelling of Elastic Properties

Theoretical models have been proposed for modelling the elastic modulus properties of composite material based on the parameters of the composites. Thus, it is the properties of components, as well as their arrangement, that determine the outcomes of the models of mechanical properties. Elastic modulus, Poisson's ratio, and the relative volume fractions of the fibre and matrix are the inputs used in mathematical modelling. To a lesser extent, fibre aspect ratio and fibre orientation are also used. In this study, the experimental results for the elastic modulus were compared with the theoretical values obtained from micromechanical modelling, based on the following models.

(a)   Rule of Mixtures (ROM) and Inverse Rule of Mixtures (IROM) Models

The ROM is one of the simplest models for the prediction of the elastic properties of composite materials. Presuming that the matrix and fibre experience the same strain and that this strain is a result of uniform stress applied over a uniform cross-sectional area, the elastic modulus of the composite material in one direction (E_1) can be determined according to the ROM and the IROM equations. For apparent elastic modulus in the fibre direction, the ROM equation is (Ku et al. 2011)

$$E_1 = E_f V_f + E_m V_m \tag{2.16}$$

where E_f, E_m, V_f, and V_m are the respective moduli and volume fractions for the fibre and matrix materials.

   The ROM is useful for aligned continuous fibre composites, particularly when there is the correct assumption of equal strain in the two components. Elastic modulus of a composite in the two directions (E_2) is calculated, presuming that the applied transverse stress is equal in the fibre and matrix. This means that E_2 is determined using the IROM, as given by Ku et al. (2011)

$$E_2 = \frac{E_f E_m}{V_m E_f + V_f E_m} \tag{2.17}$$

When composites have well-bonded reinforcements, the values predicted by the ROM mixtures or the IROM equations serve as the upper and lower bounds for elastic modulus in the principal fibre direction (Facca et al. 2006).

(b)   Halpin–Tsai Model

Halpin and Tsai developed a semi-empirical model that is widely used for modelling the elastic properties of short fibre-reinforced composites. For short fibre-reinforced composites, the Halpin–Tsai equation, in the following form, is used to predict the elastic modulus (Tucker and Liang 1999):

$$E = E_m \left(\frac{1 + \xi \mu V_f}{1 - \eta V_f} \right)$$
(2.18)

The parameter η is given as

$$\eta = \frac{(E_f/E_m) - 1}{(E_f/E_m) + \xi}$$
(2.19)

where ξ in Eqs. 2.18 and 2.19 is a shape fitting parameter to fit the Halpin–Tsai model to experimental data. This parameter considers the packing arrangements and geometry of the reinforcing fibre. The following equation (Bourmaud and Baley 2009) gives ξ when the elastic modulus in the principal fibre direction is required, and the fibres are circular in shape:

$$\xi = 2(l/d)$$
(2.20)

where l is the length of the fibre in one direction and d is the diameter of the fibre.

(c)   Tsai–Pagano Model

Tsai and Pagano developed a method to model elastic modulus in those composites containing short fibres with random orientation (Esfandiari 2008). This model has similarities to Halpin and Tsai's equation. It is given as

$$E = \frac{3}{8} E_1 + \frac{5}{8} E_2$$
(2.21)

where E is the elastic modulus of the composite, and E_1 and E_2 are the elastic moduli of fibre-reinforced composites containing short fibres with random orientation, as given by the Halpin–Tsai model (Lee et al. 2009):

$$E_i = E_m \left(\frac{1 + \xi_i \eta_i V_f}{1 - \eta_i V_f} \right)$$
(2.22)

$$\eta_i = \frac{(E_f/E_m) - 1}{(E_f/E_m) + \xi_i}$$
(2.23)

$$\xi_i = 2\frac{l_f}{d_f} \text{ for } i = 1 \text{ or } \xi_i = 0.5 \text{ for } i = 2 \tag{2.24}$$

(d)   Cox–Krenchel Model

The Cox–Krenchel model is a relatively simple mathematical equation for modelling. This yielded good agreement with the experimental elastic modulus values for a range of glass fibre lengths and volume fractions. The model also performed acceptably well for certain natural fibre composites (Garkhail et al. 2000). The composite elastic modulus, E, is related to the fibre and matrix moduli, E_f and E_m, and the fibre volume fraction, V_f, by using a ROM type of relationship (Andersons et al. 2006):

$$E = \eta_{0E}\eta_{1E}E_fV_f + (1 - V_f)E_m \tag{2.25}$$

where η_{0E} is the orientation factor and η_{lE} is the fibre length efficiency factor. In the case of reinforcing fibres of length, l, the fibre length efficiency factor is given by Andersons et al. (2006)

$$\eta_{1E} = 1 - \frac{\tanh(\beta l/2)}{\beta l/2} \tag{2.26}$$

where the value of β can be expressed as

$$\beta = \frac{1}{r_f}\sqrt{\frac{2E_m/(1 + v)}{E_f \ln(\pi/4V_f)}} \tag{2.27}$$

where r_f is the fibre radius and v is Poisson's ratio of the matrix.

2.9   Mathematical Modelling of Particulate-Reinforced Composites

There are several theoretical frameworks that have been developed to support the prediction of elastic modulus of polymer particulate-reinforced composites. These sophisticated theories have been developed according to the requirements of different material or geometric parameters (Ahmed and Jones 1990; Dong et al. 2011). Conventionally, the elastic properties of a particulate–polymer composite's components (particle and matrix), its particle loading, and its aspect ratio are used in determining the elastic modulus (Ahmed and Jones 1990). For example, for spherical particles, when the aspect ratio of particles equals unity, the elastic modulus of components and particle loading, or particle size will be used to provide the composite modulus. The composite modulus is normally enhanced by adding particles to the matrix since the modulus of particles is usually much higher than that of the polymer matrices (Dong

et al. 2011; Fu et al. 2008). While the theories used for predicting elastic modulus of polymer particulate-reinforced composites are to an extent satisfactory, the theories for predicting the strength and fracture toughness of particulate-reinforced systems are less developed (Fu et al. 2008; Yan et al. 2006). From this point, the present study will limit the prediction of the mechanical properties of the composites to their elastic modulus. Table 2.2 outlines the name, formula, and nomenclature of six mathematical models for predicting elastic modulus. These mathematical models were used to compare experimental data from this study with the models to determine the applicability of the empirical relationships. The parameter values that correspond to the materials properties for mathematical model implementation are presented in Table 2.3.

Table 2.2 Mathematical models used to compare with experimental data of this work

Model name	Model formula	Nomenclature
Paul (upper bound) Ishai–Cohen (lower bound)	$\frac{E_c}{E_m} = \frac{1+(\delta-1)V_p^{2/3}}{1+(\delta-1)(V_p^{2/3}-V_p^{1/3})}$ $\frac{E_c}{E_m} = 1 + \frac{V_p}{\delta/(\delta-1)-V_p^{1/3}}$ $\delta = E_p/E_m$	E_c = Elastic modulus of composite E_m = Elastic modulus of matrix E_p = Elastic modulus of particles V_p = Volume fraction of particles v_m = Poisson's ratio of matrix ϕ_{max} = Maximum packing fraction of particles
Kerner	$\frac{E_c}{E_m} = 1 + \frac{V_p}{(1-V_p)}\frac{15(1-v_m)}{(8-10v_m)}$	
Frankel–Acrivos	$\frac{E_c}{E_m} = 1 + \frac{9}{8}\left[\frac{(V_p/\phi_{max})^{1/3}}{1-(V_p/V_{max})^{1/3}}\right]$	
Guth	*For spherical-shaped particles* $E_c = E_m(1 + 2.5V_p + 14.1V_p^2)$	
Counto	$\frac{1}{E_c} = \frac{1-V_p^{1/2}}{E_m} + \frac{1}{(1-V_p^{1/2})/V_p^{1/2}E_m+E_p}$	

Table 2.3 Values of parameters used in mathematical modelling

Parameters	Values	References
Average of aspect ratio of HNTs α	7[a]	
Elastic modulus of VER E_m (GPa)	2.9[b]	
Poisson ratio of matrix v_m	0.39	Prashantha et al. (2011)
Average of elastic modulus of HNTs E_p (GPa)	30	Guo et al. (2008), Abdelwahab et al. (2012)
Maximum packing fraction ϕ_{max}	0.637	Marsh (2007)
Density of VER	1.14[c]	
Density of HNTs	2.11[d]	

[a] Calculated based on 50 numbers of HNT particles using SEM and TEM micrographs
[b,c,d] Our experimental data

References

Abdelwahab M, Agag T, Akelah A et al (2012) Synthesis and characterization of styrene modified vinylester resin-clay nanocomposites. Polym Eng Sci 52:125–132

Ahmed S, Jones FR (1990) A review of particulate reinforcement theories for polymer composites. J Mater Sci 25:4933–4942

Andersons J, Spārniņš E, Joffe R (2006) Stiffness and strength of flax fiber/polymer matrix composites. Polym Compos 27:221–229

Bourmaud A, Baley C (2009) Rigidity analysis of polypropylene/vegetal fibre composites after recycling. Polym Degrad Stab 94:297–305

Dhakal HN, Zhang ZY, Richardson MOW (2007) Effect of water absorption on the mechanical properties of hemp fibre reinforced unsaturated polyester composites. Compos Sci Technol 67(7–8):1674–1683

Dong Y, Chaudhary D, Ploumis C et al (2011) Correlation of mechanical performance and morphological structures of epoxy micro/nanoparticulate composites. Compos A 42:1483–1492

Esfandiari A (2008) The statistical investigation of mechanical properties of PP/natural fibers composites. Fibers Polym 9:48–54

Espert A, Vilaplana F, Karlsson S (2004) Comparison of water absorption in natural cellulosic fibres from wood and one-year crops in polypropylene composites and its influence on their mechanical properties. Compos A 35:1267–1276

Facca AG, Kortschot MT, Yan N (2006) Predicting the elastic modulus of natural fibre reinforced thermoplastics. Compos A 37:1660–1671

Fu SY, Feng XQ, Lauke B et al (2008) Effects of particle size, particle/matrix interface adhesion and particle loading on mechanical properties of particulate–polymer composites. Compos B 39:933–961

Garkhail SK, Heijenrath RWH, Peijs T (2000) Mechanical properties of natural-fibre-mat-reinforced thermoplastics based on flax fibres and polypropylene. Appl Compos Mater 7:351–372

Guo Z, Lei K, Li Y et al (2008) Fabrication and characterization of iron oxide nanoparticles reinforced vinyl-ester resin nanocomposites. Compos Sci Technol 68:1513–1520

Ku H, Wang H, Pattarachaiyakoop N et al (2011) A review on the tensile properties of natural fiber reinforced polymer composites. Compos B 42:856–873

Lee BH, Kim HJ, Yu WR (2009) Fabrication of long and discontinuous natural fiber reinforced polypropylene biocomposites and their mechanical properties. Fibers Polym 10:83–90

Liu W, Hoa SV, Pugh M (2008) Water uptake of epoxy–clay nanocomposites: model development. Compos Sci Technol 68:156–163

Low IM, Mai YW (1992) Fracture properties and failure mechanisms in pure and toughened epoxy resins. In: Cheremisinoff NP (ed) Handbooks of ceramics & composite materials. Marcel Dekker Publishers, New York, pp 105–160

Low IM, McGrath M, Lawrence D et al (2007) Mechanical and fracture properties of cellulose-fibre-reinforced epoxy laminates. Compos A 38:963–974

Marsh G (2007) Composites help propel GKN Aerospace growth. Reinf Plast 51:26–29

Mohan TP, Kanny K (2011) Water barrier properties of nanoclay filled sisal fibre reinforced epoxy composites. Compos A 42(4):385–393

Prashantha K, Schmitt H, Lacrampe MF et al (2011) Mechanical behaviour and essential work of fracture of halloysite nanotubes filled polyamide 6 nanocomposites. Compos Sci Technol 71:1859–1866

Reddy M, Gupta R, Bhattacharya S et al (2007) Structure-property relationship of melt intercalated maleated polyethylene nanocomposites. Korea-Aust Rheol J 19(3):133–139

Tucker ICL, Liang E (1999) Stiffness predictions for unidirectional short-fiber composites: review and evaluation. Compos Sci Technol 59:655–671

Yan W, Lin RJT, Bhattacharyya D (2006) Particulate reinforced rotationally moulded polyethylene composites—Mixing methods and mechanical properties. Compos Sci Technol 66:2080–2088

Chapter 3
Materials Properties: Physical Characteristics

Abstract Cellulose fibre-reinforced epoxy and vinyl-ester ecocomposites were fabricated in conjunction with inorganic nano-fillers. XRD, FTIR, and SEM studies were carried out to evaluate the composition and microstructure of these ecocomposites and eco-nanocomposites. The effect of water absorption on mechanical and physical properties of these ecocomposites and eco-nanocomposites was investigated. The values of maximum water uptake and diffusion coefficient were found to increase with an increase in fibre content but the presence of nano-filler provided a barrier to water diffusion.

Keywords Polymer ecocomposites · Nanocomposites · Cellulose fibres · Nanofnano-fillers · Epoxy resin · Vinyl-ester resin · Water uptake · Diffusion coefficient · XRD · FTIR · SEM · Aspect ratio · Microstructure

3.1 Cellulose Fibre/Epoxy Ecocomposites

(a) X-ray diffraction analysis of RCF

The X-ray diffraction patterns of RCF are given in Fig. 3.1 showing a typical crystal lattice of native cellulose (cellulose I) (Georget et al. 1999). The main patterns of cellulose fibre are shown at $2\beta = 15.5, 16.5$, and $22.8°$ correspond to (101), (10ī), and (002) planes, respectively (Park et al. 2010). The peak (002) is the major crystalline peak of cellulose I. The fibre crystallinity index (CrI) of RCF is determined by using Segal empirical method (Tserkia et al. 2005). This method offers a quick and simple calculation of the crystallinity index by using the following equation Roncero et al. (2005):

$$CrI = \frac{(I_{002} - I_{am})}{I_{002}} \times 100$$

where I_{002} is the maximum intensity of the 002 crystalline peak and I_{am} is the minimum intensity of the amorphous materials between 101 and 002 peaks as shown in Fig. 3.1.
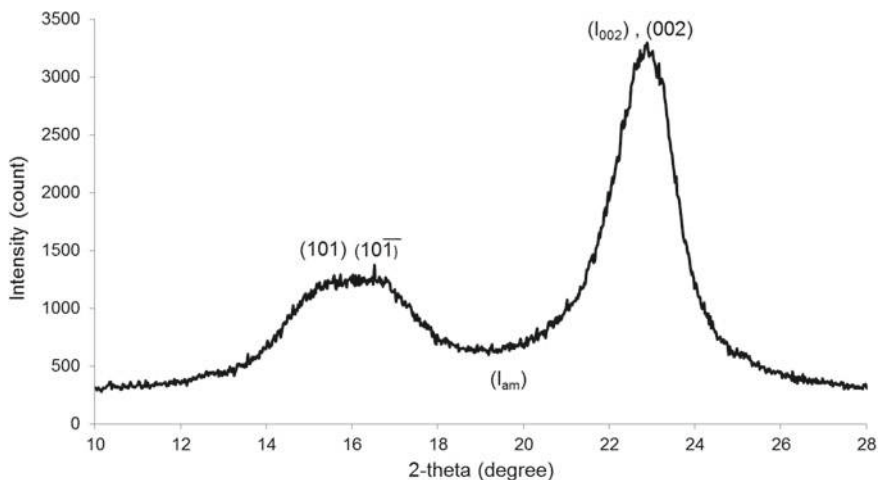
Fig. 3.1 X-ray diffraction patterns of RCF

The crystallinity index of RCF is found to be about 81.8%. Several studies used the same method to measure the crystallinity index of variety of cellulose fibres. For example, Rong et al. (2001) found that the cellulose crystallinity of untreated sisal fibre was 62.8%. Tserkia et al. (2005) reported that the crystallinity of flax, hemp and wood fibres were 86.1, 79.9, 65.1%, respectively. El-Sakhawy and Hassan (2021) found that the crystallinity index of bleached bagasse, rice straw, and cotton stalks fibres after treated by HCl acid were 76.0, 78.0, and 77.0%, respectively. Mwaikambo et al. (2002) found that the crystallinity index of hemp, sisal, jute, and kapok fibres were 87.9, 70.9, 71.4, and 45.8%, respectively. Joonobi et al. (2010) reported that the crystallinity index of kenaf fibre is about 41%.

(b)   FTIR analysis of RCF and RCF/epoxy ecocomposite

FTIR spectra of both RCF and RCF/epoxy ecocomposite are shown in Fig. 3.2. The FTIR spectra show a broad peak in the region between 3340 and 3275 cm^{-1} corresponds to the hydroxyl (OH) stretching vibration of free and hydrogen bonded –OH groups (Karbowiak et al. 2011; Lasagabaster et al. 2006). The peak at around 2902 cm^{-1} in the spectra of the RFC is probably associated with the (CH) stretching of cellulose fibre (Sgriccia et al. 2008; Oh et al. 2005; Bledzki et al. 2010). The absorbance peaks observed at around 1654 cm^{-1} is due to the (OH) bending vibration of absorbed water (Tserkia et al. 2005; Karbowiak et al. 2011; Lasagabaster et al. 2006). The peaks at 1422 and 1368 cm^{-1} can be attributed to CH_2 and CH_3 bending vibration of cellulose fibres, respectively (Karbowiak et al. 2011). The absorption peaks around 1000–1100 cm^{-1} may correspond to C–O stretching of cellulose fibre (Deka and Maji 2011). However, the presence of epoxy in the composites can be recognized by number of peaks. The composites spectra show peaks at 2921 and 2853 cm^{-1}, which may belong to the asymmetric and symmetric CH_2 and CH_3 of
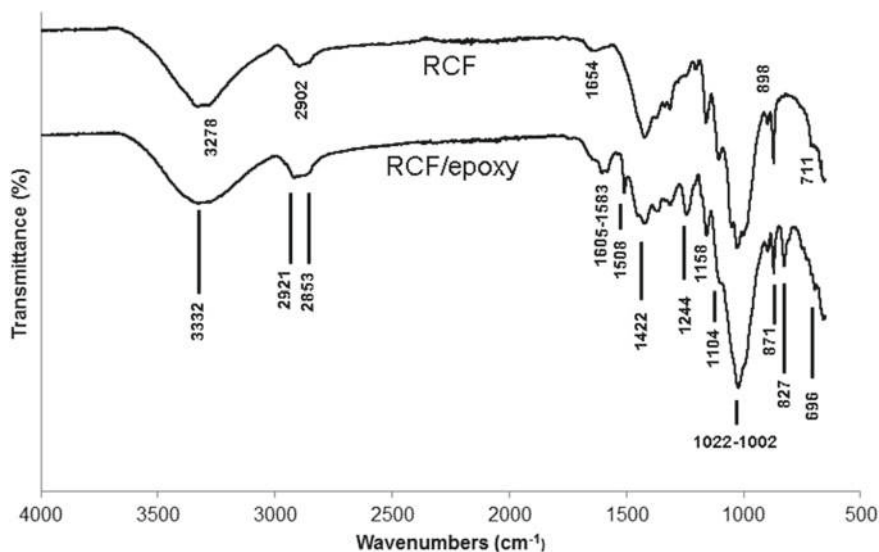
Fig. 3.2 FTIR spectra of RCF and RCF/epoxy ecocomposites

epoxy resin (Shukla et al. 2008). The peaks at 1605, 1583, and 1508 cm^{-1} correspond to the benzene ring of epoxy or C=C stretching of aromatic ring (Chozhan et al. 2007). The peaks appear at 1244 and 918 cm^{-1} are attributed to the C–O stretching of epoxide ring vibration (Shukla et al. 2008; Chozhan et al. 2007; Rajasekaran et al. 2008). Finally, the absorption band at 827 cm^{-1} could be assigned to the 1,4-substitution of aromatic ring for epoxy resin (Khan et al. 2011; Nikolic et al. 2010).

3.2 Nano-SiC/Cellulose Fibre/Epoxy Eco-Nanocomposites

(a) Characterization of Nanocomposites
(i) *Synchrotron radiation diffraction (SRD)*

The SRD diffractograms for epoxy/n-SiC nanocomposites and n-SiC powder are shown in Fig. 3.3. The n-SiC patterns show crystalline pattern structure with five sharp peaks in the range of 2β = 30–70°. Figure 3.3 also shows epoxy having an amorphous structure without distinct repeating unit. The addition of n-SiC particles to epoxy matrix clearly increased the crystallinity of the epoxy/n-SiC composites due to the presence of sharp narrow diffraction peaks. It also can be seen that the highest of the diffraction peaks of n-SiC increased as nano-filler content increased in the epoxy/n-SiC composites.
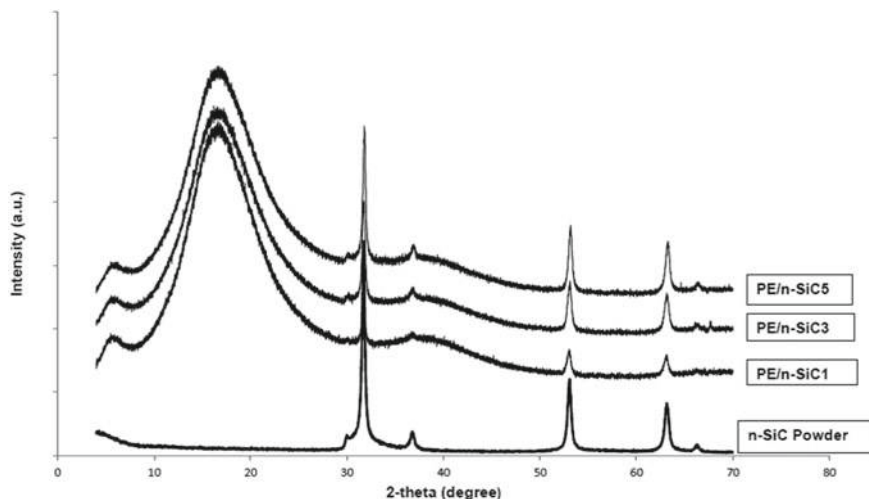
Fig. 3.3 Synchrotron radiation diffraction (SRD) patterns of n-SiC powder and epoxy/n-SiC nanocomposites

(ii)   *Transmission electron microscopy (TEM)*

TEM images of the epoxy nanocomposite with different contents of n-SiC particles are shown in Fig. 3.4. The lower magnification images in Fig. 3.4a–c give a general observation of n-SiC particles dispersion into the epoxy matrix. The n-SiC particles are homogeneously dispersed inside the epoxy matrix except for some particle agglomerations can be clearly seen at higher n-SiC loading. These agglomerations increase as n-SiC particle content increases. As it was observed during sample fabrication, the matrix viscosity significantly increased as nanoparticles concentration increased, which made particles dispersion rather poor and easily to aggregate in micro-size. At higher magnification images Fig. 3.4d–f, n-SiC particles have spherical shape with crystalline structure. Table 3.1 shows the compositions of synthesized n-SiC/epoxy and RCF-epoxy/n-SiC nanocomposites.

3.3   Nano-Filler/Epoxy Nanocomposites

(a)   TEM Observations

Images in Fig. 3.5a–c show the dispersion for 5 wt% of nanoclay, halloysite nanotube (HNT), and n-SiC within the epoxy matrix, respectively. The dispersion of these fillers was quite homogenous with some particle agglomerations that found to increase as filler content increased due to the increase in matrix viscosity. High magnification TEM images for nanoclay (Cloisite 30B), HNT, and n-SiC in the epoxy matrix are shown in Fig. 3.5d–f. It can be seen in Fig. 3.5d that mixing the
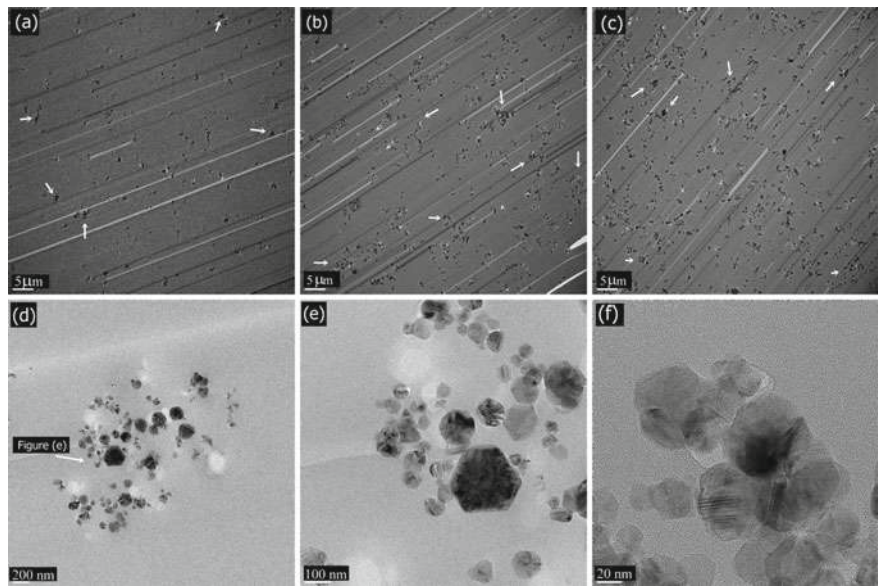
Fig. 3.4 TEM micrographs of epoxy nanocomposites reinforced with different n-SiC concentration: **a** 1 wt%, **b** 3 wt%, **c** 5 wt%, and **d–f** are high magnification TEM images of n-SiC particles inside epoxy matrix [The white arrows indicate n-SiC clusters]

Table 3.1 Compositions of synthesized n-SiC/epoxy and RCF-epoxy/n-SiC nanocomposites

n-SiC/epoxy sample	n-SiC (wt%)	RCF/SiC/epoxy sample	SiC (wt%)
Pure epoxy (PE)	0	PE/RCF	0
PE/SiC1	1	PE/RCF/ SiC1	1
PE/SiC3	3	PE/RCF/ SiC3	3
PE/SiC5	5	PE/RCF/ SiC5	5

nanoclay platelet with epoxy resin resulted in intercalated structure with d-spacing ranges from 2.3 to 4.3 nm compared to 1.8 nm of nanoclay platelet. Separated single layers of clay platelet can be also observed. Figure 3.5e shows that HNT has hollow nanotubular structure with an average diameter of about 20–40 nm and length ranging from 500 nm to 1.6 μm, while Fig. 3.5f indicates that n-SiC particles are spherical in shape with diameter ranging from 40 to ≥100 nm.

(b)   FTIR Analyses

The FTIR spectra of epoxy and epoxy nanocomposites filled with nanoclay, HNT, and n-SiC in dry condition is investigated. Figure 3.6 presents the main FTIR bands of epoxy and its nanocomposites. The FTIR spectra showed the broad band in the region 3317–3373 cm^{-1} corresponds to the stretching vibration of the hydroxyl
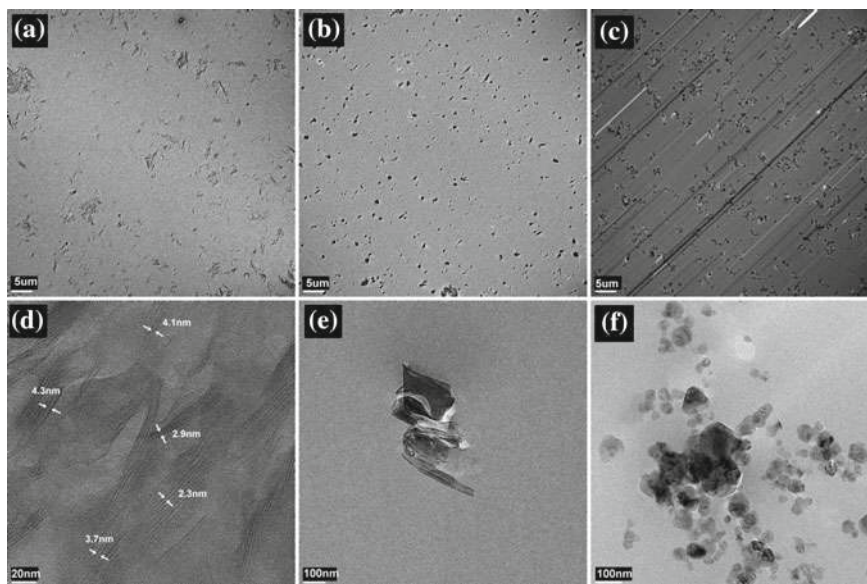
Fig. 3.5 TEM images of epoxy-based nanocomposites filled with nanoclay (**a**, **d**), HNT (**b**, **e**), and n-SiC (**c**, **f**)

groups (OH) of free and hydrogen bonded –OH groups (Lasagabaster et al. 2006). The peak at 1647 cm^{-1} is assigned to the (OH) bending vibration (Tserkia et al. 2005). The absorption peaks at 2869 and 2921 cm^{-1} are attributed to C–H symmetric and asymmetric stretching vibration (Pasbakhsh et al. 2010). The absorption peaks at 1607, 1582, and 1508 cm^{-1} are associated with characteristic adsorptions of the benzene ring of epoxy or C=C stretching of aromatic ring (Chozhan et al. 2007). The absorption bands at 1362 and 1453 cm^{-1} can be attributed to CH_3 and CH_2 bending vibration, respectively (Nikolic et al. 2010). The C–O stretching of epoxide ring vibration showed peaks at 1237 and 917 cm^{-1}. The peak appeared at 826 cm^{-1} could be assigned to the 1,4-substitution of aromatic ring for epoxy resin. There are number of peaks existed in the FTIR spectra due to the presence of nanoclay, HNT, and n-SiC into epoxy system. For example, the peaks appeared at 3621 and 3695 cm^{-1} in the HNT/epoxy spectrum correspond to Al_2OH stretching of HNT (Mayandi et al. 2020). The absorption bands at 911 and 1031 cm^{-1} are attributed to Al-OH vibrations and Si–O stretching vibrations in the HNT. In the FTIR spectrum of n-SiC/epoxy nanocomposites, the peaks found at 911 and 1105 cm^{-1} may correspond to Si–C bonds and Si–O–C bonds between n-SiC and epoxy matrix, respectively (Zhou et al. 2008). The spectrum of nanoclay-filled epoxy composite showed peak at 3631 cm^{-1}, which belongs to the (OH) stretching for Al–OH and Si–OH of nanoclay (Ramadan et al. 2010). Otherwise, the intensity of some peaks in the nanoclay/epoxy composites changed due to the presence of nanoclay.
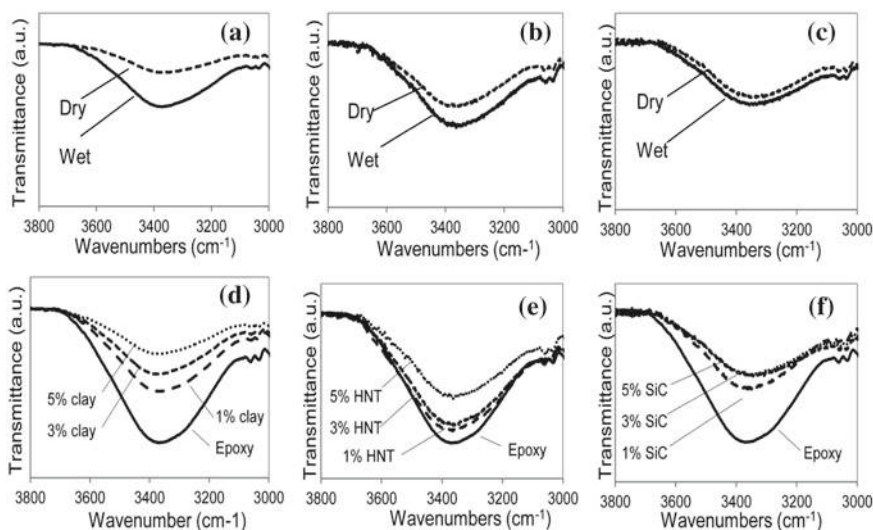
Fig. 3.6 FTIR (3000–3800 cm^{-1}) of epoxy-based nanocomposites. **a** dry and wet nanoclay/epoxy, **b** dry and wet HNT/epoxy, **c** dry and wet n-SiC/epoxy, **d** wet nanoclay/epoxy series, **e** wet HNT/epoxy series, and **f** wet n-SiC/epoxy series

Plots in Fig. 3.6a–c show the principle peak of the hydroxyl group (OH) for dry and wet nanoclay/epoxy nanocomposites, HNT/epoxy nanocomposites, and n-SiC/epoxy nanocomposites, respectively. This peak represents the water indirectly and directly bonded to the hydroxyl group and can be used as an indicator to water content in the materials. It can be seen in Fig. 3.6a–c that after water absorption the peak of interest is found to increase compared to dry composites for all composites. Furthermore, the effect of nano-filler addition on the water absorption of epoxy system was investigated by studying the hydroxyl group (OH) peak at the range of 3317–3373 cm^{-1}. Plots in Fig. 3.6d–f show the effect of nanoclay, HNT, and n-SiC in reducing water uptake in epoxy-based nanocomposites, respectively. In general, it can be observed that the peak of interest decreases as the filler content increases. This confirms that the addition of nano-filler decreases the amount of absorbed water. The reduction in water uptake is most pronounced for nanocomposites filled with n-SiC particles. This result agrees with the weight gain study of water absorption.

3.4 Nanoclay/Cellulose Fibre/Epoxy Eco-Nanocomposites

(a)   Nanostructural Characterization
(i)   *Wide-angle X-ray scattering (WAXS)*

X-ray diffraction (XRD) is used to calculate the basal spacing (*d*-spacing) of nanoclay. WAXS patterns obtained for Cloisite (30B) organoclay, pure epoxy, and
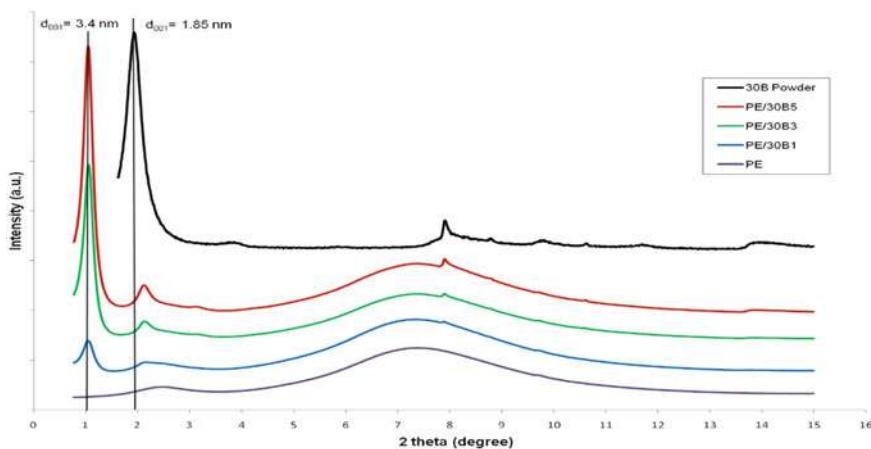
Fig. 3.7 WAXS patterns of cloisite 30B, pure epoxy, and epoxy nanocomposites

epoxy/clay are shown in Fig. 3.7. Epoxy has an amorphous structure without any diffraction peaks. In contrast, the organoclay exhibits a strong (001) peak at $2\beta = 1.92°$, which corresponds to a d-spacing or basal spacing of 1.85 nm. The diffraction patterns of all epoxy/clay nanocomposites exhibited similar plots with the (001) peak shifted to a lower angle compared to the nanoclay control powder, indicating an increase in the inter-layer distance between the clay platelets. The basal spacing of (001) is 3.4 nm at $2\beta = 1.03°$. This result indicates the intercalated structure of the fabricated nanocomposites.

(ii)   *Transmission electron microscopy (TEM)*

TEM images for epoxy/clay nanocomposites loaded with 1–5 wt% of Cloisite 30B nanoclay are shown in Figs. 3.8 and 3.9. The lower magnification images in Fig. 3.8a–c give a general view of the nanoclay dispersion within the epoxy matrix. The
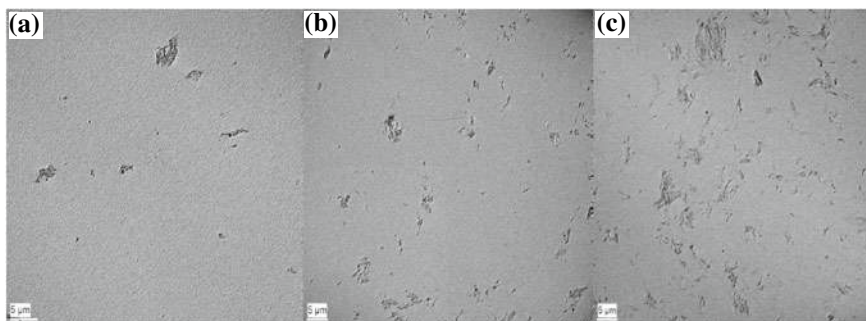
Fig. 3.8   TEM micrographs at low magnification of epoxy nanocomposites reinforced with different nanoclay concetration: **a** 1 wt%, **b** 3 wt%, and **c** 5 wt%
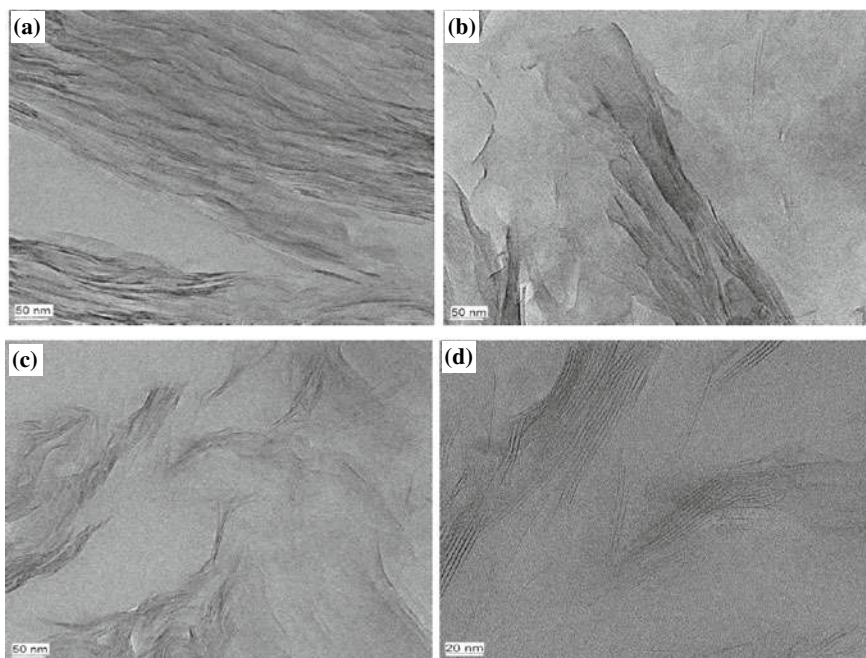
Fig. 3.9 TEM micrographs at high maginifaction of epoxy nancomposites reinforced with different nanoclay concetration: **a** 1 wt%, **b** 3 wt%, and **c** 5 wt%. **d** basal spacing between the interlayers of clay/epoxy nanocomposites Morphology of clay/epoxy nanocomposites

nanoclay platelets are uniformly dispersed within the epoxy matrix. However, large agglomerations can be clearly observed at higher clay loading which implies that the degree of platelet dispersion decreases as the nanoclay concentration increases due to the increase in matrix viscosity. High-magnification images in Fig. 3.9a–d show the layer structure of clay platelets. It can be seen in Fig. 3.9d that epoxy was intercalated between the clay layers shifting them apart, which confirmed the intercalated structure of the resulted nanocomposites. The d-spacing of (001) planes in nanoclay layers were 1.85 nm. However, as a result of intercalation with epoxy resin, the corresponding d-spacing increased to 2.93 nm. This observation relatively agrees with the X-ray diffraction results, which have indicated that the spacing between the clay layers in the nanocomposites was in the range of 3.4 nm.

(b)   Morphology of clay/epoxy nanocomposites

In a previous study by Alamri and Low (Alamri and Low 2012a), wide-angle X-ray scattering (WAXS) and transmission electron microscopy (TEM) were used to investigate the dispersion of the nanoclay in the resulting epoxy/clay nanocomposites. Results showed an intercalation and homogeneous dispersion of nanoclay platelet with some agglomerations. Based on WAXS results, the basal spacing of (001) was 3.4 nm compared to 1.85 nm for nanoclay powder. In this study, we

present more investigation on the nanocomposites structure that used as a matrix for RCF-reinforced epoxy/clay nanocomposites. High-magnification TEM images of epoxy reinforced with 1 and 5 wt% nanoclay are shown in Fig. 3.10a–b. A combination of intercalated and exfoliated clay platelets in epoxy systems can be clearly observed. Figure 3.10a shows the intercalation regions where a multi-layered structure of nanoclay is penetrated by the polymer chains as labelled by letter A and shows exfoliation regions where single layers of nanoclay are surrounded by the polymer chains (labelled by letter B). Figure 3.10b reveals the basal spacing of nanoclay layers in the epoxy matrix. The measured d-spacing ranges from 2.65 to 7.98 nm compared to 1.8 nm of nanoclay platelet. This indicates that in general, the major structure of the nanoclay/epoxy matrix is intercalated with some exfoliated regions. Mixed of intercalated and exfoliated structure was also achieved by Zainuddin et al. (2010) in their study of nanoclay/epoxy nanocomposites.

(c)   Porosity

Porosity of RCF/epoxy and nanoclay-filled RCF/epoxy composites are shown in Fig. 3.11. The dotted line in Fig. 3.11 represents the porosity of pure epoxy. A significant increase in porosity can be observed for all RCF composites when compared to pure epoxy. The addition of nanoclay shows no significant effect on the porosity of these composites.

(d)   FTIR

FTIR spectra of both dry and wet RCF/epoxy composite and 5 wt% nanoclay-filled RCF/epoxy nanocomposites are shown in Fig. 3.12. The FTIR spectra of all samples show a broad peak in the region between 3340 and 3290 cm^{-1}. This fundamental peak corresponds to the hydroxyl (OH) stretching vibration and is often divided into
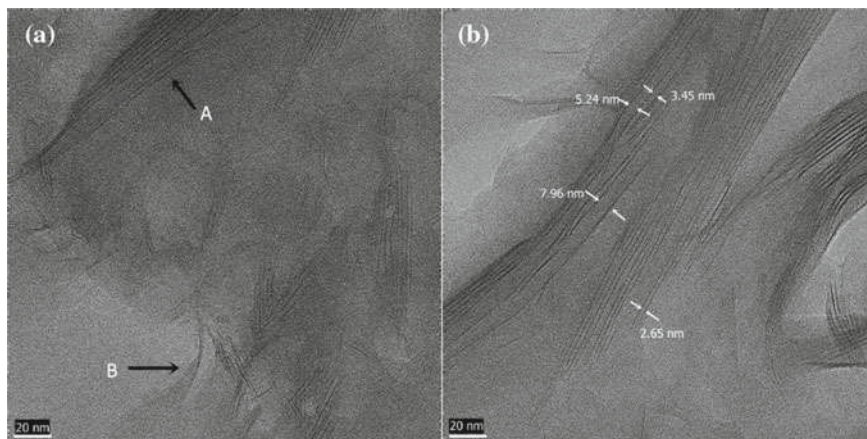

Fig. 3.10   TEM images of epoxy nanocomposites filled with **a** 1.0 wt% and **b** 5.0 wt% nanoclay [Labels A and B indicate intercalated and exfoliated regions, respectively]
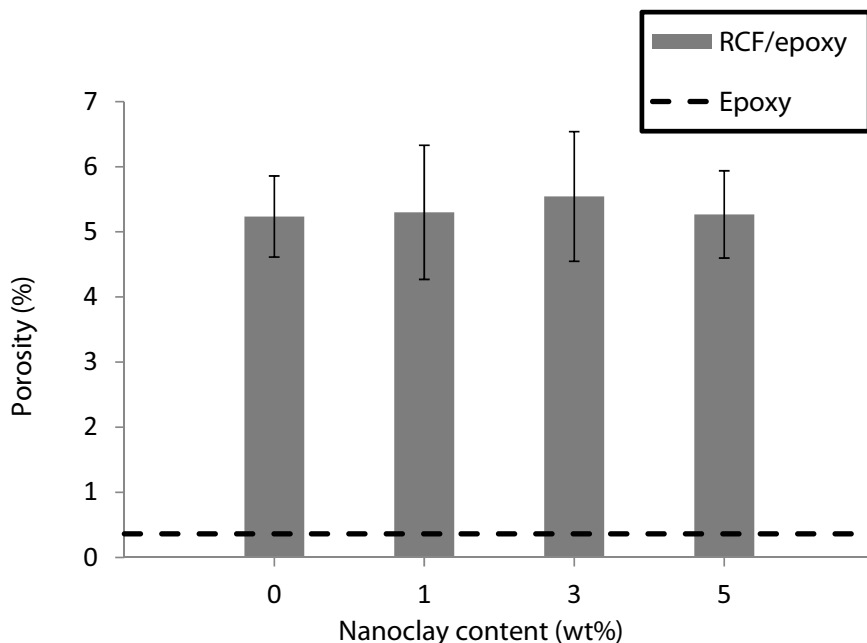
Fig. 3.11 The porosity of RCF/epoxy nanocomposites as a function of nanoclay content

two peaks. The one with higher frequency is often due to the hydroxyl peak of liquid water and is attributed to unassociated water or loosely bound water, where water indirectly bonded to the hydroxyl groups through another water molecule (Karbowiak et al. 2011; Lasagabaster et al. 2006). However, the peak with lower frequency is usually related to strongly bound water, where water directly bonded to the hydroxyl group though hydrogen bonds (Sonawane et al. 2009; Joussein et al. 2005). Other signs of water absorption can be seen in the peaks at around 1642 ± 1 cm^{-1} and 692 cm^{-1}, which correspond to in plane (OH) bending vibration and out of plane vibrations of O–H group, respectively. The peak at 2902 ± 2 cm^{-1} is attributed to the (CH) stretching of cellulose fibre (Sgriccia et al. 2008; Oh et al. 2005). This peak is present in all RCF-reinforced epoxy composites and nanocomposites due to the presence of CH in the chemical structure of cellulose fibre. The absorption band at 1428 cm^{-1} and 1370 cm^{-1} are assigned to CH$_2$ and CH$_3$ bending vibration of cellulose fibres, respectively.

In addition, there are numbers of peaks are related to the presence of epoxy group in the composites. For example, the peaks at around 2928 and 2871 cm^{-1} may correspond to asymmetric and symmetric CH$_2$ and CH$_3$ of epoxy resin (Shukla et al. 2008). The carbonyl group if the epoxide ring produces a peak at 1724 cm^{-1} (Chozhan et al. 2007). The FTIR bands at 1607, 1585, and 1508 cm^{-1} are due to the benzene ring of epoxy or C=C stretching of aromatic ring. The peaks at 1243 and 918 cm^{-1} show the epoxide ring vibration of epoxy resin, which belongs to the
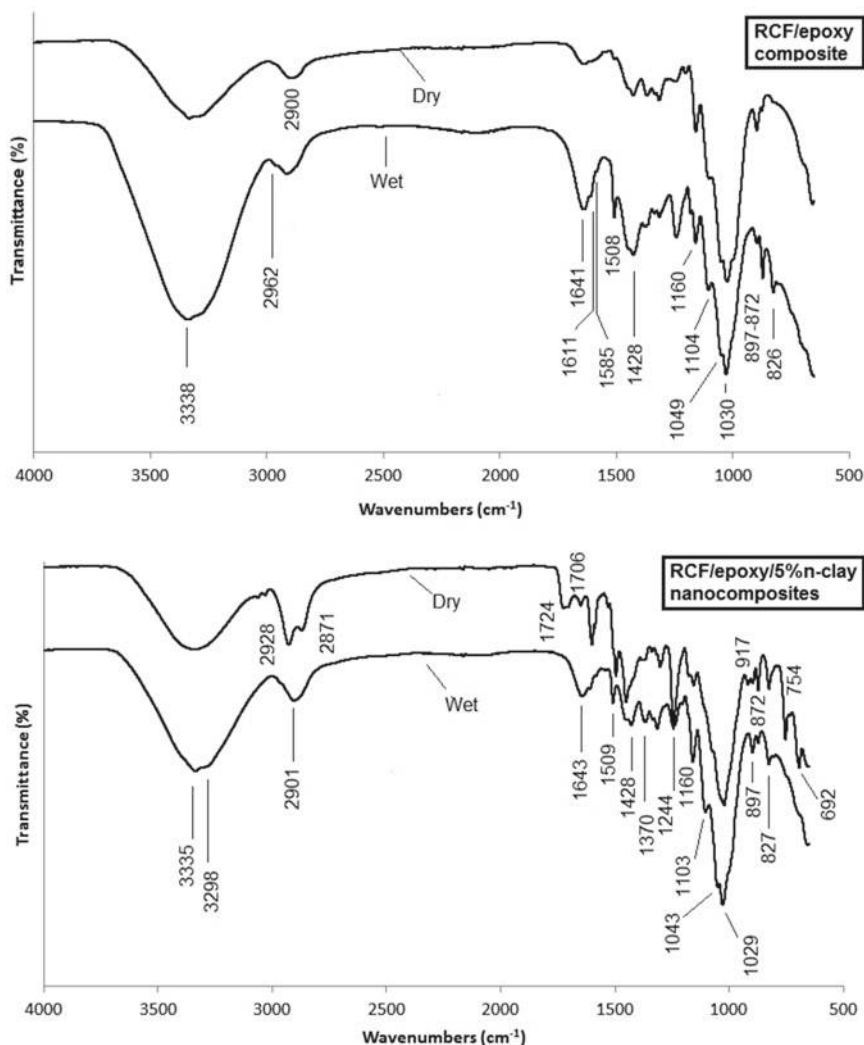
Fig. 3.12 FTIR analysis for dry and wet RCF/epoxy and 5 wt% nanoclay-filled RCF/epoxy ecocomposites

stretching absorption of C–O in the epoxide ring (Rajasekaran et al. 2008). Peaks appear in the range of 1160–1029 cm^{-1} corresponds to C–O stretching of cellulose fibre and epoxy resin. The 1,4-substitution of aromatic ring is observed at 826 cm^{-1} for epoxy resin (Khan et al. 2011; Nikolic et al. 2010). Finally, the peak at 753 cm^{-1} is due Si–O–Al symmetric vibration which confirms the formation of nanocomposites (Fig. 3.12b) (Sonawane et al. 2009).

The main objective of using the FTIR spectroscopy was to investigate the effect of nanoclay addition on the water absorption behaviour of RCF reinforced epoxy
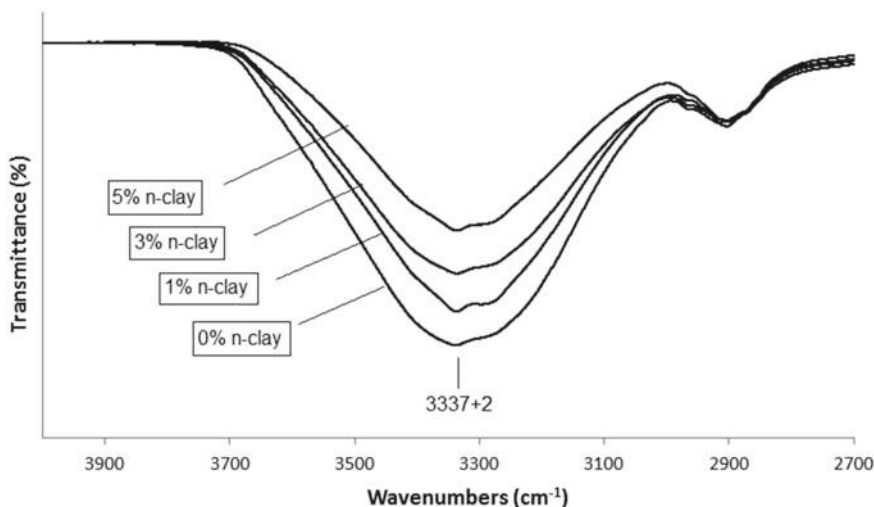
Fig. 3.13 FTIR spectra of wet nanoclay-filled RCF/epoxy ecocomposites

composites. Attention has been focused onto the fundamental OH stretching vibration centred at 3337 ± 1 cm^{-1}, since this peak indicates the water content. It can be seen from Fig. 5.6 that the peak of interest at around 3337 cm^{-1} significantly increased for all wet composites due the immersion in water compared to dry composites. The presence of OH groups in the cellulose fibres attracts the water molecule, resulting in significant water absorption.

Figure 3.13 illustrates the fundamental OH stretching vibration of wet RCF/epoxy composites filled with 0, 1, 3, and 5 wt% nanoclay. It can be observed that unfilled RCF/epoxy composite displays the highest peak among other filled RCF/epoxy nanocomposites. The presence of nanoclay effectively reduces the water uptake for nanoclay-filled RCF/epoxy composites.

The decrease in water uptake is the result of enhancement in the barrier properties of the nanocomposites due to the presence of high aspect ratio nanoclay platelets. Other interesting observation is that the intensity of the fundamental OH peak gradually decreases as nanoclay content increases with maximum reduction occurred at 5 wt% nanoclay loading. This result agrees with the weight gain study of water absorption in the previous section.

3.5 Halloysite/Cellulose Fibre/Epoxy Eco-Nanocomposites

(a)   Synchrotron powder diffraction (SRD)

The SRD patterns of HNT powder and PE/HNT nanocomposites are shown in Fig. 3.14. The HNTs show a sharp peak at 10.73° which correspond to [001] basal
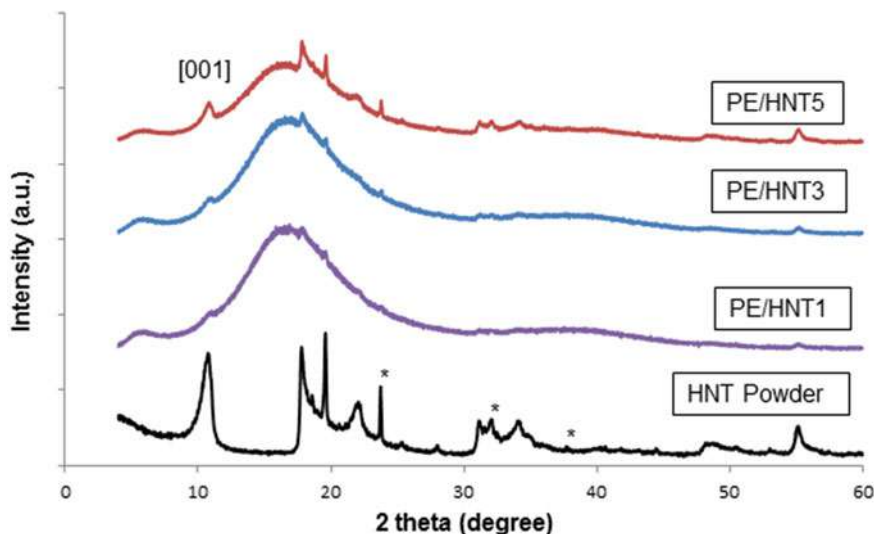
Fig. 3.14 Synchrotron radiation diffraction patterns of HNT powder and epoxy/HNT nanocomposites (Q: quartz)

spacing of 0.735 nm (Pasbakhsh et al. 2010). In addition to halloysite, there are also small amounts of quartz in the powders as has been reported by Joussein et al. (2005) and Deng et al. (2008). Epoxy/HNT nanocomposites patterns show no change in HNTs peaks positions. However, the height of the diffraction peaks of HNT increases as halloysite content increases in HNT/epoxy nanocomposites.

(b)   Transmission electron microscopy (TEM)

TEM images for epoxy/HNT materials loaded with 1, 3, and 5 wt% HNTs are shown in Fig. 3.15. The low-magnification images in Fig. 3.15a–c give a general view of the HNTs dispersion within the epoxy matrix. The HNTs are uniformly dispersed within the epoxy matrix. However, bigger agglomerations of HNTs can be clearly observed at higher clay loading. This suggests the quality of HNT dispersion decreases as clay concentration increases due to the increase in matrix viscosity (Mayandi et al. 2020). At higher magnification images shown in Fig. 3.15d–f, HNTs have tubular shape similar to the multi-walled carbon nanotube with an average diameter of about 20–40 nm and length ranging from 500 nm to 1.6 μm (Pasbakhsh et al. 2010).

Figure 3.15d shows the cross section of the HNTs, while Fig. 3.15f shows the longitudinal section. This would indicate that the dispersion of HNTs within the epoxy matrix is quite random. The dimension of the lumen structure of HNTs and their walls are clearly shown in Fig. 3.15e–f, which confirms the multiwall nanotubular structures of HNTs. Finally, it was reported that HNTs have two different interlayer surfaces; the inner walls contain alumina while the outer surfaces contain silica (Liu et al. 2007).
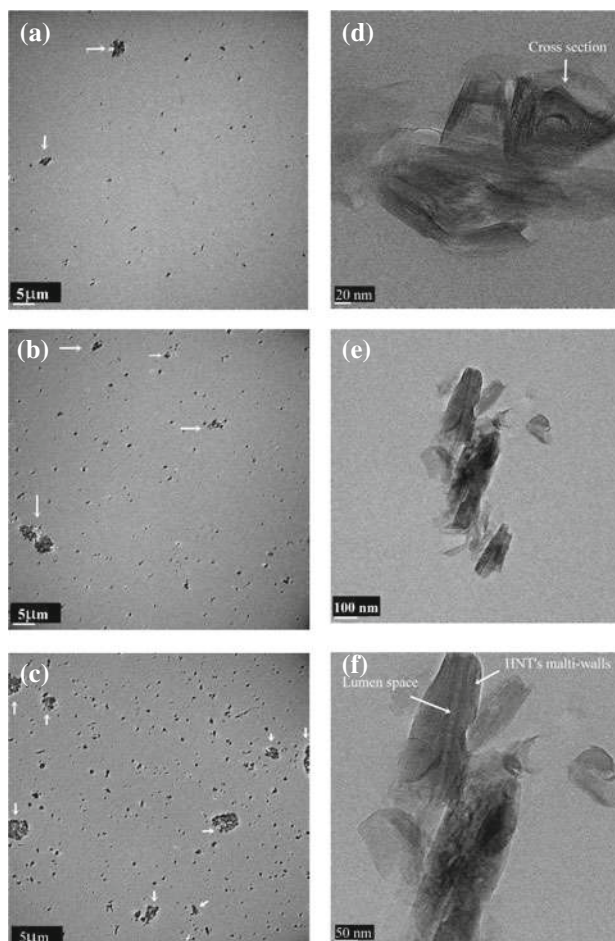
Fig. 3.15 TEM micrographs of epoxy nanocomposites reinforced with different HNTs concentration: **a** 1 wt%, **b** 3 wt%, **c** 5 wt%, and **d–f** are high magnification TEM images of HNTs

3.6 Nano-SiC/Cellulose Fibre/Epoxy Eco-Nanocomposites

(a) TEM Observations

Figure 3.16a–b shows the dispersion of 1 and 5 wt% n-SiC inside the epoxy matrix. The TEM images show that the dispersion of n-SiC particles in the epoxy matrix was quite homogenous with some particle agglomerations that found to increase with increasing filler content as seen in Fig. 3.16a–b. As mentioned in our previous work (Alamri and Low 2012b), the increase in matrix viscosity due to the increase in filler

Fig. 3.16 TEM images of
epoxy-based nanocomposites
filled with **a** 1 wt% n-SiC
and **b** 5 wt% nano-SiC
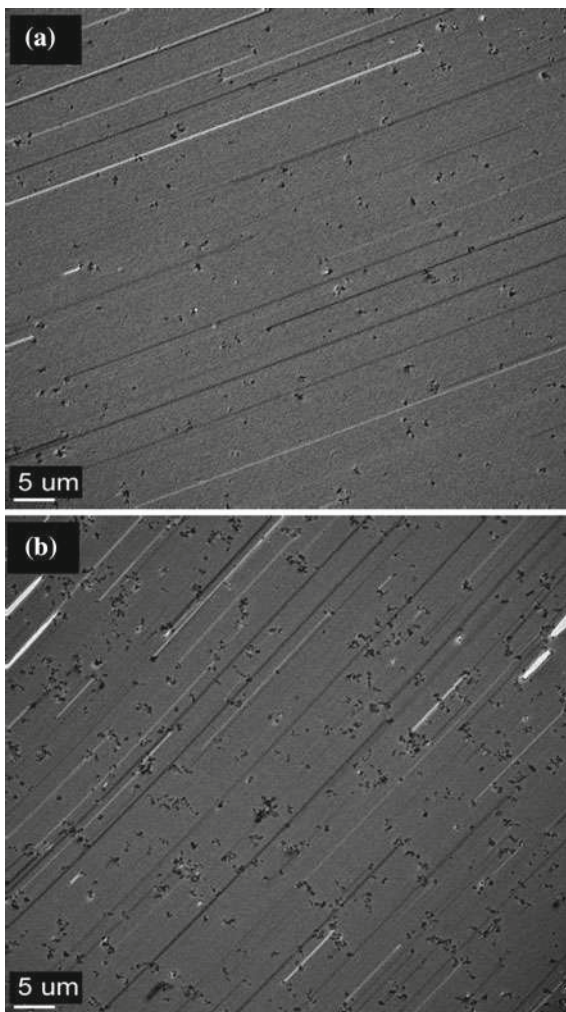
content was the reason behind the presence of particles agglomeration in composites. More details can be found in Alamri and Low 2012b, c).

(b)   Water Absorption

The amount of absorbed water in the composites M_t was determined using the following equation:

$$M_t(\%) = \left(\frac{W_t - W_o}{W_o} \right) \times 100$$

Fig. 3.17 Water absorption curves of n-SiC-filled RCF/epoxy eco-nanocomposites
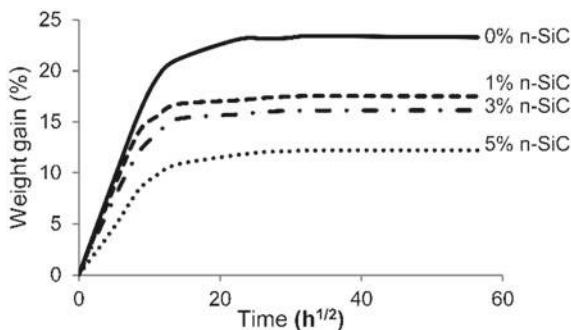
where W_t is the weight of the sample at time t and W_o is the initial weight of the sample.

The effect of the addition of n-SiC particles on the water absorption behaviour of the RCF/epoxy eco-nanocomposites is plotted in Fig. 3.17. It can be observed that all composites display identical curves to each other. This implies that the addition of n-SiC has no effect on the basic mechanism of water diffusion in RCF/epoxy composites. Similar observation was reported by Zhao and Li (2008) for water absorption of nano-Al_2O_3-filled epoxy nanocomposites. For all composites, water uptake continuously increases with the increasing time of immersion. However, water absorption content is found to decrease gradually due to the presence of n-SiC. It was reported that the presence of high aspect ratio nano-filler in polymer matrix enhances the barrier properties of the materials by creating tortuous pathway for water molecules to diffuse into the composites, which leads to a reduction in absorbed water content (Liu et al. 2005). Maximum water uptake of RCF/epoxy composites filled with 5 wt% n-SiC decreases by 47.5% compared to unfilled RCF/epoxy composites. Similarly, Mohan and Kanny (Mohan and Kanny 2011) reported a dramatic decrease in water mass uptake of nanoclay-filled sisal fibre/epoxy composites.

The water absorption behaviour in the composites can be studied as Fickian behaviour. Therefore, the following formula has been used for short immersion times (Mohan and Kanny 2011):

$$\frac{M_t}{M_\infty} = 4\left(\frac{Dt}{\pi h^2}\right)^{1/2}$$

where M_t is the moisture content at time t, M_∞ is the equilibrium moisture content, D is the diffusion coefficient, and h is the sample thickness. Therefore, the diffusivity D can be determined from the initial slope of the moisture absorption versus the square root of time:

$$D = \frac{\pi}{16}\left(\frac{M_t/M_\infty}{\sqrt{t}/h}\right)^2$$

Table 3.2 Maximum water uptake and diffusion coefficient (D) of n-SiC-filled RCF/epoxy eco-nanocomposite

| Samples	M∞ (%)	$D \times 10^{-06}$ (mm^2/sec)
RCF/epoxy	23.28	4.26
1% n-SiC/RCF/epoxy	17.51	6.06
3% n-SiC/RCF/epoxy	16.14	5.28
5% n-SiC/RCF/epoxy	12.23	4.19

The maximum water absorptions and the diffusion coefficient values of RCF/epoxy composites filled with (0, 1, 3, and 5 wt%) n-SiC are presented in Table 3.2. It can be observed that the diffusivity increases after the addition of 1 wt% n-SiC, and then decreases as filler content increases. For example, the diffusivity of 5 wt% n-SiC-filled composites decreased by 30.9% compared to 1 wt% n-SiC-filled composites. This significant reduction in diffusion coefficients may be attributed to increase in the tortuosity of diffusion path created by higher n-SiC content (Liu et al. 2005).

(c)   FTIR Observations

The effect of the moisture absorption on the (OH) stretching vibration and (OH) bending vibration of dry and wet n-SiC-filled RCF/epoxy eco-nanocomposites was investigated by FTIR. Figure 3.18a displays the FTIR spectra of 3 wt% n-SiC-filled RCF/epoxy composites in dry and wet condition. The FTIR spectra show a broad peak in the region between 3335 and 3280 cm^{-1} relates to the stretching vibration of the hydroxyl groups (OH) of both unassociated water (higher frequency peak) and strongly bound water (lower frequency peak) (Karbowiak et al. 2011; Lasagabaster et al. 2006). Other sign of water absorption can be seen in the peak at 1642 cm^{-1}, which belongs to in plane (OH) bending vibration. The effect of water absorption on these peaks is clearly seen in the FTIR spectra in Fig. 3.18a. It can be observed that the peaks of (OH) stretching and bending vibration at 3335 and 1642 cm^{-1}, respectively, increase significantly due to the water absorption. This remarkable increase is expectable due to the presence of RCF in the composites, since cellulose fibre is hydrophilic in nature and tends to absorb much of water in wet condition (Alamri and Low 2012c).

Figure 3.18b displays the fundamental OH stretching vibration and OH bending vibration of wet RCF/epoxy composites filled with 1, 3, and 5 wt% n-SiC. The intensity of the fundamental OH peak gradually decreases with increasing n-SiC content. Maximum reduction is observed for composites filled with 5 wt% n-SiC. This reduction in water absorption is attributed to the enhancement in composites barrier properties due to the presence of nano-filler. Moreover, the absorption peak of OH stretching vibration for 5 wt% filled RCF/epoxy composites is moved to higher wave number centred at 3400 cm^{-1}. This indicates an increase in free OH groups, where water molecules indirectly bonded to the hydroxyl groups through another water molecule. Similar observation was reported for bamboo husk fibre treated by silane coupling agents (Shih 2007).

Fig. 3.18 FTIR spectra of **a** 3 wt% n-SiC-filled RCF/epoxy eco-nanocomposites in dry and wet conditions and **b** n-SiC-filled RCF/epoxy eco-nanocomposites in wet condition
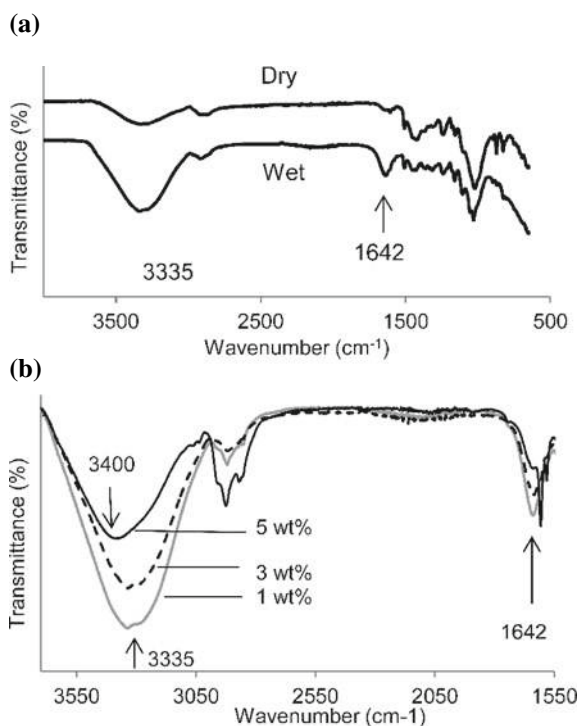
3.7 Nanoclay/Cellulose Fibre/Vinyl-Ester Eco-Nanocomposites

(a) Structure and morphology of nanocomposites

XRD patterns for both nanoclay and VER/clay nanocomposites are shown in Fig. 3.19. A sharp reflection peak is demonstrated at 4.74° at 2β for Cloisite 30B corresponding to interlaying spacing of 1.8 nm. Different results were revealed in the XRD of nanocomposites with 5 wt% nanoclay which is shifting to a broad and weak lower diffraction peak at 4.42°. This shifting is corresponding to the interlaying spacing of 2.1 nm. An intercalated nanocomposite structure was the result evident from entrance of matrix polymer into nanoclay interlayer spacing and increased d-spacing. However, at 1 and 3 wt% nanoclay, there was no reflection peak for the XRD patterns of the composites. The result could suggest an exfoliated structure with uniform dispersion of nanoclay within the matrix. Alternatively, the absence of this peak may be due to the lower nanoclay concentration in composites then that XRD reflection is absent or due to the exciting of an aggregated arrangement of clay nanolayers which indicates there is no nanocomposites formation.
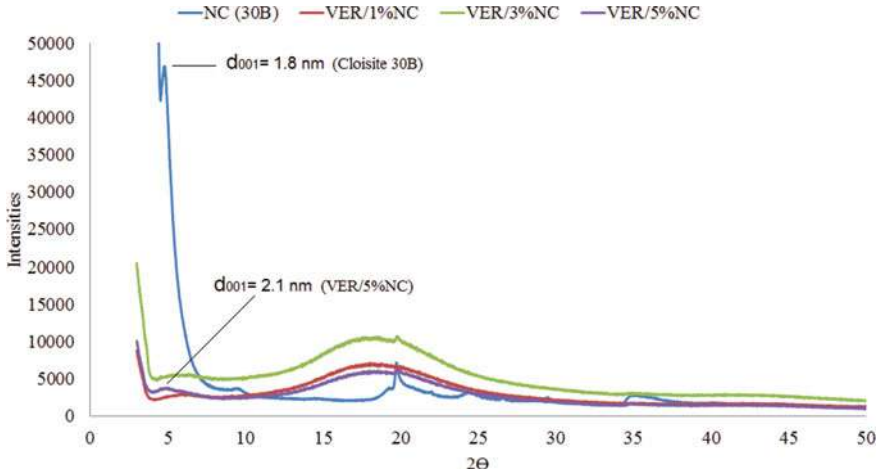
Fig. 3.19   XRD pattern of nanoclay (Cloisite 30B) and VER/nanoclay composites

(b)   Void Content

If voids exist in a composite, the fibre weight fraction w_f is given by

$$w_f = \frac{\rho_f V_f}{\rho_f V_f + \rho_m(1 - V_f - V_v)} \tag{3.1}$$

where ρ_c, ρ_f, ρ_m are the densities of composite, fibre, and matrix, respectively, and V_f and V_v are the volume fractions of fibre and voids, respectively.

If the fibre weight fraction is known, the fibre volume fraction can be found by

$$V_f = \frac{1 - V_v}{1 + \frac{\rho_f}{\rho_m}\left(\frac{1}{w_f} - 1\right)} \tag{3.2}$$

The density of composite can be obtained using the rule of mixtures as given below.

$$\rho_c = \rho_f V_f + \rho_m(1 - V_f - V_v) \tag{3.3}$$

When a composite is void-free, Eqs. (3.2) and (3.3) become

$$V_f = \frac{1}{1 + \frac{\rho_f}{\rho_m}\left(\frac{1}{w_f} - 1\right)} \tag{3.4}$$

$$\rho_c = \rho_f V_f + \rho_m(1 - V_f) \tag{3.5}$$

Substituting Eqs. (3.4) into (3.5) yields

$$\rho_c = \rho_m + \frac{\rho_f - \rho_m}{1 + \frac{\rho_f}{\rho_m}\left(\frac{1}{w_f} - 1\right)} \tag{3.6}$$

First, the VER/RCF composites are assumed to be void-free, and the density of RCF sheets was derived to be $\rho_{RCF} = 1.542$ g/cm^3 from the densities of VER/RCF composites and VER (Table 3.3) using Eq. (3.6). The fibre volume fraction is 32.76%.

(c)   Water uptake characteristics

Water absorption curves of the ecocomposites and eco-nanocomposites are shown in Fig. 3.20. Results showed that samples followed typical Fickian diffusion behaviours. Water absorption, according to the theory, occurs rapidly at the beginning of exposure of the matter with water, however, after time, the absorption rate slows down until reaching the point of equilibrium. Nanoclay addition reduces the uptake of water. Nanoclay platelets cause this behaviour as they have a high aspect ratio (Kim et al. 2005) where the water molecules path is distributed. The presence of the nanoclay platelets means that the water molecules path is altered from the direct-fast diffusion

Table 3.3 Measured thicknesses, densities, and void contents

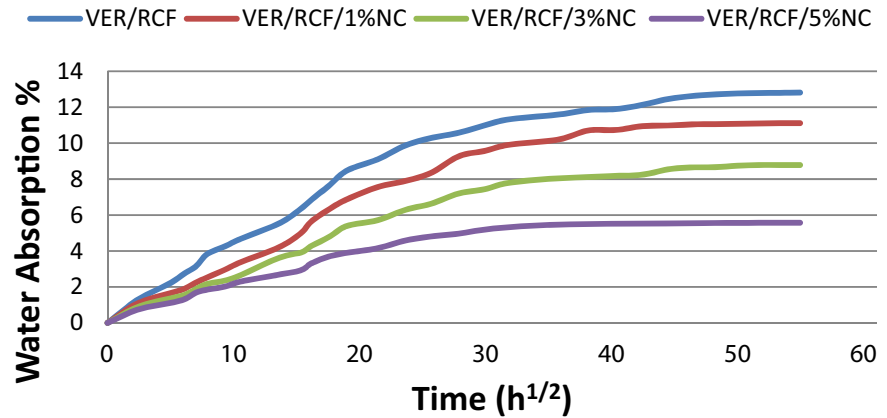| Samples	NC Wt.%	Measured density (g/cm^3)	Void content (%)
VER/RCF	0	1.263	0
VER/RCF/1%NC	1	1.273	0
VER/RCF/3%NC	3	1.277	0.12
VER/RCF/5%NC	5	1.269	1.17

Fig. 3.20 Water absorption behaviour of various vinyl-ester ecocomposites and eco-nanocomposites

Table 3.4 Maximum water uptake M_∞ and Diffusion coefficients D of VER/RCF eco and VER/RCF/NC eco-nanocomposites

Samples	M_∞ (%)	D (mm²/s)
VER/RCF	12.81	0.989×10^{-6}
VER/RCF/1%NC	11.13	0.832×10^{-6}
VER/RCF/3%NC	8.78	0.827×10^{-6}
VER/RCF/5%NC	5.57	1.16×10^{-6}

into the polymer matrix to a maze-like obstacle-ridden path decreasing the overall uptake of water (Ray and Okamoto 2003; Zeng et al. 2005). Table 3.4 shows the maximum water uptake M_∞ and diffusion coefficient D values of all composite.

Table 3.4 shows that as nanoclay loading is increased, the amount of water absorbed is decreased. This shows that nanoclay limits water absorption in composites. This is a desirable property for commercial applications. However, as the nanoclay loading is increased, there is no statistically significant change in the diffusion behaviours of the composites as per the diffusion coefficient. In other words, no trend between the nanoclay content and the water's diffusivity values is observed (Mohan and Kanny 2011; Wu et al. 2022).

(d)   FTIR

The following FTIR spectrums of ecocomposite and nanocomposites identify the main absorbance peaks of water-sensitive bands. The FTIR spectrums in both dry and wet conditions are presented (Fig. 3.21).

The main peak in each of the figures represents the hydroxyl (OH) stretching that occurs between 3000 and 3700 cm^{-1}. This hydroxyl stretching at this higher frequency is a fundamental phenomenon which corresponds to the hydroxyl peak of liquid water and is often assigned to unassociated water alternatively with loosely bound water, and indirectly bonded water bonded to the hydroxyl groups using other water molecules. Moreover, the lower frequency region peak is associated with strongly bound water as characterized by water bound directly by hydrogen bonds to hydroxyl groups of composite components (Lasagabaster et al. 2006, 2009).

When these hydroxyl groups interact with water, water adsorption occurs. Evidence for this is the hydroxyl groups which are part of the water molecules displaying in-plane bending at 1650 cm^{-1} (Karbowiak et al. 2011). Out-of-plane vibrations of the hydroxyl groups cause the broad band which is evident at 700 cm^{-1}. These vibrations are referred to as librations—a collective normal multiple water molecule mode (Lasagabaster et al. 2006).

In addition to these peaks, there are peaks arising between 1000 and 1110 cm^{-1} due to Si–O stretching, peaks at around 915 cm^{-1} due to Al–O/Al–OH stretching, and peaks at ~851 cm^{-1} due to Al–Mg–OH deformation. CH_2 bending vibration causes peaks around 1460 cm^{-1} and CH_3 bending vibration causes peaks 1350 cm^{-1}. These peaks are due to nanoclay vibrations (Sonawane et al. 2009; Leslie and Karen 2004). All composites displayed peaks at ~2900 cm^{-1}. It is expected that these peaks are due to CH stretching, as CH is present in the chemical structures of vinyl-ester and cellulose fibres stretching (Sgriccia et al. 2008; Oh et al. 2005). The benzene
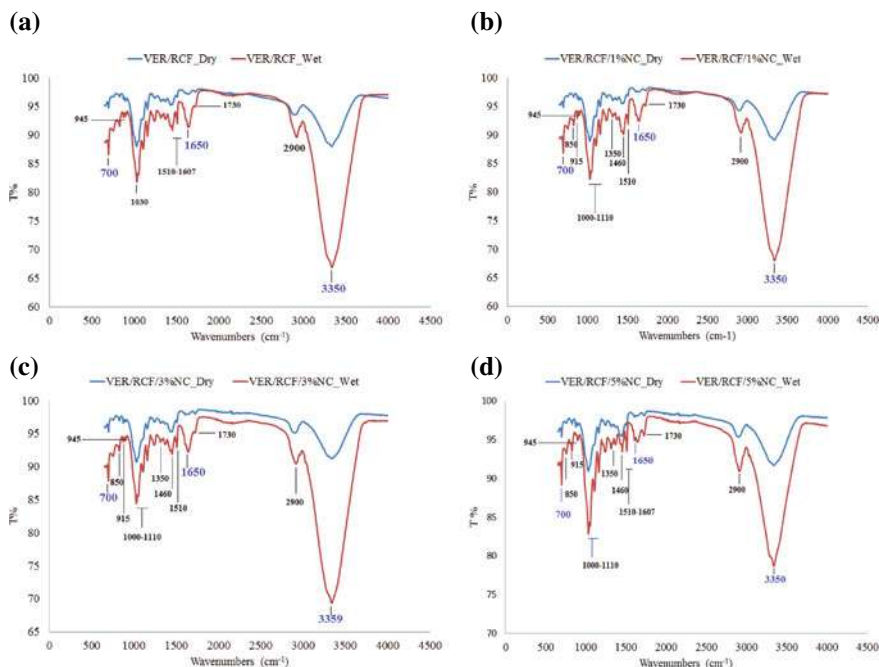
Fig. 3.21 FTIR Dry and Wet spectrums of **a** VER/RCF, **b** VER/RCF/1%NC, **c** VER/RCF/3%NC, and **d** VER/RCF/5%NC samples

ring of vinyl-ester is believed to cause the exhibited absorptions between 1607 and 1510 cm^{-1} (Scott et al. 2002). Out-of-plane bending of carbon–hydrogen bonds in the vinyl group of the vinyl-ester monomer is believed to cause the absorbance at 945 cm^{-1} (Brill and Palmese 2000). As well as, a specific absorption band from vinyl-ester at around 1030 cm^{-1} is a resulting from C–O–C bending vibrations (Oh et al. 2005). Finally, the C=O stretching of the acetyl groups of hemicellulose is believed to cause the peak at ~1730 cm^{-1} (Sgriccia et al. 2008).

The peak of interest in this study is the peak centred at 3350 cm^{-1} (Fig. 3.22). This peak indicates the water content. Even in dry conditions, this peak is still present due to the HO groups which are part of the chemical structure of cellulose fibres. After the water absorption experiment, the peak was found to increase in response to immersion in water for 120 days. The FTIR spectra for the different composite samples included in the study indicated that water immersion led to an increase in the quantities of moisture absorbed and that these quantities were different for each composite.

The peak due to water content which centred at 3350 cm^{-1}, was studied to identify the effect of nanoclay addition on water uptake behaviours of ecocomposites and eco-nanocomposites. Nanoclay addition decreases the amount of water absorption in composites. In particular, the addition of 5 wt% nanoclay provided substantial
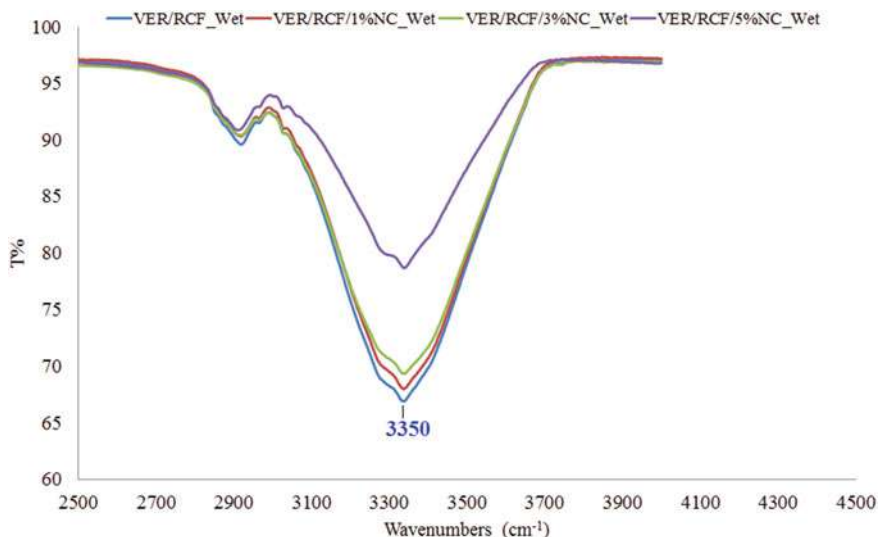
Fig. 3.22 Comparison between FTIR spectrums peaks of water content of various samples

water absorption resistance to composites as evidenced by both the weight gain study and FTIR analysis.

3.8 Halloysite/Cellulose Fibre/Vinyl-Ester Eco-Nanocomposites

(a)   X-ray diffraction analysis (XRD)

XRD patterns for pure HNTs and VER/HNT composites with 1%, 3%, and 5 wt% of HNTs are shown in Fig. 3.23. A diffraction peak at 2β of ~12.27° corresponding to the (001) plane can be seen in XRD pattern for pure HNTs. Two additional diffraction peaks at 2β at ~20.15° and ~ 24.95° corresponding to (020) and (002) basal reflections are noticeable (Joussein et al. 2005; Liu et al. 2007). Trace amounts of quartz and feldspar are also evident and are represented by (*) and (+), respectively. The presence of these minerals in HNTs has also been noted by other researchers (Joussein et al. 2005; Deng et al. 2008).

For pure HNTs, a diffraction peak at a $2\beta = 12.27°$ corresponds to a basal spacing of 0.721 nm. For VER/HNT composites, this diffraction peak has shifted towards lower 2β values or larger basal spacing. The diffraction peaks, with corresponding basal spacing shown in parenthesis, for samples of VER/1%HNTs, VER/3%HNTs, and VER/5%HNTs were 11.87° (0.745 nm), 12.07° (0.733 nm), and 12.15° (0.728 nm), respectively (see Table 3.5). This increase in the basal spacing of HNTs in the composites sample suggests the existence of intercalation between vinyl-ester chains and
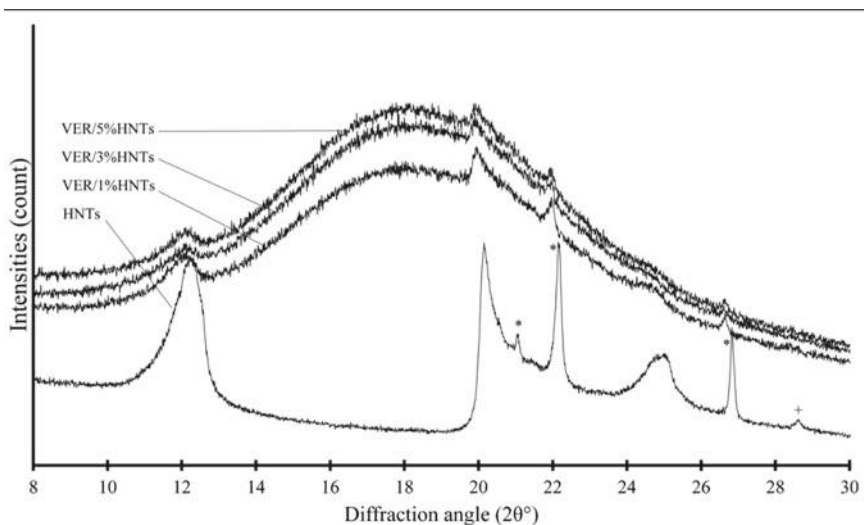
Fig. 3.23 XRD pattern of pure HNTs and VER/HNT samples

Table 3.5 XRD results of HNTs and VER/HNT samples

Specific plane	(001)		(020)		(002)	
2β/d-spacing	2θ	d (nm)	2θ	d (nm)	2θ	d (nm)
HNTs	12.27	0.721	20.15	0.44	24.95	0.357
VER/1%HNTs	11.87	0.745	19.85	0.447	–	–
VER/3%HNTs	12.07	0.733	19.92	0.445	–	–
VER/5%HNTs	12.15	0.728	19.98	0.444	–	–

the HNTs, thus confirming the formation of nanocomposites as also found in other studies (Liu et al. 2007; Rooj et al. 2010).

(b)   Microstructures of HNTs and Nanocomposites

SEM and TEM images of HNTS are shown in Fig. 3.24. The images show that the majority of HNTs exist in a tubular shape, however, short tubular HNTs, and semi-rolled HNTs can also be seen. The image indicates that HNTs have a length ranging from 500 nm to 3 μm. From the image, the average outer diameters of the HNTs ranged from 100 to 300 nm, whereas the average inner diameters ranged from 50 to 150 nm. The length/diameter ratio (i.e. aspect ratio) of HNTs varied between 3 and 15. Being a natural product, the size distribution of HNTs is expected to be large.

The TEM micrographs in Fig. 3.25a–c display the uniform dispersion of HNT fillers in the vinyl-ester (VER) matrix. The extent of dispersion is acceptable even though a few micro-sized HNT clusters can be found. HNTs were randomly dispersed in the matrix with short inter-tube distances resulting in formation of HNT-rich
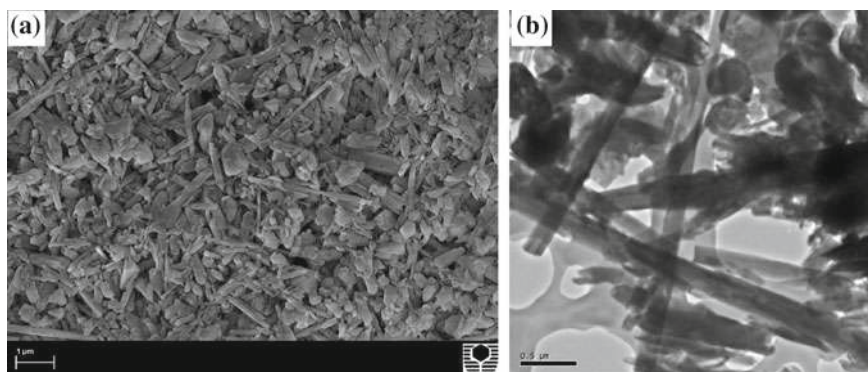
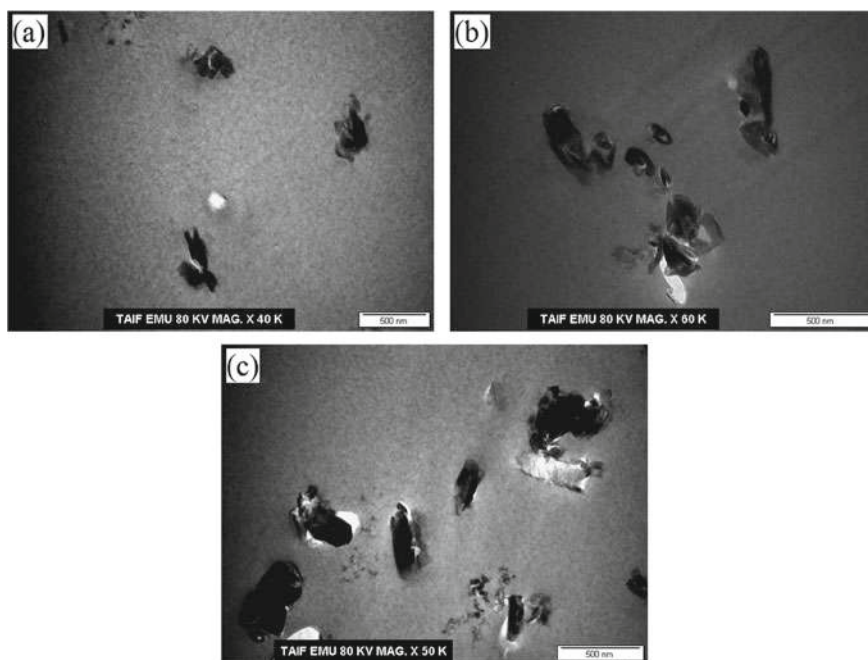**Fig. 3.24** **a** SEM micrograph of HNTs particles and **b** TEM micrograph of HNT particles

Fig. 3.25 Dispersion of HNTs particles within cured VER with **a** 1 wt% of HNTs, **b** 3 wt% of HNTs **c** 5 wt% of HNTs

region and long inter-tube distances resulting in VER-rich region being formed as seen in Fig. 3.26a. The HNT-rich regions give the appearance of HNT clusters. However, a closer examination reveals that VER has filled spaces between these clusters (Fig. 3.26b). In other words, the morphology of the HNT/VER composites displays a continuous phase and a discontinuous phase. The continuous phase is the
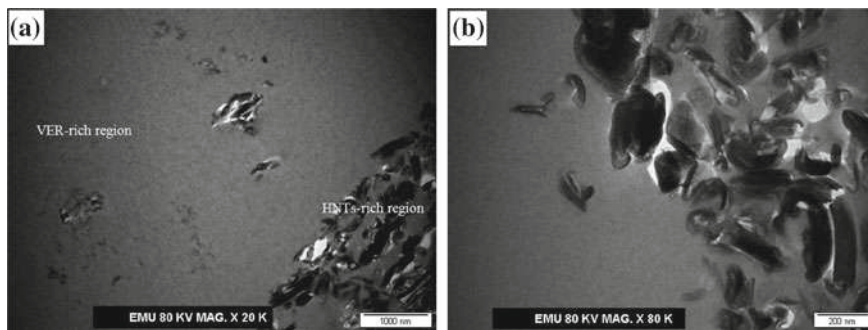
Fig. 3.26 TEM micrographs of VER/HNT samples: **a** VER-rich region and HNT-rich region and **b** spaces between HNT particles cluster clearly filled by VER

VER-rich regions in which a good dispersion of individual HNT clusters is clear. In contrast, the agglomeration of HNT clusters embedded in this continuous phase forms the rigid discontinuous phase (Deng et al. 2008; Ye et al. 2007).

(c)   Water Uptake

Water absorption curves of the ecocomposites and eco-nanocomposites are shown in Fig. 3.27. When the samples were first exposed to water, the process of water
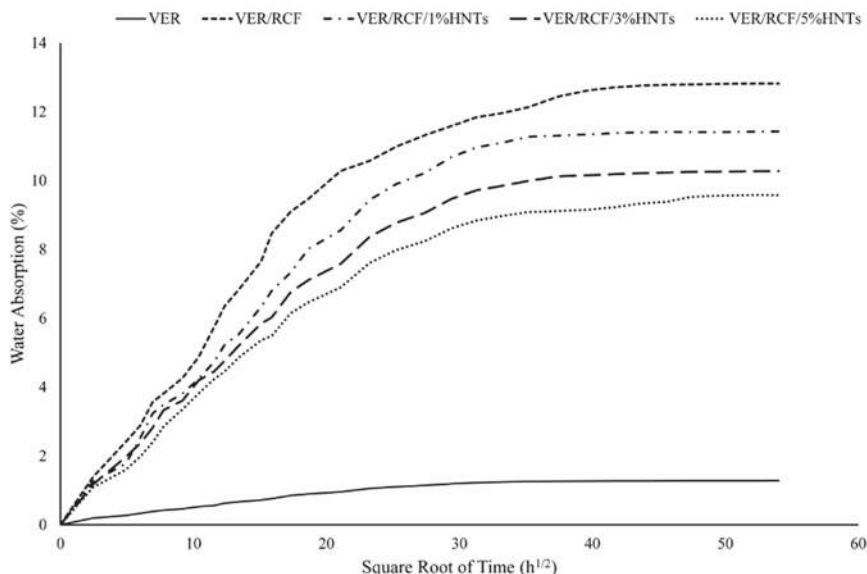

Fig. 3.27 Water absorption behaviour of VER, VER/RCF, VER/RCF/1%HNTs, VER/RCF/3HNTs, and VER/RCF/5%HNTs

Table 3.6 Maximum water uptake M_∞ and Diffusion coefficients D of VER/RCF eco and VER/RCF/HNTs eco-nanocomposites

Samples	RCF content (%)	HNT content (%)	M_∞ (%)	D (mm^2/s)
VER	0	0	1.29	2.72×10^{-6}
VER/RCF	40	0	12.83	2.81×10^{-6}
VER/RCF/1%HNTs	40	1	11.44	2.56×10^{-6}
VER/RCF/3%HNTs	40	3	10.28	2.16×10^{-6}
VER/RCF/5%HNTs	40	5	9.58	2.99×10^{-6}

absorption occurred rapidly then gradually the absorption rate slowed down until equilibrium, these behaviours follow the Fickian diffusion behaviour (Dhakal et al. 2007). Clearly, increasing the HNT addition to the system has resulted in a reduction in the uptake of water. The most plausible explanation for this is that HNTs interfere with the transfer paths of water molecule by transforming the original path of direct-fast diffusion into a torturous or maze-like path which slows water absorption and reduces the overall uptake of water. The impermeability of nanocomposites provided by HNTs prevents their complete saturation and causes maximum water uptake to be lower (Ladhari et al. 2010; Corobea et al. 2008). The maximum water uptake M_∞ and diffusion coefficient D values for all composites are shown in Table 3.6. The amount of water absorbed decreased as the HNT loading increased, thus indicating the desirable effect of HNTs in reducing water absorption in the composites.

(d)   FTIR Analysis

The FTIR spectra of ecocomposites and eco-nanocomposites in dry and wet conditions are shown in Fig. 3.28a–b. A broad peak representing the stretching of hydroxyl groups between 3000 and 3700 cm^{-1} can be seen for each spectrum in dry conditions due to OH ions present in VER, RCF, and HNTs (Baiardo et al. 2002; Du et al. 2008; Jinhua et al. 2010). This broad peak will be reference for the description of water absorption behaviour.

Additional peaks also caused by the presence of VER, RCF, and HNTs can be seen in addition to this broad peak. A strong peak at ~2924 cm^{-1} and weaker peak at around 2870 cm^{-1} caused by the presence of VER and RCF can be seen in all spectra displayed. It is expected that these peaks are due to symmetric and asymmetric vibration from CH (Mohit et al. 2021). The absorption peak at 830 cm^{-1} is believed to be caused by bending vibrations of the vinylic group in vinyl ester, whereas the peak near 947 cm^{-1} is believed to be caused by out-of-plane bending of vinyl ester monomer (Sultania et al. 2010). The bending vibration peak at ~1450 cm^{-1} for methyl groups, and 1350 and 1380 cm^{-1} for methylene groups are due to symmetric and asymmetric vibration from CH (Jebrane and Sèbe 2008). Absorption peaks seen at 1607 and 1510 cm^{-1} are attributed to the benzene ring of vinyl-ester, while peaks at ~1720 and 1180 cm^{-1} are due to the carbonyl groups of the ester linkage (Scott et al. 2002). The presence of HNTs is believed to cause at least three more peaks. The peak
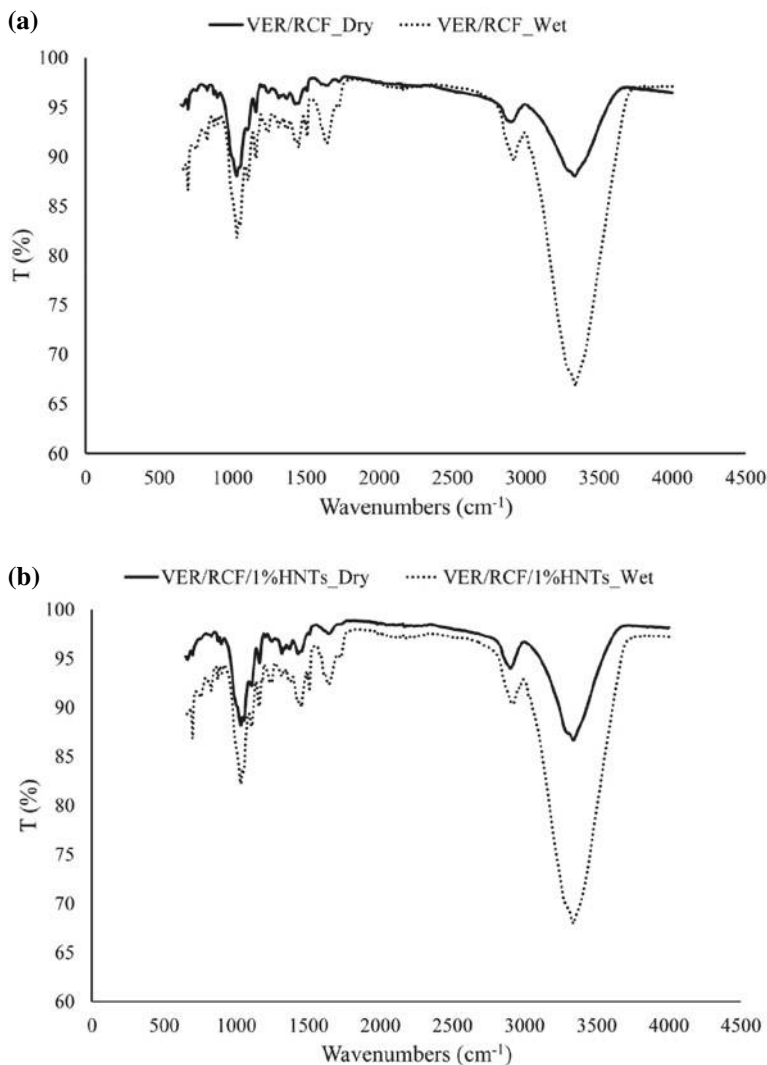
Fig. 3.28 FTIR Dry and Wet spectrums of **a** VER/RCF ecocomposites, **b** VER/RCF/1%HNT eco-nanocomposites, **c** VER/RCF/3%HNT eco-nanocomposites, and **d** VER/RCF/5%HNT eco-nanocomposites

at around 1030 cm^{-1} is caused by perpendicular Si–O stretching, whereas the peak at 1113 cm^{-1} is caused by apical Si–O vibration. The stretching of Al–O/Al–OH bonds is responsible for the peak at ~912 cm^{-1} (Sultania et al. 2010).

   The water absorption of composites for 120 days caused an increase in the broad peak of hydroxyl stretching. The higher frequency region of the peak is due to hydroxyl stretching which is caused by the hydroxyl peak of absorbed liquid water.
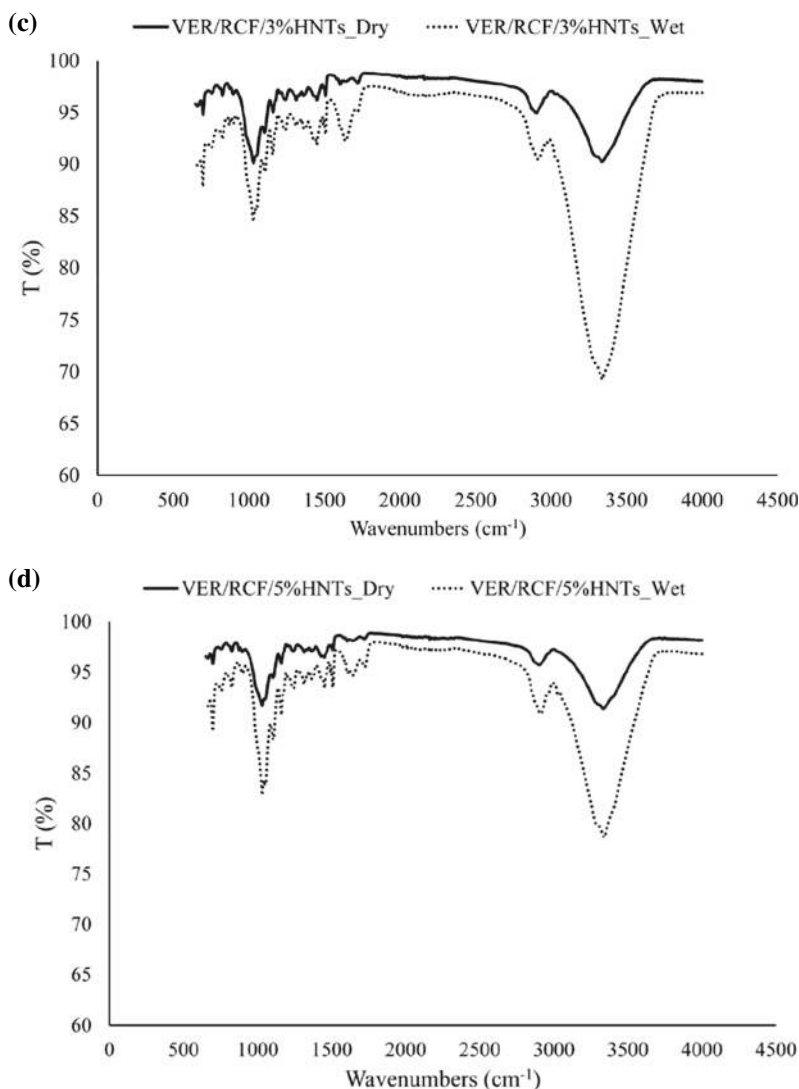
(c)

(d)

Fig. 3.28   (continued)

The effects of absorbed liquid water are considered to include the effects of unasso-
ciated water, loosely bound water, as well as the indirectly bonded water which may
be bonded to the hydroxyl groups using other water molecules. The lower frequency
region of the peak is a result of hydroxyl stretching caused by hydroxyl stretching
of strongly bound water. Strongly bound water is produced when direct hydrogen
bonds are formed between the hydroxyl groups of absorbed water and the composite
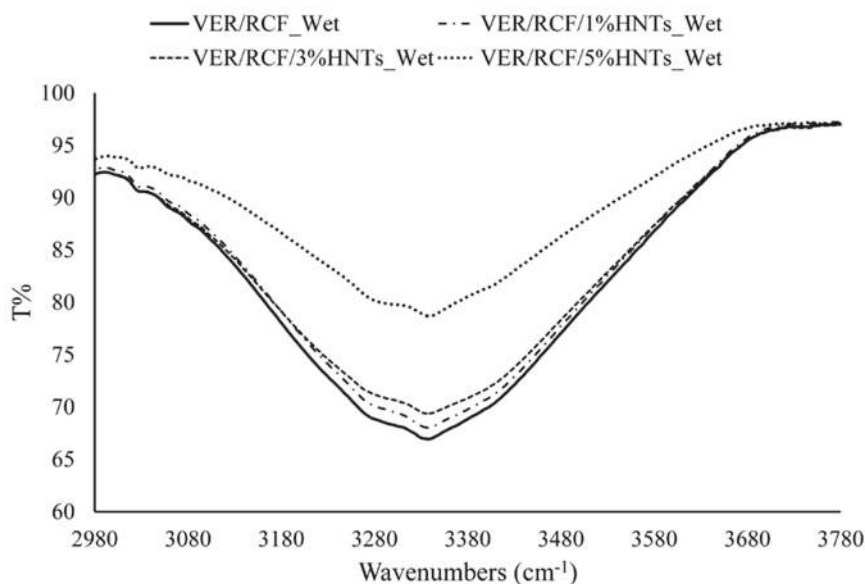components (Lasagabáster et al. 2009).

Fig. 3.29 Comparison between FTIR spectrums peaks of water content of ecocomposites and eco-nanocomposites

The broad peaks, centred at around 3340 cm^{-1}, are shown in Fig. 3.29. These peaks increased after 120 days of immersion in water. The respective FTIR spectra reveal that there were differing quantities of moisture absorbed for each composite. The addition of HNTs was found to lead to a decrease in water uptake behaviours. This provides further support for the premise that HNT addition increases the resistance to water absorption. When compared to 1 and 3 wt% HNTs, the addition of 5 wt% HNTs led to the greatest resistance to water absorption as evidenced by the studies on weight gain and FTIR.

3.9 Nano-SiC/Cellulose Fibre/Viny-Ester Eco-Nanocomposites

(a) Density and Porosity

Table 3.7 shows the values of density and porosity for pure, ecocomposite, and eco-nanocomposite samples. The addition of RCF and n-SiC was found to increase the density of the composites. The porosities in ecocomposites and eco-nanocomposites were found to be much higher compared to the pure samples. Due to the incompatibility between the hydrophilic natural fibres and hydrophobic polymer matrices, the presence of natural fibres in the composite samples has created voids at the interfacial

Table 3.7 Density and porosity results of pure, ecocomposite, and eco-nanocomposite samples

Sample	RCF Content (wt%)	n-SiC Content (wt%)	Density (g/cm^3)	Porosity (%)
VER	0	0	1.14 ± 0.01	0.52 ± 0.01
VER/RCF	40	0	1.26 ± 0.02	3.97 ± 0.03
VER/RCF/1%n-SiC	40	1	1.28 ± 0.01	3.32 ± 0.01
VER/RCF/3%n-SiC	40	3	1.29 ± 0.01	2.99 ± 0.02
VER/RCF/5%n-SiC	40	5	1.32 ± 0.02	2.88 ± 0.03

areas between RCF and matrices (Kim et al. 2005; Dhakal et al. 2007). However, the addition of n-SiC has reduced the porosities of the eco-nanocomposite samples which can be attributed to the improvement of RCF–VER interfacial adhesion. The high specific surface area and high surface energy of n-SiC due to its nano-sized dimension can facilitate rapid phase interactions within the polymer matrix. Therefore, RCF–VER interfacial adhesion can be improved. Furthermore, n-SiC provides strong electrostatic attractive forces at the fibre–matrix interfaces serving to impart additional adhesion between the fibres and the matrix (Chee et al. 2020; Shi et al. 2011).

(b)   Water Uptake

Figure 3.30 shows the water absorption curves of the ecocomposites and eco-nanocomposites. The Fickian diffusion behaviour was observed for each of the samples immersed in water for prolonged period with water absorption occurring rapidly in the beginning and then slowing down prior to reaching equilibrium (Dhakal et al. 2007). The addition of n-SiC has led to a slight reduction in the overall uptake
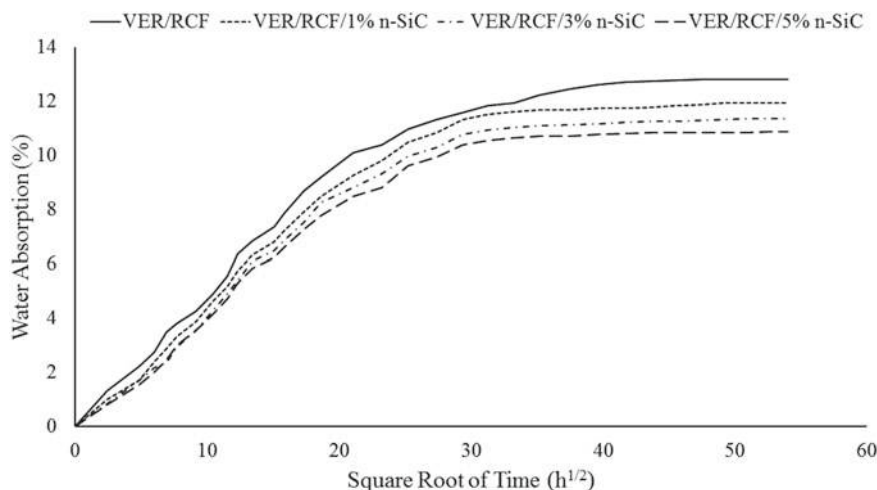

Fig. 3.30 Water absorption behaviour of ecocomposites and eco-nanocomposites

Table 3.8 Maximum water uptake M_∞ and Diffusion coefficients D of VER/RCF eco and VER/RCF/n-SiC eco-nanocomposites

Sample	RCF (wt%)	n-SiC (wt%)	M_∞ (%)	D (mm^2/s)
VER/RCF	0	0	12.8	2.86×10^{-6}
VER/RCF/1% n-SiC	40	1	11.9	2.76×10^{-6}
VER/RCF/3% n-SiC	40	3	11.4	2.75×10^{-6}
VER/RCF/5% n-SiC	40	5	10.9	2.77×10^{-6}

of water in each of the eco-nanocomposite samples. Table 3.8 shows that as n-SiC loading is increased, the amount of water uptake is decreased. This indicates that n-SiC addition inhibits water absorption in eco-nanocomposites. As the equilibrium water content reduces, however, there is no statistically significant change in the diffusion behaviours of the composites. This finding supports the view that there is no direct relationship between water content and diffusivity value as was reported by previous studies (Mohan and Kanny 2011; Wu et al. 2022). These findings imply that a critical determinant of water uptake may be the rate of water flow into the immersed composite. The following equation provides a method for measuring water transmission rate (Mohan and Kanny 2011):

$$WTR = \frac{M_\infty(g)}{TSA(m^2) \times T(days)}$$

where *WTR* is the water transmission rate, M_∞ is the maximum of water uptake, *TSA* is total surface area of specimen since the specimen was exposed to the water in all directions, and *T* is the time to reach the maximum water uptake.

Figure 3.31 shows that with increasing n-SiC content, there is a slight reduction in WTR. This measurement (i.e. WTR) provides a better understanding of water uptake behaviours of composites as it is representative of water flow in three dimensions of the samples. In contrast, diffusivity is the measurement of one-dimensional water flow along the thickness of the samples.

In general, reinforcing composites with nanoparticles can lead to dramatic improvements in the barrier properties of the resultant samples by virtue of the need for the permeating molecules to wiggle around the nanoparticles. Also, the pathway tortuosity of diffusion depends strongly on the aspect ratio or length/width ratio of the nanoparticles. Hence, particles with large aspect ratios will be more likely to form composites with high barrier properties (Liu et al. 2008). The low aspect ratio of n-SiC because of its spherical shape suggests that its addition will only impart moderate barrier properties. As mentioned previously, the reduction of water uptake in eco-nanocomposites may be attributed to the improvement of fibres/matrix interfacial bonding because of n-SiC addition. Better interfacial adhesion can reduce the width of the interface areas existing between fibres and matrix, thus causing a reduction in the amount of water absorption (Qin et al. 2011).
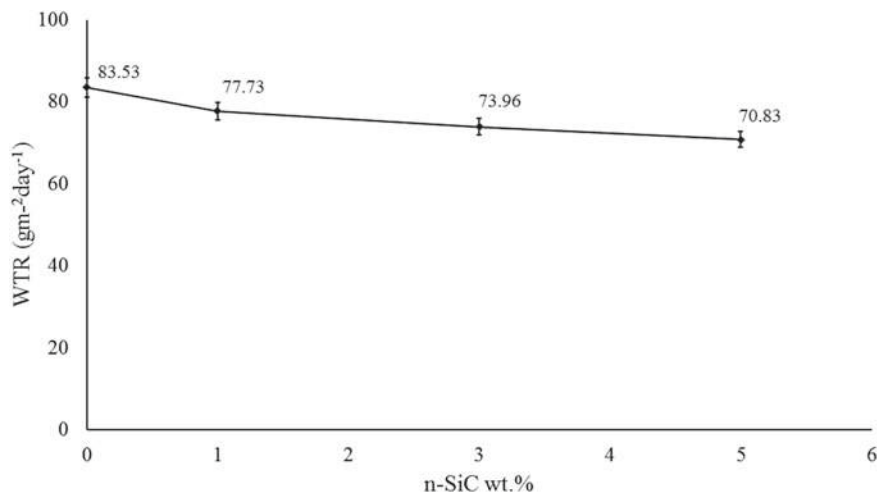
Fig. 3.31 Water transmission rate for pure VER, ecocomposites, and eco-nanocomposites

References

Alamri H, Low IM (2012a) Characterization of epoxy hybrid composites filled with cellulose fibres and nano-SiC. J Appl Polym Sci 126:E221–E231

Alamri H, Low IM (2012b) Mechanical, thermal and microstructural characteristics of cellulose fibre reinforced epoxy/organoclay nanocomposites. Composites B 43:2762–2771

Alamri H, Low IM (2012c) Mechanical properties and water absorption behaviour of recycled cellulose fibre reinforced epoxy composites. Polym Testing 31(5):620–628

Baiardo M, Frisoni G, Scandola M et al (2002) Surface chemical modification of natural cellulose fibers. J Appl Polym Sci 83(1):38–45

Bledzki AK, Mamun AA, Volk J (2010) Barley husk and coconut shell reinforced polypropylene composites: The effect of fibre physical, chemical and surface properties. Compos Sci Technol 70:840–846

Brill RP, Palmese GR (2000) An investigation of vinyl–ester-styrene bulk copolymerization cure kinetics using fourier transform infrared spectroscopy. J Appl Polym Sci 76:1572–1582

Chee SS, Jawaid M, Sultan MTH et al (2020) Effects of nanoclay on physical and dimensional stability of bamboo/kenaf/nanoclay reinforced epoxy hybrid nanocomposites. J Market Res 9(3):5871–5880

Chozhan CK, Alagar M, Sharmila RJ et al (2007) Thermo mechanical behaviour of unsaturated polyester toughened epoxy–clay hybrid nanocomposites. J Polym Res 14:319–328

Corobea MC, Donescu D, Grishchuk S et al (2008) Organophilic layered silicate modified vinylester-urethane hybrid resins: Structure and properties. Polym Polym Compos 16(8):547–554

Deka BK, Maji TK (2011) Study on the properties of nanocomposite based on high density polyethylene, polypropylene, polyvinyl chloride and wood. Composites A 42:686–693

Deng S, Zhang J, Ye L et al (2008) Toughening epoxies with halloysite nanotubes. Polymer 49:5119–5127

Dhakal HN, Zhang ZY, Richardson MOW (2007) Effect of water absorption on the mechanical properties of hemp fibre reinforced unsaturated polyester composites. Compos Sci Technol 67(7–8):1674–1683

Du M, Guo B, Lei Y et al (2008) Carboxylated butadiene–styrene rubber/halloysite nanotube nanocomposites: Interfacial interaction and performance. Polymer 49(22):4871–4876

Georget DM, Cairns P, Smith AC et al (1999) Crystallinity of lyophilised carrot cell wall components. Int J Biol Macromol 26:325–331

Jebrane M, Sèbe G (2008) A new process for the esterification of wood by reaction with vinyl esters. Carbohyd Polym 72(4):657–663

Jinhua W, Xiang Z, Bing Z et al (2010) Rapid adsorption of Cr (VI) on modified halloysite nanotubes. Desalination 259(1–3):22–28

Joonobi M, Harun J, Tahir P et al (2010) Characteristics of nanofibers extracted from kenaf core. BioResources 5(4):2556–2566

Joussein E, Petit S, Churchman J et al (2005) Halloysite clay minerals—a review. Clay Miner 40:383–426

Karbowiak T, Ferret E, Debeaufort F et al (2011) Investigation of water transfer across thin layer biopolymer films by infrared spectroscopy. J Membr Sci 370:82–90

Khan R, Khare P, Baruah BP et al (2011) Spectroscopic, kinetic studies of polyaniline-flyash composite. Adv Chem Eng Sci 1:37–44

Kim JK, Hu C, Woo RSC et al (2005) Moisture barrier characteristics of organoclay–epoxy nanocomposites. Compos Sci Technol 65(5):805–813

Ladhari A, Ben Daly H, Belhadjsalah H et al (2010) Investigation of water absorption in clay-reinforced polypropylene nanocomposites. Polym Degrad Stab 95(4):429–439

Lasagabaster A, Abad MJ, Barral L et al (2006) FTIR study on the nature of water sorbed in polypropylene (PP)/ethylene alcohol vinyl (EVOH) films. Eur Polymer J 42:3121–3132

Lasagabáster A, Abad MJ, Barral L et al (2009) Application of FTIR spectroscopy to determine transport properties and water–polymer interactions in polypropylene (PP)/poly(ethylene-co-vinyl alcohol) (EVOH) blend films: effect of poly(ethylene-co-vinyl alcohol) content and water activity. Polymer 50(13):2981–2989

Leslie SL, Karen KG (2004) Investigation of polymer and nanoclay orientation distribution in nylon6/montmorillonite nanocomposite. Polymer 45:5933–5939

Liu W, Hoa SV, Pugh M (2005) Fracture toughness and water uptake of high-performance epoxy/nanoclay nanocomposites. Compos Sci Technol 65:2364–2373

Liu W, Hoa SV, Pugh M (2008) Water uptake of epoxy–clay nanocomposites: model development. Compos Sci Technol 68(1):156–163

Liu M, Guo B, Du M et al (2007) Properties of halloysite nanotube–epoxy resin hybrids and the interfacial reactions in the systems. Nanotechnology 18:455703

Mayandi K, Rajini N, Ayrilmis N et al (2020) An overview of endurance and ageing performance under various environmental conditions of hybrid polymer composites. J Market Res 9(6):15962–15988

Mohan TP, Kanny K (2011) Water barrier properties of nanoclay filled sisal fibre reinforced epoxy composites. Composites A 42(4):385–393

Mohit H, Sanjay MR, Siengchin S et al (2021) Effect of TiC nanoparticles reinforcement in coir fiber based bio/synthetic epoxy hybrid composites: mechanical and thermal characteristics. J Polym Environ 29(8):2609–2627

Mwaikambo LY, Ansell MP (2002) Chemical modification of hemp, sisal, jute, and kapok fibres by alkalization. J Appl Polym Sci 84:2222–2234

Nassar MMA, Alzebdeh KI, Pervez T et al (2021) Progress and challenges in sustainability, compatibility, and production of eco-composites: a state-of-art review. J Appl Polym Sci 138. https://doi.org/10.1002/app.51284

Nikolic G, Zlatkovic S, Cakic M et al (2010) Fast Fourier transform IR characterization of epoxy GY systems crosslinked with aliphatic and cycloaliphatic EH polyamine adducts. Sensors 10:684–696

Oh SY, Yoo DI, Shin Y et al (2005) FTIR analysis of cellulose treated with sodium hydroxide and carbon dioxide. Carbohyd Res 340:417–428

Park S, Baker JO, Himmel ME et al (2010) Cellulose crystallinity index: measurement techniques and their impact on interpreting cellulose performance. Biotechnol Biofuels 3:10–17

Pasbakhsh P, Ismail H, Fauzi M et al (2010) EPDM/modified halloysite nanocomposites. Appl Clay Sci 48:405–413

Qin L, Qiu J, Liu M et al (2011) Mechanical and thermal properties of poly(lactic acid) composites with rice straw fiber modified by poly(butyl acrylate). Chem Eng J 166(2):772–778

Rajasekaran R, Karikalchozhan C, Alagar M (2008) Synthesis, characterization and properties of organoclaymodified polysulfone/epoxy interpenetrating polymer network nanocomposites. Chin J Polym Sci 26(6):669–678

Ramadan AR, Esawi AM, Gawad AA (2010) Effect of ball milling on the structure of Na+-montmorillonite and organo-montmorillonite (Cloisite 30B). Appl, Clay Sci 47:196–202

Ray SS, Okamoto M (2003) Polymer/layered silicate nanocomposites: a review from preparation to processing. Prog Polym Sci 28:1539–1641

Roncero MB, Torres AL, Colom JF et al (2005) The effect of xylanase on lignocellulosic components during the bleaching of wood pulps. Biores Technol 96:21–30

Rong MZ, Zhang MQ, Lui Y et al (2001) The effect of fibre treatment on the mechanical properties of unidirectional sisal-reinforced epoxy composites. Compos Sci Technol 61:1437–1447

Rooj S, Das A, Thakur V et al (2010) Preparation and properties of natural nanocomposites based on natural rubber and naturally occurring halloysite nanotubes. Mater Des 31:2151–2156

Scott TF, Cook WD, Forsythe JS (2002) Kinetics and network structure of thermally cured vinyl ester resins. Eur Polym J 38(4):705–716

Sgriccia N, Hawley MC, Misra M (2008) Characterization of natural fiber surfaces and natural fiber composites. Composites A 39:1632–1637

Shi J, Shi SQ, Barnes HM et al (2011) Kenaf bast fibers-Part ii: inorganic nanoparticle impregnation for polymer composites. Int J Polym Sci. https://doi.org/10.1155/2011/736474

Shih YF (2007) Mechanical and thermal properties of wastewater bamboo husk fibre reinforced epoxy composites. Mater Sci Eng, A 445–446:289–295

Shukla DK, Kasisomayajula SV, Parameswaran V (2008) Epoxy composites using functionalized alumina platelets as reinforcements. Compos Sci Technol 68:3055–3063

Sonawane SH, Chaudhari PL, Ghodke SA et al (2009) Ultrasound assisted synthesis of polyacrylic acid–nanoclay nanocomposite and its application in sonosorption studies of malachite green dye. Ultrason Sonochem 16:351–355

Sultania M, Yadaw SB, Rai JSP et al (2010) Laminates based on vinyl ester resin and glass fabric: a study on the thermal, mechanical and morphological characteristics. Mater Sci Eng, A 527(18–19):4560–4570

Tserkia V, Zafeiropoulos NE, Simon F et al (2005) A study of the effect of acetylation and propionylation surface treatments on natural fibres. Composites A 36:1110–1118

Wu Y, Liang Y, Mei C et al (2022) Advanced nanocellulose-based gas barrier materials: present status and prospects. Chemosphere 286:131891

Ye Y, Chen H, Wu J et al (2007) High impact strength epoxy nanocomposites with natural nanotubes. Polymer 48:6426–6433

Zainuddin S, Hosura MV, Zhoua Y et al (2010) Experimental and numerical investigations on flexural and thermal properties of nanoclay–epoxy nanocomposites. Mater Sci Eng A 527:7920–7926

Zeng QH, Yu AB, Lu GQ et al (2005) Clay-Based polymer nanocomposites: research and commercial development. J Nanosci Nanotechnol 5:1574–1592

Zhao H, Li RKY (2008) Effect of water absorption on the mechanical and dielectric properties of nano-alumina filled epoxy nanocomposites. Composites A 39:602–611

Zhou T, Wang X, Mingyuan G et al (2008) Study of the thermal conduction mechanism of nano-SiC/DGEBA/EMI-2,4 composites. Polymer 49:4666–4672

Chapter 4
Materials Properties: Mechanical Characteristics

Abstract Cellulose-fibre-reinforced epoxy and vinyl-ester ecocomposites were fabricated in conjunction with inorganic nano-fillers. The effect of cellulose fibre and/or nano-filler dispersion on the mechanical properties of these composites has been characterized. The fracture surface morphology and toughness mechanisms were investigated by SEM. Results indicated that mechanical properties increased as a result of fibre and nano-filler additions. In particular, the presence of cellulose fibres significantly increased the mechanical properties of ecocomposites.

4.1 Cellulose Fibre/Epoxy Ecocomposites

(a)   Effect of fibre content on the mechanical properties
(i)   *Flexural stress–strain behaviour*

Figure 4.1 presents the stress–strain curve of selected RCF/epoxy specimens loaded with 19 and 46 wt% RCF. These composites generally display non-catastrophic fracture behaviour. Composites filled with low RCF loading show a linear behaviour at very low strain (0.003%), followed by a knee in the curve. After that a reduction in the modulus occurs and the composite fails at low stress. In contrast, composites filled with higher RCF loading show linear behaviour at higher strain (0.013%), followed by a slight reduction in slope until the composite fails at higher stress. This means that composites filled with higher RCF loading display higher flexural strength and modulus than composites filled with lower RCF loading. Moreover, the areas under the two curves give an indication that composites filled with higher RCF loading have higher toughness than those filled with lower RCF loading.

There are two failure modes which probably occur in the composite materials under three-point bending. One is called the flexural failure mode which exists at the upper and lower surface of the specimen. This type of failure happens when the specimen fails abruptly in a linear manner. The other type of failure is called the shear failure mode and occurs at the neutral axis of the specimen as a result of interlaminar
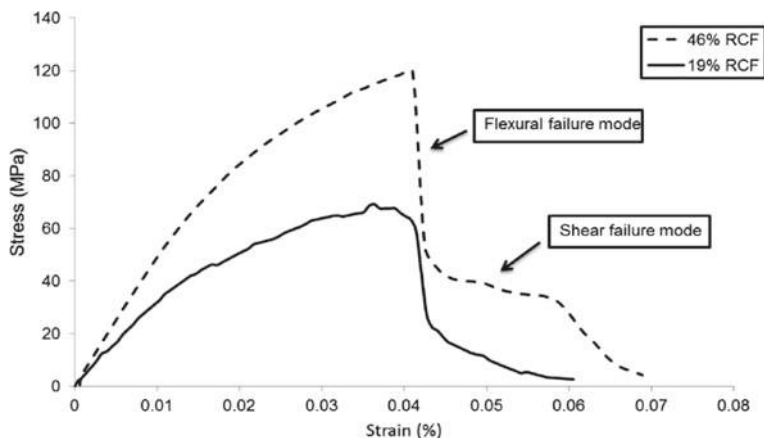
Fig. 4.1 Typical stress–strain curves of RCF/epoxy composites filled with 19 and 46 wt% RCF

stress. This failure happens when the specimen fails in more graceful manner and the slope of the curve decreases gradually to zero (Nassar et al. 2021). However, according to the stress–strain curves, the failure mode of the RCF-reinforced epoxy composites consists of both flexural and shear failure modes. The composites first fail in the flexural mode, followed by the shear failure mode. This means that the failure first occurs in the top and bottom RCF layers, then the interlaminar failure takes place in the neutral axis of the composites.

(ii)   *Flexural strength and modulus*

The effect of fibre content on flexural strength of dry RCF-reinforced epoxy composites is plotted in Fig. 4.2 (dark bars). At dry conditions, flexural strength is found to increase as fibre content increases. Flexural strength of neat epoxy increases by
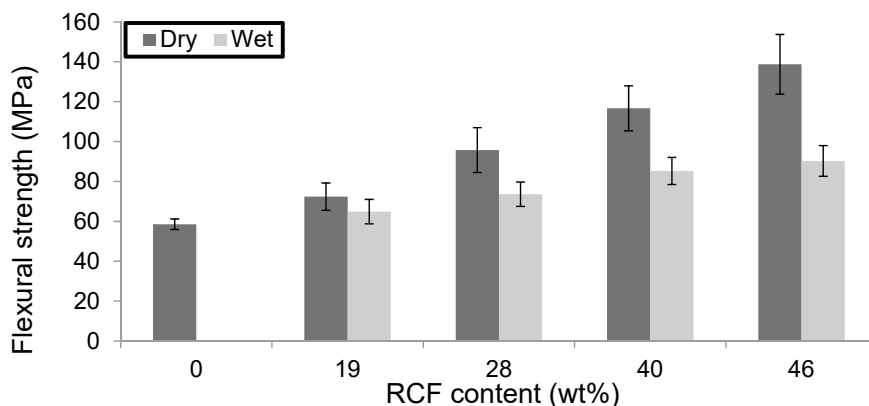

Fig. 4.2 Effect of fibre content on the flexural strength of dry and wet RCF/epoxy composites

23.6, 63.5, 99.4, and 137.1% after the addition of 19, 28, 40, and 46 wt% RCF, respectively. This enhancement in RCF/epoxy flexural strength is due to the ability of cellulose fibre in resisting the bending force. The lower flexural strength at lower RCF content may be attributed to the lower loads transferred from the matrix to the fibres, thus resulting in lower load carried by the fibres (Alonso-Montemayor et al. 2022). However, the significant increase in flexural strength at higher RCF content is due to the increase in stress transferred to the fibre as a result of the increased bonding at fibre–matrix interface. Le Guen and Newman (2007) investigated the flexural properties of pulped leaf fibre-reinforced epoxy composites where they reported an increase in both flexural strength and modulus as the fibre volume fraction increased.

Normally the strength of fibre-reinforced polymer composites increases as the fibre content increases. A maximum strength value is reached at a fibre volume fraction called the optimum or maximum fibre volume fraction. Any further increase in fibre content beyond the optimum fibre fraction can lead to a reduction in strength. This reduction in strength beyond the maximum fibre fraction is attributed to the lack of interfacial adhesion between the fibre and the matrix as a result of the increase in fibre–fibre interaction (Chai et al. 2021).

Rong et al. (2001) reported an overall enhancement in flexural strength and modulus of sisal/epoxy composites as fibre content increased up to ~75 vol%. Chai et al. (2021) reported that the ultimate flexural strength for date palm fibres/polyester composites was obtained at 9 wt% of fibre content. Adding more fibre caused a reduction in strength. Athijayamani et al. (2009) studied the flexural strength of roselle/sisal-reinforced polyester composites and they reported that flexural strength increased as fibre content increased from 10 to 30 wt%. Ruoyuan et al. (2010) reported that the maximum flexural strength and modulus of silk fibre-reinforced PBS composites occurred at fibre content 40 wt%. Further increase in fibre content led to reduction in both strength and modulus. They attributed the reduction in flexural properties to insufficient filling of PBS matrix into fibres.

The effect of moisture absorption on flexural strength is shown in Fig. 4.2 (light bars). Flexural strength for all samples decreases due to the water absorption. Comparing to dry samples, the percentages of reduction in flexural strength of samples loaded with 19, 28, 40, and 46 wt% RCF are 10.4, 23.1, 26.9, and 34.9%, respectively. This means that in wet condition flexural strength decreases progressively as fibre content increases due to an increase in moisture content (Athijayamani et al. 2009). The reduction in flexural strength of wet composites is mainly due to the reduction in bonding at the fibre–matrix interface, which results in lower stress transferred from the matrix to the fibres. Similar results were reported by Dhakal et al. (2007) and Athijayamani et al. (2009).

The flexural modulus versus fibre weight percentage for RCF/epoxy composites for dry and wet conditions is shown in Fig. 4.2. In the case of dry composites, flexural modulus shows similar trend to flexural strength. As fibre content increases, flexural modulus increases. The addition of 19 wt% of RCF increases flexural modulus by 262.1% compared to neat epoxy, while flexural modulus increased by 536.8% at 46 wt% of RCF. Significant increase in flexural modulus of plant fibre-reinforced

polymer composites was also reported by Rong et al. (2001), Dhakal et al. (2007), and Le Guen and Newman (2007). The influence of water absorption on flexural modulus of RCF/epoxy composites is seen in Fig. 4.3 where flexural modulus decreases as a result of water absorption and this reduction is most pronounced for composites with high cellulose-fibre content.

(iii)   *Fracture toughness*

The effect of cellulose-fibre content on facture toughness of dry RCF/epoxy is presented in Fig. 4.4 (dark bars). The addition of recycled cellulose fibre gradually
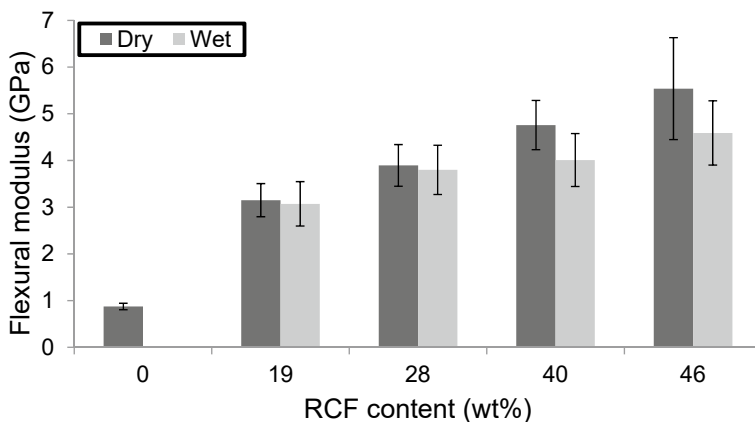

Fig. 4.3 Effect of fibre content on the flexural modulus of dry and wet RCF/epoxy composites
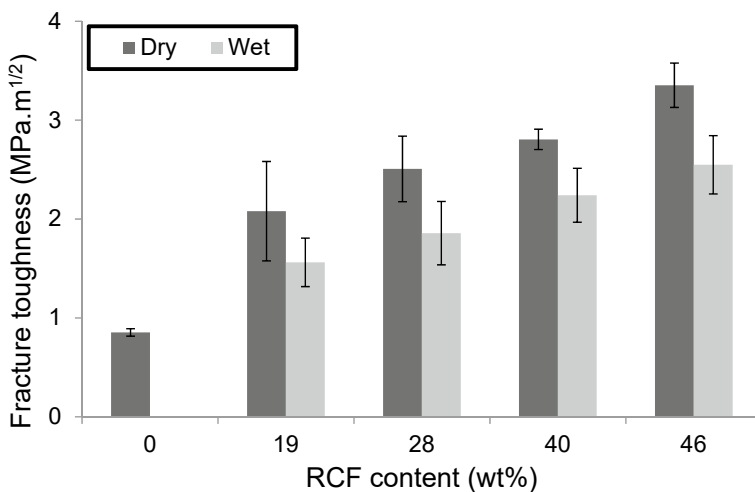

Fig. 4.4 Effect of fibre content on the fracture toughness of dry and wet RCF/epoxy composites

increases the fracture toughness of RCF/epoxy composites compared to neat epoxy. Cellulose fibres play a significant role in enhancing facture toughness of polymer matrixes through several energy absorbing events such as fibre pull-out, fibre fracture, and fibre bridging (Alamri and Low 2012a, b; Low et al. 2009). The fracture toughness of epoxy reinforced with 46% wt% RCF increases by a maximum 294.1% compared to neat epoxy. This significant enhancement in facture toughness at higher RCF content is due to the extensive fibre pull-outs, fibre fracture, and fibre bridging as can be seen in the SEM images shown later. Saber et al. (2021) reported that facture toughness of hemp and jute fibre-reinforced polyester composites increased as fibre volume fraction increased. In the present study, the values of fracture toughness of epoxy reinforced with 0, 19, 28, 40, and 46 wt% cellulose fibres are 0.85, 2.08, 2.51, 2.80, and 3.35 MPa m$^{1/2}$, respectively.

The effect of water absorption on fracture toughness of RCF/epoxy composites is shown in Fig. 4.4 (light bars). Generally, there is a reduction in fracture toughness due to moisture absorption. However, there is still a modest increase in fracture toughness as fibre content increases. Composites with higher fibre content in both dry and wet conditions display higher fracture toughness due to an increase in fibre pull-outs, fibre debonding, and fibre bridging, which in turn increase the resistance in crack propagation.

(iv) *Impact strength*

Impact strength is an essential property that gives an indication of the overall material toughness (Ruoyuan et al. 2010). Impact strength of fibre-reinforced polymer is governed by the matrix–fibre interfacial bonding, and properties of matrix and fibres. When the composites undergo a sudden force, the impact energy is dissipated by the combination of fibre pull-outs, fibre fracture, and matrix deformation (Wambua et al. 2003). Normally in fibre-reinforced polymer composites, impact strength increases as fibre content increases due to the increase in fibre pull-out and fibre breakage (Mishra et al. 2003).

The effect of fibre weight fraction for dry and wet RCF/epoxy composites is illustrated in Fig. 4.5. It can be observed that impact strength significantly increases as RCF content increases for both dry and wet composites. The presence of RCF layers in epoxy matrix increases the ability of these composites to absorb impact energy better than unreinforced polymer. In dry conditions, the addition of RCF with contents of 19, 28, 40, and 46 wt% increases impact strength compared to neat epoxy by 59.9, 132.8, 184.0, and 286.3%, respectively. Similarly, Wambua et al. (2003) reported that impact strength of kenaf-reinforced polypropylene composites increased as fibre weight fraction increased. Impact strength increased slightly as kenaf fibre content increased from 30 to 40 wt% then increased dramatically as kenaf fibre content increased from 40 to 50 wt%. However, Bledzki and Frauk (2004) reported a decrease in impact strength of wood fibre/polypropylene composites as fibre content increased from 40 to 60 wt%.

In wet conditions, impact strength generally increases as a result of water absorption for 2 weeks. This phenomenon is also observed by other researchers (Low et al. 2009; Kumar et al. 2022). Kumar et al. (2022) reported an increase in unnotched
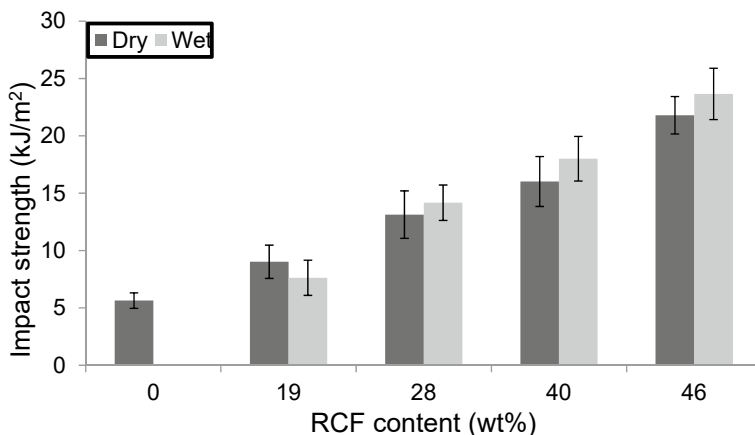
Fig. 4.5 Effect of fibre content on the impact strength of dry and wet RCF/epoxy composites

impact strength of jute fibre/polypropylene composites after immersing in water for 14 days. Similarly, Low et al. (2009) reported an enhancement in unnotched impact strength of cellulose-fibre-reinforced epoxy composites after soaking in sea water for 2 weeks.

(b)   SEM observation on facture surface

The SEM images in Fig. 4.6 show the typical fracture surfaces of RCF-reinforced epoxy composites loaded with fibre contents of 19, 28, 40, and 46 wt%. Generally, fibre pull-outs, fibre debonding, fibre breakage, and matrix fracture can be observed after the fracture test for all composites. Such toughness mechanisms can lead to increase in fracture properties of samples reinforced with RCF sheets. The effect of fibre content on the fracture surface is clearly seen in Fig. 4.6a–d. Composites filled with lower fibre content (19 and 28) wt% show an increase in matrix-rich regions compared to composites filled with higher fibre content. An increase in matrix-rich regions means that the matrix is not restrained by enough fibres (Sivaperumal and Jancirani 2021). In this case, there is insufficient fibre to carry the transferred load from the matrix. Therefore, composites exhibit highly localized strains at low stresses, which lead to low mechanical properties (Sivaperumal and Jancirani 2021).

However, images in Fig. 4.6c–d display fracture surface with higher fibre-rich regions of composites filled with 40 and 46 wt% RCF. An increase in fibre-rich regions means that the matrix is sufficiently restrained with fibres and the stress is more evenly distributed leading to increase in composite stiffness (Sivaperumal and Jancirani 2021). In this case, the stress is effectively transferred from the matrix to the fibres resulting in an increase in mechanical properties. Moreover, an increase in energy dissipation due to the increase in fibre fracture, fibre debonding, fibre pull-out, fibre bridging, and matrix deformation is observed for composites loaded with higher fibre content as shown in Fig. 4.6c–d. This confirms the increase in fracture toughness for these composites.
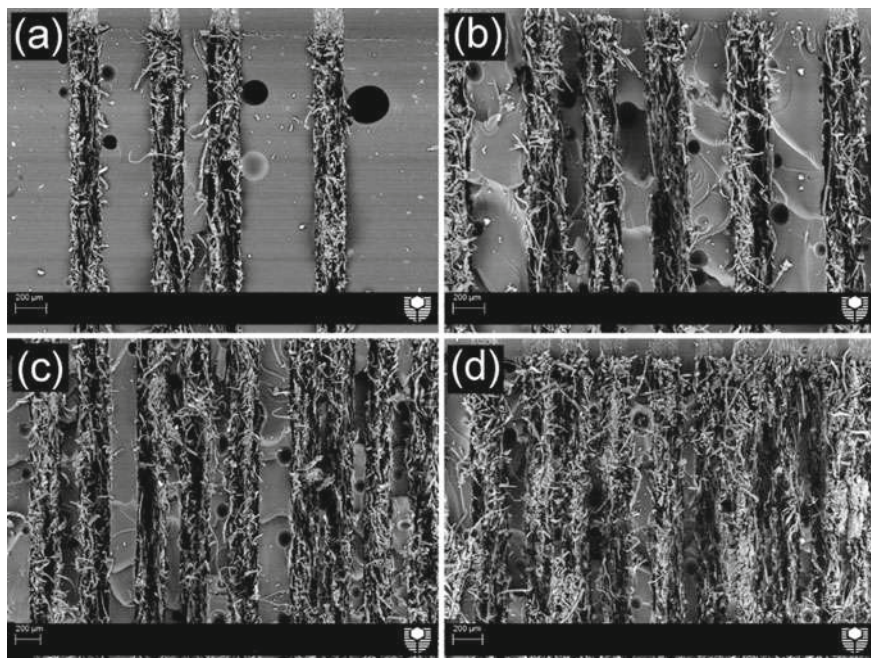
Fig. 4.6 SEM images of fracture surface of RCF/epoxy composites with fibre content of **a** 19 wt%, **b** 28 wt%, **c** 40 wt%, and **d** 46 wt%

Images in Fig. 4.7a–b show the high magnification images of the fracture surface of RCF/epoxy composites loaded with 28 and 46 wt% fibres. It can be observed that composites loaded with higher fibre content show better fibre–matrix interfacial bonding than those loaded with lower fibre content. Fibre debonding and gaps between fibres and matrix are more prevalent in composites with lower fibre content. This finding is an agreement with the result obtained by Pothan et al. (2003).
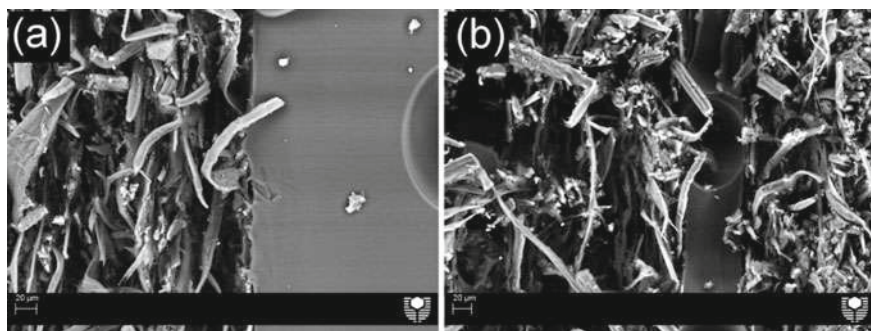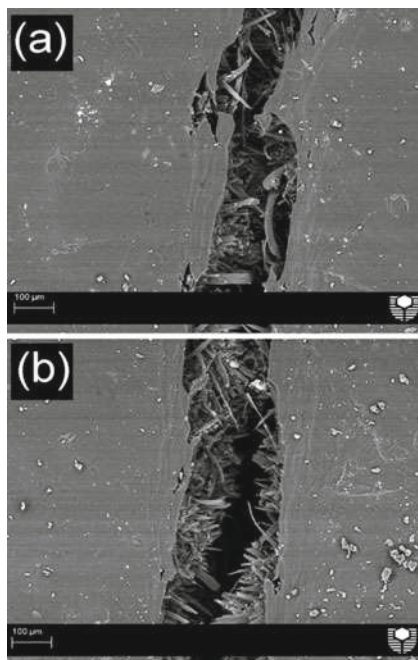

Fig. 4.7 High magnification SEM images of surface fracture of RCF/epoxy composites loaded with **a** 28 wt% RCF and **b** 46 wt% RCF

Fig. 4.8 SEM images of crack propagation in RCF/epoxy composites loaded with 46 wt% fibre showing characteristics of **a** crack bridging, and **b** fibre fracture and pull-outs

Images in Fig. 4.8a–b show the crack propagation in RCF/epoxy composites with 46 wt% fibre content. Extensive fibre fracture, fibre bridging, and matrix fracture can be clearly observed. Such fracture mechanisms lead to enhance the mechanical properties in the composites.

4.2 Nanoclay/Cellulose Fibre/Epoxy Eco-nanocomposites

(a)   Mechanical Properties

(i)   *Flexural strength*

In general, the incorporation of nanoclay platelets into epoxy matrix led to a modest enhancement in flexural strength for all nanocomposite samples as shown in Fig. 4.9a. The addition of 1 wt% nanoclay resulted in the highest flexural strength of all nanocomposite samples. The flexural strength of epoxy/nanoclay composites containing 1 wt% nanoclay was increased by 45.6% compared to neat epoxy. However, the addition of more clay caused a marked decrease in flexural strength. This can be due to the poor dispersion of the nanoclay in the epoxy resin at higher clay contents (Qi et al. 2006). At high concentration of clay, nanoclay platelet poorly dispersed inside the matrix forming platelet agglomerations which act as stress concentrators which in turn cause reduction in flexural strength. Zainuddin
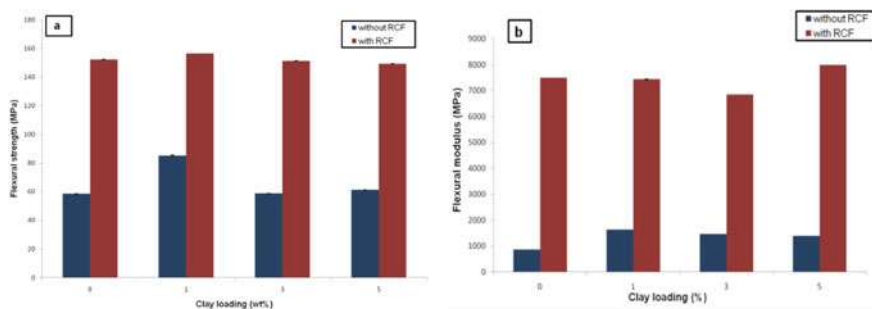
Fig. 4.9   **a** Flexural strength as a function of clay content for epoxy and its nanocomposites with and without RC; **b** Flexural modulus as a function of clay content for epoxy and its nanocomposites with and without RCF

et al. (2010) investigated the flexural properties of nanoclay–epoxy nanocomposites fabricated with 1–3 wt% loading of montmorillonite. Results showed that flexural strength was increased as a maximum up to 8.7% for samples reinforced by only 2 wt% of nanoclay over neat epoxy. Poor dispersion of nanoclay was thought to lead to poor mechanical properties. Moreover, it was observed in our study that the viscosity of the matrix increased as clay content increased, which allowed small air bubbles to be trapped in the resin during mixing process forming tiny voids in the sample. This in turn resulted in sample failure at relatively low stress. In contrast, with a lower loading of nanoclay, the potential of the formation of micro-voids is less, and the dispersion is more uniform which both lead to strength improvement (Xu and Hoa 2008).

The flexural strength of RCF-reinforced epoxy/clay nanocomposites is also shown in Fig. 4.9a. The presence of the RCF sheets has significantly improved the flexural strength for all samples. The flexural strength of neat epoxy increased from 58.5 to 152.3 MPa after the addition of RCF sheets. This enhancement in flexural properties is clearly due to the ability of recycled cellulose fibres to withstand bending force of the composites (Satapathy et al. 2010). The inclusion of 1 wt% nanoclay platelet to the RCF/epoxy composites was found to have positive effect on flexural strength.

However, adding more clay (i.e. 3 and 5 wt%) led to a slight reduction in flexural strength. Previous studies have shown enhancement in strength properties of fibre-based epoxy nanocomposites. Bozkurt et al. (2007) studied the mechanical properties of non-crimp glass fibre-reinforced layered clay/epoxy nanocomposites. They observed that flexural properties increased with the addition of clay due the enhancement in the interface between the glass fibre and epoxy matrix. In similar study, Zulfli and Shyang (2010) reported an improvement in flexural strength and modulus for glass fibre-reinforced epoxy/clay nanocomposites due to the addition of treated nanoclay. The presence of clay is believed to increase the interface between the glass fibre and epoxy matrix (Zulfli and Shyang 2010).

The flexural modulus can be used as an indicator of the stiffness of the materials in static bending condition. Figure 4.9b also shows the values of flexural modulus

for all samples. The addition of 1 wt% nanoclay in epoxy matrix has increased the flexural modulus by 87.6% over neat epoxy. In addition, the presence of RCF has a tremendous effect on flexural modulus for epoxy and its nanocomposites. Flexural modulus of epoxy was increased by about 760% after the addition of RCF sheet.

(ii)   *Fracture toughness*

The influence of nanoclay on fracture toughness of epoxy/nanoclay composites is shown in Fig. 4.10. The fracture toughness of neat epoxy and epoxy/clay nanocomposites reinforced with 0, 1, 3, and 5 wt% nanoclay was 0.85, 1.11, 0.93, and 0.97 MPa m$^{1/2}$, respectively. Once again, it was observed that reinforcement with 1.0 wt% of nanoclay could achieve better fracture properties with improvement reaching up to 30%. This enhancement in epoxy fracture toughness after adding nanoclay platelet is like the work of Kim et al. (2008) who reported that adding (0.5, 1.5, and 3 wt%) nanoclay platelets to epoxy matrix increased fracture toughness by about 20, 46, and 50%, respectively. However, Fig. 4.10 also shows that facture toughness of epoxy nanocomposites decreased slightly when more clay was added. It has been reported that poor dispersion of high content of nano-fillers leads to agglomeration which acts as a stress concentration that can initiate tiny cracks, which leads to crack propagation (Deng and Tang 2010).

The influence of RCF sheets on fracture toughness is clearly shown in Fig. 4.10. As expected, samples reinforced with RCF sheets showed a significant increase in fracture toughness in all samples. For example, the addition of RCF in epoxy resin increased the fracture toughness by about 350%. This extraordinary enhancement is due to the unique properties of cellulose fibre in resisting fracture which resulted in increased energy dissipation from crack deflection at the fibre–matrix interface, fibre debonding, fibre bridging, fibre pull-out, and fibre fracture. This result is supported by the work of Lui and Huges (2008) and Maleque and Belal (2007) where they reported an enhancement in fracture toughness when cellulose fibres were added to
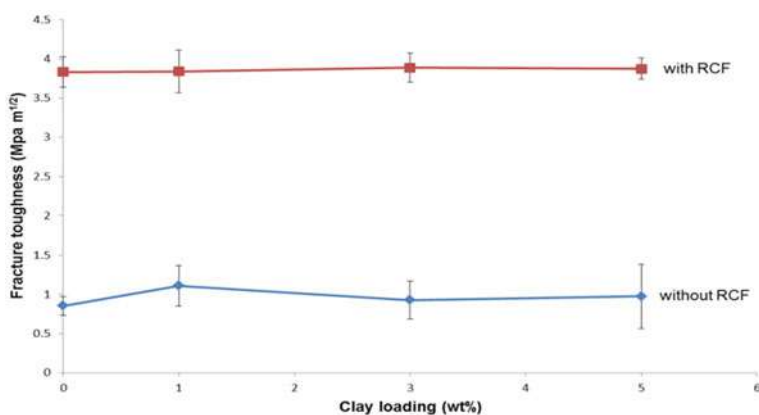

Fig. 4.10 Fracture toughness as a function of clay content for epoxy and its nanocomposites with and without RCF

epoxy matrix. The addition of nanoclay to the RCF/epoxy composites was found to have insignificant or negligible increase in fracture toughness. The fracture toughness for RCF/epoxy composite and RCF/epoxy nanocomposites reinforced with nanoclay loading 0, 1, 3, and 5 wt% was 3.8, 3.8, 3.9, and 3.9 MPa m$^{1/2}$, respectively. This result agrees with the work done by McGrath et al. (McGrath et al. 2004). They studied the mechanical properties of cellulose fibre/epoxy composites reinforced with kaolinite and micro-sized ZrO_2. It was found that fracture toughness increased with the addition of either kaolinite or ZrO_2 or both particles.

(iii)   *Impact strength*

Impact strength can be defined as the ability of the material to withstand impact loading. As shown in Fig. 4.11, the presence of nanoclay platelets slightly enhanced the impact strength for epoxy nanocomposites with maximum improvement reaching up to 22.45% at 5 wt% nanoclay loading. The impact strength of epoxy/clay nanocomposites increased as clay content increased. The impact strength of neat epoxy increased from 5.6 kJ/m^2 to 6.1, 6.9, and 6.9 kJ/m^2 after the addition of 1, 3, and 5 wt% of clay, respectively. Similarly, significant enhancement in impact strength was reported by Ye et al. (2007). Based on their observation, the addition of 2.3 wt% halloysite nanotubes (HNTs) could increase the impact strength of neat epoxy four times without affecting the flexural properties and thermal stability.

The presence of RCF significantly improved impact strength by approximately 444% over pure epoxy from 5.6 to 30.7 kJ/m^2. This huge achievement is because cellulose fibre has a better ability to absorb impact energy than unreinforced polymer. This result concurs with the work of Maleque and Belal (2007) where they investigated the mechanical properties of pseudo-stem banana fibre–epoxy composites and found that the presence of banana-woven fabric increased the impact strength over the neat epoxy by approximately 40%. However, the addition of nanoclay to RCF/epoxy composites showed two different scenarios. At low clay content (1 wt%),
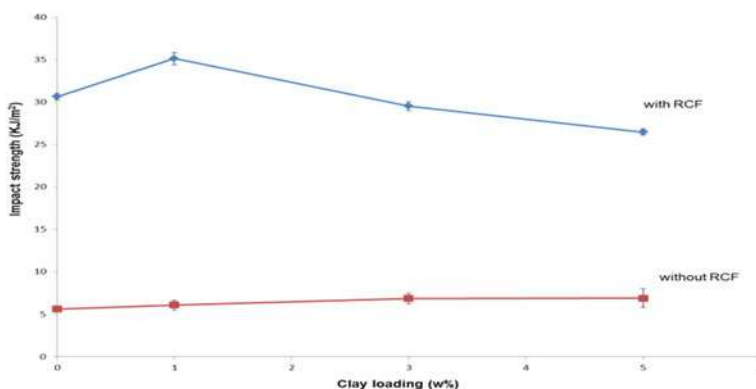

Fig. 4.11 Impact strength as a function of clay content for epoxy and its nanocomposites with and without RCF
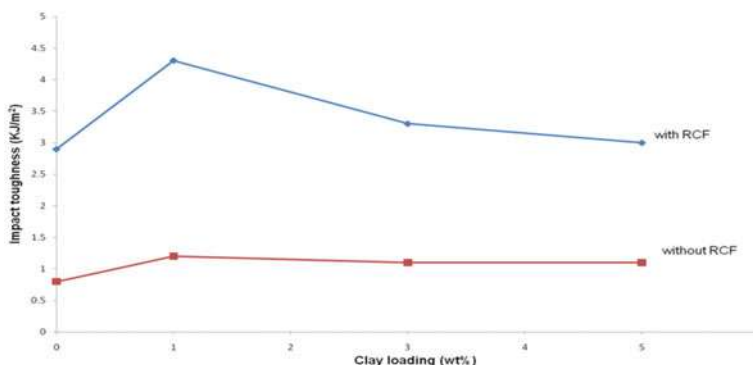
Fig. 4.12 Impact toughness as a function of clay content for epoxy and its nanocomposites with and without RCF

the impact strength of neat epoxy increased by 15% from 30.7 to 35.2 kJ/m^2. But as clay loading increased, the impact strength significantly decreased with 3.7 and 13.7% reduction at clay contents 3 and 5 wt%, respectively, compared to neat epoxy. This reduction in impact strength at higher clay loading was due to the formation of clay agglomerates and voids as a result of increased system viscosity due to the presence of nanoclay which in turn reduced the fibre–matrix adhesion (Khan et al. 2010).

(iv)   *Impact toughness*

The impact toughness in terms of energy release rate (G_{IC}) of epoxy/clay nanocomposites and RCF/epoxy/clay nanocomposites has been shown in Fig. 4.12. Several interesting characteristics are noteworthy. Firstly, the presence of RCF significantly enhanced the impact toughness of epoxy matrix. The impact toughness for pure epoxy and RCF-reinforced epoxy are 0.8 and 2.9 kJ/m^2, respectively. This result indicates that recycled cellulose fibres improved the impact toughness of the pure epoxy material by approximately 262.5%. This extraordinary enhancement in toughness properties as discussed before is because RCF displays a variety of fracture mechanisms in the crack path to resist crack propagation. These fracture mechanisms include fibre breakage, fibre pull-out, fibre debonding, and fibre bridging which require high energy to be absorbed. This may explain why composites reinforced by RCF displayed higher toughness. Secondly, the addition of nanoclay in different concentration to the RCF/epoxy composites increased the impact toughness by 48.3, 13.8, and 3.5% at clay loading 1, 3, and 5 wt%, respectively. Once again and like the impact strength behaviour, impact toughness displayed maximum value at 1 wt% nanoclay load which then dramatically decreased as clay contents increased.

Lastly, quite good improvements in impact toughness were observed for epoxy nanocomposites without RCF reinforcement. The incorporation of 1, 3, and 5 wt% nanoclay increased impact toughness of neat epoxy by 50, 37.5, and 37.5%, respectively. An increase in impact toughness of epoxy due to the addition of nano-filler

was also reported by Ma et al. (2008) where they found that the inclusion of silica nanoparticles increased the toughness properties in terms of energy release rate (G_{1C}) of epoxy system by 81% at 20 wt% silica load. In general, the enhancement in toughness properties as was observed by number of studies for polymers reinforced with nano-fillers was due to several toughness mechanisms for dissipating energy such as crack pinning, particle debonding, plastic void growth, plastic deformation, and particle pull-out (Ma et al. 2008; Zhao et al. 2008; Wetzel et al. 2006; Tang et al. 2011; Chen et al. 2008).

(v)   *Failure Micromechanisms and Energy Dissipative Processes*

The fracture surfaces of pure epoxy and epoxy nanocomposites reinforced with 1 and 5 wt% nanoclay are shown in Fig. 4.13. As a result of adding nanoparticles, epoxy/clay nanocomposites display a rougher fracture surface than that of neat resin. An increase in fracture surface roughness can be used as indicator to the presence of crack pinning mechanisms, which increase fracture toughness by increasing crack
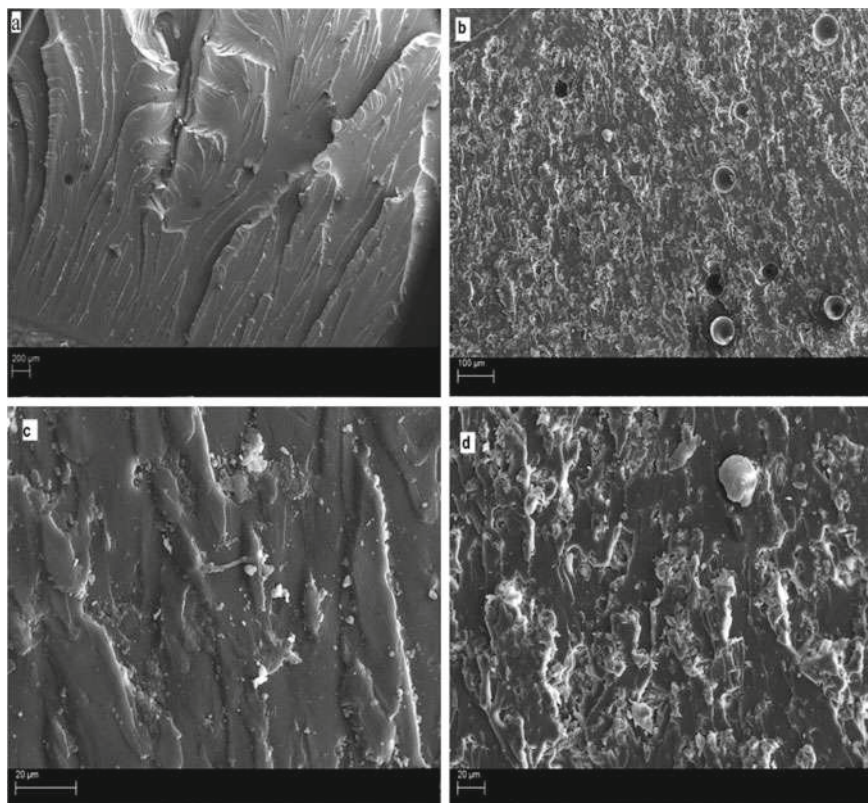

Fig. 4.13 Scanning electron micrographs after fracture toughness testing for: low magnification **a** PE; **b** PE/30B5 and high magnification; **c** EP/30B1; and **d** EP/30B5

propagation length during deformation (Zhao et al. 2008; Wetzel et al. 2006; Tang et al. 2011). On the other hand, the fracture surface of pure epoxy was very smooth and featureless, which indicates typical brittle fracture behaviour with lack of significant toughness mechanisms (Tang et al. 2011). Figure 4.13c–d shows high magnification SEM micrograph of fracture surface for epoxy-reinforced with 1 and 5 wt% nanoclay platelets, respectively. A variety of possible toughness mechanisms such as crack pinning, particle debonding, plastic void growth, plastic deformation, and particle pull-out can be observed. Such toughness mechanisms can lead to higher fracture toughness properties through resisting crack propagation (Ma et al. 2008; Zhao et al. 2008; Wetzel et al. 2006; Tang et al. 2011; Chen et al. 2008).

Figure 4.14 shows the SEM micrographs of the fracture surface for RCF/epoxy composite and RCF/epoxy nanocomposites reinforced with 1 and 5 wt% clay after fracture toughness test. A variety of toughness mechanisms such as shear deformation, crack bridging, fibre pull-out and fibre fracture and matrix fracture can be clearly observed which impart good fracture properties of samples reinforced by RCF. It can be seen from Fig. 4.14e–f that the sample of RCF mat composite didn't completely break into two pieces. This is because fibres bridge the cracks and enhance the crack propagation resistance which led to improvement in fracture toughness. It also can be observed that the adhesion between the fibre and the matrix is quite good. These super toughness mechanisms of RCF were the major factor of increasing mechanical properties of samples reinforced with RCF when compared to samples without RCF.

4.3 Nano-SiC/Cellulose Fibre/Epoxy Eco-nanocomposites

(a)   Flexural strength and modulus

Figures 4.15 and 4.16 illustrate the effect of n-SiC particles on the flexural strength and modulus of epoxy nanocomposites. Both flexural strength and modulus increase due to the presence of n-SiC particles. Flexural strength of epoxy increases by a maximum 21.5% with the addition of only 1 wt% n-SiC. The enhancement in flexural strength may be ascribed to the good dispersion of n-SiC particles into the matrix, which increases matrix/n-SiC interaction surface providing good stress transferring from the matrix to the nano-fillers resulting in an improvement in sample strength properties. However, with further n-SiC loading (3 and 5%), flexural strength tends to decrease to values less than pure epoxy. The reason could be due to high concentration of n-SiC, n-SiC particles poorly dispersed inside the matrix forming particles agglomerations, which could weaken the adhesion strength between the matrix and the filler (Qi et al. 2006; Zainuddin et al. 2010; Xu and Hoa 2008). Besides, these agglomerations may act as stress concentrators, which in turn cause reduction in flexural strength (Qi et al. 2006; Zainuddin et al. 2010; Xu and Hoa 2008). Zainuddina et al. (2010) investigated the flexural properties of epoxy/clay nanocomposites. Nanocomposites were fabricated with 1–3 wt% loading of montmorillonite-layered silicate via magnetic stirring mixing for 5 h. Result showed that flexural strength
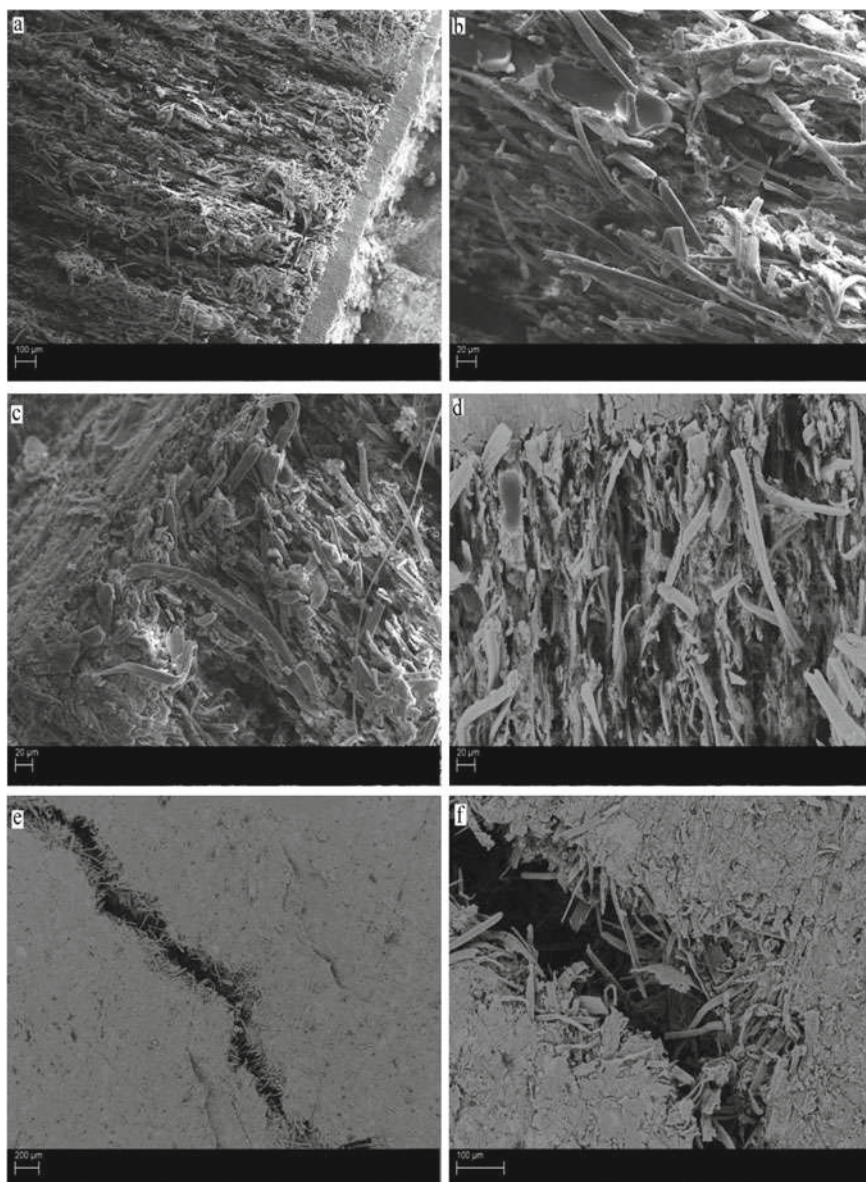
Fig. 4.14 SEM micrographs of facture surface: **a** PE/RCF low magnification, **b** PE/RCF high magnification, **c** PE/RCF/30B1, **d** PE/RCF/30B5, **e** crack propagation (low magnification), and **f** crack propagation (high magnification)
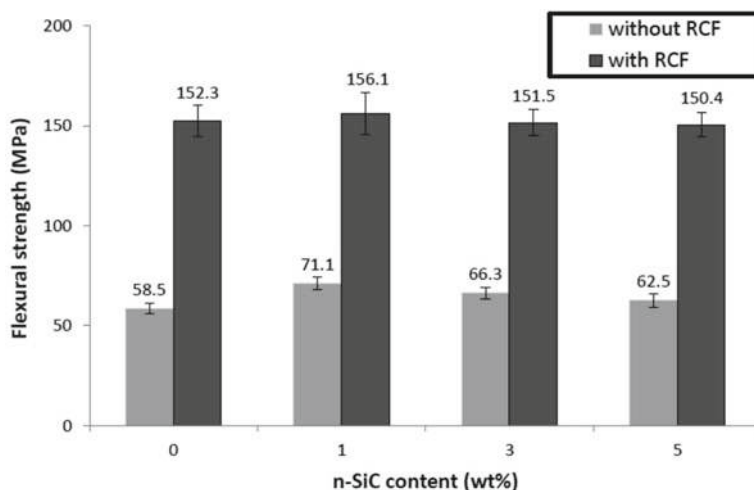
Fig. 4.15 Flexural strength as a function of n-SiC content in unfilled composites and RCF-filled composites
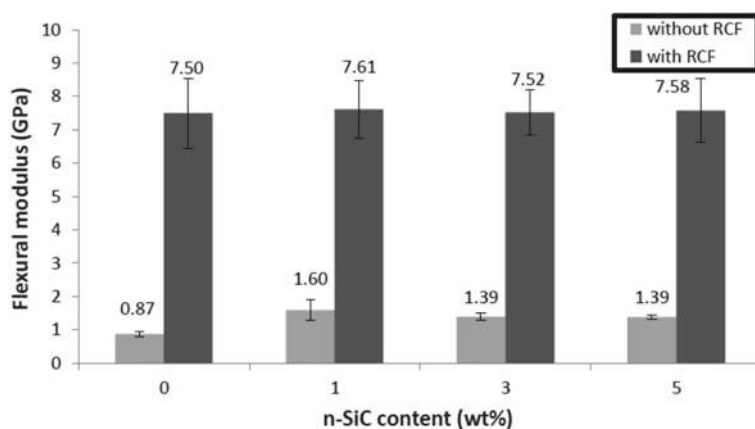
Fig. 4.16 Flexural modulus as a function of n-SiC content in unfilled composites and RCF-filled composites

was increased by a maximum up to 8.7% for samples reinforced with only 2 wt% of nanoclay compared to neat epoxy. Authors stated that poor dispersion of nanoclay led to poor mechanical properties (Zainuddin et al. 2010). Flexural modulus of epoxy nanocomposites is demonstrated in Fig. 4.16. Flexural modulus has similar trend to flexural strength values. The addition of (1, 3, and 5) wt% n-SiC significantly increases the modulus of epoxy system by 83, 59.2, and 58.9%, respectively. This expected result is due to the fact that n-SiC particles have higher modulus than epoxy

resin. Therefore, the presence of these rigid particles into the epoxy matrix increases the modulus of epoxy nanocomposites when compared to neat resin (Ma et al. 2008).

The flexural strength of RCF-reinforced n-SiC/epoxy nanocomposites is shown in Fig. 4.15. The presence of the RCF layers significantly improved the flexural strength for all kinds of samples. The flexural strength of the neat epoxy resin increases from 58.5 to 152.3 MPa after the addition of RCF layers with enhancement reaches up to 160%. This enhancement in flexural properties is due to the advantages of recycled cellulose fibres in resisting bending force of the composites (Satapathy et al. 2010). In the case of RCF-reinforced n-SiC/epoxy nanocomposites, the insertion of 1 wt% n-SiC slightly increases the flexural strength of RCF/epoxy composites. However, adding more SiC (3 and 5 wt%) lead to an insignificant reduction in strength. These results agree with those obtained by Satapathy et al. (2010) in their study on the influence of SiC particles derived from rice husk on flexural strength of jute/epoxy composites. Flexural strength was found insignificantly decreased after adding 10 and 20 wt% of SiC particles (Satapathy et al. 2010). The presence of RCF into epoxy matrix significantly increases the flexural modulus by about seven times compared to neat epoxy. Adding n-SiC particles to the RCF/epoxy slightly increases flexural modulus (Fig. 4.16).

(b)   Impact strength and toughness

The impact strength of epoxy nanocomposites and RCF-reinforced epoxy nanocomposites is plotted in Fig. 4.17. The presence of n-SiC particles increases the impact strength for epoxy nanocomposites with maximum improvement 35.5% at 5 wt% n-SiC load. The impact strength of neat epoxy increases from 5.6 kJ/m^2 to 7.5, 7.0, and 7.6 $^{kJ}/m^2$ after the addition of 1, 3, and 5 wt% of n-SiC, respectively. Similar significant enhancement in impact strength was reported by Lu et al. (2009). They investigated the mechanical properties of hybrid epoxy/SiO_2 nanocomposites. It was

Fig. 4.17 Impact strength as a function of n-SiC content in unfilled composites and RCF-filled composites

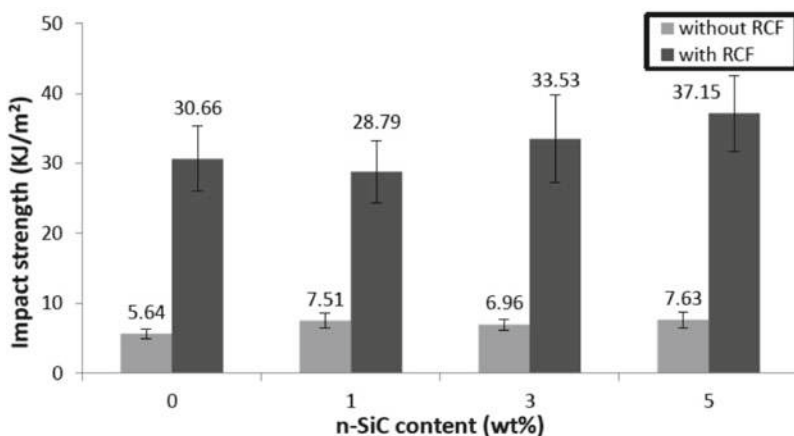found that impact strength for nanocomposites filled with 2 wt% SiO_2 increased by maximum 43.3% when compared to neat epoxy. However, adding more SiO_2 content (2.5 and 3) wt% caused impact strength to decrease due to the poor dispersion of SiO_2 particles at higher filler content. As illustrated in Fig. 4.17, the presence of RCF significantly improves impact strength by approximately 444% over pure epoxy from 5.6 to 30.7 kJ/m^2. This great achievement is because cellulose fibre has a better ability to absorb impact energy than unreinforced polymer. This result agrees with the work of Maleque and Belal (2007). They studied the mechanical properties of pseudo-stem banana fibre–epoxy composites and found that the presence of banana-woven fabric increased the impact strength over the neat epoxy by approximately 40%. The effect of the addition of n-SiC on impact strength properties of RCF/epoxy nanocomposites is shown in Fig. 4.17. Impact strength of n-SiC-filled RCF/epoxy nanocomposites increases as n-SiC loading increases. The impact strength of RCF/epoxy displays a maximum increase of 21% with only 5 wt% of n-SiC particles. This can be explained; it was observed an increase in n-SiC clusters into epoxy nanocomposites due to the increase in n-SiC loading as seen in Fig. 4.14a–c. These clusters may act as crack stoppers and increase the ability of the material to absorb energy by forming tortuous pathways for crack propagation, resulting in the impact strength to increase (Deng et al. 2009).

The impact toughness in terms of the energy release rate (G_{1C}) for n-SiC/epoxy nanocomposites is illustrated in Fig. 4.18. Impact toughness gradually increases as the n-SiC content increases yielding a maximum at 5 wt% n-SiC load. The addition of 1, 3, and 5 wt% n-SiC into epoxy matrix significantly enhances impact toughness by 25.0, 50.0, and 62.5% over neat epoxy, respectively. This remarkable enhancement in toughness properties for nanocomposites is due to several toughness mechanisms for dissipating energy such as crack pinning, particle debonding, plastic void growth, plastic deformation, and particle pull-out as has been reported by number of studies for polymers reinforced with nano-fillers (Ma et al. 2008; Zhao et al. 2008; Wetzel
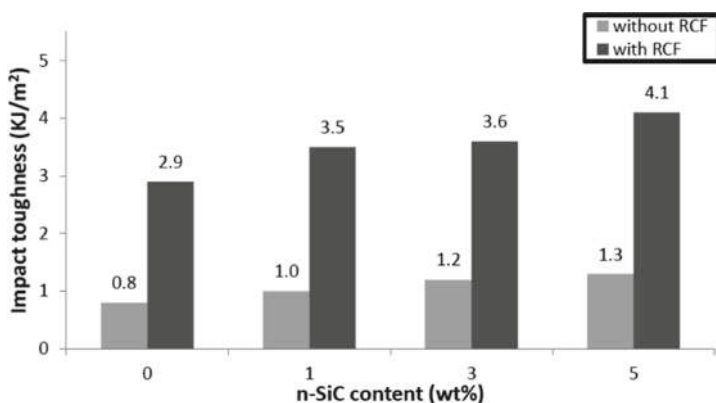

Fig. 4.18 Impact toughness as a function of n-SiC content in unfilled composites and RCF-filled composites

et al. 2006; Tang et al. 2011; Chen et al. 2008). Ma et al. (2008) reported an increase in impact toughness of epoxy system due to the addition of nano-filler. Authors found that the inclusion of silica nanoparticles increased the toughness properties in terms of energy release rate (G_{1C}) of epoxy system by 81% at 20 wt% silica loads. In the case of RCF/epoxy nanocomposites, the inclusion of RCF layers into epoxy resin remarkably enhances the impact toughness by about 262.5%. This extraordinary enhancement in toughness properties is because RCF displays a variety of fracture mechanisms in the crack path to resist crack propagation (Low et al. 2009). These fracture mechanisms such as fibre breakage, fibre pull-out, fibre debonding, and fibre bridging require high energy to be absorbed. The presence of n-SiC particles into RCF/epoxy increases impact toughness by 10.3, 24.1, and 27.6% at (1, 3, and 5) wt% n-SiC load, respectively. The extra improvement in impact toughness for RCF-based nanocomposites is due to the participation of n-SiC in resisting the crack growth.

(c)   Fracture toughness

The influence of n-SiC particles on fracture toughness of epoxy/n-SiC composites is shown in Fig. 4.19. Fracture toughness increases due to the presence of n-SiC particles. The addition of only 1 wt% n-SiC significantly increases facture toughness by a maximum of 89.4% compared to neat epoxy. However, fracture toughness tends to decline as n-SiC content increases to (3 and 5) wt%. This could be due to the poor dispersion of n-SiC and forming particle agglomeration at higher filler content as can be seen in Fig. 4.14a–c (Deng et al. 2009). This significant enhancement in fracture toughness is like the work of Chen et al. (2008). They found that the addition of (1 and 5) wt% of nano-silica to epoxy matrix increased fracture toughness by about 30%. However, adding more silica (10 wt%) led to decrease in toughness.

The effect of RCF layers on fracture toughness is clearly shown in Fig. 4.19. As expected, samples reinforced with RCF layers show a significant increase in fracture
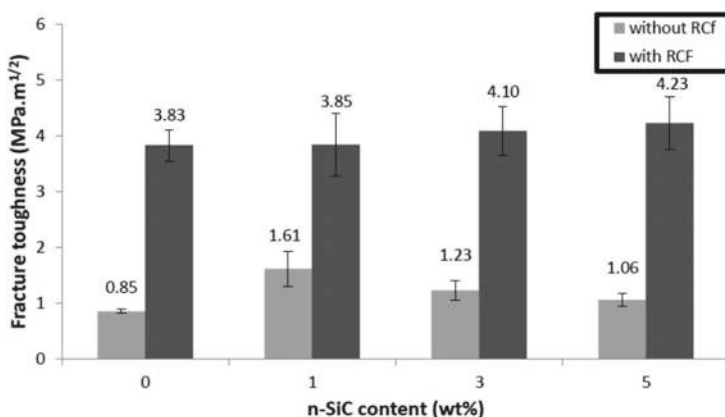

Fig. 4.19   Fracture toughness as a function of n-SiC content in unfilled composites and RCF-filled composites

toughness in all samples. For example, the addition of RCF in epoxy resin increased fracture toughness by about 350%. This extraordinary enhancement as can be seen later in Fig. 4.21 is due to the unique properties of cellulose fibre in resisting fracture, which resulted in increased energy dissipation from crack deflection at the fibre–matrix interface, fibre debonding, fibre bridging, fibre pull-out, and fibre fracture (Low et al. 2009). This result is supported by the work of Lui and Huges (2008) and Maleque and Belal (2007). They reported an enhancement in fracture toughness when cellulose fibre was added to epoxy matrix. In the case of epoxy eco-nanocomposites, the addition of n-SiC to the RCF/epoxy composites gradually increases the fracture toughness for all n-SiC-filled RCF/epoxy samples. Fracture toughness of RCF/epoxy reinforced with 5 wt% n-SiC increases by maximum 10% over unfilled RCF/epoxy samples. This reveals that fracture toughness in RCF/epoxy eco-nanocomposites is mostly dominated by recycled cellulose fibres with slight effect of n-SiC particles.

(d)   Failure micromechanisms

The fracture surfaces of pure epoxy and epoxy nanocomposites reinforced with 1 and 5 wt% n-SiC particles are shown in Fig. 4.20. It can be seen from Fig. 4.20a that the fracture surface of pure epoxy is very smooth and featureless, which indicates typical brittle fracture behaviour with lack of significant toughness mechanisms (Tang et al. 2011). However, epoxy/n-SiC nanocomposites show rougher fracture surfaces than
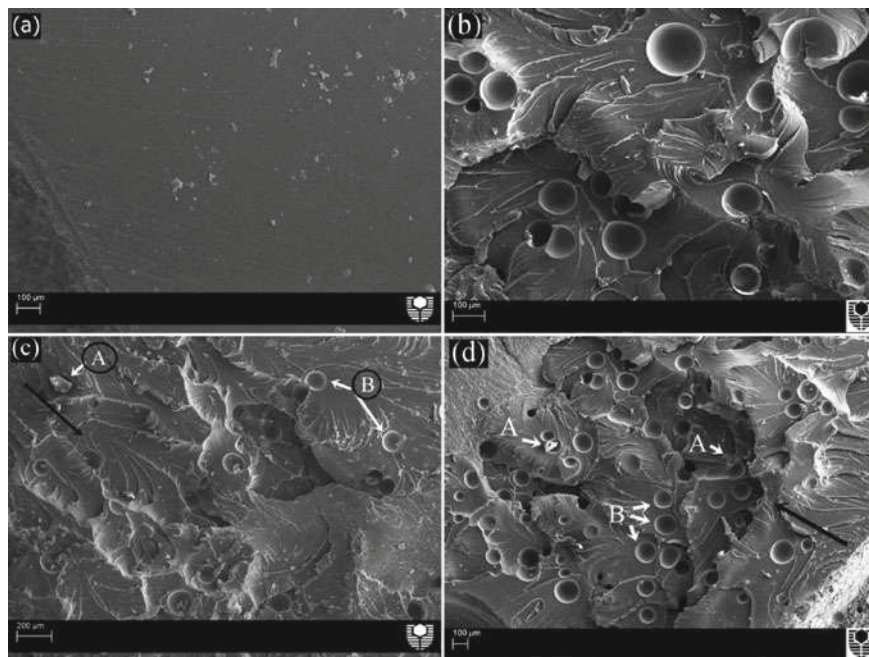

Fig. 4.20 Scanning electron micrographs showing the fracture surfaces of: **a** PE; **b** PE/SiC5 (high magnification); **c** PE/SiC1; and **d** PE/SiC5 [Legend: A = n-SiC clusters and B = voids]

that of neat resin because of the addition of nano-fillers as can be seen in Fig. 4.20c–d.
An increase in fracture surface roughness can be used as indicator to the presence of
crack pinning mechanisms, which increase fracture toughness by increasing crack
propagation length during deformation (Zhao et al. 2008; Wetzel et al. 2006; Tang
et al. 2011). Figure 4.20b shows high magnification SEM micrograph of fracture
surface for epoxy reinforced with 5 wt% n-SiC particles. Several possible toughness
mechanisms such as crack pinning, particle debonding, plastic void growth, plastic
deformation, and particle pull-out can be observed. Such toughness mechanisms
can lead to higher fracture toughness properties through resisting crack propagation
(Ma et al. 2008; Zhao et al. 2008; Wetzel et al. 2006; Tang et al. 2011; Chen et al.
2008). Moreover, particles agglomerations and voids in micro-scale are observed for
epoxy/n-SiC nanocomposites. Samples with 5 wt% n-SiC show increase in particle
agglomerates and voids than samples filled with 1 wt% n-SiC. This result agrees
with TEM results.

 Figure 4.21a, b illustrates low magnification image of RCF/epoxy sample and
RCF/epoxy filled with 1 wt% n-SiC, while Fig. 4.21c, d shows high magnification
image of same samples. A variety of toughness mechanisms such as shear defor-
mation, crack bridging, fibre pull-out and fibre fracture and matrix fracture can be
clearly observed, which lead to good fracture properties of samples reinforced by
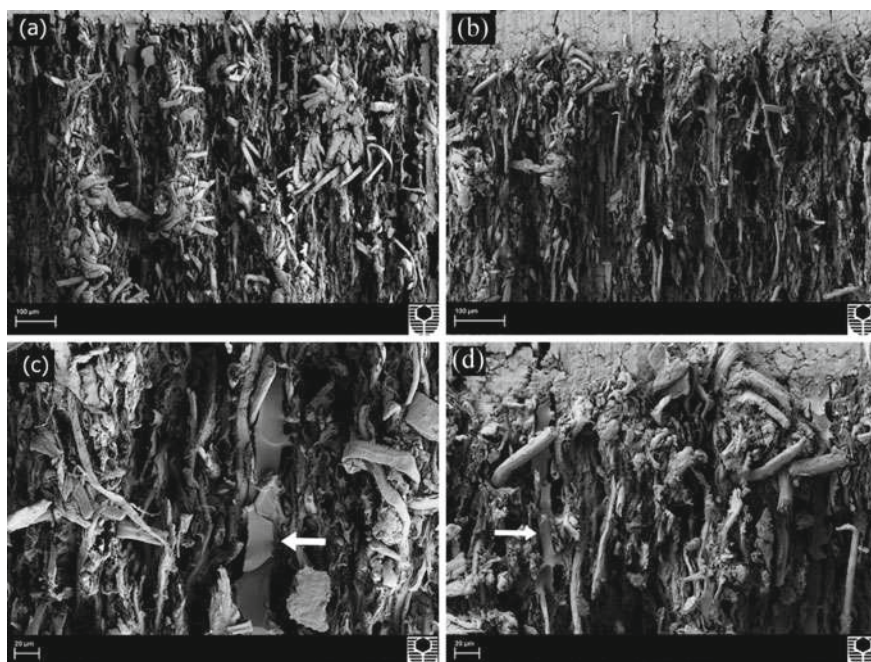

Fig. 4.21 Scanning electron micrographs showing the fracture surfaces of: **a** PE/RCF; **b**
PE/RCF/SiC1; **c** PE/RCF (high magnification); and **d** PE/RCF/SiC1 (high magnification) [the white
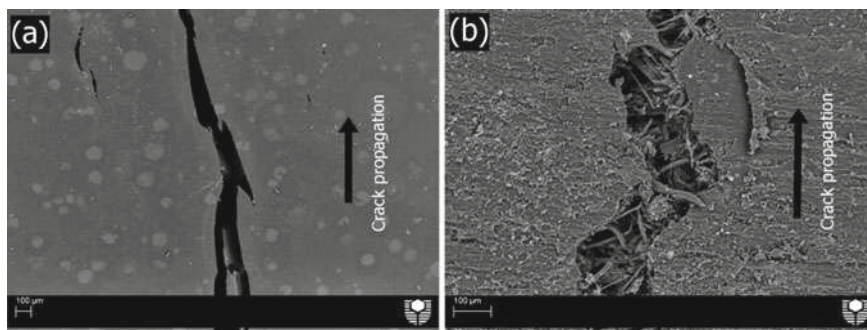arrow indicates the matrix]

Fig. 4.22 Scanning electron micrographs showing the crack propagation behaviour in: **a** PE/SiC1 and **b** PE/RCF/SiC1

RCF layers. Figure 4.22a, b displays the back-scattered SEM images of crack propagation in epoxy/n-SiC and RCF/epoxy/n-SiC nanocomposites filled with 1% wt n-SiC. It is observed that samples reinforced with RCF layers didn't completely break into two pieces. This is because fibres bridge the cracks and enhance the crack propagation resistance, which lead to improvement in fracture toughness. The tortuous pathway for the crack propagations indicates the high energy absorbance by the RCF sheets. These super toughness mechanisms of RCF are the major factors of increasing mechanical properties of samples reinforced with RCF when compared to samples without RCF.

4.4 Nano-filler/Epoxy Nanocomposites

(a) Flexural strength and modulus

Table 4.1 summarizes the flexural strength and modulus of nano-filler-reinforced epoxy nanocomposites in both dry and wet conditions. In general, water absorption has a negative influence on flexural strength and modulus of epoxy-based nanocomposites. Flexural strength of unmodified epoxy and modified epoxy-based nanocomposites decreases after subjecting to water compared to dry nanocomposites. This reduction in flexural strength can be attributed to the plasticization effect of water absorption in epoxy matrix. This can lead to reduction in the interfacial strength between the epoxy and reinforcing particles resulting in drop in flexural strength values (Lee et al. 2010). For example, the flexural strength of water-absorbed epoxy decreases by 12.2% compared to epoxy in dry condition. In the case of nanoclay/epoxy nanocomposites, the flexural strengths of wet specimens filled with 1, 3, and 5 wt% nanoclay decrease by 38.3, 10.3, and 13.4%, respectively, compared to nanoclay-filled epoxy in dry condition. Similarly, for HNT/epoxy nanocomposites, the flexural strengths of wet specimens modified with 1, 3, and 5 wt% HNT decrease

**Table 4.1** Flexural strength and modulus of epoxy and its nanocomposites before and after water treatment

Samples	Before placing in water		After placing in water	
	Flexural strength (MPa)	Flexural modulus (GPa)	Flexural strength (MPa)	Flexural modulus (GPa)
Epoxy	58.5 ± 2.6	0.9 ± 0.1	51.4 ± 3.1	0.7 ± 0.2
+1% nanoclay	85.2 ± 2.5	1.6 ± 0.4	52.6 ± 4.3	1.3 ± 0.2
+3% nanoclay	58.7 ± 3.9	1.5 ± 0.1	52.7 ± 4.3	1.3 ± 0.2
+5% nanoclay	61.2 ± 3.5	1.4 ± 0.2	53.0 ± 3.9	1.3 ± 0.2
+1% HNT	70.7 ± 6.2	1.5 ± 0.2	55.8 ± 6.5	1.4 ± 0.2
+3% HNT	68.2 ± 8.1	1.3 ± 0.1	52.5 ± 4.9	1.3 ± 0.2
+5% HNT	64.5 ± 4.7	1.4 ± 0.1	53.1 ± 3.5	1.4 ± 0.2

by 21.1, 23.0, and 17.6%, respectively, compared to dry HNT-filled epoxy. Furthermore, for n-SiC/epoxy nanocomposites, the flexural strengths of wet specimens filled with 1, 3, and 5 wt% n-SiC decrease by 15.9, 14.8, and 12.0%, respectively, in comparison to n-SiC-filled epoxy. Several studies have reported reduction in flexural strength of epoxy-based nanocomposites due to water absorption. For instance, Abacha et al. (2007) reported a decrease in flexural strength and modulus of clay/epoxy nanocomposites due to the water absorption. Buehler and Seferis (2000) also reported a drop in flexural strength values of carbon fibre/epoxy and glass fibre/epoxy composites as a result of moisture absorption.

The effect of nano-fillers on enhancing the flexural strength of wet epoxy matrix was investigated and compared to neat epoxy in wet condition. Table 4.1 shows no significant change in flexural strength due to the presence of nanoclay. For example, the flexural strength increases by 2.2 and 3.0% after the addition of 1 and 5 wt% nanoclay, respectively. For HNT/epoxy nanocomposites, maximum flexural strength (about 8.5% over neat epoxy) is obtained at 1 wt% HNT loading. Similarly, the addition of 1 wt% n-SiC increases flexural strength by 16.3% over unmodified wet epoxy. The increase in flexural strength of water-treated nanocomposites after the addition of nano-fillers can be attributed to the enhancement in the interfacial bonding between the filler and the matrix, thus increasing the surface area of matrix/filler interaction. As a result, this leads to good stress transfer from the matrix to the nano-fillers, thus resulting in improved flexural strength. In a similar study, Hossain et al. (2011) investigated the effect of nanoclay on the flexural strength of carbon fibre-reinforced epoxy composites after immersing in sea water for 30, 60, and 180 days. Their results showed that flexural strength increased due to the presence of nanoclay.

However, the decrease in flexural modulus is more expressed for nanocomposites filled with nanoclay than other nanocomposites. The reduction in flexural modulus can be attributed to the plasticization effect of water absorption on the epoxy matrix (Zhao and Li 2008). DSC analysis was conducted on neat epoxy before and after water treatment to evaluate the effect of water absorption on T_g. Figure 4.23 shows

Fig. 4.23 The DSC curves of neat epoxy before and after water treatment
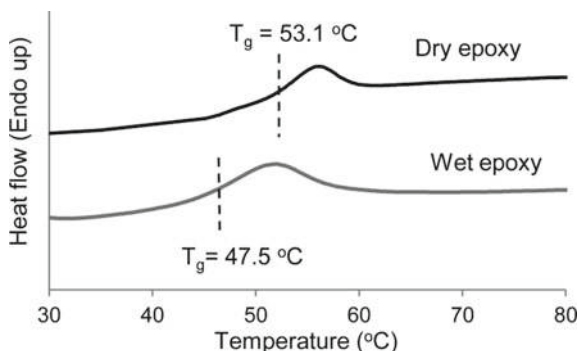
that T_g significantly decreased from 53.1 to 47.5 due to the plasticization effect of absorbed water. Similar observation was obtained by Zhao and Li (2008).

In the case of wet nanocomposites, the addition of nano-fillers increases the flexural modulus for all types of nanocomposites. The flexural modulus of epoxy modified with 1 wt% of nanoclay, HNT, and n-SiC increases by 80.7, 89.5, and 98.2%, respectively, as compared to wet unmodified epoxy. The enhancement in flexural modulus can be due to the presence of rigid fillers that have higher modulus than epoxy matrix (Alamri and Low 2012a). Any further increase in fillers loading shows slight decrease in the modulus values. The reduction in flexural modulus due to the water absorption was also observed in several studies. Hossain et al. (2011) observed a reduction in flexural modulus of carbon fibre/epoxy composites filled with nanoclay after immersing in water for 180 days. However, the addition of nanoclay increased flexural modulus of nanoclay-filled composites in wet condition compared to unfilled composites. Buehler and Seferis (2000) found that flexural modulus of carbon fibre/epoxy and glass fibre/epoxy composites decreased after water absorption.

(b)   Fracture toughness

Table 4.2 displays the fracture toughness of nano-filler/epoxy nanocomposites in both dry and wet conditions. Surprisingly, fracture toughness for all types of nanocomposites is observed to increase due to exposing to a moist environment. This can be explained by increasing the ductility of the composites due to the plasticization effect of absorbed water, which tends to increase in fracture toughness (Buehler and Seferis 2000). Similarly, Wang et al. (2006) observed an increase in fracture toughness of neat epoxy and exfoliated clay/epoxy nanocomposites after subjecting to water for 30 days.

In details, fracture toughness of unmodified epoxy in wet condition increases by 48.9% compared to dry epoxy. In the case of nanoclay/epoxy nanocomposites, facture toughness of wet composites modified with 1, 3, and 5 wt% nanoclay platelets increase by 29.3, 51.4, and 36.0%, respectively, compared to same nanocomposites in dry condition. Similarly, fracture toughness of wet HNT/epoxy nanocomposites filled with 1, 3, and 5 wt% HNT increases by 30.7, 57.4, and 11.1%, respectively,

Table 4.2 Fracture toughness and impact strength of epoxy and its nanocomposites before and after water treatment

Samples	Before placing in water		After placing in water	
	Fracture toughness MPa m$^{1/2}$	Impact strength kJ/m^2	Fracture toughness MPa m$^{1/2}$	Impact strength kJ/m^2
Epoxy	0.9 ± 0.1	5.6 ± 0.7	1.3 ± 0.2	6.2 ± 1.4
+1% nanoclay	1.1 ± 0.1	6.1 ± 1.3	1.4 ± 0.3	7.4 ± 1.5
+3% nanoclay	0.9 ± 0.1	6.9 ± 1.4	1.4 ± 0.2	6.6 ± 1.5
+5% nanoclay	1.0 ± 0.2	7.8 ± 2.7	1.3 ± 0.3	7.3 ± 1.7
+1% HNT	1.3 ± 0.2	5.6 ± 1.1	1.7 ± 0.2	6.5 ± 1.8
+3% HNT	1.0 ± 0.1	6.4 ± 0.7	1.6 ± 0.5	6.3 ± 1.8
+5% HNT	1.2 ± 0.1	7.0 ± 0.9	1.3 ± 0.3	6.2 ± 1.5
+1% n-SiC	1.6 ± 0.3	7.5 ± 1.1	2.2 ± 0.3	9.1 ± 1.8
+3% n-SiC	1.2 ± 0.2	7.0 ± 0.8	2.1 ± 0.3	7.9 ± 2.2
+ 5% n-SiC	1.1 ± 0.1	7.6 ± 1.2	1.9 ± 0.3	8.2 ± 1.4

as compared to dry nanocomposites. Moreover, fracture toughness of n-SiC/epoxy nanocomposites reinforced with 1, 3, and 5 wt% n-SiC increases by 34.1, 67.2, and 76.4%, respectively, when compared to dry nanocomposites.

The effect of nano-filler addition on the fracture toughness of wet epoxy-based nanocomposites was studied. All types of nanocomposites show similar fracture toughness trend. A maximum value achieved at 1 wt% filler loading, followed by a decrease in fracture toughness value with further increase in filler content. Fracture toughness of composites filled with 1 wt% of nanoclay, HNT, and n-SiC increases by 10.6, 36.7, and 70.3%, respectively, compared to wet unfilled epoxy matrix. Nanocomposites reinforced with n-SiC particles show better fracture toughness than other nanocomposites. The enhancement in fracture toughness can be attributed to the increased resistance to crack propagation via number of possible toughness mechanisms such as crack pinning, particle debonding, plastic void growth, plastic deformation, and particle pull-out (Alamri and Low 2012a). Similarly, Buehler and Seferis (2000) reported an increase in fracture toughness of carbon fibre/epoxy composites after placement in water medium for 1200 h. Plasticization effect of water and increased fibre bridging were reported to be the reasons of the enhancement in fracture toughness.

(c)   Impact strength

The effect of water absorption on the impact strength of nano-filler-reinforced epoxy nanocomposites is also presented in Table 4.2. Nanocomposites filled with either nanoclay or HNT show no clear trend of the influence of water on impact strength. For nanocomposites filled with n-SiC, a significant increase in impact strength can be observed due to water absorption. In the case of wet condition, the impact strength of epoxy matrix increases due to the presence of nano-fillers. The increase in impact strength is more pronounced for nanocomposites modified with n-SiC particles. For all types of nanocomposites, reinforcing with 1 wt% of nano-filler displays the highest value compared to other fillers content. Impact strength of nanocomposites reinforced with 1 wt% of nanoclay, HNT, and n-SiC increases by 20.0, 4.9, and 46.1%, respectively, compared to wet unfilled epoxy matrix. The increase in impact strength is due to the increase in the flexibility of the epoxy chains as a result of the plasticization action of the absorbed water (Sombatsompop and Chaochanchaikul 2004). Low et al. (2009) reported an increase in impact strength for recycled cellulose-fibre-reinforced epoxy composites due to the plasticization effect of sea water.

(d)   SEM Observations

The SEM micrographs of fracture surfaces of the water-treated epoxy and epoxy nanocomposites are shown in Figs. 4.24 and 4.25. Low magnification images for unfilled epoxy and epoxy filled with nanoclay, HNT, and n-SiC, respectively, are shown in Fig. 4.24a–d. All types of samples show different degree of surface roughness. The surface of neat epoxy displays lower roughness than nanocomposites as seen in Fig. 4.24a. River markings can be clearly observed for neat epoxy with quite smooth fracture surface indicating very fast and straight crack propagation (Alamri and Low 2012a). However, it is evident that the presence of nano-fillers increases the roughness of the fracture surfaces. An increase in fracture surface roughness is an indicator of crack pinning mechanism, which increases the absorbed energy of fracture by increasing the crack length during deformation (Alamri and Low 2012a). The formation of micro-voids is more pronounced in n-SiC nanocomposites. It was reported that the presence of micro-voids led to increase in fracture toughness. This explains why nanocomposites filled with n-SiC particles exhibited the highest fracture toughness among other nanocomposites.

High magnification SEM images of epoxy nanocomposites filled with nanoclay, HNT, and n-SiC are shown in Fig. 4.25a–d. In general, several toughness mechanisms such as crack pinning, particle debonding, plastic void growth, plastic deformation, and particle pull-outs can be observed. Such toughness mechanisms can increase the energy dissipated by resisting crack propagation during deformation, which lead to an increase in fracture toughness values (Alamri and Low 2012a). Close observation of Figs. 4.24 and 4.25 indicates that plastic deformation due to the presence of clay clusters is the dominant toughening mechanism for nanocomposites filled with nanoclay (Tang et al. 2011). For nanocomposites filled with HNT, crack pinning and bowing are the main toughening mechanisms (Sánchez-Soto et al. 2007). In the case of nanocomposites filled with n-SiC, Figs. 4.24d and 4.25d show the existence of
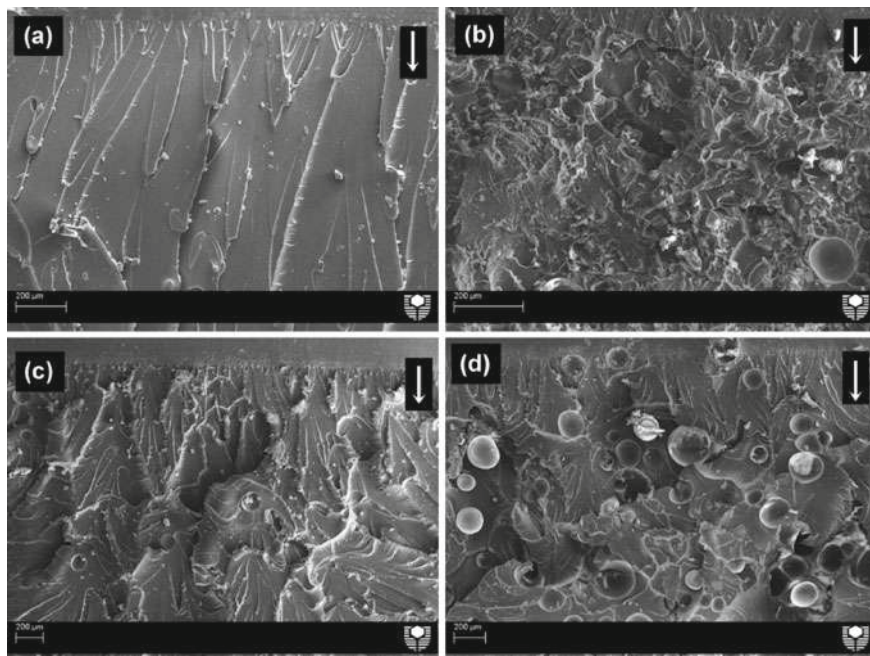
Fig. 4.24 SEM images showing the details of fracture surfaces for **a** unfilled epoxy **b** epoxy/nanoclay 5 wt%, **c** epoxy/HNT 5 wt%, and **d** epoxy/n-SiC 5 wt% [white arrow indicates the direction of crack propagation]

micro-voids, which reveals that plastic deformation of the matrix around the voids and crack deflection due to the presence of these voids are primary toughening mechanisms.

4.5 Halloysite/Cellulose Fibre/Epoxy Eco-nanocomposites

(a) Mechanical Properties of HNT/Epoxy Nanocomposites

The flexural strength, flexural modulus, impact strength, fracture toughness, and impact toughness of HNT/epoxy composites are shown in Figs. 4.26, 4.27, 4.28, 4.29 and 4.30. In general, the incorporation of HNT into epoxy matrix enhances the mechanical properties for all nanocomposite samples. The enhancement in flexural strength is shown in Fig. 4.26 as a function of HNT content. The addition of 1 wt% HNTs has resulted in the highest flexural strength of all nanocomposite samples. Flexural strength of epoxy/HNT composites containing 1 wt% HNTs was increased by 20.8% compared to neat epoxy. This can be linked to the better dispersion of nano-fillers at low HNTs loading. However, adding more HNTs slightly decreases the flexural strength. This can be due to the presence of filler agglomerations and
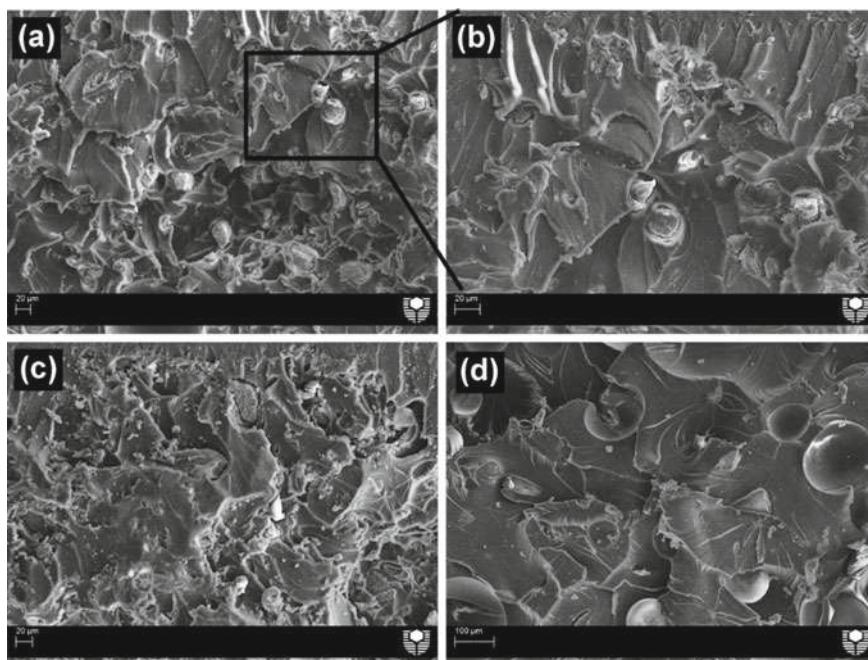
Fig. 4.25 SEM images showing the details of fracture surfaces for epoxy-based nanocomposites filled with nanoclay (**a**, **b**), HNT (**c**), and n-SiC (**d**)

Fig. 4.26 Flexural strength as a function of HNT content for epoxy and its nanocomposites reinforced with or without RCF
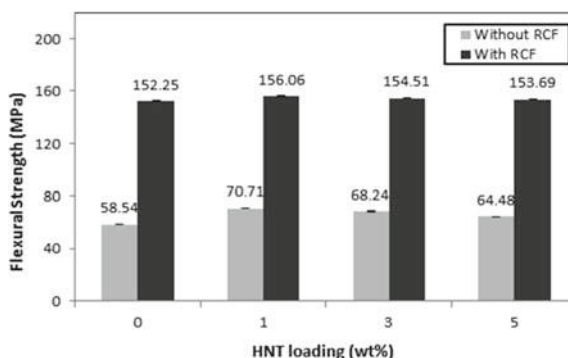
micro-voids at higher HNTs contents (Xu and Hoa 2008). At high concentration of HNTs, they are poorly dispersed within the matrix forming agglomerations that act as stress concentrators, which in turn cause reduction in flexural strength (Zainuddin et al. 2010). Additionally, it was observed an increase in matrix viscosity due to the increase in HNTs content, which in turn allowed small air bubbles to be trapped in the resin during the mixing process forming tiny voids in the sample. This in turn resulted in sample failure at relatively low stress. In contrast, with a lower loading of HNTs, the

Fig. 4.27 Flexural modulus as a function of HNT content for epoxy and its nanocomposites reinforced with or without RCF

Fig. 4.28 Impact strength as a function of HNT content for epoxy and its nanocomposites reinforced with or without RCF

Fig. 4.29 Fracture toughness as a function of HNT content for epoxy and its nanocomposites reinforced with or without RCF

potential of micro-void formation is less, and the dispersion is more uniform which both lead to strength improvement (Xu and Hoa 2008). Similar observations have been reported by Prashantha et al. (2011) in their study of halloysite nanotube-filled polypropylene nanocomposites. It was found that the addition of HNTs resulted in a slight improvement in flexural strength of neat polymer. However, at higher
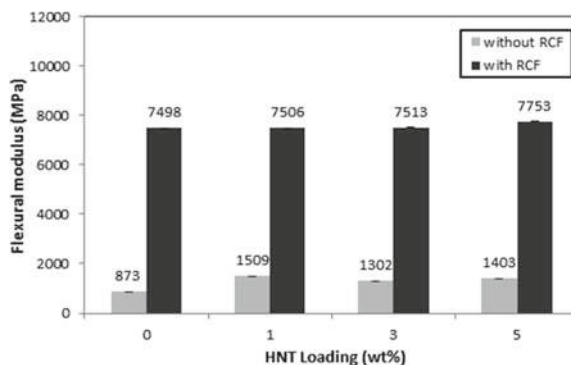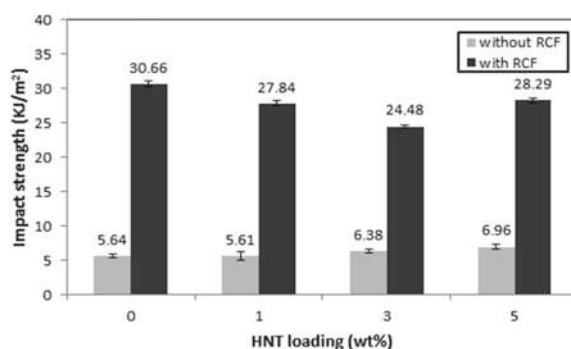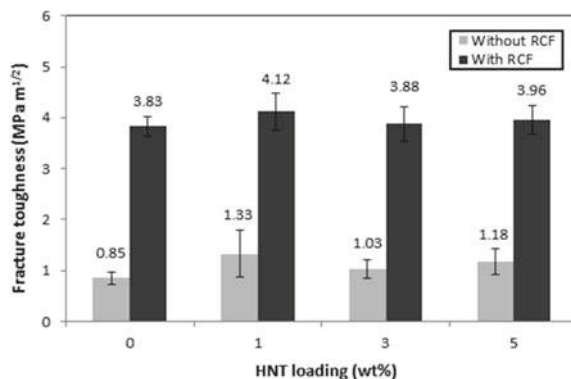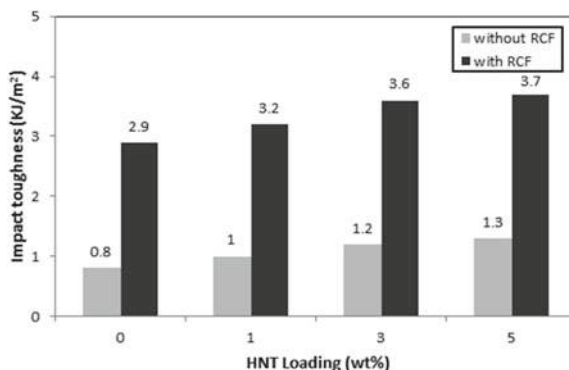
Fig. 4.30 Impact toughness
as a function of HNT content
for epoxy and its
nanocomposites reinforced
with or without RCF

HNT loading (8 wt%), flexural strength decreased due to the tendency of HNTs to agglomerate (Prashantha et al. 2011). Figure 4.27 demonstrates the flexural modulus of HNT/epoxy nanocomposites as a function of HNTs loading. The introduction of HNTs into epoxy matrix significantly increases the flexural modulus for all epoxy nanocomposites samples. The addition of 1 wt% HNTs in epoxy matrix increases the flexural modulus by 72.8% over neat epoxy. This means that the presence of halloysite nanotubes increases the stiffness of the matrix. This enhancement in modulus can be explained by the strong stiffening effect of the HNT fillers which themselves have a higher modulus than epoxy.

Impact strength can be defined as the ability of the material to withstand impact loading. As shown in Fig. 4.28, the presence of halloysite nanotubes gradually increases the impact strength for epoxy nanocomposites with maximum enhancement reaching up to 23.4% at 5 wt% HNT loading. The impact strength of neat epoxy increases from 5.6 kJ/m^2 to 6.4 and 7.0 kJ/m^2 after the addition of 3 and 5 wt% of HNTs, respectively. At high HNT loading, HNT clusters may act as crack stoppers and increase the ability of the material to absorb energy by forming tortuous pathways for crack propagation, resulting in the impact strength to increase. Similarly, remarkable improvement in impact strength was reported by Ye et al. (2007). Based on their observation, the addition of 2.3 wt% HNTs could increase the impact strength of neat epoxy four times without affecting the flexural properties and thermal stability. The discrepancy in results between our work and that of Ye et al. could be attributed to the geometry and condition of samples tested. In our study, the samples were not notched whereas notched samples were used by Ye et al.

The role of halloysite nanotubes on fracture toughness of epoxy/HNT nanocomposites is shown in Fig. 4.29. The fracture toughness of neat epoxy and epoxy/HNT nanocomposites reinforced with 1, 3, and 5 wt% HNTs are 0.85, 1.33, 1.03, and 1.18 MPa m$^{1/2}$, respectively. Fracture toughness increased by 56.5, 21.2, and 38.8% when 1, 3, and 5 wt% HNTs are added. This significant enhancement in fracture toughness is like the study of Deng and Tang (2010). They reported a significant enhancement in facture toughness of HNT/epoxy nanocomposites compared to neat epoxy. In their study, fracture toughness increased by 38 and 47% when 5 and 10 wt%

halloysite were added. This was due to the toughness mechanisms of halloysite tube such as particle pull-out and debonding. Once again, it was observed in our study that reinforcement with 1.0 wt% of halloysite tubes displayed superior fracture properties than those reinforced with higher contents of HNTs. It has been reported that nanoparticles easily tend to agglomerate at higher filler contents acting as stress concentration that can initiate tiny cracks, which leads to crack propagation (Deng et al. 2009; Alhuthali and Low 2021).

Figure 4.30 displays the impact toughness in terms of the energy release rate of epoxy/HNT nanocomposites. The addition of 1, 3, and 5 wt% HNTs significantly increases impact toughness of neat epoxy by 25.0, 50.0, and 62.5%, respectively. This remarkable enhancement in toughness properties for nanocomposites is due to several toughness mechanisms for dissipating energy such as crack pinning, particle debonding, plastic void growth, plastic deformation, and particle pull-out as was reported by number of studies for polymers reinforced with nano-fillers (Ma et al. 2008; Zhao et al. 2008; Wetzel et al. 2006; Tang et al. 2011; Chen et al. 2008). Ma et al. (2008) reported an increase in impact toughness of epoxy system due to the addition of nano-filler. They found that the inclusion of silica nanoparticles increased the toughness properties in terms of energy release rate (G_{1C}) of epoxy system by 81% at 20 wt% silica loads.

(b)   Mechanical Properties of RCF-Reinforced HNT/Epoxy Nanocomposites

The flexural strength, flexural modulus, impact strength, fracture toughness, and impact toughness of RCF-reinforced HNT/epoxy nanocomposites are also plotted in Figs. 4.26, 4.27, 4.28, 4.29 and 4.30. In general, the addition of RCF into epoxy matrix and HNT/epoxy nanocomposites significantly increases the mechanical properties compared to neat epoxy and its nanocomposites. This is due to the unique properties of cellulose fibres in enhancement polymer mechanical properties. Figure 4.26 displays the flexural strength of RCF/HNT/epoxy composites as a function of HNT loading. First, the presence of RCF into epoxy matrix significantly increases the flexural strength of neat epoxy by 160.3% from 58.5 to 152.3 MPa. This significant enhancement in flexural properties is clearly due to the ability of recycled cellulose fibres in resisting bending force of the composites (Satapathy et al. 2010). The addition of halloysite nanotubes to the RCF/epoxy composites is found to have a positive effect on flexural strength when compared to unfilled RCF/epoxy composites. This slight improvement in flexural strength can be related to the enhanced RCF–matrix interface due to the presence of HNT tubes. However, flexural strength gradually decreases as HNTs content increases. This decline in flexural strength can be due to the lack in stress transferring between matrix and RCF as a result of increased matrix viscosity. Previous studies showed enhancement in strength properties of fibre-based epoxy nanocomposites. Ceretti et al. (2019) and Ye et al. (2011) investigated the mechanical properties of carbon fibre-reinforced epoxy/HNT composites. Flexural properties slightly increased due to the addition of HNTparticles. In another study, Zulfli and Shyang (2010) reported an improvement in flexural strength and modulus of glass fibre-reinforced epoxy/clay nanocomposites due to the addition of treated nanoclay. The presence of clay enhanced the interface between the glass

fibre and epoxy matrix. The addition of RCF to epoxy system significantly increases flexural modulus by seven times as seen in Fig. 4.27. Adding HNTs to RCF/epoxy samples slightly enhances flexural modulus.

Figure 4.28 illustrates the impact strength of epoxy reinforced with RCF sheets and halloysite nanotubes. The presence of RCF sheets significantly increases the impact strength of unfilled epoxy by approximately 444% from 5.6 to 30.7 kJ/m^2. This enormous achievement is because cellulose fibre has a better ability to absorb impact energy than unreinforced polymer. This result is in accordance with the work of Maleque and Belal (2007), where they investigated the mechanical properties of pseudo-stem banana fibre-epoxy composites and found that the presence of banana-woven fabric increased the impact strength over the neat epoxy by approximately 40%. However, the incorporation of HNTs into RCF/epoxy composites slightly reduces the impact strength compared to unfilled RCF/epoxy composites, Fig. 4.28. Samples reinforced with 5 wt% HNTs display better impact strength than those reinforced with 1 and 3 wt% HNTs. Impact strengths of RCF/epoxy nanocomposites filled with 1, 3, and 5 wt% HNTs are 27.8, 24.5, and 28.3 kJ/m^2, respectively.

The role of RCF sheets on fracture properties of unfilled epoxy composites and HNT-filled epoxy nanocomposites is plotted in Fig. 4.29. The addition of RCF sheets remarkably increases the fracture toughness for all samples when compared to the same samples without RCF. For example, the addition of RCF in epoxy resin increases the fracture toughness by about 350% compared to neat epoxy. This incredible improvement is due to the unique properties of cellulose fibre in resisting fracture, which resulted in increased energy dissipation from crack deflection at the fibre–matrix interface, fibre debonding, fibre bridging, fibre pull-out, and fibre fracture. This result is supported by the work of Lui and Huges (2008). They investigated the toughness and fracture behaviour of epoxy matrix composites reinforced with woven flax fibre textiles. It was found that the fracture toughness of the composites was increased by two to four times due to the presence of woven flax fibre when compared to pure epoxy samples. In the case of RCF/epoxy nanocomposites, the addition of HNTs to the RCF/epoxy composites shows no significant differences in fracture toughness with a maximum increase (7.6%) at 1 wt% HNTs load. This reveals that fracture toughness in RCF/epoxy nanocomposites is mostly dominated by recycled cellulose fibres with slight effect of HNTs. Khan et al. (2011) investigated the fracture properties of carbon fibre/clay-reinforced epoxy nanocomposites. Results showed that the incorporation of (1, 3, and 5) wt% nanoclay gradually increased the fracture toughness by (8, 19, and 23%), respectively. Authors concluded that several toughness mechanisms such as formation of voids, crack pining, and micro-cracking were responsible for toughness enhancement (Khan et al. 2011).

The impact toughness in terms of the energy release rate of HNTs/epoxy nanocomposites reinforced with RCF sheets is plotted in Fig. 4.30 as a function of HNTs content. As expected, the influence of RCF sheets on the impact toughness of HNT/epoxy and unfilled epoxy matrices is remarkable. The impact toughness of pure epoxy increases from 0.8 to 2.9 kJ/m^2 due to the addition of RCF sheets. This result indicates that recycled cellulose fibres improve the impact toughness of the

epoxy resin by approximately 262.5%. This extraordinary enhancement in toughness properties as discussed before is because RCF displays a variety of fracture mechanisms in the crack path to resist crack propagation. These fracture mechanisms include fibre breakage, fibre pull-out, fibre debonding, and fibre bridging which require high energy to be absorbed. The incorporation of HNTs in different concentration to the RCF/epoxy composites gradually enhances the impact toughness by 10.3, 24.1, and 27.6% at HNTs content 1, 3, and 5 wt%, respectively. The extra improvement in impact toughness for RCF-based nanocomposites is due to the participation of HNTs in resisting the crack growth.

(c)   Fracture Surfaces and Toughening mechanisms

Figure 4.31 shows the facture surfaces of pure epoxy and epoxy nanocomposites containing 1 and 5 wt% of HNTs. It can be seen from Fig. 4.31a that the fracture surface of pure epoxy is very smooth and featureless, which indicates typical brittle fracture behaviour with lack of significant toughness mechanisms (Tang et al. 2011). However, epoxy/HNT nanocomposites display a rougher fracture surface than that of neat resin because of the presence of nanoparticles as indicated in Fig. 4.31c–d. An increase in fracture surface roughness can be used as indicator to the presence of crack pinning mechanisms, which increase fracture toughness by increasing crack propagation length during deformation (Zhao et al. 2008; Wetzel et al. 2006; Tang
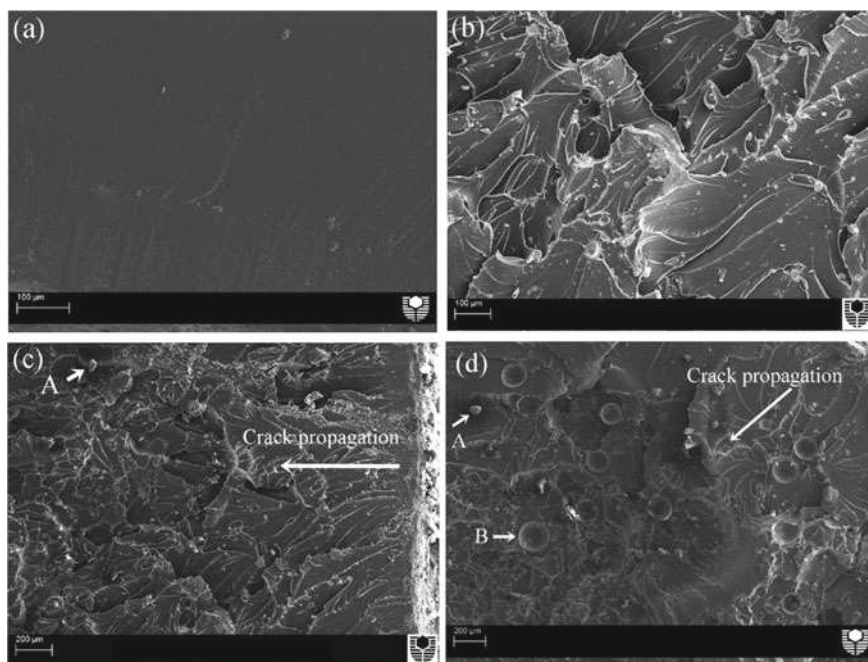

Fig. 4.31 Scanning electron micrographs after fracture toughness testing for: **a** PE; **b** PE/HNT1; **c** PE/HNT1; and **d** PE/HNT5 [Legend: A = HNTs clusters and B = voids]

et al. 2011). Figure 4.31b shows high magnification SEM micrograph of fracture surface for epoxy reinforced with 1% HNTs. A range of possible toughness mechanisms such as crack pinning, particle debonding, plastic void growth, plastic deformation, and particle pull-out can be observed. Such toughness mechanisms can lead to higher fracture toughness properties through resisting crack propagation (Ma et al. 2008; Zhao et al. 2008; Wetzel et al. 2006; Tang et al. 2011; Chen et al. 2008). When compared between samples filled with 1 and 5 wt% HNT, Fig. Figure 4.31c–d, sample with high HNT loading has large particle agglomerations than those filled with lower HNTs loading as confirmed by TEM images in Fig. 4.25a–c. These particle clusters act as a stress concentrator leading to low facture toughness. Moreover, an increase in particle pull-out and void formation is observed for samples with higher HNT loading. This can be attributed to the lack in HNT–matrix interfacial adhesion. This observation confirms the result of fracture toughness test, which indicates that epoxy reinforced with 1 wt% HNT has the highest fracture toughness value compared to samples filled with either 3 or 5 wt% HNT.

Figure 4.32 illustrates the SEM micrograph of the fracture surface for RCF/epoxy composite and RCF/epoxy nanocomposites reinforced with 5 wt% HNTs after fracture toughness test. Images in Fig. 4.32a–b show the low magnification images of RCF/epoxy sample and RCF/epoxy filled with 5 wt% HNT, while images in Fig. 4.32c–d show the high magnification images of same samples. A variety of toughness mechanisms such as shear deformation, crack bridging, fibre pull-out and fibre fracture and matrix fracture can be clearly observed which lead to good fracture properties of samples reinforced by RCF sheets. These SEM images confirm the enhancement in mechanical properties due to the presence of RCF sheets. Moreover, a closer look of Fig. 4.32c–d (white arrows) shows that HNT/epoxy matrix displays rougher fracture surface than unmodified epoxy matrix, which indicates the positive participation of HNT/epoxy matrix in the energy absorption during fracture test. This observation confirms the slight enhancement in fracture toughness for RCF/epoxy samples filled with HNTs compared to unfilled RCF/epoxy samples.

Images in Fig. 4.32e–f display low and high magnification back-scattered SEM images of crack propagation in RCF/epoxy sample. It was observed that samples filled with RCF sheets did not completely break into two pieces. This is because fibres bridge the cracks and enhance the crack propagation resistance which led to improvement in fracture toughness. The tortuous pathway for the crack propagations indicates the high energy absorbance by the RCF sheets. It also can be observed that the adhesion between the fibre and the matrix is quite good. These super toughness mechanisms of RCF are the major factors of increasing mechanical properties of samples reinforced with RCF when compared to samples without RCF.
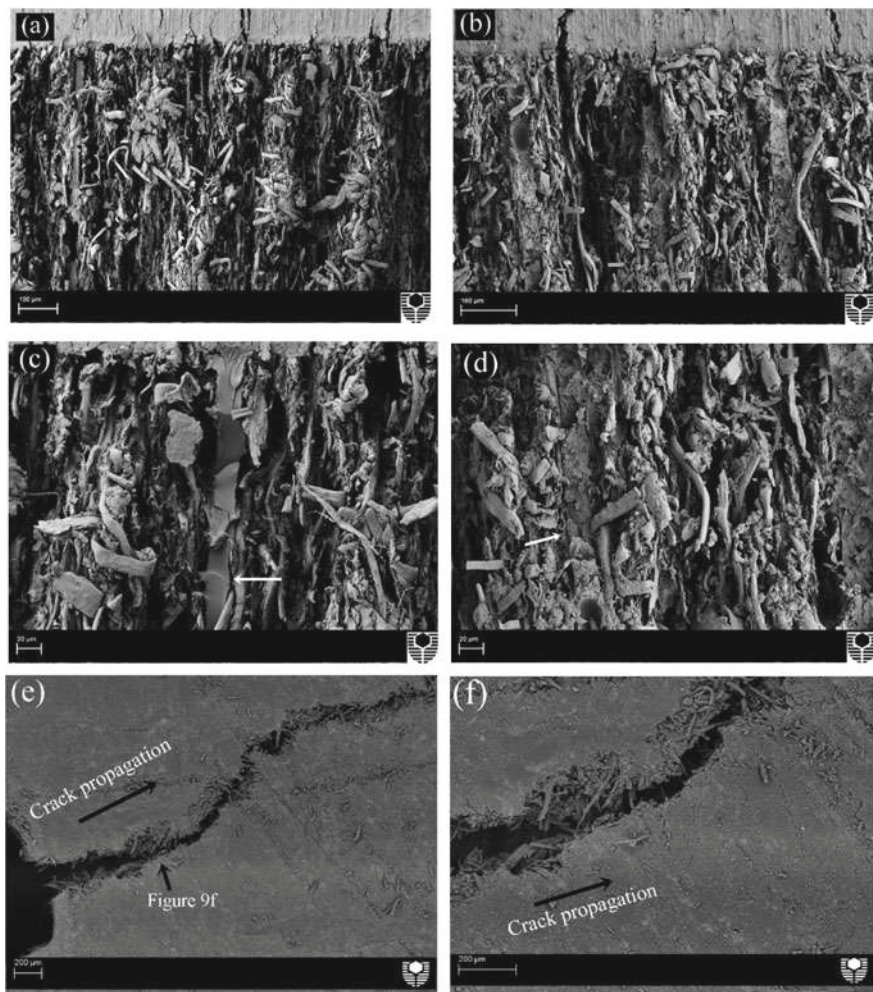
Fig. 4.32 Scanning electron micrographs after fracture toughness testing for **a** PE/RCF; **b** PE/RCF/HNT5; **c** PE/RCF (high magnification) and **d** PE/RCF/HNT5 (high magnification), **e** crack propagation, and **f** crack propagation (high magnification). White arrow indicates the location of epoxy matrix

4.6 Cellulose Fibre/Vinyl-Ester Eco-nanocomposites

(a) Mechanical Properties

Flexural strength and impact strength are measures of strength properties. Results for flexural strength (Fig. 4.33) revealed that ecocomposites and eco-nanocomposite had greater strength than pure samples. Results for impact strength (Fig. 4.34) also indicated that ecocomposites and eco-nanocomposite were stronger than the pure
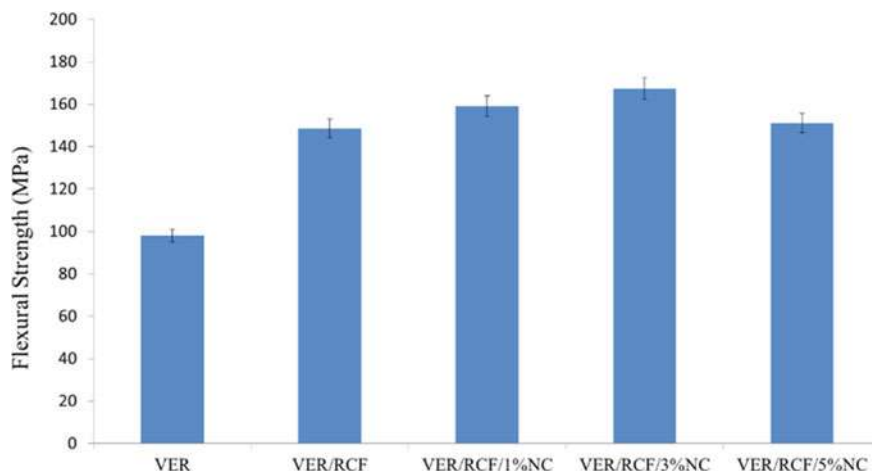
Fig. 4.33 Flexural strength of vinyl-ester eco and nano-ecocomposites
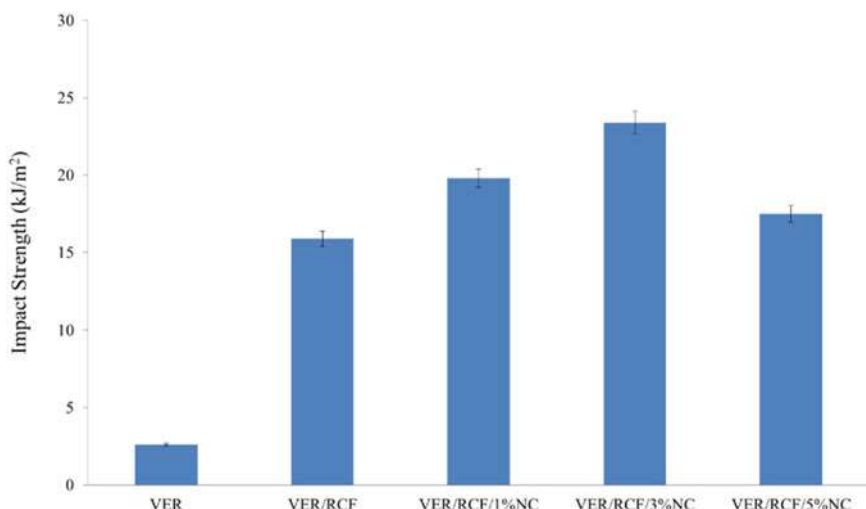
Fig. 4.34 Impact strength of vinyl-ester eco and eco-nanocomposites

samples. Specifically, compared to the pure sample, the ecocomposite's flexural strength was greater by approximately 33.98%. Cellulose fibres' high strength and modulus and the strong matrix–fibre interfacial adhesion contribute to the observed enhanced flexural properties (Chen et al. 2009; Espert et al. 2004; Bakare et al. 2010). The improved strength properties of polymer reinforced with natural fibres composites have also been documented in other studies (Low et al. 2009; Wambua et al. 2003; Shahinur and Hasan 2020). The addition of 1, 3 wt% nanoclay showed 38.43 and 41.42% respective increase in flexural strength.

The addition of 5 wt% nanoclay reduced flexural strength however. The failure of 5 wt% nanoclay addition to further enhance strength properties is because of the processing events. At higher clay content, viscosity increases during mixing of resin and nanoclay rendering degassing insufficient before curing. A complete degassing process is essential for the composite to minimize void formation. For nanocomposites containing 5 wt% of clay, the degassing process is particularly critical as the formation of voids causes specimen failure even on exposure to very low strains. The highly viscous mixture that results when 5 wt% nanoclay is added to polymer also has further undesirable effects on fibre–matrix adhesion. Since high viscosity causes a reduction in wettability, interfacial adhesion between matrix and fibres is more likely which also reduce the resultant material's strength (Ashori and Nourbakhsh 2009; Kumar and Allamraju 2019).

The pure sample impact strength was 2.6 kJ/m^2. Ecocomposites were found to be many magnitudes stronger at 15.9 kJ/m^2. The addition of 1 and 3 wt% nanoclay gave impact strength results of 17.9 and 20.0 kJ/m^2, respectively. The addition of 5 wt% nanoclay did not give a higher impact strength result. The high viscosity of the mixture reduced interfacial adhesion of matrix and fibre reducing strength properties.

Impact strength and flexural strength results all indicate improved values due to nanoclay addition. Despite the problems described above regarding the addition of 5 wt% nanoclay, strength property results in both impact strength and flexural strength which were greater than the unmodified ecocomposites. The fibre–matrix adhesion is a primary determinant in composite quality. In a fibre-reinforced composite, the role of the matrix is to transfer the load to the stiff fibres through shear stresses at the interface, and this process requires a good bond between the polymeric matrix and the fibres (Chen et al. 2009; Bakare et al. 2010). Studying the fracture surfaces of modified samples (eco-nanocomposites) and unmodified samples ecocomposites using SEM reveals the effect of nanoclay additon on fibre–matrix adhesion.

Images in Fig. 4.35 show the fracture surfaces of all samples using SEM. The images display fibre pull-outs from the matrix. The disparity in the length of fibres, the fibre surfaces, and matrix–fibre gaps is apparent in each of the composites. The pull-out lengths, the extent that individual fibres are isolated, was greater for in the unmodified composites (Fig. 4.35a) in comparison to the modified composites (Fig. 4.35b–d). Also, the number of fibres that was pulled out was greater in the unmodified sample. This phenomenon is a result of poor adhesion between the fibres and the matrix materials (Silva et al. 2006; Stocchi et al. 2007).

The fibre surfaces in unmodified ecocomposite appear clean. This suggests poor adhesion as no matrix materials have adhered to the fibres (Rosa et al. 2010; Mylsamy and Rajendran 2011). In contrast, the modified eco-nanocomposite fibre surfaces are rough indicating better adhesion between the fibres and the matrix materials. Finally, the matrix–fibre gaps appear larger in the unmodified composites compared to the small gaps of the modified composites. The fracture surface images are indicative of nanoclay addition's positive effect on matrix–fibre adhesion (Suppakarn and Jarukumjorn 2009; Reddy et al. 2020).

The RCF composites feature fracture toughness and impact toughness greater than those of the pure samples (Figs. 4.36 and 4.37). Cellulose fibres interact with the

(a)   (b)

(c)   (d)
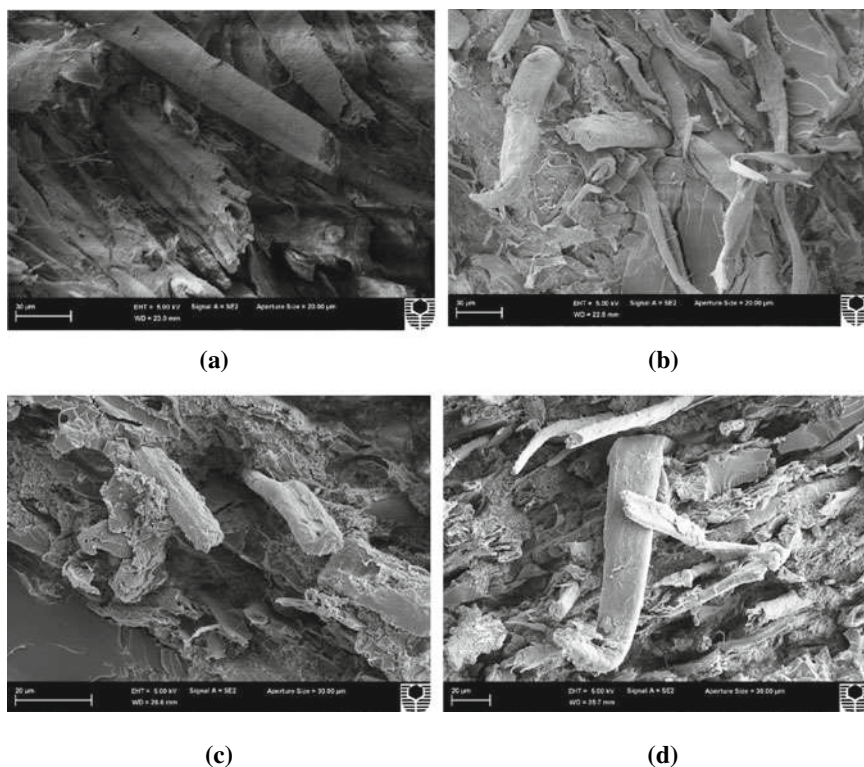
Fig. 4.35 SEM images of fracture surfaces of **a** eco-composite, **b** eco-nanocomposite with 1 wt% nanoclay loading, **c** eco-nanocomposite with 3 wt% nanoclay loading, **d** eco-nanocomposite with 5 wt% nanoclay loading all samples were subjected to three-point fracture toughness test

matrix to provide a composite which has better crack deflection, energy dissipation, and fracture resistance properties (Low et al. 2009; Wambua et al. 2003; Shahinur and Hasan 2020).

Typically, natural fibre–polymer composites display crack deflection, debonding between fibre and matrix, pull-out effect, and a fibre-bridging mechanism, which all contribute to fracture toughness. In terms of the matrix alone, plastic deformation provides toughness using an energy dissipation mechanism (Mylsamy and Rajendran 2011; Suppakarn and Jarukumjorn 2009; Reddy et al. 2020; Singh et al. 2021). However, this mechanism is hindered by the addition of fibres. Nonetheless, the overall material is tougher due to the toughness mechanisms provided by natural fibres.

In this study, the fracture toughness of ecocomposites was, at its highest, 60% greater than the baseline pure matrix (Fig. 4.36). Increasing nanoclay addition, however, led to a reduction in fracture toughness. It was previously discussed that nanoclay addition results in desirable strength properties due to fibre–matrix adhesion improvement. However, this improvement of fibre–matrix adhesion makes the
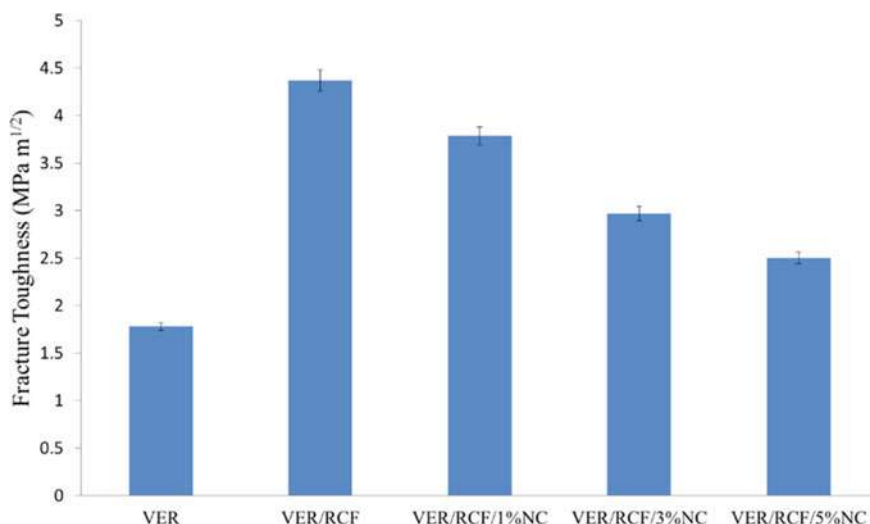
Fig. 4.36 Fracture toughness of ecocomposite and eco-nanocomposites
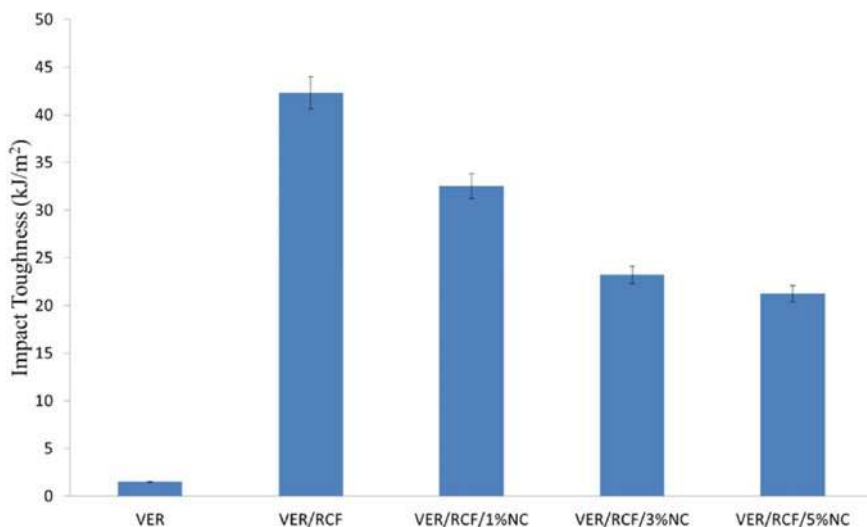
Fig. 4.37 Impact toughness of ecocomposite and eco-nanocomposites

eco-nanocomposite brittle as indicated in the lower fracture toughness results for the samples. The addition of nanoclay causes fibre–matrix adhesion to be high which prevents the materials' energy absorption mechanisms provided by fibre pull-outs and fibre debonding (Silva et al. 2006). The images in Fig. 4.35 reveal how without nanoclay, the fibres in the ecocomposite slide out from the matrix in a greater length and number (Fig. 4.35a), however, with nanoclay, the fibres pulled out are shorter

and in less number (Fig. 4.35b–d) indicating the strong interfacial adhesion of the eco-nanocomposites (Mylsamy and Rajendran 2011).

For this reason, a similar trend was observed with impact toughness (Fig. 4.37). Eco-composite impact toughness was markedly greater than the baseline pure matrix sample with 42.3 kJ m^2 and 1.5 ^{kJ}/m^2 as respective results. Increasing the loading of nanoclay decreased impact toughness properties again. Fibre pull-outs and fibre fracture were determined by the dominant toughness mechanisms as evidenced by the images in Fig. 4.35.

(b)   Calculations of Flexural Strength and Modulus

From the load–deflection data obtained from testing, flexural strength (π_F), modulus (E_F), and strain to failure (ρ_F) can be calculated using ASTM D790 (ASTM International 2007):

$$\pi_F = \frac{3 P_{\max} L}{2bh^2} \left[1 + 6 \left(\frac{D}{L} \right)^2 - 4 \left(\frac{h}{L} \right) \left(\frac{D}{L} \right) \right]$$

$$E_F = \frac{m L^3}{4bh^3}$$

$$\rho_F = \frac{6Dh}{L^2}$$

where L, b, and h are the span, width, and depth of the specimen, m is the slope of the tangent to the initial straight-line portion of the load–deflection curve, D is the maximum deflection before failure, and $P_{\max}$ is the maximum load encountered before failure.

For each weight loading, five tests were conducted for each configuration, and the average values and variations were determined and presented. Following the testing, specimens were also inspected under an optical microscope in order to investigate any anomalies in flexural performance.

(c)   Flexural Modulus

Since the ecocomposites contain voids, they are three-phase materials and the modulus is given by Cohen and Ishai (1967)

$$E_{VER/RCF/NC} = E_{VER/RCF} \left(\frac{1 - V_\theta^{2/3}}{1 - V_\theta^{2/3} + V_\theta} \right)$$

$$\left[\frac{1 + \left(E_{NC}/E_{VER/RCF} - 1 \right) V_{NC}^{2/3}}{1 + \left(E_{NC}/E_{VER/RCF} - 1 \right) \left(V_{NC}^{2/3} - V_{NC} \right)} \right]$$
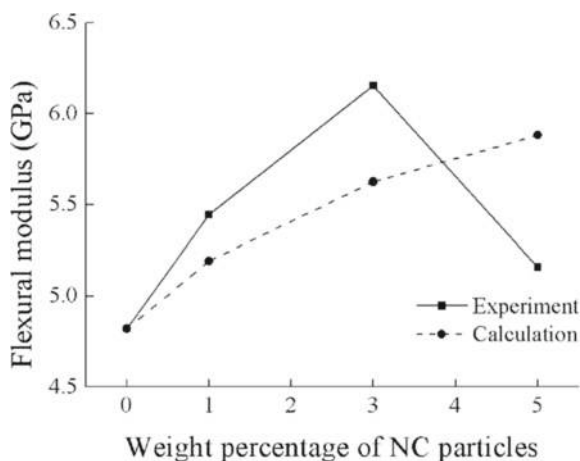
Fig. 4.38 Comparison between flexural moduli from the experiments and calculation

where $E_{VER/RCF/NC}$, E_{NC}, and $E_{VER/RCF}$ are the elastic moduli of the composite, nanoclay particles, and matrix, respectively. The tensile modulus and tensile strength of Cloisite 30B are 170 and 1 GPa, respectively (Yasmin et al. 2006).

Because of the linear load–displacement relationships, the elastic modulus and the flexural modulus are very close. The flexural moduli from the experiments and calculation are shown in Fig. 4.38. It is seen that good agreement is found. The general trend is flexural modulus increases with weight percentage of nanoclay particles except the 5% NC specimens, where their decreased flexural modulus is due to their highest void content.

(d)   Flexural Strength

The flexural strengths from the experiments are shown in Fig. 4.39. It is also seen that the flexural strength of the 5% NC specimens decreases due to their highest void content.

4.7   Halloysite/Vinyl-Ester Nanocomposites

(a)   Toughness Properties

The results of fracture toughness and impact toughness are shown in Table 4.3. The results show that the addition of HNTs has led to enhanced toughness values for all VER/HNT composite samples. For example, compared to the fracture toughness of pure VER (1.81 MPa m$^{1/2}$), the fracture toughness of VER/HNT samples was higher with 17% increase for HNT loading of 1.0 wt%, 34% increase for 3.0 wt% loading, and 46% increase for 5.0 wt% loading. Similarly, the addition of HNTs at 1, 3, and
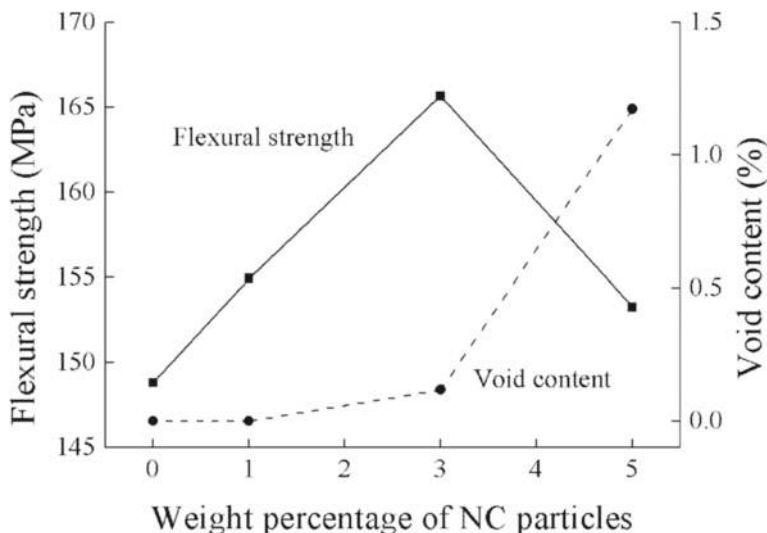
Fig. 4.39 Void content effect on flexural strength

Table 4.3 Fracture properties of VER and VER/HNTs nanocomposites

Samples	HNTs content (wt%)	Fracture toughness (MPa m$^{1/2}$)	Impact toughness (kJ/m^2)
VER	0	1.81 ± 0.05	1.52 ± 0.08
VER/1%HNTs	1	2.12 ± 0.16	2.93 ± 0.16
VER/3%HNTs	3	2.43 ± 0.07	3.34 ± 0.13
VER/5%HNTs	5	2.64 ± 0.12	4.14 ± 0.15

5 wt% increased the impact toughness of pure VER (1.52 kJ/m^2) by 93, 118, and 172%, respectively.

Figure 4.40a shows the fracture surface of pure VER which is flat and smooth except for some river line markings near the crack initiation site which indicates typical brittle fracture behaviour or low fracture toughness (Wang et al. 2005). In contrast, the non-planar fracture surfaces of VER/HNT nanocomposites are shown in Fig. 4.40b–d. These figures depict an increasing roughness of the fracture surfaces with increasing loading of HNTs. The roughness of the fracture surface is an indicator of the quantity of energy dissipated during fracture (Chen and Evans 2006). With increasing HNT content, the fracture surfaces of these samples become rougher and the crack bifurcation is more evident. Such visual features suggest crack pinning due to the rigidness of HNTs in hindering crack propagation (Tang et al. 2011).

SEM images in Fig. 4.41a–c reveal micro-sized white fillers on the fracture surfaces of the VER/HNT nanocomposites. These fine white fillers are HNT clusters
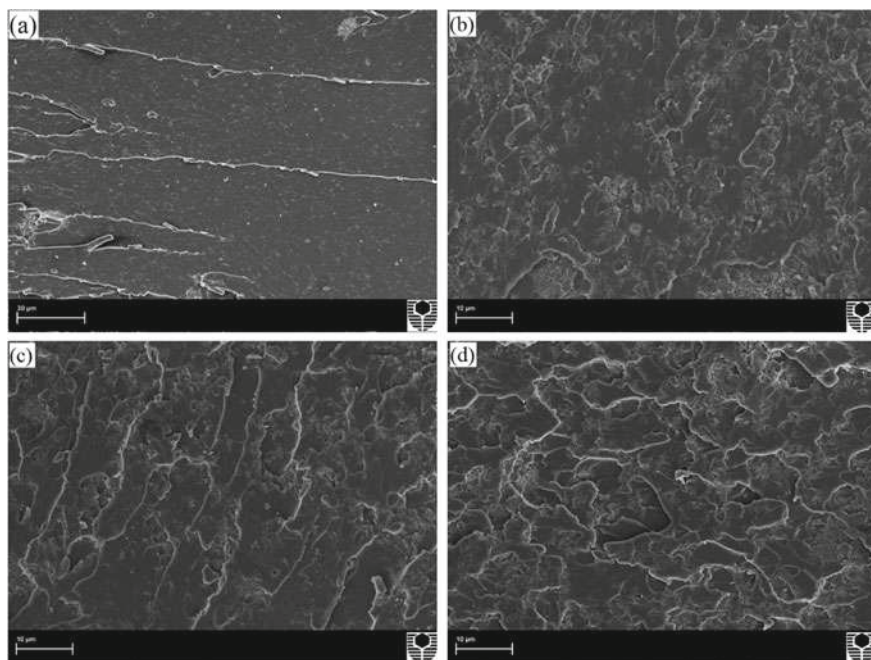
Fig. 4.40 SEM images of fracture surfaces of **a** VER, **b** VER/HNTS composite with 1 wt% HNTs loading, **c** VER/HNTs composite with 3 wt% HNTs loading, and **d** VER/HNTs composite with 5 wt% HNTs loading. All samples had been subjected to fracture toughness test

and are evenly distributed within the matrix. These clusters can increase toughness by stopping the propagation of cracks through interacting with passing cracks and resisting crack advancement (Mylsamy et al. 2019). Plastic deformation of VER around clusters is also evident. Plastic deformation and crack pinning by these clusters are the principal toughening mechanisms observed in this study. These clusters are believed to resemble micro-sized rigid inorganic particles, which when confronting cracks hinder the crack propagation and cause crack pinning, twisting, and plastic deformation in particulate polymer composite (Wetzel et al. 2006; Ye et al. 2011; Meng and Hu 2004).

The effectiveness of HNTs in imparting toughness needs to be assessed against alternative fillers such as nanoclay or rubbery particles. In an attempt to improve the fracture toughness of vinyl-ester, nanoclay and/or core shell rubber (CSR) particles were used by Subramaniyan and Sun (2007). Their results showed that an improvement in fracture toughness of 12% was achieved by CSR, whereas the addition of nanoclay and nanoclay/CSR caused a reduction in fracture toughness by 16 and 6%, respectively. Therefore, HNTs may be preferable to nanoclay for improving the toughness of vinyl esters.
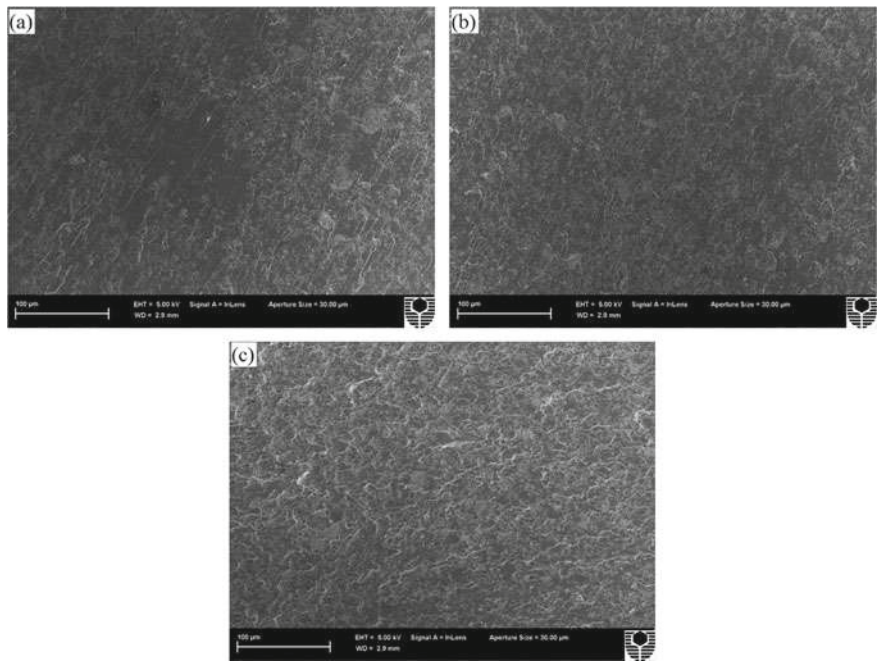
Fig. 4.41 Fracture surfaces of VER/HNTs composites with **a** 1 wt% of HNTs loading, **b** 3 wt% HNTs loading, and 5 wt% HNTs loading, showing crack pinning and plastic deformation around HNTs particle clusters

(b)   Flexural Strength and Modulus

The flexural modulus, flexural strength, and impact strength of VER/HNT composites are summarized in Table 4.4, and the improvements in these properties due to HNT addition are evident. With regard to flexural modulus, the addition of HNTs has led to an improvement from 2.90 GPa to 3.11, 3.31, and 3.42 GPa for HNT loading of 1, 3, and 5 wt%, respectively. The addition of HNTs caused a moderate increase in flexural strength and impact strength. When pure VER is reinforced with 1, 3, and 5 wt% HNTs, the flexural strength of resultant nanocomposites increased to 45.9, 51.1, and 56.5 MPa, respectively. Similarly, the addition of HNTs at 1, 3, and

Table 4.4 Mechanical properties of VER and VER/HNTs nanocomposites

Samples	HNTs content (wt%)	Flexural modulus (GPa)	Flexural strength (MPa)	Impact strength (kJ/m^2)
VER	0	2.90 ± 0.04	42.0 ± 2.4	2.60 ± 0.08
VER/1%HNTs	1	3.11 ± 0.02	45.9 ± 2.1	3.32 ± 0.14
VER/3%HNTs	3	3.31 ± 0.05	51.1 ± 1.8	4.14 ± 0.08
VER/5%HNTs	5	3.46 ± 0.04	56.5 ± 2.0	4.45 ± 0.91
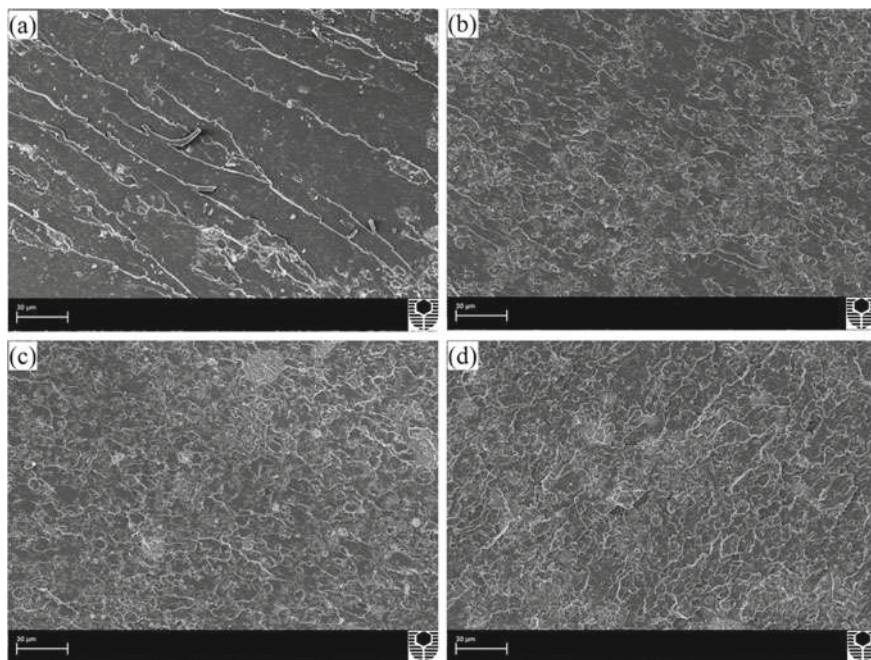
Fig. 4.42 SEM micrographs of fracture surfaces of **a** pure VER/HNTS composite, VER/HNTs composites with 1 wt% HNTs loading, **c** VER/HNTs composite with 3 wt% HNTs loading, and **d** VER/HNTs composite with 5 wt% HNTs loading. All samples had been subjected to flexural strength test

5 wt% increased the impact strength to 3.32, 4.12, and 4.45 kJ/m^2, respectively. Based on these results, the nanocomposites containing HNTs displayed increased modulus and strength properties when compared to neat VER. This observation is further supported by the fracture surface shown in Fig. 4.42a–d. When comparing Fig. 4.42a of VER with Fig. 4.42b–d of VER/HNT nanocomposites, the roughness and tortuosity of the fracture surfaces can be seen to increase with increasing HNT loading.

In general, the elastic modulus of a polymer matrix is enhanced by adding fillers that are rigid (Kaully et al. 2008). Since HNTs have higher elastic modulus (30 GPa) than VER (2.90 GPa) and by virtue of the rule of mixtures, an improved elastic modulus was obtained for all VER/HNT nanocomposites. On the other hand, with respect to strength of particulate-reinforced polymer composites, the size (micro/nanoscale) of particles in relation to the specific surface area (Dong et al. 2011), interfacial bonding between particles and matrix (Hedicke-Höchstötter et al. 2009), and degrees of particle dispersion (Ning et al. 2007) are factors necessary for enhanced strength properties. These dynamics drive the load transfer between reinforcing particles and matrix which is efficient and ultimately results in better strength properties for the composites.

Fig. 4.43 SEM micrograph showing favourable adhesion between VER and HNTs

Compared to micro-scale fillers the nanoscale fillers, such as the HNTs, have a high specific surface area which allow dense interfacial interaction with the polymer matrix. Typically, the specific surface area for halloysite nanotubes is about 65 m^2/g (Ismail et al. 2008). This large contact surface area can provide a favourable adhesion and bonding between filler and matrix which increases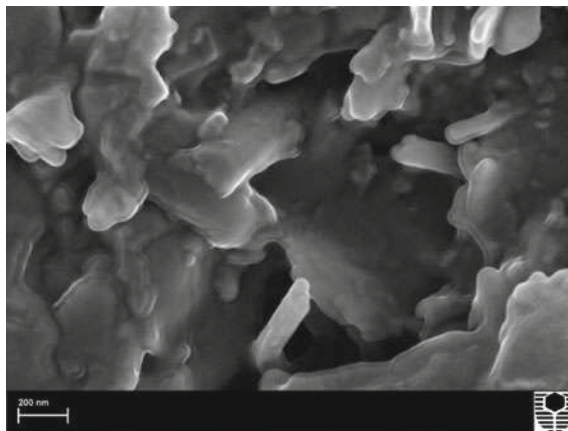 the strength of the composite. The SEM image in Fig. 4.43 shows this favourable adhesion between VER and HNTs, where there are no obvious cavities at the particle/matrix interfaces. Finally, the inter-tubular interaction between HNTs and VER can indicate a good bonding state between filler and matrix, which can serve to increase the strength properties (Ismail et al. 2008). All these mechanisms mentioned above are believed to underpin the increased strength properties and overall mechanical properties of the nanocomposites of this study.

(c)   Comparisons with Theoretical Models

The experimental data on flexural modulus in this study were compared with well-known mathematical models of elastic modulus (see Fig. 4.44). One test of validity is the Reuss–Voigt model, which is an approximate theory, identifying upper and lower bounds of values for a predicted solution of elastic modulus for particulate-reinforced composites. The validity of elastic modulus for most particulate micro- and nanocomposites can be tested using the Reuss–Voigt model by comparing experimental data elastic modulus values with the lower and upper bounds provided by this model (Fu et al. 2008). Results that fall between the bounds are believed to be valid. In the case of composites reinforced with a filler of large aspect ratio and strong adhesion between filler and matrix, the upper bound of Reuss–Voigt model is appropriate. In the case of rigid spherical fillers, the lower bound is applicable (Piechota et al. 2021; Alam 2010). The model supports the validity of elastic modulus results in this study. All experimental and predicted data value fell between the upper and lower bounds. Interestingly, the experimental data lie close to the upper bounds.
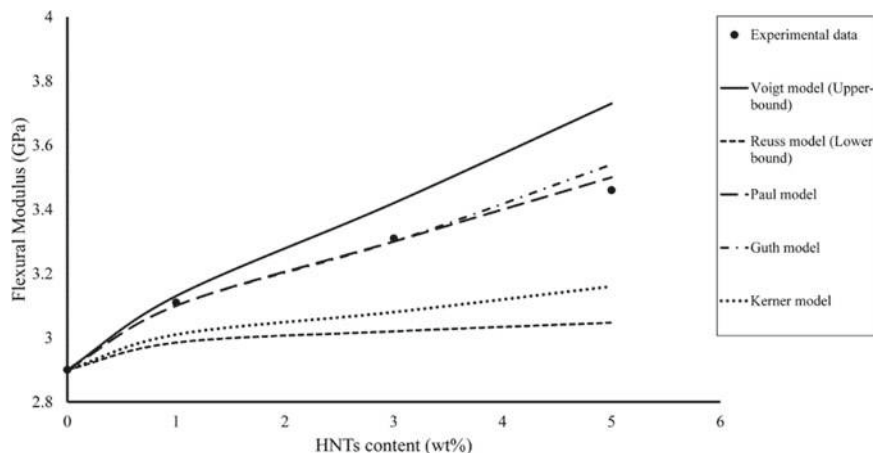
Fig. 4.44 Comparison of experimental data for flexural modulus against HNTs content with results extrapolated from published models

This can be attributed to the large aspect ratio of HNTs and the good adhesion between HNTs and VER. Both the Paul model and the Guth model agree well with the experimental results. The assumption of a perfect adhesion between the particles and matrix underpins the Paul model (Dong et al. 2011; Hashim et al. 2021). Thus, the experimental data is believed to support adequate adhesion between the filler and matrix in the nanocomposite samples. The microstructures observed by SEM and TEM also supported adequate interfacial bonding between HNTs and VER. The Guth model not also assumes perfect adhesion between filler and matrix, but also assumes perfect dispersion and large particle aspect ratio (Fu et al. 2008; Hashim et al. 2021). Thus, the experimental results here support adequate adhesion between the filler and matrix, acceptable dispersion, and that the majority of HNTs were found to exist in a tubular shape with an aspect ratio of between 3 and 15.

Nonetheless, both models of Paul and Guth have over-predicted the modulus of the samples in this study for cases where the volume fraction increased to 5 wt%. This discrepancy is most likely explained by the formation of HNT clusters in the 5 wt% nanocomposites. These clusters within the samples can affect the load-bearing capability and result in a lower elastic modulus (Yan et al. 2006). At the same time, overall aspect ratio of HNTs can be reduced due to the formation of clusters (Gantenbein et al. 2011) and during processing due to the shearing effect which breaks the HNTs (Ning et al. 2007). The models of Paul and Guth do not take into consideration the formation of clusters or the reduction in aspect ratio of the fillers. The Kerner model is a measure of validity for composite systems in which the modulus of filler is many times higher than the modulus of the matrix (Kaully et al. 2008; Dong et al. 2011). The relative modulus ratio of fillers to matrix in this study is low which explains the lack of agreement between experimental data when compared to the Kerner model.

In summary, based on current findings and the results of other studies (Ahmad et al. 2008; Masouras et al. 2008), the aspect ratio of fillers and the state of adhesion between fillers and matrix are both significant factors that should be considered when predicting the elastic modulus of particulate-reinforced composites. The postulation that adhesion between fillers and matrix is a significant determinant of elastic modulus contradicts the findings of earlier studies as reviewed by Hashim et al. (2021) and Fu et al. (2008). In contrast to the results of this study, some of the earlier investigations suggested that adhesion between fillers and matrix was an insignificant or irrelevant factor in relation to the prediction of elastic modulus for particulate–polymer composites.

4.8 Halloysite/Cellulose Fibre/Vinyl-Ester Eco-nanocomposites

(a)   Characteristics of elastic modulus and strength

Table 4.5 displays the results for elastic modulus, flexural strength, and impact strength. Compared to pure VER, ecocomposites and eco-nanocomposites had greater elastic modulus. In particular, the elastic modulus of ecocomposites VER/RCF increased by 162.3%. The improvement in elastic modulus is due to the higher initial modulus of the cellulose fibres acting as backbones in the composites (Guo et al. 2010).

The flexural strength of ecocomposite (148.4 MPa) was more than three times that of the pure sample (41.9 MPa). These significant enhancements in strength properties are attributed to the reinforcing effect imparted by cellulose fibres which are of high strength and modulus. Moreover, the ability of cellulose fibres in resisting bending force is also a contributor in the improved flexural strength (Chen et al. 2009). Since the role of matrix is to transfer the load to the stiff fibres through shear stresses at the interface, a good bond between the polymeric matrix and the fibres is required in this process.

Table 4.5 Elastic modulus and strength properties of pure VER, VER/RCF, and VER/RCF/HNT samples

Samples	RCF content (%)	HNT content (%)	Elastic modulus (GPa)	Flexural strength (MPa)	Impact strength (kJ/m^2)
VER	0	0	2.97 ± 0.2	41.9 ± 1.4	2.6 ± 0.2
VER/RCF	40	0	4.82 ± 1.1	148.4 ± 1.7	15.9 ± 1.2
VER/RCF/1%HNTs	40	1	5.11 ± 1.3	156.1 ± 1.5	16.81 ± 1.5
VER/RCF/3%HNTs	40	3	5.75.1 ± 1.2	161.2 ± 1.7	18.86 ± 1.3
VER/RCF/5%HNTs	40	5	5.24 ± 0.9	150.2 ± 1.3	16.12 ± 1.2

When compared to pure VER, the impact strength of ecocomposites was found to be six times larger at 15.9 kJ/m^2. As impact strength is defined as the ability of a material to resist fracture under conditions of stress applied at high speed, the marked enhancement of impact strength in the ecocomposites can be attributed to cellulose fibres having a superior ability to absorb impact energy compared to pure polymer (Arul et al. 2020). Similarly, good interfacial bonding is required for composites to exhibit enhanced impact strength. This is because when there is good bonding between fibres and matrix, the load requires for debonding or fibre pull-outs will be high and thus high impact resistance can be expected (Kim and Seo 2006). Previous studies have documented these improvements in elastic modulus and strength properties in polymer composites reinforced with natural fibres (Arul et al. 2020; Kim and Seo 2006; Facca et al. 2006).

The addition of HNTs to VER/RCF composites resulted in eco-nanocomposites with increased elastic modulus. Compared to unfilled ecocomposites, eco-nanocomposites reinforced with 1, 3, and 5 wt% of HNTs exhibited enhanced elastic moduli of 5.1, 5.8, and 5.2 GPa, respectively. Halloysite nanotubes have a high specific surface area which is favourable for interfacial interaction with the polymer matrix, thus promoting stronger bonding at the interfaces. Hence, HNTs are expected to hinder the mobility of surrounding chains in the polymer matrix, thus increasing the matrix stiffness (Zuiderduin et al. 2003). Moreover, HNTs have a higher elastic modulus (i.e. 10.1 GPa) when compared to pure VER (2.97 GPa) or VER/RCF samples (4.8 GPa).

The addition of HNTs imparted a moderate increase in both flexural strength and impact strength. When ecocomposites were reinforced with 1, 3, and 5 wt% HNTs, the flexural strength of eco-nanocomposites increased from 148.4 MPa to 156.1, 161.2, and 150.2 MPa, respectively. Similarly, the addition of HNTs at 1, 3, and 5 wt% increased the impact strength from 15.9 kJ/m^2 to 16.8, 18.9, and 16.1 kJ/m^2, respectively.

The SEM micrographs in Fig. 4.45 show the fracture surfaces of all samples. The investigation of the quality of fibre–matrix adhesion is based on fibre pull-outs, disparity in fibre lengths, fibre surfaces, and fibre–matrix gaps. Figure 4.45a shows that the pull-out lengths, the extent that individual fibres are debonded, were greater in the ecocomposites when compared to eco-nanocomposites shown in images of Fig. 4.45b–d. Moreover, Fig. 4.45a shows that the number of fibres that were pulled out was greater in the ecocomposites when compared to eco-nanocomposites. The greater pull-out lengths and greater number of fibres pulled out in ecocomposites is a consequence of poor interfacial adhesion and can be contrasted with the stronger fibre–matrix adhesion in eco-nanocomposites (Stocchi et al. 2007; Kim and Seo 2006). In the case of weak fibre–matrix adhesion, cracks propagate along the debonded fibre–matrix interfaces and result in greater fibre pull-out length and number. In contrast, when fibre–matrix adhesion is strong, the propagation of cracks along the debonded interfaces is less and thus less fibre pull-outs.

Interestingly, with loading of HNTs the length and number of fibres pulled out was clearly reduced compared to ecocomposites. In eco-nanocomposites with 3 wt%
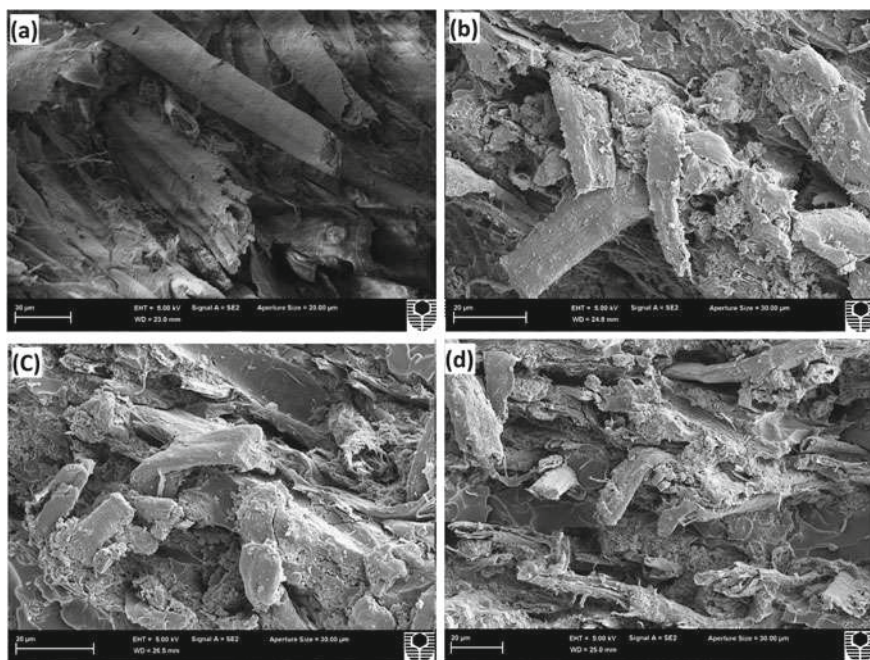
Fig. 4.45 SEM images of fracture surfaces of **a** eco-composite, **b** eco-nanocomposite with 1 wt% HNT loading, **c** eco-nanocomposite with 3 wt% HNT loading, and **d** eco-nanocomposite with 5 wt% HNT loading. All samples were subjected to three-point fracture toughness test

HNTs almost no fibre pull-outs are observed, and the fibres can be seen to be fractured instead due to strong interfacial bonding. Another distinguishing feature of the ecocomposites is the clean appearance of the fibre surfaces. This clean appearance is another indicator of poor adhesion between the matrix and fibres. This contrasts with the rough appearance of fibre surfaces in eco-nanocomposites as a result of strong fibre–matrix adhesion (Deng and Tang 2010). Finally, the matrix–fibre gaps appear larger in the ecocomposites compared to the eco-nanocomposites. These observations indicate that the addition of HNTs leads to stronger adhesion between fibre–matrix with concomitant strength improvements. The high surface area of HNTs increases the contact area within the matrix and thereby increases the interfacial bonding between the fibre and the polymer matrix (Chandradass et al. 2008; Avilés et al. 2011). In addition, HNTs can provide strong attractive forces to further enhance adhesion between the fibres and the matrix (Kumar et al. 2021).

With regard to the addition of 5 wt% HNTs, it was found that this concentration led to less improvement in strengths when compared to 1 and 3 wt% HNTs. Processing events are believed to underpin the failure of 5 wt% HNTs addition to further improve the strength. When there is a high loading of HNTs, the viscosity increases during mixing of resin and HNTs rendering insufficient degassing before curing. It is vital that during processing a complete degassing process is ensured for the composite
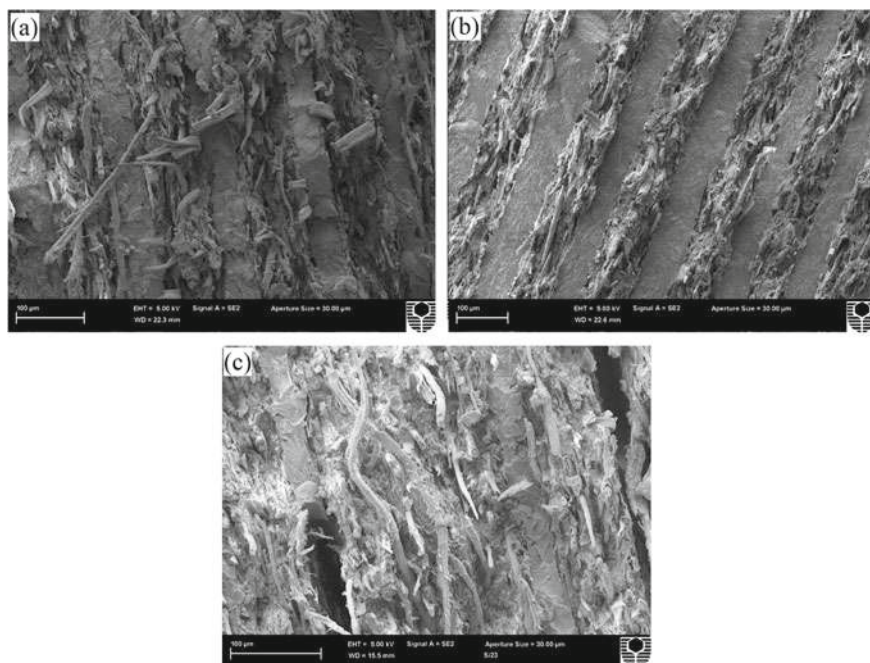
Fig. 4.46 SEM images show the fracture surfaces of samples with **a** 1 wt% HNTs, **b** 3 wt% HNTs, and **c** 5 wt% HNTs have with voids

to minimize void formation. The formation of voids in composites can act as stress concentrators to reduce the strength (Fu et al. 2008). The SEM images in Fig. 4.46 compare the fracture surfaces due to void formation in sample with 5 wt% HNTs with void-free samples with 1 and 3 wt% HNTs.

The ASTM D2734-94 standard was used to determine void content or porosity of the composite samples. The void contents for ecocomposites and 1, 3, and 5 wt% eco-nanocomposites were determined to be 3.3% and 1.1, 0.57, and 3.1%, respectively. Eco-nanocomposites exhibited a lower void content when compared to ecocomposites. Eco-nanocomposites with 3 wt% exhibited the lowest void content (0.57%). However, the void content for 5 wt% (3.1%) was almost the same as the unfilled ecocomposites (3.3%). A plausible explanation is that the addition of 5 wt% HNTs caused an increase in the resin viscosity, thus resulting in a reduction of fibre wettability by the matrix or interfacial adhesion.

SEM observations of fibre/matrix adhesion combined with the calculation values of void content support the observed strength results. Thus, the higher strengths exhibited by 3 wt% eco-nanocomposites are attributed to strong fibre/matrix adhesion and low void content. In contrast, weaker fibre/matrix adhesion and higher void contents resulted in lower strength.

Table 4.6 Toughness properties of pure VER, VER/RCF, and VER/RCF/HNT samples

Sample	RCF content (%)	HNT content (%)	Fracture toughness (MPa m$^{1/2}$)	Impact toughness (kJ/m^2)
VER	0	0	1.8 ± 0.2	1.5 ± 0.2
VER/RCF	40	0	4.4 ± 0.5	42.3 ± 2.1
VER/RCF/1%n-SiC	40	1	3.84 ± 0.3	36.5 ± 1.5
VER/RCF/3%n-SiC	40	3	3.06 ± 0.2	26.2 ± 1.3
VER/RCF/5%n-SiC	40	5	3.12 ± 0.9	29.3 ± 1.2

(b)   Fracture Toughness

Table 4.6 shows that, compared to pure samples, the ecocomposites have greater fracture toughness and impact toughness. The improved fracture toughness may be attributed to the pronounced display of crack deflection, interfacial debonding, fibre bridging, and pull-outs in these materials (Kim and Seo 2006; Alhuthali et al. 2012). When compared to pure VER samples which are quite brittle like all thermosetting resins (1.8 MPa m$^{1/2}$), ecocomposites are much tougher with 4.4 MPa m$^{1/2}$. Similarly, compared to pure samples, with an impact toughness of 1.5 kJ/ m^2, ecocomposites are also much tougher with an impact toughness of 42.3 kJ/m^2. However, toughness properties were reduced on increasing the loading of HNTs. Addition of 1, 3, and 5 wt% HNTs reduced the fracture toughness to 3.8, 3.1, and 3.1 MPa m$^{1/2}$, respectively. Similar reductions in impact toughness were observed impact toughness.

4.9   Nano-SiC/Cellulose Fibre/Viny-Ester Eco-nanocomposites

(a)   Elastic Modulus and Strength

Elastic modulus, flexural strength, and impact strength results are provided (Table 4.7). Compared to neat VER (2.97 GPa), the elastic moduli of the ecocomposites and eco-nanocomposites were found to be greater. There was a 162.3% increase in the elastic modulus of VER/RCF ecocomposite (4.81 GPa). This enhancement is believed to be attributable to the higher initial modulus of the cellulose fibres (Espert et al. 2004).

Compared to neat VER (41.9 MPa), the flexural strength of ecocomposites was significantly greater (148.4 MPa). The enhancement in strength is believed to be attributable to a reinforcing effect imparted by the high-strength and high-modulus cellulose fibres as well as the resistance to bending force that the fibres provide. Fibre–matrix interaction is also critical to composite strength. Good bonding between polymeric matrix and the fibres facilitates the role of the matrix in transferring load to stiff fibres through shear stresses at the interface (Qin et al. 2011).

Table 4.7 Elastic modulus and strength properties of pure VER, VER/RCF, and VER/RCF/n-SiC samples

Samples	RCF content (%)	n-SiC content (%)	Elastic modulus (GPa)	Flexural strength (MPa)	Impact strength (kJ/m^2)
VER	0	0	2.9 ± 0.2	41.9 ± 1.4	2.6 ± 0.2
VER/RCF	40	0	4.8 ± 1.1	148.4 ± 1.7	15.9 ± 1.2
VER/RCF/1% n-SiC	40	1	5.8 ± 1.2	173.1 ± 1.5	21.8 ± 1.4
VER/RCF/3% n-SiC	40	3	6.2 ± 1.2	176.1 ± 1.7	24.6 ± 1.3
VER/RCF/5% n-SiC	40	5	6.9 ± 1.4	179.4 ± 1.3	27.4 ± 1.1

Compared to neat VER (2.6 kJ/m^2), the impact strength of the ecocomposites was significantly greater (15.9 kJ/m^2). This increase in strength is attributed to the superior ability of cellulose fibres in impact energy absorption compared to that of the pure polymer.

Energy absorption in fibre–polymer composite materials occurs through the energy dissipation mechanisms of fibre pull-out and fibre debonding. Favourable fibre–matrix interaction promotes good interfacial bonding which is also a significant factor for enhancing impact strength (Arul et al. 2020). These improvements in elastic modulus and strength properties in polymer composites reinforced with natural fibres have been reported by earlier studies (Wambua et al. 2003; Arul et al. 2020).

The addition of n-SiC was found to enhance the elastic moduli of the samples. The elastic modulus of the unfilled ecocomposites was 4.8 GPa whereas addition of 1, 3, and 5 wt% of n-SiC led to eco-nanocomposites with elastic moduli of 5.8, 6.2, and 6.9 GPa, respectively. The n-SiC used in this study, as other nano-fillers, has a high specific surface area, which is believed to provide dense interfacial interaction with polymer matrix. It is believed that the presence of n-SiC affects the mobility of surrounding chains in the polymer matrix which leads to increased matrix stiffness. Another reason believed to lead to increased matrix stiffness is the very high initial elastic modulus of the n-SiC (470 GPa) compared to that of pure VER (2.9 GPa) and the VER/RCF ecocomposites (4.8 GPa). By the rule of mixtures, this high initial elastic modulus is believed to also contribute to the increased elastic modulus of each the eco-nanocomposites observed in this study (Ma et al. 2008; Zuiderduin et al. 2003). These two effects of n-SiC are believed to contribute to the overall stiffness of the composite.

The addition of n-SiC was also found to enhance the flexural strength and impact strength of the samples. The flexural strength of the unfilled ecocomposites was 148.4 MPa whereas addition of 1, 3, and 5 wt% n-SiC led to eco-nanocomposites with flexural strengths of 173.1, 176.1, and 179.4 MPa, respectively. The addition of 1, 3, and 5 wt% of n-SiC also increased the impact strength of the samples from

15.9 kJ/m^2 for unfilled ecocomposite to 21.8, 24.6 and 27.4 kJ/m^2 respectively for the eco-nanocomposites. Fibre–matrix adhesion, as mentioned, is an important determinant of composite quality. In fibre-reinforced composites, the matrix has the role of transferring load from the matrix to the fibres. This occurs through shear stresses at the interface. Effective transfer of load requires a strong bond to be formed between the polymeric matrix and the fibres (Chen et al. 2009; Herrera-Franco and Valadez-González 2005).

The fracture surfaces of all composites are shown in Fig. 4.47 which reveals an extensive occurrence of fibre pull-outs. In addition, these micrographs also reveal useful information about the fibre surfaces and interfacial debondings. It is worth noting that the pull-out lengths and the number of pull-outs were greater in ecocomposites (see Fig. 4.47a) when compared to eco-nanocomposites (see Fig. 4.47b–d). This supports the notion that the strength of interfacial adhesion is stronger in eco-nanocomposites compared to ecocomposites. In the presence of weak interfacial adhesion, cracks tend to propagate through the fibre–matrix interfaces and result in greater fibre pull-out lengths and numbers. In contrast, when fibre–matrix adhesion is strong, propagation of cracks through the fibre–matrix interfaces is less and thus less fibre pull-outs are observed. Interestingly, as the loading of n-SiC increased from 1 to 3% and then to 5%, the lengths and numbers of fibre pull-outs were reduced. For example, in eco-nanocomposites with 5 wt% n-SiC almost no fibre pull-outs were
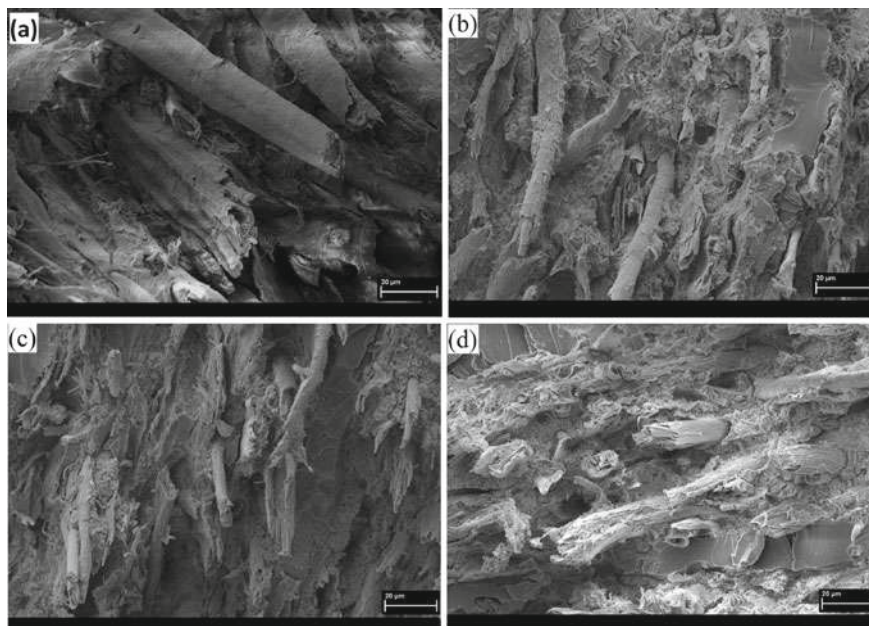

Fig. 4.47 SEM images of fracture surfaces: **a** ecocomposite, **b** eco-nanocomposite with 1 wt% n-SiC loading, **c** eco-nanocomposite with 3 wt% n-SiC loading, **d** eco-nanocomposite with 5 wt% n-SiC loading. All samples were subjected to three-point bending test

observed, and the fibres were broken off with no interfacial debonding. These observations are a result of strong adhesion between the fibres and the matrix (Stocchi et al. 2007; Abdelmouleh et al. 2007). The micrographs also show the roughness of the fibre surface increases with increasing n-SiC loading. Ecocomposites with no n-SiC addition have fibre surfaces which appear smooth which indicate poor interfacial adhesion (Rosa et al. 2010). In addition, the interfacial gaps due to debonding appear larger in ecocomposites when compared to eco-nanocomposites. These fracture surface images indicate that the addition of n-SiC has led to the display of a stronger matrix–fibre adhesion.

The notion of thermal expansion mismatch may explain the improvements in observed interfacial adhesion for eco-nanocomposites. Because of thermal expansion mismatch, stresses can develop at the interface between matrix and filler of composite materials. The magnitude of radial (β_r) and tangential (β_t) stresses induced as a result of thermal expansion mismatch can be estimated from the following equation (Low 1990a, 1990b):

$$-\pi_r = 2\pi_t = \frac{\Delta\alpha\,\Delta T}{(1 + v_m/2E_m) + (1 - 2v_f/E_f)}$$

$$\leq \Delta\alpha\,\Delta T\,E_m$$

where α, T, v, and E represent the linear thermal expansion coefficient, temperature, Poisson's ratio, and elastic modulus, respectively. The matrix is referred to using (m) and dispersed filler is (f). The thermal expansion characteristics of the phases at the interface play a dominant role in determining the nature of these stresses.

In this study, the polymer matrix is reinforced with RCF and n-SiC. These two phases have a lower thermal expansion coefficient (1×10^{-6} and 2.77×10^{-6} °C^{-1}, respectively) (Duigou et al. 2010; Slack and Bartram 1975) when compared to VER (56.8×10^{-6} °C^{-1}). Therefore, $\Delta\alpha$ for the two systems, RCF/VER and n-SiC/VER, is negative. In the case of RCF/VER, a compressive radial stress of approximately 3.24 MPa is induced at the RCF/VER interface with the production of tensile tangential stresses in the matrix. Compressive radial stresses of about 3.47 MPa are generated at the n-SiC/VER interface in concert with the production of tensile tangential stresses in the matrix. These stresses serve to increase the intrinsic bond developed at the interfaces between VER and both fillers (i.e. RCF and n-SiC) (Low 1990a, 1990b). Under this circumstance and due to the presence of these lower thermal expansion fillers extra compressive stresses can be induced at the filler/VER interfaces which serve to improve the interfacial adhesion. Thus, the improved strengths of eco-nanocomposites can be attributed to enhance adhesion at the fibre–matrix interfaces due to the addition of n-SiC as discussed previously.

Table 4.8 Toughness of pure VER, VER/RCF, and VER/RCF/n-SiC samples

Samples	RCF content (%)	n-SiC content (%)	Fracture toughness (MPa m$^{1/2}$)	Impact toughness (kJ/m^2)
VER	0	0	1.8 ± 0.2	1.5 ± 0.2
VER/RCF	40	0	4.4 ± 0.5	42.3 ± 2.1
VER/RCF/1%n-SiC	40	1	2.9 ± 0.1	28.7 ± 1.7
VER/RCF/3%n-SiC	40	3	2.7 ± 0.2	26.4 ± 1.2
VER/RCF/5%n-SiC	40	5	2.5 ± 0.1	23.1 ± 1.3

(b)   Fracture Toughness

The ecocomposites had significantly greater fracture toughness and impact toughness compared to the pure samples (Table 4.8). As expected, ecocomposites displayed greater values of fracture toughness and impact toughness relative to the control. It is the interaction of cellulose fibres with the polymer matrix that is believed to enable ecocomposites to exhibit the desirable energy dissipating, crack deflection, and fracture resistance properties (Ma et al. 2008). In this study, the fracture toughness and impact toughness of ecocomposites were significantly enhanced when compared to the control. The favourable fracture toughness properties that natural fibre–polymer composites typically display are believed to be determined through crack deflection, debonding between fibre and matrix, the pull-out effect, and a fibre-bridging mechanism (Zuiderduin et al. 2003).

A plausible explanation for the enhanced toughness properties found for the ecocomposites in this study is the effect of toughness mechanisms provided by RCF. Pure samples had a fracture toughness of 1.8 MPa m$^{1/2}$ whereas ecocomposites had a fracture toughness of 4.4 MPa m$^{1/2}$. Similarly, the impact toughness of ecocomposites (42.3 kJ/m^2) was significantly higher than the impact toughness of the pure samples (1.5 kJ m^2). However, increasing the loading of n-SiC reduced the sample toughness properties. For example, the addition of 5 wt% n-SiC reduced the fracture toughness from 4.4 to 2.5 MPa m$^{1/2}$ and the impact toughness from 42.3 to 23.1 kJ/m^2. The addition of n-SiC, as mentioned, resulted in strength improvements by virtue of enhanced interfacial adhesion. However, fibre–matrix adhesion enhancement causes the eco-nanocomposites to become more brittle inhibiting fibre debonding and fibre pull-out and ultimately leading to lower fracture toughness (Ma et al. 2008; Stocchi et al. 2007).

Figure 4.48 displays the load–displacement curves for fracture testing of VER, ecocomposites, and eco-nanocomposites. For the composite samples, after the initial rise, nonlinearity occurs until the peak fracture load. This shift from linearity to nonlinearity is indicative of improved toughness in the composite samples. For pure VER, the figure shows catastrophic failure at a lower fracture load. In contrast, for ecocomposite samples, the results suggest better durability with these materials initially resisting fracture and failing only at a much higher fracture load. Moreover, the ecocomposites failed in a graceful manner exhibiting a discontinuous fracture or multiple "stick–slip" fracture. Repeated occurrence of crack initiation, arrests,
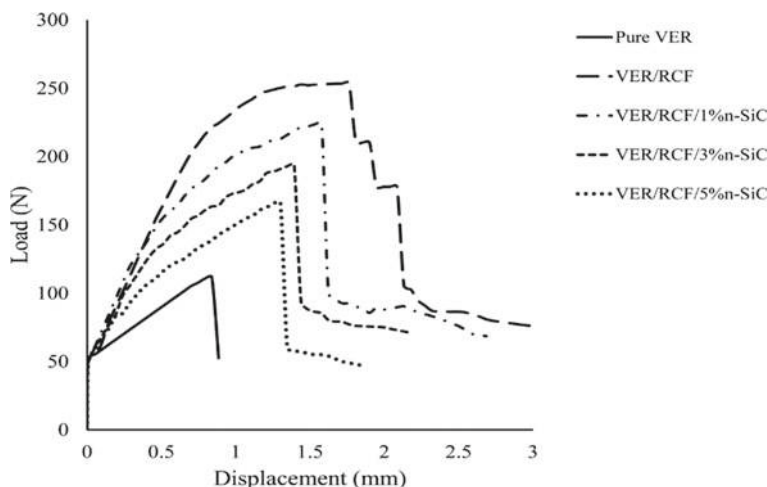
Fig. 4.48 Load–displacement curves of pure VER, VER/RCF, and VER/RCF/n-SiC samples during flexural toughness testing

and fibres debonding at the RCF sheet/epoxy interfaces is the most plausible explanation for the observed nonlinearity. SEM images of the fracture surfaces support this explanation (see Fig. 4.47a). For the eco-nanocomposites, these samples exhibited a dramatic failure at lower fracture load than the ecocomposites. The dramatic failures of eco-nanocomposites are indicative of simultaneous fracture of the matrix and the fibres. This explanation is consistent with the appearance of the fracture surfaces of these samples (see Fig. 4.47b–d). However, it should be noted that the pronounced display of nonlinear fracture behaviour in both ecocomposites and eco-nanocomposites implies that the principles of linear elastic fracture mechanics are invalid for the measured K_{IC} values and these quoted values are apparent but not "true" fracture toughness. As such, these materials will invariably exhibit an R-curve fracture behaviour by virtue of extensive slow crack growth and fibre bridging at the crack wake.

References

Abacha N, Kubouchi M, Tsuda K et al (2007) Performance of epoxy-nanocomposite under corrosive environment. Exp Polym Lett 1(6):364–369

Abdelmouleh M, Boufi S, Belgacem MN et al (2007) Short natural-fibre reinforced polyethylene and natural rubber composites: effect of silane coupling agents and fibres loading. Compos Sci Technol 67(7–8):1627–1639

Ahmad FN, Jaafar M, Palaniandy S et al (2008) Effect of particle shape of silica mineral on the properties of epoxy composites. Compos Sci Technol 68:346–353

Alam P (2010) A mixtures' model for porous particle–polymer composites. Mech Res Commun 37:389–393

Alamri H, Low IM (2012a) Characterization of epoxy hybrid composites filled with cellulose fibres and nano-SiC. J Appl Polym Sci 126:E221–E231

Alamri H, Low IM (2012b) Microstructural, mechanical and thermal characteristics of recycled cellulose fiber- halloysite-epoxy hybrid nanocomposites. Polym Compos 33:589–600

Alhuthali A, Low IM, Dong C (2012) Characterisation of the water absorption, mechanical and thermal properties of recycled cellulose fibre reinforced vinyl-ester eco-nanocomposites. Compos B Eng 43(7):2772–2781

Alhuthali A, Low IM (2021) Vinyl-ester composites reinforced with natural fibers and nanofillers, Chapter 9. In: Low I-M, Dong Y (eds) Composite materials. Elsevier, pp 227–244. ISBN 9780128205129

Alonso-Montemayor FJ, Narro-Céspedes RI, Neira-Velázquez MG et al (2022) Biofibers for polymer reinforcement: Macro and micro mechanical points of view. In: Handbook of research on bioenergy and biomaterials: consolidated and green Processes. Apple Academic Press - CRC Press, pp 479–498

Arul M, Sasikumar KSK, Sambathkumar M et al (2020) Mechanical and fracture study of hybrid natural fiber reinforced composite—coir and sugarcane leaf sheath. Mater Today Proc 33(7):2795–2797

Ashori A, Nourbakhsh A (2009) Characteristics of wood–fiber plastic composites made of recycled materials. Waste Manage 29:1291–1295

ASTM International (2007) Standard test methods for flexural properties of unreinforced and reinforced plastics and electrical insulating materials, in D790

Athijayamani A, Thiruchitrambalam M, Natarajan U et al (2009) Effect of moisture absorption on the mechanical properties of randomly oriented natural fibers/polyester hybrid composite. Mater Sci Eng, A 517:344–353

Avilés F, Cauich-Rodríguez JV, Rodríguez-González JA et al (2011) Oxidation and silanization of MWCNTs for MWCNT/vinyl ester composites. Express Polym Lett 5(9):766–776

Bakare IO, Okieimen FE, Pavithran C et al (2010) Mechanical and thermal properties of sisal fiber-reinforced rubber seed oil-based polyurethane composites. Mater Des 31:4274–4280

Bledzki AK, Faruk O (2004) Creep and impact properties of wood fibre–polypropylene composites: influence of temperature and moisture content. Compos Sci Technol 64:693–700

Bozkurt E, Kaya E, Tanoğlu M (2007) Mechanical and thermal behaviour of non-crimp glass fibre reinforced layered clay/epoxy nanocomposites. Compos Sci Technol 67:3394–3403

Buehler FU, Seferis JC (2000) Effect of reinforcement and solvent content on moisture absorption in epoxy composite materials. Composites A 31:741–748

Ceretti A, Daniel V, da Silva E et al (2019) The role of dispersion technique and type of clay on the mechanical properties of clay/epoxy composites. Macromol Symp 383:1800055

Chai H, Wang X, Rehman WU et al (2021) Study on water absorption and mechanical properties of CNF–Ti reinforced epoxy resin composites.Plast Rubber Compos.https://doi.org/10.1080/146 58011.2021.2017127

Chandradass J, Ramesh Kumar M, Velmurugan R (2008) Effect of clay dispersion on mechanical, thermal and vibration properties of glass fiber-reinforced vinyl ester composites. J Reinf Plast Compos 27(15):1585–1601

Chen B, Evans JRG (2006) Elastic moduli of clay platelets. Scripta Mater 54:1581–1585

Chen C, Justice RS, Schaefer DW et al (2008) Highly dispersed nanosilica-epoxy resins with enhanced mechanical properties. Polymer 49:3805–3815

Chen H, Miao M, Ding X (2009) Influence of moisture absorption on the interfacial strength of bamboo/vinyl ester composites. Compos A Appl Sci Manuf 40(12):2013–2019

Cohen LJ, Ishai O (1967) The elastic properties of three-phase composites. J Compos Mater 1(4):390–403

De Rosa IM, Santali C, Sarasini F (2010) Mechanical and thermal characterization of epoxy composites reinforced with random and quasi-unidirectional untreated Phormium tenax leaf fibers. Mater Des 31:2397–2405

Deng S, Tang Y (2010) Increasing load-bearing capacity of wood-plastic composites by sandwiching natural and glass fabrics. J Reinf Plast Compos 29(20):3133–3148

Deng S, Zhang J, Ye L (2009) Halloysite–epoxy nanocomposites with improved particle dispersion through ball mill homogenisation and chemical treatments. Compos Sci Technol 69:2497

Dhakal HN, Zhang ZY, Richardson MOW (2007) Effect of water absorption on the mechanical properties of hemp fibre reinforced unsaturated polyester composites. Compos Sci Technol 67:1674–1683

Dong Y, Chaudhary D, Ploumis C et al (2011) Correlation of mechanical performance and morphological structures of epoxy micro/nanoparticulate composites. Composites A 42:1483–1492

Espert A, Vilaplana F, Karlsson S (2004) Comparison of water absorption in natural cellulosic fibres from wood and one-year crops in polypropylene composites and its influence on their mechanical properties. Composites A 35(11):1267–1276

Facca AG, Kortschot MT, Yan N (2006) Predicting the elastic modulus of natural fibre reinforced thermoplastics. Composites A 37(10):1660–1671

Fu SY, Feng XQ, Lauke B et al (2008) Effects of particle size, particle/matrix interface adhesion and particle loading on mechanical properties of particulate–polymer composites. Compos B Eng 39(6):933–961

Gantenbein D, Schoelkopf J, Matthews GP et al (2011) Determining the size distribution-defined aspect ratio of rod-like particles. Appl Clay Sci 53:538–543

Guo Q, Cheng B, Kortschot M et al (2010) Performance of long Canadian natural fibers as reinforcements in polymers. J Reinf Plast Compos 29(21):3197–3207

Hashim MKR, Abdul Majid MS, Ridzuan MJM (2021) Review of fatigue responses of fiber-reinforced polymer (FRP) composite. In: Jawaid M, Hamdan A, Hameed Sultan MT (eds) Structural health monitoring system for synthetic, hybrid and natural fiber composites. Composites science and technology. Springer, Singapore. https://doi.org/10.1007/978-981-15-8840-2_9

Hedicke-Höchstötter K, Lim GT, Altstädt V (2009) Novel polyamide nanocomposites based on silicate nanotubes of the mineral halloysite. Compos Sci Technol 69:330–334

Herrera-Franco PJ, Valadez-González A (2005) A study of the mechanical properties of short natural-fiber reinforced composites. Composites B 36(8):597–608

Hossain MK, Imran KA, Hosur MV et al (2011) Degradation of mechanical properties of conventional and nanophased carbon-epoxy composites in seawater. J Eng Mater Technol 133(4):41004

Ismail H, Pasbakhsh P, Fauzi MNA et al (2008) Morphological, thermal and tensile properties of halloysite nanotubes filled ethylene propylenediene monomer (EPDM) nanocomposites. Polym Testing 27:841–850

Kaully T, Siegmann A, Shacham D (2008) Mechanical behavior of highly filled natural $CaCO_3$ composites: effect of particle size distribution and interface interactions. Polym Compos 29:396–408

Khan SU, Iqbal K, Munir A et al (2010) Quasi-static and impact fracture behaviours of CFRPs with nanoclay-filled epoxy matrix. Composites A 42:53–264

Khan SU, Iqbal K, Munir A et al (2011) Quasi-static and impact fracture behaviors of CFRPs with nanoclay-filled epoxy matrix. Composites A 42:253–264

Kim HJ, Seo DW (2006) Effect of water absorption fatigue on mechanical properties of sisal textile-reinforced composites. Int J Fatigue 28(10):1307–1314

Kim BC, Park SW, Lee DG (2008) Fracture toughness of the nano-particle reinforced epoxy composite. Compos Struct 86:69–77

Kumar PSS, Allamraju KV (2019) A review of natural fiber composites (jute, sisal, kenaf). Mater Today Proc 18(7):2556–2562

Kumar S, Prasad L, Patel VK et al (2021) Physico-mechanical properties and Taguchi optimized abrasive wear of alkali treated and fly ash reinforced Himalayan Agave fiber polyester composite. J Nat Fibers. https://doi.org/10.1080/15440478.2021.1982818

Kumar P, Ram CS, Srivastava JP et al (2022) Physical and chemical properties of cotton fiber-based composites.https://doi.org/10.1002/9783527832996.ch8

Le Guen MJ, Newman RH (2007) Pulped phormium tenax leaf fibres as reinforcement for epoxy composites. Composites A 38:2109–2115

Le Duigou A, Davies P, Baley C (2010) Interfacial bonding of flax fibre/Poly(l-lactide) bio-composites. Compos Sci Technol 70(2):231–239

Lee JH, Rhee KY, Lee JH (2010) Effects of moisture absorption and surface modification using 3-aminopropyltriethoxysilane on the tensile and fracture characteristics of MWCNT/epoxy nanocomposites. Appl Surf Sci 256:7658–7667

Low IM (1990a) Effects of residual stresses on the failure micromechanisms in toughened epoxy systems. J Mater Sci 25(4):2144–2148

Low IM (1990b) Toughening of epoxies by thermal expansion mismatch. J Appl Polym Sci 39:759–762

Low IM, Somers J, Kho HS et al (2009) Fabrication and properties of recycled cellulose fibre-reinforced epoxy composites. Compos Interfaces 16(7–9):659–669

Lu SR, Jiang YM, Wei C (2009) Preparation and characterization of EP/SiO$_2$ hybrid materials containing PEG flexible chain. J Mater Sci 44:4047

Lui Q, Hughes M (2008) The fracture behaviour and toughness of woven flax fibre reinforced epoxy composites. Composites A 39:1644–1652

Ma J, Mo MS, Du XS et al (2008) Effect of inorganic nanoparticles on mechanical property, fracture toughness and toughening mechanism of two epoxy systems. Polymer 49(16):3510–3523

Maleque MA, Belal FY (2007) Mechanical properties study of pseudo-stem banana fibre reinforced epoxy composite. Arab J Sci Eng 32(2B):359–364

Masouras K, Silikas N, Watts DC (2008) Correlation of filler content and elastic properties of resin-composites. Dent Mater 24:932–939

McGrath M, Vilaiphand W, Vaihola S et al (2004) Synthesis and properties of clay-ZrO$_2$-cellulose fibre-reinforced polymeric nano-hybrids. In: Structural integrity and fracture: proceedings off the international conference, SIF 2004, pp 265–270

Meng J, Hu X (2004) Synthesis and exfoliation of bismaleimide–organoclay nanocomposites. Polymer 45:9011–9018

Mishra S, Mohanty AK, Drzal LT et al (2003) Studies on mechanical performance of biofibre/glass reinforced polyester hybrid composites. Compos Sci Technol 63:1377–1385

Mylsamy K, Rajendran I (2011) The mechanical properties, deformation and thermomechanical properties of alkali treated and untreated Agave continuous fibre reinforced epoxy composites. Mater Des 32:3076–3084

Mylsamy B, Palaniappan SK, Subramani SP et al (2019) Impact of nanoclay on mechanical and structural properties of treated Coccinia indica fibre reinforced epoxy composites. J Market Res 8(6):6021–6028

Nassar MMA, Alzebdeh KI, Pervez T et al (2021) Progress and challenges in sustainability, compatibility, and production of eco-composites: a state-of-art review. J Appl Polym Sci 138:e51284. https://doi.org/10.1002/app.51284

Ning NY, Yin QJ, Luo F et al (2007) Crystallization behavior and mechanical properties of polypropylene/halloysite composites. Polymer 48:7374–7384

Piechota K, Czaja K, Bączek M et al (2021) Effect of a new amido-imidazolium compound as a clay modifier on properties of polypropylene composites. https://doi.org/10.1002/pc.26428

Pothan LA, Oommen Z, Thomas S (2003) Dynamic mechanical analysis of banana fibre reinforced polyester composites. Compos Sci Technol 63:283–293

Prashantha K, Lacrampe MF, Krawczak P (2011) Processing and characterization of halloysite nanotubes filled polypropylene nanocomposites based on a masterbatch route: effect of halloysites treatment on structural and mechanical properties. Express Polym Lett 5:295–307

Qi B, Zhang QX, Bannister M et al (2006) Investigation of the mechanical properties of DGEBA-based epoxy resin with nanoclay additives. Compos Struct 75:514–519

Qin L, Qiu J, Liu M et al (2011) Mechanical and thermal properties of poly(lactic acid) composites with rice straw fiber modified by poly(butyl acrylate). Chem Eng J 166(2):772–778

Reddy RA, Yoganandam K, Mohanavel V (2020) Effect of chemical treatment on natural fiber for use in fiber reinforced composites—review. Mater Today Proc 33(7):2996–2999

Rong MZ, Zhang MQ, Lui Y et al (2001) The effect of fibre treatment on the mechanical properties of unidirectional sisal-reinforced epoxy composites. Compos Sci Technol 61:1437–1447

Ruoyuan S, Teruo K, Haruhiro I (2010) Papermaking from waste silk and its application as reinforcement of green composites. J Text Eng 56(3):71–76

Saber D, Alghtani AH, Ahmed EM et al (2021) Enhancement of barrier and mechanical performance of steel coated with epoxy filled with micron and nano alumina fillers. Mat Res. https://doi.org/10.1590/1980-5373-mr-2021-0413

Sánchez-Soto M, Pagés P, Lacorte T et al (2007) Curing FTIR study and mechanical characterization of glass bead filled trifunctional epoxy composites. Compos Sci Technol 67:1974–1985

Satapathy A, Jha AK, Mantry S et al (2010) Processing and characterization of jute-epoxy composites reinforced with SiC derived from rice husk. J Reinf Plast Compos 29(18):2869–2878

Shahinur S, Hasan M (2020) Jute/coir/banana fiber reinforced bio-composites: critical review of design, fabrication, properties and applications. In: Hashmi S, Choudhury IA (eds) Encyclopedia of renewable and sustainable materials. Elsevier, pp 751–756

Silva RV, Spinelli D, Bose WW et al (2006) Fracture toughness of natural fibers/castor oil polyurethane composites. Compos Sci Technol 66:1328–1335

Singh R, Singh B, Gupta M et al (2021) Mechanical properties and dimensional stability of jute/VER-isocyanate hybrid matrix composites. Polym Polym Compos 29:S803–S816

Sivaperumal R, Jancirani J (2021) Characterization of amino silane modified ramie fibre, OMMT nanoclay-reinforced epoxy resin composite. Silicon. https://doi.org/10.1007/s12633-021-01502-9

Slack GA, Bartram SF (1975) Thermal expansion of some diamondlike crystals. J Appl Phys 46(1):89–98

Sombatsompop N, Chaochanchaikul K (2004) Effect of moisture content on mechanical properties, thermal and structural stability and extrude texture of poly(vinyl chloride)/wood sawdust composites. Polym Int 53:1210–1218

Stocchi A, Bernal C, Vazquez A et al (2007) A silicone treatment compared to traditional natural fiber treatments: effect on the mechanical and viscoelastic properties of jute–vinyl ester laminates. J Compos Mater 41(16):2005–2024

Subramaniyan AK, Sun CT (2007) Toughening polymeric composites using nanoclay: crack tip scale effects on fracture toughness. Composites A 38:34–43

Suppakarn N, Jarukumjorn K (2009) Mechanical properties and flammability of sisal/PP composites: effect of flame-retardant type and content. Composites B 40:613–618

Tang Y, Deng S, Ye L et al (2011) Effects of unfolded and intercalated halloysites on mechanical properties of halloysite–epoxy nanocomposites. Compos Part A Appl Sci Manuf 42(4):345–354

Wambua P, Ivens J, Verpoest I (2003) Natural fibres: can they replace glass in fibre reinforced plastics? Compos Sci Technol 63:1259–1264

Wang K, Chen L, Wu J et al (2005) Epoxy nanocomposites with highly exfoliated clay: mechanical properties and fracture mechanisms. Macromolecules 38:788–800

Wang L, Wang K, Chen L et al (2006) Hydrothermal effects on the thermomechanical properties of high-performance epoxy/clay nanocomposites. Polym Eng Sci 46(2):215–221

Wetzel B, Rosso P, Haupert F et al (2006) Epoxy nanocomposites—fracture and toughening mechanisms. Eng Fract Mech 73(16):2375–2398

Xu Y, Hoa SV (2008) Mechanical properties of carbon fibre reinforced epoxy/clay nanocomposites. Compos Sci Technol 68:854–861

Yan W, Lin RJT, Bhattacharyya D (2006) Particulate reinforced rotationally moulded polyethylene composites—mixing methods and mechanical properties. Compos Sci Technol 66:2080–2088

Yasmin A, Luo JJ, Abot JL et al (2006) Mechanical and thermal behavior of clay/epoxy nanocomposites. Compos Sci Technol 66(14):2415–2422

Ye Y, Chen H, Wu J et al (2007) High impact strength epoxy nanocomposites with natural nanotubes. Polymer 48:6426–6433

Ye Y, Chen H, Wu J et al (2011) Interlaminar properties of carbon fiber composites with halloysite nanotube-toughened epoxy matrix. Compos Sci Technol 71:717–723

Zainuddin S, Hosura MV, Zhoua Y et al (2010) Experimental and numerical investigations on flexural and thermal properties of nanoclay–epoxy nanocomposites. Mater Sci Eng A 527:7920–7926

Zhao H, Li RKY (2008) Effect of water absorption on the mechanical and dielectric properties of nano-alumina filled epoxy nanocomposites. Composites A 39:602–611

Zhao S, Schadler LS, Hillborg H et al (2008) Improvements and mechanisms of fracture and fatigue properties of well-dispersed alumina/epoxy nanocomposites. Compos Sci Technol 68:2976–2982

Zuiderduin WCJ, Westzaan C, Huétink J et al (2003) Toughening of polypropylene with calcium carbonate particles. Polymer 44(1):261–275

Zulfli NHM, Shyang CW (2010) Flexural and morphological properties of epoxy/glass fibre/silane-treated organo montmorillonite composites. J Phys Sci 21:41–50

Chapter 5
Materials Properties: Moisture Absorption and Durability

Check for updates

Abstract The role of water absorption on the physical and mechanical properties of cellulose fibre-reinforced epoxy and vinyl-ester ecocomposites and econanocomposites were investigated. Water absorption was found to decrease as the nanoclay content increased. The flexural strength, flexural modulus, and fracture toughness significantly decreased as a result of water absorption. However, the properties of impact strength and impact toughness were found to increase after exposing to water. The addition of nanoclay slightly minimized the effect of moisture on the mechanical properties. SEM images showed that water absorption severely damaged the cellulose fibres and the bonding at fibre–matrix interfaces in wet composites.

Keywords Nanocomposites · Cellulose fibres · Nanoclay · Water uptake · Moisture diffusion · Microstructure · SEM · TEM · Mechanical properties · Flexural strength · Flexural modulus · Impact strength · Impact toughness · Fracture toughness

5.1 Cellulose Fibre/Epoxy Ecocomposites

(a) Effect of fibre content on water absorption behaviour

The amount of water uptake in the composites was determined using the following equation:

$$M_t(\%) = \left(\frac{W_t - W_o}{W_o} \right) \times 100$$

where W_t is the weight of the sample at time t and W_o is the initial weight of the sample.

Figure 5.1 illustrates the effect of fibre content on the water absorption behaviour of the RCF/epoxy ecocomposites. Water absorption increases with an increase in time of immersion for all samples. The water uptake rate is linear and very rapid in the beginning of the exposure, after which it slows down and reaches the saturation level (Dhakal et al. 2007; Kim and Seo 2006). It can be observed that water absorption increases as fibre content increases. This result is expected due the hydrophilic
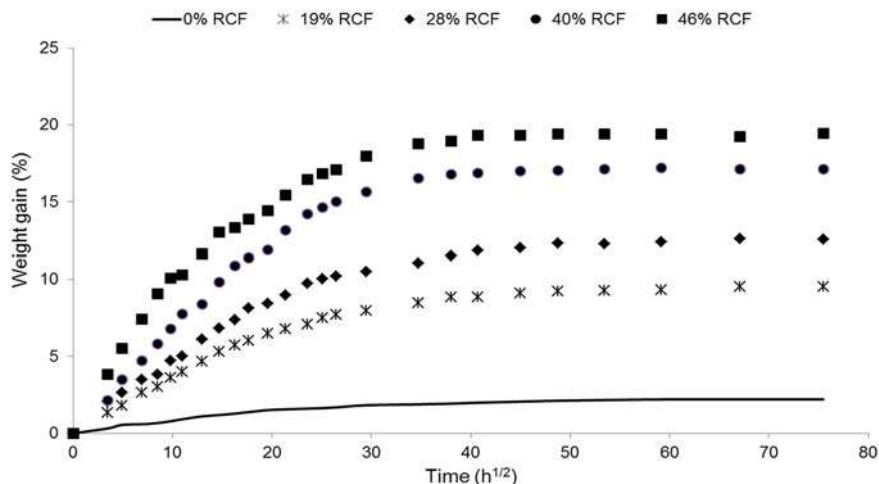
Fig. 5.1 Water absorption curves of RCF/epoxy ecocomposites

nature of cellulose fibres. Therefore, an increase in cellulose-fibre content leads to an increase in water absorption content (Kim and Seo 2006). Moreover, cellulose fibres have a central hollow region (i.e. the lumen) which allows much water to be absorbed via the capillary effect. Thus, as fibre loading increases in the composites, more interfacial area exists leading to an increase in water absorption. A similar study on moisture behaviour of plant fibre/polymer composites was done by Dhakal et al. (2007). Unsaturated polyester was reinforced with 2, 3, 4, and 5 layers of hemp fibre. It was found that moisture absorption increased as fibre content increased. Because of the hydrophilic nature of cellulose fibres, composites reinforced with cellulose fibres always tend to absorb much water than other types of composites. Rizal et al. (2021) also indicated in their study on kenaf fibre-reinforced unsaturated polyester composites that as fibre loading increased, moisture absorption also increased by virtue of the high cellulose content.

The water absorption behaviour in the samples can be studied as Fickian behaviour. Therefore, for short immersion times the following formula has been used (Mohan and Kanny 2011; Reddy et al. 2010):

$$\frac{M_t}{M_\infty} = 4\left(\frac{Dt}{\pi h^2}\right)^{1/2}$$

The maximum water absorptions and the diffusion coefficient values of RCF-reinforced epoxy composites series are listed in Table 5.1. The addition of cellulose fibre increases the rate of water diffusion. Diffusivity increases slightly as fibre content increases from 0 to 40%. However, at 46% RCF loading, the diffusivity significantly increases by 52.7% compared to neat epoxy. This can be attributed to

Table 5.1 Maximum water uptake and diffusion coefficient (D) of RCF/epoxy ecocomposites

Samples	RCF content (wt%)	M_∞ (%)	$D \times 10^{-07}$ (mm^2/s)
Epoxy	0	2.21	9.17
RCF/epoxy	19	9.52	9.53
RCF/epoxy	28	12.59	9.30
RCF/epoxy	40	1714	10.20
RCF/epoxy	46	19.46	14.00

the increases in fibre content (Dhakal et al. 2007). Furthermore, exposing to moisture causes the fibres to swell resulting in formation of micro-cracks and voids at the fibre–matrix interface region. This in turn leads to increase in water diffusion via these microcarcks and voids (Dhakal et al. 2007).
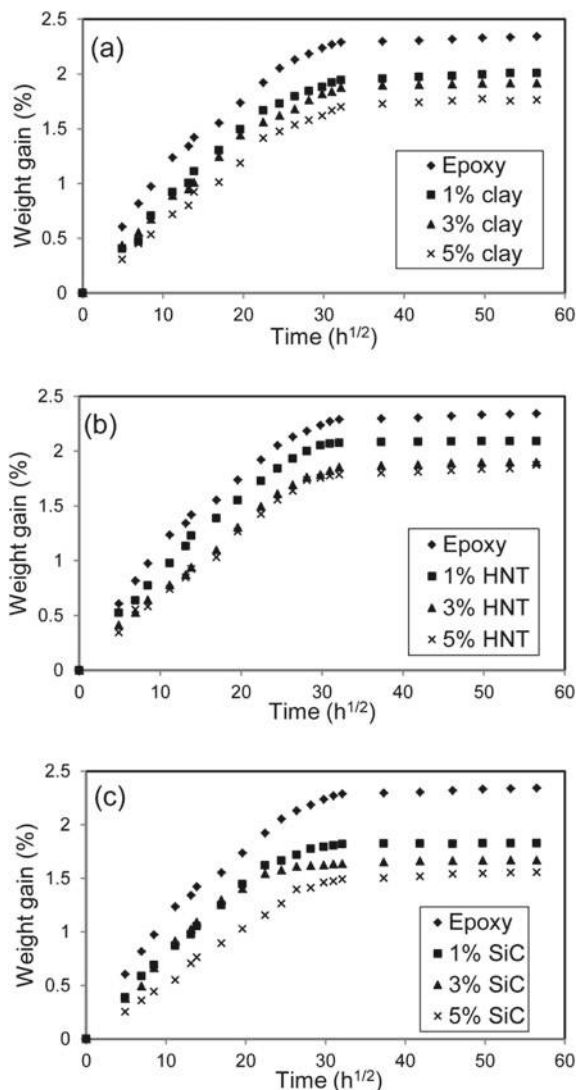
5.2 Nano-Filler/Epoxy Nanocomposites

(a) Effect of Nano-Filler on Water Absorption

The water absorption curve of nanoclay/epoxy nanocomposites, HNT/epoxy nanocomposites, and n-SiC/epoxy nanocomposites are illustrated in Fig. 5.2a–c, respectively. All nanocomposites exhibit typical water absorption behaviour of polymers that follow Fick's low (Pradhan et al. 2021; Liu et al. 2005). In general, the presence of nano-fillers is found to decrease the water uptake of modified composites compared to neat epoxy. This phenomenon is due to the excellent barrier properties of these nano-fillers (Liu et al. 2005; Jodatnia and Rash-Ahmadi 2022). The presence of high aspect ratio nano-fillers can create a tortuous pathway for water molecules to diffuse into the composites (Jodatnia and Rash-Ahmadi 2022).

In the case of nanoclay-reinforced epoxy nanocomposites, the maximum water uptake decreases gradually with increasing clay contents (Liu et al. 2005). The maximum water absorption of nanoclay-filled epoxy nanocomposites decreases by 14.1, 17.9, and 24.8% after the addition of 1, 3, and 5 wt% nanoclay, respectively, when compared to neat epoxy. Similarly, the presence of 1, 3, and 5 wt% HNT decreases the water absorption by 10.3, 18.8, and 20.1%, respectively. Interestingly, the nanocomposites filled with n-SiC show better barrier properties than other filled nanocomposites. The incorporation of 1, 3, and 5 wt% n-SiC decreases water uptake by 21.8, 28.6, and 33.3%, respectively, as compared to neat epoxy. For all nanocomposites, water uptake decreases with increasing filler content. This can be attributed to the increase in the tortuosity effect with increasing filler content (Liu et al. 2005; Jodatnia and Rash-Ahmadi 2022). Several studies showed that the maximum water absorption of polymer system decreased due the presence of nano-filler (Mohan and Kanny 2011; Reddy et al. 2010; Pradhan et al. 2021; Liu et al. 2005). Pradhan et al. (2021) reported a reduction in maximum water uptake for different types of epoxy

Fig. 5.2 Water absorption
curves of epoxy-based
nanocomposites filled with
nanoclay (**a**), HNT (**b**), and
n-SiC (**c**)

systems reinforced with layered silicate. Similarly, Jodatnia and Rash-Ahmadi (2022) investigated the water absorption of Al_2O_3/epoxy nanocomposites. Results showed that the water uptake of epoxy decreased after the addition of Al_2O_3 nanoparticles.

Table 5.2 shows the maximum water uptake and the effective diffusion coefficient of neat epoxy and epoxy nanocomposites filled with nanoclay, HNT, and n-SiC. The diffusivity of nanocomposites generally decreases due to the addition of nano-fillers. Compared to neat epoxy, significant reduction in diffusivity (30.0, 31.7, and 36.3%) were achieved with only 5 wt% of nanoclay, HNT, and n-SiC content, respectively. The reduction in the diffusivity may be attributed to the tortuosity of diffusion path

Table 5.2 Maximum water uptake and diffusion coefficient (D) of epoxy-based nanocomposites filled with nanoclay, HNT, and n-SiC particles

Sample	Maximum water uptake (%)	Diffusion coefficients (D) (10^{-7} mm^2/s)
Epoxy	2.34	11.75
Epoxy/nanoclay (1%)	2.01	9.98
Epoxy/nanoclay (3%)	1.92	10.10
Epoxy/nanoclay (5%)	1.76	8.23
Epoxy/HNT (1%)	2.09	10.87
Epoxy/HNT (3%)	1.90	8.47
Epoxy/HNT (5%)	1.87	8.03
Epoxy/n-SiC (1%)	1.83	11.35
Epoxy/n-SiC (3%)	1.67	13.84
Epoxy/n-SiC (5%)	1.56	7.48

created by the nano-filler addition (Pradhan et al. 2021). Similar results were obtained by Kim et al. (2005). It was found that the addition of 5 wt% nanoclay (I30P and Cloisite 20A) decreased the diffusivity of epoxy by 36 and 39%, respectively.

(b)   Role of Water Absorption

The effect of water absorption on the mechanical properties of epoxy nanocomposites was investigated after placing the specimens in water for 6 months period at room temperature and compared with the same nanocomposites in dry conditions. All mechanical tests were carried out at room temperature for wet samples. The data of the nanocomposites in dry condition have been demonstrated here only for the purpose of benchmarking. More details about the mechanical properties of epoxy-based nanocomposites filled with nanoclay, HNT, and n-SiC particles in dry condition can be found in the work of Limpadapun and Sukmanee (2021), Alamri and Low (2012).

(i)   *Flexural strength and modulus*

Table 5.3 summarizes the flexural strength and modulus of nano-filler-reinforced epoxy nanocomposites in both dry and wet conditions. In general, water absorption has a negative influence on flexural strength and modulus of epoxy-based nanocomposites. Flexural strength of unmodified epoxy and modified epoxy-based nanocomposites decreases after subjecting to water compared to dry nanocomposites. This reduction in flexural strength can be attributed to the plasticization effect of water absorption in epoxy matrix. This can lead to reduction in the interfacial strength between the epoxy and reinforcing particles resulting in drop in flexural strength values (Alhuthali and Low 2021). For example, the flexural strength of water-absorbed epoxy decreases by 12.2% compared to epoxy in dry condition.

Table 5.3 Flexural strength and modulus of epoxy and its nanocomposites before and after water treatment

Sample	Before placing in water		After placing in water	
	Flexural strength (MPa)	Flexural modulus (GPa)	Flexural strength (MPa)	Flexural modulus (GPa)
Epoxy	58.5 ± 2.6	0.9 ± 0.1	51.4 ± 3.1	0.7 ± 0.2
+1% nanoclay	85.2 ± 2.5	1.6 ± 0.4	52.6 ± 4.3	1.3 ± 0.2
+3% nanoclay	58.7 ± 3.9	1.5 ± 0.1	52.7 ± 4.3	1.3 ± 0.2
+5% nanoclay	61.2 ± 3.5	1.4 ± 0.2	53.0 ± 3.9	1.3 ± 0.2
+1% HNT	70.7 ± 6.2	1.5 ± 0.2	55.8 ± 6.5	1.4 ± 0.2
+3% HNT	68.2 ± 8.1	1.3 ± 0.1	52.5 ± 4.9	1.3 ± 0.2
+5% HNT	64.5 ± 4.7	1.4 ± 0.1	53.1 ± 3.5	1.4 ± 0.2
+1% n-SiC	71.1 ± 3.2	1.6 ± 0.3	59.8 ± 4.3	1.4 ± 0.3
+3% n-SiC	66.3 ± 2.9	1.4 ± 0.2	56.5 ± 5.8	1.3 ± 0.3
+5% n-SiC	61.9 ± 3.2	1.4 ± 0.1	54.5 ± 3.4	1.4 ± 0.3

In the case of nanoclay/epoxy nanocomposites, the flexural strengths of wet specimens filled with 1, 3, and 5 wt% nanoclay decrease by 38.3, 10.3, and 13.4%, respectively, compared to nanoclay filled epoxy in dry condition. Similarly, for HNT/epoxy nanocomposites, the flexural strengths of wet specimens modified with 1, 3, and 5 wt% HNT decrease by 21.1, 23.0, and 17.6%, respectively, compared to dry HNT-filled epoxy. Furthermore, for n-SiC/epoxy nanocomposites, the flexural strengths of wet specimens filled with 1, 3, and 5 wt% n-SiC decrease by 15.9, 14.8, and 12.0%, respectively, in comparison to n-SiC-filled epoxy. Several studies have reported reduction in flexural strength of epoxy-based nanocomposites due to water absorption. For instance, Abacha et al. (2007) reported a decrease in flexural strength and modulus of clay/epoxy nanocomposites due to the water absorption. Buehler and Seferis (2000) also reported a drop in flexural strength values of carbon fibre/epoxy and glass fibre/epoxy composites as a result of moisture absorption.

The effect of nano-fillers on enhancing the flexural strength of wet epoxy matrix was investigated and compared to neat epoxy in wet condition. Table 5.3 shows no significant change in flexural strength due to the presence of nanoclay. For example, the flexural strength increases by 2.2 and 3.0% after the addition of 1 and 5 wt% nanoclay, respectively. For HNT/epoxy nanocomposites, maximum flexural strength (about 8.5% over neat epoxy) is obtained at 1 wt% HNT loading. Similarly, the addition of 1 wt% n-SiC increases flexural strength by 16.3% over unmodified wet epoxy. The increase in flexural strength of water-treated nanocomposites after the addition of nano-fillers can be attributed to the enhancement in the interfacial bonding between the filler and the matrix, thus increasing the surface area of matrix/filler interaction. As a result, this leads to good stress transfer from the matrix to the nano-fillers, thus resulting in improved flexural strength. In a similar study, Hossain et al.

Fig. 5.3 The DSC curves of neat epoxy before and after water treatment
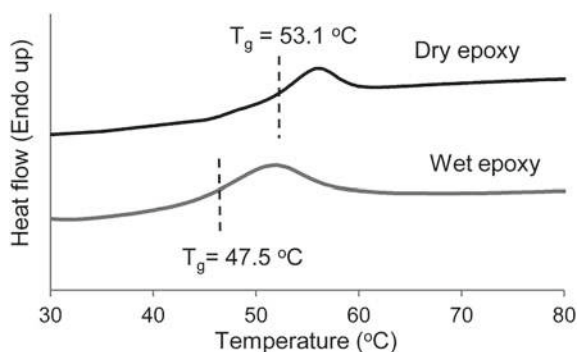
(2011) investigated the effect of nanoclay on the flexural strength of carbon fibre-reinforced epoxy composites after immersing in sea water for 30, 60, and 180 days. Their results showed that flexural strength increased due to the presence of nanoclay.

The effect of water absorption on the flexural modulus of nano-filler-reinforced epoxy nanocomposites is presented in Table 5.3. Briefly, it can be argued that flexural modulus was not significantly influenced by water absorption for most of the nanocomposites. However, the decrease in flexural modulus is more expressed for nanocomposites filled with nanoclay than other nanocomposites. The reduction in flexural modulus can be attributed to the plasticization effect of water absorption on the epoxy matrix (Jodatnia and Rash-Ahmadi 2022). DSC analysis was conducted on neat epoxy before and after water treatment to evaluate the effect of water absorption on T_g. Figure 5.3 shows that T_g significantly decreased from 53.1 to 47.5 due to the plasticization effect of absorbed water. Similar observation was obtained by Jodatnia and Rash-Ahmadi (2022).

In the case of wet nanocomposites, the addition of nano-fillers increases the flexural modulus for all types of nanocomposites. The flexural modulus of epoxy modified with 1 wt% of nanoclay, HNT, and n-SiC increases by 80.7, 89.5, and 98.2%, respectively, as compared to wet unmodified epoxy. The enhancement in flexural modulus can be due to the presence of rigid fillers that have higher modulus than epoxy matrix (Alamri and Low 2012). Any further increase in fillers loading shows slight decrease in the modulus values. The reduction in flexural modulus due to the water absorption was also observed in several studies. Hossain and co-workers (2011) observed a reduction in flexural modulus of carbon fibre/epoxy composites filled with nanoclay after immersing in water for 180 days. However, the addition of nanoclay increased flexural modulus of nanoclay-filled composites in wet condition compared to unfilled composites. Buehler and Seferis (2000) found that flexural modulus of carbon fibre/epoxy and glass fibre/epoxy composites decreased after water absorption.

Table 5.4 Fracture toughness and impact strength of epoxy and its nanocomposites before and after water treatment

Samples	Before placing in water		After placing in water	
	Fracture toughness MPa $m^{1/2}$	Impact strength kJ/m^2	Fracture toughness MPa $m^{1/2}$	Impact strength kJ/m^2
Epoxy	0.9 ± 0.1	5.6 ± 0.7	1.3 ± 0.2	6.2 ± 1.4
+1% nanoclay	1.1 ± 0.1	6.1 ± 1.3	1.4 ± 0.3	7.4 ± 1.5
+3% nanoclay	0.9 ± 0.1	6.9 ± 1.4	1.4 ± 0.2	6.6 ± 1.5
+5% nanoclay	1.0 ± 0.2	7.8 ± 2.7	1.3 ± 0.3	7.3 ± 1.7
+1% HNT	1.3 ± 0.2	5.6 ± 1.1	1.7 ± 0.2	6.5 ± 1.8
+3% HNT	1.0 ± 0.1	6.4 ± 0.7	1.6 ± 0.5	6.3 ± 1.8
+5% HNT	1.2 ± 0.1	7.0 ± 0.9	1.3 ± 0.3	6.2 ± 1.5
+1% n-SiC	1.6 ± 0.3	7.5 ± 1.1	2.2 ± 0.3	9.1 ± 1.8
+3% n-SiC	1.2 ± 0.2	7.0 ± 0.8	2.1 ± 0.3	7.9 ± 2.2
+5% n-SiC	1.1 ± 0.1	7.6 ± 1.2	1.9 ± 0.3	8.2 ± 1.4

(ii)   *Fracture toughness*

Table 5.4 displays the fracture toughness of nano-filler/epoxy nanocomposites in both dry and wet conditions. Surprisingly, fracture toughness for all types of nanocomposites is observed to increase due to exposing to a moist environment. This can be explained by increasing the ductility of the composites due to the plasticization effect of absorbed water, which tends to increase in fracture toughness (Buehler and Seferis 2000). Similarly, Wang et al. (2006) observed an increase in fracture toughness of neat epoxy and exfoliated clay/epoxy nanocomposites after subjecting to water for 30 days.

In details, fracture toughness of unmodified epoxy in wet condition increases by 48.9% compared to dry epoxy. In the case of nanoclay/epoxy nanocomposites, facture toughness of wet composites modified with 1, 3, and 5 wt% nanoclay platelets increase by 29.3, 51.4, and 36.0%, respectively, compared to same nanocomposites in dry condition. Similarly, fracture toughness of wet HNT/epoxy nanocomposites filled with 1, 3, and 5 wt% HNT increases by 30.7, 57.4, and 11.1%, respectively, as compared to dry nanocomposites. Moreover, fracture toughness of n-SiC/epoxy nanocomposites reinforced with 1, 3, and 5 wt% n-SiC increases by 34.1, 67.2, and 76.4%, respectively, when compared to dry nanocomposites.

The effect of nano-filler addition on the fracture toughness of wet epoxy-based nanocomposites was studied. All types of nanocomposites show similar fracture toughness trend. A maximum value achieved at 1 wt% filler loading, followed by a decrease in fracture toughness value with further increase in filler content. Fracture toughness of composites filled with 1 wt% of nanoclay, HNT, and n-SiC increases by 10.6, 36.7, and 70.3%, respectively, compared to wet unfilled epoxy matrix. Nanocomposites reinforced with n-SiC particles show better fracture toughness than

other nanocomposites. The enhancement in fracture toughness can be attributed to the increased resistance to crack propagation via number of possible toughness mechanisms such as crack pinning, particle-debonding, plastic void growth, plastic deformation, and particle pull-out (Alamri and Low 2012). Similarly, Buehler and Seferis (2000) reported an increase in fracture toughness of carbon fibre/epoxy composites after placement in water medium for 1200 h. Plasticization effect of water and increased fibre-bridging were reported to be the reasons of the enhancement in fracture toughness.

(iii)   *Impact strength*

The effect of water absorption on the impact strength of nano-filler-reinforced epoxy nanocomposites is also presented in Table 5.4. Nanocomposites filled with either nanoclay or HNT show no clear trend of the influence of water on impact strength. For nanocomposites filled with n-SiC, a significant increase in impact strength can be observed due to water absorption. In the case of wet condition, the impact strength of epoxy matrix increases due to the presence of nano-fillers. The increase in impact strength is more pronounced for nanocomposites modified with n-SiC particles. For all types of nanocomposites, reinforcing with 1 wt% of nano-filler displays the highest value compared to other fillers content. Impact strength of nanocomposites reinforced with 1 wt% of nanoclay, HNT, and n-SiC increases by 20.0, 4.9, and 46.1%, respectively, compared to wet unfilled epoxy matrix. The increase in impact strength is due to the increase in the flexibility of the epoxy chains as a result of the plasticization action of the absorbed water (Nassar et al. 2021). Low and co-workers (2007) reported an increase in impact strength for recycled cellulose fibre-reinforced epoxy composites due to the plasticization effect of sea water.

(c)   SEM Observations

The SEM micrographs of fracture surfaces of the water-treated epoxy and epoxy nanocomposites are shown in Figs. 5.4 and 5.5. Low magnification images for unfilled epoxy and epoxy filled with nanoclay, HNT, and n-SiC, respectively, are shown in Fig. 5.4a–d. All types of samples show different degree of surface roughness. The surface of neat epoxy displays lower roughness than nanocomposites as seen in Fig. 5.5a. River markings can be clearly observed for neat epoxy with quite smooth fracture surface indicating very fast and straight crack propagation (Alamri and Low 2012). However, it is evident that the presence of nano-fillers increases the roughness of the fracture surfaces. An increase in fracture surface roughness is an indicator of crack pinning mechanism, which increases the absorbed energy of fracture by increasing the crack length during deformation. The formation of micro-voids is more pronounced in n-SiC nanocomposites. It was reported that the presence of micro-voids led to increase in fracture toughness (Alamri and Low 2012). This explains why nanocomposites filled with n-SiC particles exhibited the highest fracture toughness among other nanocomposites.

High-magnification SEM images of epoxy nanocomposites filled with nanoclay, HNT, and n-SiC are shown in Fig. 5.5a–d. In general, several toughness mechanisms such as crack pinning, particle debonding, plastic void growth, plastic deformation,
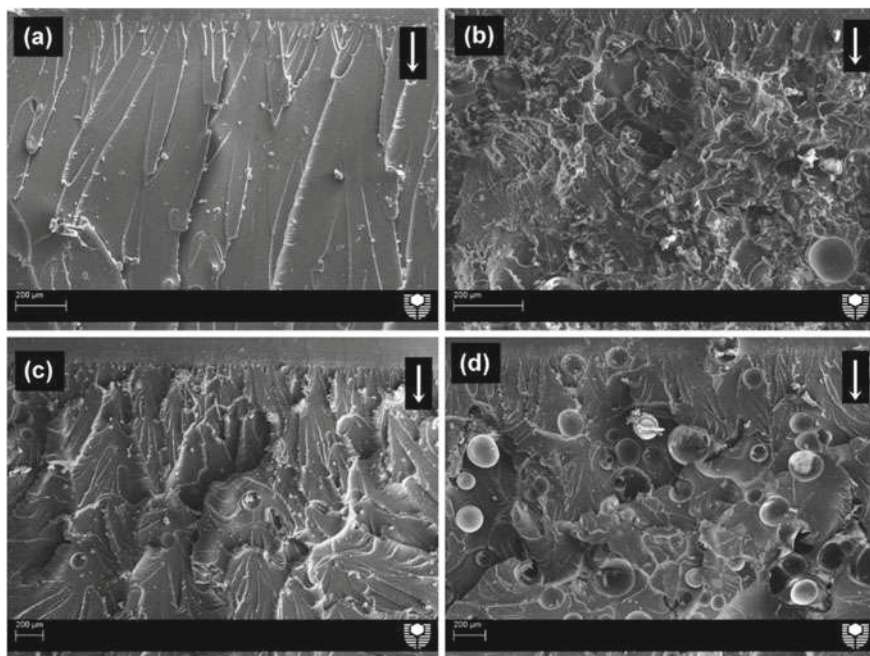
Fig. 5.4 SEM images showing the details fracture surfaces for **a** unfilled epoxy, **b** epoxy/nanoclay 5 wt%, **c** epoxy/HNT 5 wt%, and **d** epoxy/n-SiC 5 wt% [White arrow indicates the direction of crack propagation]

and particle pull-outs can be observed. Such toughness mechanisms can increase the energy dissipated by resisting crack propagation during deformation, which lead to an increase in fracture toughness values (Alamri and Low 2012). Close observation of Figs. 5.5 and 5.6 indicates that crack pinning and plastic deformation due to the presence of clay clusters are the dominant toughening mechanisms for nanocomposites filled with nanoclay (Tang et al. 2011). For nanocomposites filled with HNT, crack pinning and bowing are the main toughening mechanisms (Sánchez-Soto et al. 2007). In the case of nanocomposites filled with n-SiC, Figs. 5.4d and 5.5d show the existence of micro-voids, which reveals that the plastic deformation of the matrix around the voids and the crack deflection due to the presence of these voids are primary toughening mechanisms.

5.3   Nanoclay/Cellulose Fibre/Epoxy Eco-Nanocomposites

(a)   Water absorption

Figure 5.6 displays the water absorption results of nanoclay-filled and unfilled RCF/epoxy composites. The weight gain of the samples is plotted as a function

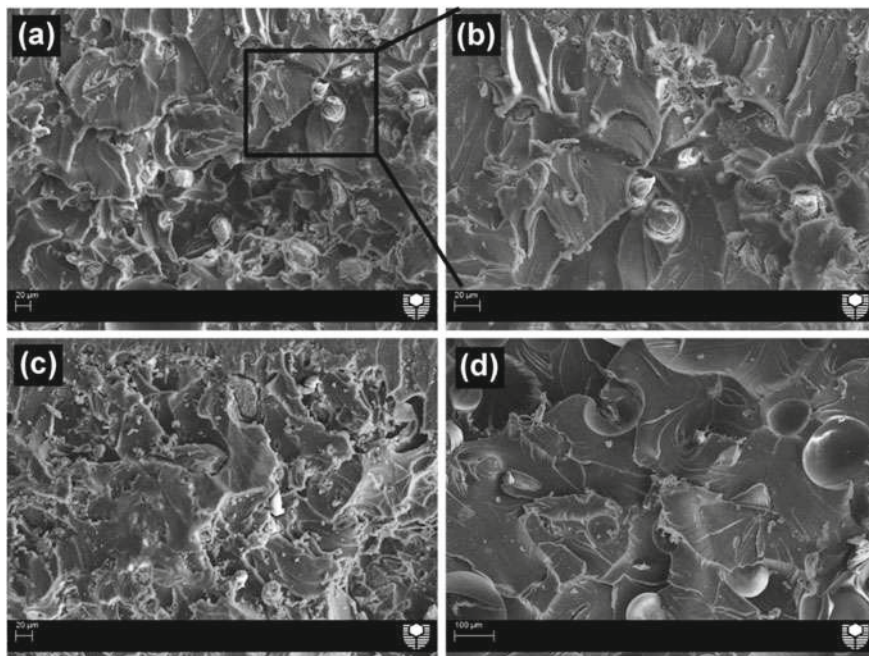**Fig. 5.5** SEM images showing the details of fracture surfaces e for epoxy-based nanocomposites filled with nanoclay (**a** and **b**), HNT (**c**), and n-SiC (**d**)
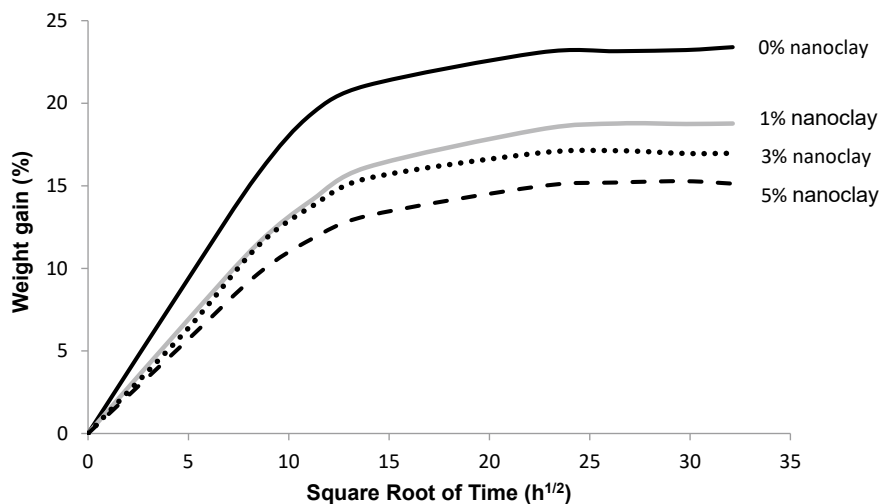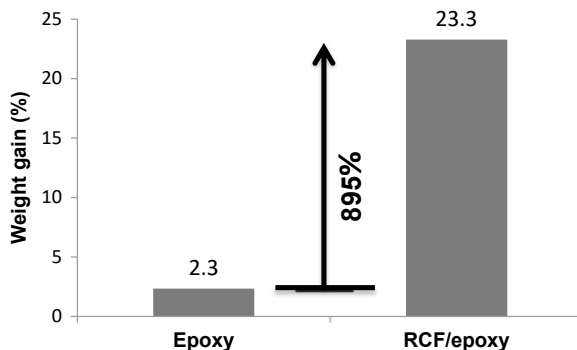

Fig. 5.6 Water absorption curves of RCF/epoxy ecocomposites and nanoclay-filled nanocomposites

Fig. 5.7 Maximum water uptake of pure epoxy and RCF/epoxy ecocomposites

of square root of time. It can be seen from Fig. 5.3 that the water uptake continuously increased with the increase in time of immersion for all specimens. Typical Fickian diffusion behaviours are observed for all samples. Water uptake rate is linear and very rapid in the beginning of the exposure, after that, it slows down and reaches the saturation level (Kim and Seo 2006).

The presence of RCF sheets dramatically increases the water absorption of RCF-reinforced epoxy when compared to pure epoxy (Fig. 5.7). This result was expected due to the hydrophilic nature of cellulose fibres, which leads to absorbing much water depending on the environmental condition. The chemical reason for this is due the presence of hydroxyl groups in the cellulose structure which attract water molecules and bind with them through hydrogen bonding (Kim and Seo 2006; Fraga et al. 2006; Doan et al. 2007). Similar observation has been made by Dhakal et al. (2007) on hemp fibre-reinforced unsaturated polyester composites. Results showed that water uptake increased as hemp fibre content increased.

However, the incorporation of nanoclay effectively decreases the water absorption for nanoclay filled RCF/epoxy samples compared to unfilled RCF/epoxy samples. Maximum water uptake continuously decreases with increasing clay content. This can be explained; the presence of nanoclay in the RCF/epoxy composites creates a tortuous pathway for water molecules to diffuse and hence hinders the permeation of water into the composites, resulting in decreased equilibrium water content as reported in the literature (Liu et al. 2005; Jodatnia and Rash-Ahmadi 2022; Deka and Maji 2011). The maximum water absorptions and the diffusion coefficient values of unfilled composites and filled composites series are listed in Table 5.5. It can

Table 5.5 Maximum water uptake and diffusion coefficient (D) of nanoclay-filled RCF/epoxy eco-nanocomposites

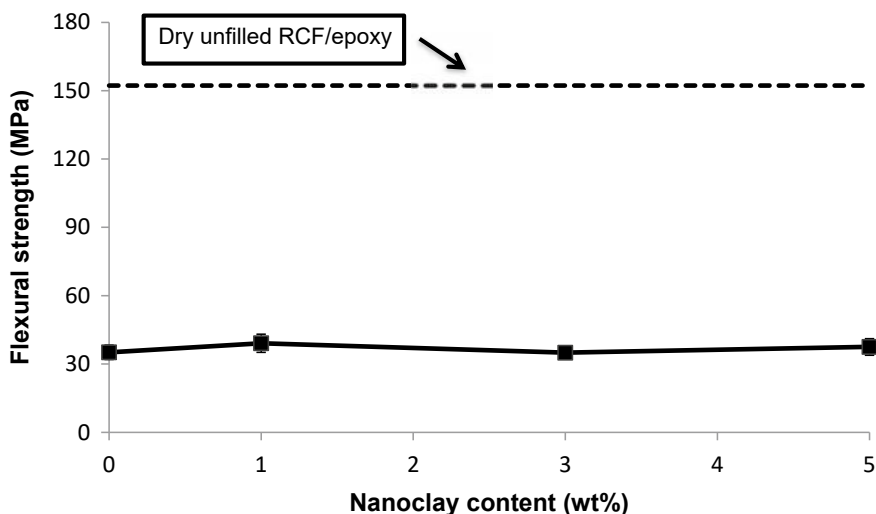| Samples	Nanoclay content (wt%)	M∞ (%)	D (mm²/s)
RCF/Epoxy	0	23.28	4.26×10^{-06}
RCF/Epoxy	1	18.78	3.52×10^{-06}
RCF/Epoxy	3	17.04	4.00×10^{-06}
RCF/Epoxy	5	15.39	3.66×10^{-06}

Fig. 5.8 Flexural strength of wet nanoclay-filled RCF/epoxy eco-nanocomposites

be observed that maximum water uptake of RCF/epoxy decreased significantly by about 34% when 5 wt% nanoclay added. However, even though the addition of nanoclay decreases the diffusion coefficients of clay-filled composites, no clear trend is observed for the diffusivity values with varying nanoclay content (Pradhan et al. 2021).

(b)   Role of Moisture Absorption on Mechanical Properties

Figure 5.8 shows flexural strength for hybrid RCF-reinforced epoxy/clay nanocomposites after placement in water medium. A significant drop can be seen in flexural strength for wet nanoclay-filled and unfilled RCF/epoxy composites compared to dry unfilled RCF/epoxy (presented in the graph as dotted line). Flexural strength of RCF-reinforced epoxy decreased by 77% from 152.3 to 35.1 MPa after immersing in water for 6 months. This significant reduction in flexural strength is because of water absorption in the degradation of fibre–matrix interface region, which in turn reduces stress transferring from matrix to fibres resulting in low flexural strength. However, the presence of nanoclay has a positive effect on enhancing the flexural strength of water-immersed samples. Flexural strength of composites filled with 1 and 5 w% nanoclay increases by 11.4 and 6.7%, respectively, compared to unfilled wet composites.

Flexural modulus results are shown in Fig. 5.9. Exposure to moisture caused a considerable drop in flexural modulus for wet composites. Flexural modulus of wet RCF/epoxy composites decreased by 82.7% compared to dry RCF/epoxy composites. This reduction in modulus properties is due to the increase in composites ductility
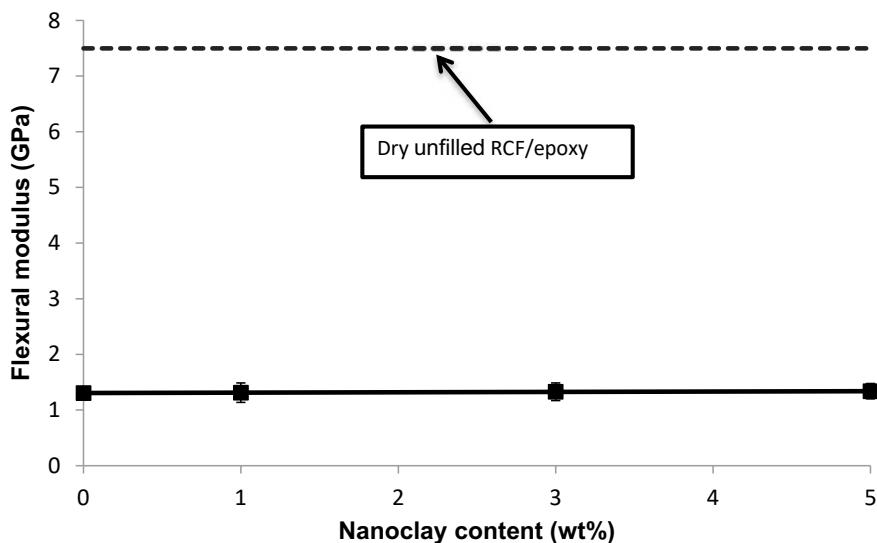
Fig. 5.9   Flexural modulus of wet nanoclay-filled RCF/epoxy composites

as a result of water absorption (Jodatnia and Rash-Ahmadi 2022). However, the incorporation of nanoclay leads to very slight enhancement in flexural modulus when compared to unfilled composites.

Fracture toughness of wet RCF/epoxy composites filled with nanoclay is plotted in Fig. 5.10. Fracture toughness clearly decreased because of moisture absorption. The reduction in fracture toughness for RCF/epoxy filled with 0, 1, 3, and 5 wt%

Fig. 5.10   Fracture toughness of wet nanoclay-filled RCF/epoxy eco-nanocomposites

nanoclay compared to dry unfilled RCF/epoxy composite is ~61, 54, 56, and 52%, respectively. This substantial reduction in fracture toughness can be explained as, moisture absorption causes swelling of fibres, which could create micro-cracks in the sample and eventually could lead to failure in fracture toughness (Athijayamani et al. 2009). Moreover, water molecules can diffuse into the fibre–matrix interfaces through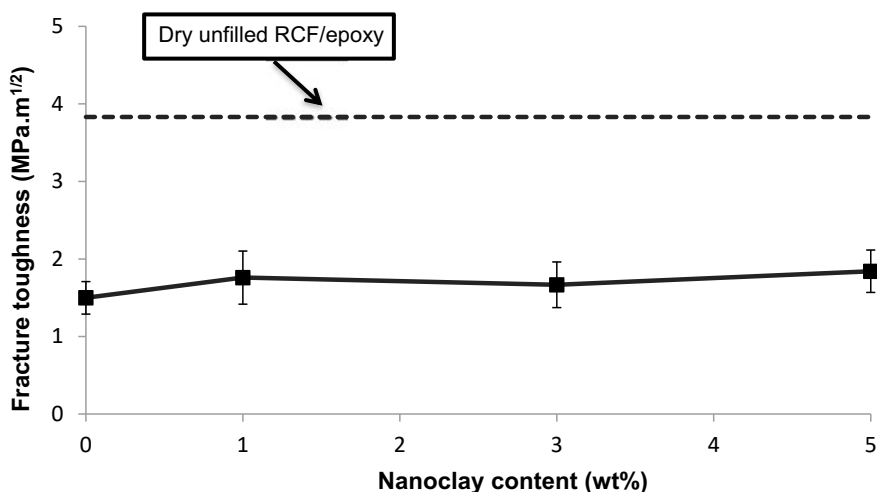 these micro-cracks, which result in debonding fibres and weakening the fibre–matrix interface, as proved by SEM images later (Kim and Seo 2006; Athijayamani et al. 2009).

However, it can be observed that the addition of nanoclay reduced the effect of water absorption on facture toughness by displaying better improvement in toughness properties than those of unfilled RCF/epoxy ecocomposites. Fracture toughness of wet composites filled with 1, 3, and 5 w% nanoclay increases by 17.3, 11.3, and 22.5% compared to unfilled wet composites. This enhancement in fracture toughness for wet samples filled with nanoclay can be attributed to the capability of well-dispersed nanoclay platelets on crack pinning and stopping tiny cracks from propagation into the matrix (Dorigato et al. 2011). In addition, the high aspect ratio of nanoclay platelet plays an essential role in decreasing water absorption in nanocomposites by introducing tortuous path for water molecules to diffuse and eventually minimizes the effect of moisture absorption on the mechanical properties of nanoclay-filled composites.

Un-notched impact strength values of nanoclay-filled RCF/epoxy composites after immersing in water are demonstrated in Fig. 5.11. Interestingly, all wet samples display better impact strength than dry unfilled RCF/epoxy sample. For examples, impact strength of unfilled RCF/epoxy composites increased by 28.6% after exposed to water for 6 months. Similar increase in Un-notched impact strength due to the
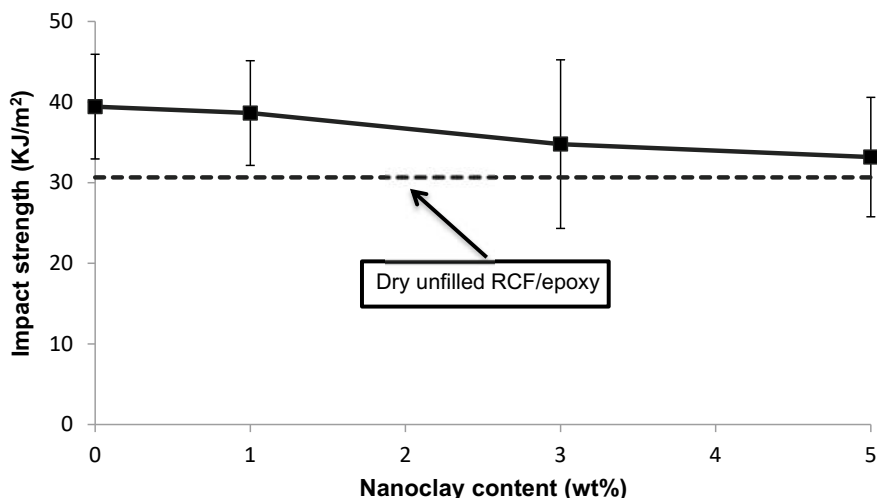

Fig. 5.11 Un-notched impact strength of wet nanoclay-filled RCF/epoxy samples
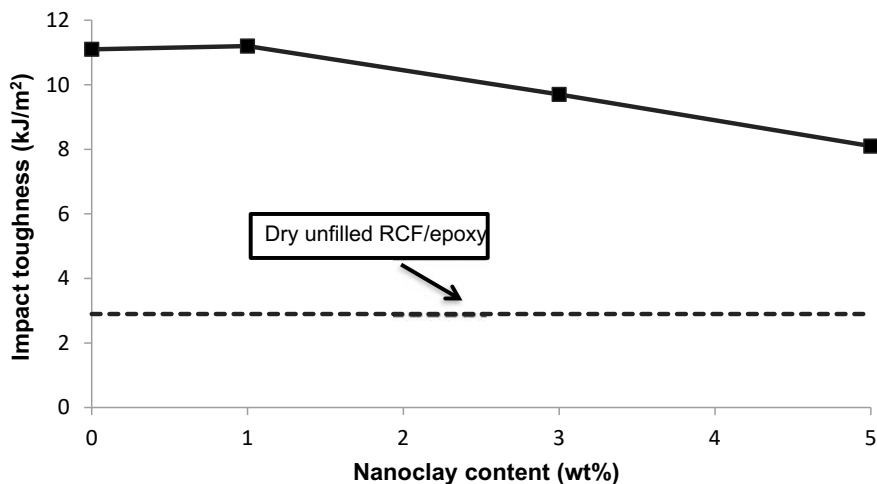
Fig. 5.12 Impact toughness of wet nanoclay-filled RCF/epoxy samples

immersing in water for 14 days of jute fibre/polypropylene composites was reported by Chandel et al. (2022). The increase in impact strength of wet samples can be attributed to the plasticization effect of water absorption on RCF/epoxy composites (Dhakal et al. 2007; Low et al. 2009). However, after the addition of nanoclay, impact strength progressively decreases as nanoclay content increases. This result indicates that although the water absorption improves the overall impact energy of nanoclay-filled and unfilled RCF/epoxy composite systems, the effect of water absorption on the impact energy is lower when nanoclay is added. This indicates that the presence of nanoclay platelet resists the influence of the plasticization effect of water absorption on composites mechanical properties.

Figure 5.12 illustrates the effect of water absorption on impact toughness in terms of energy release rate (G_{IC}) of nanoclay-filled RCF-reinforced epoxy composites. Like impact strength results, impact toughness significantly increases for all samples after immersing in water for 6 months. This improvement in fracture toughness can be attributed to the water plasticization effect on RCF-reinforced epoxy composites after the exposure to water. Moreover, water absorption can cause cellulose-fibre swelling, which in turn increases fibre resistance to impact energy (Dhakal et al. 2007). A similar observation had been reported in an earlier work by Low and co-workers (2009) in cellulose fibre-reinforced epoxy composites. These authors reported a significant increase in both impact strength and toughness after immersing samples in seawater for 2 weeks.

(c)   Fracture Mechanisms

Figure 5.13 illustrates the fracture surface micrograph of the composites before and after placement in water. The micrographs of dry and wet 5 wt% nanoclay-filled RCF/epoxy composites are shown in Fig. 5.12a, b. It can be clearly seen that dry
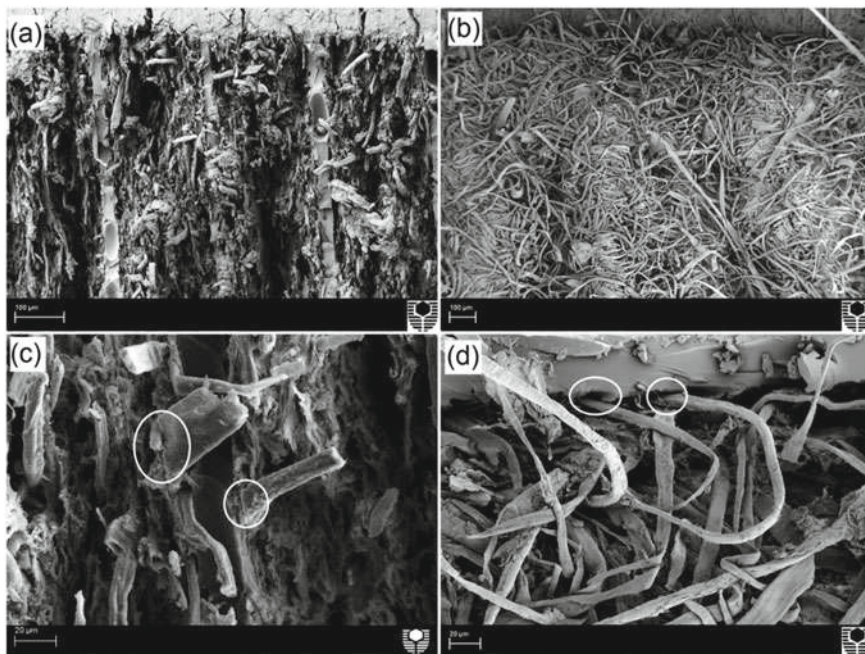
Fig. 5.13 SEM images of the fracture surface **a** dry RCF/epoxy/nanoclay 5wt%, **b** wet RCF/epoxy/nanoclay 5wt%, **c** dry RCF/epoxy, and **d** wet RCF/epoxy

composites show rougher fracture surface than wet composites. Fibres fracture can be easily observed in dry composites while it is hard to be seen in wet composites. However, the presence of unbroken fibres in wet composites after fracture test reveals that fibres were easily pulled out from the matrix, which indicates the lack of adhesion between fibre and matrix.

High-magnification images of dry and wet RCF/epoxy composites are shown in Fig. 5.13c, d. Good fibre–matrix adhesion is observed for dry composites (no gap between fibre and matrix), while weak fibre–matrix interface is observed for wet composites, (indicated in white circles). This fibre debonding (characterized by the appearance of gap between fibre and matrix) is a clear evidence of weak fibre–matrix interfacial adhesion in the structure of wet composites. This observation is like that obtained by Mohan and Kanny (2011). In wet environment, water molecule penetrates the composites through micro-cracks and diffuses along the fibre–matrix interfaces causing debonding between fibre and matrix by replacing the matrix–fibre covalent bond with weaker hydrogen bonds (Kim and Seo 2006; Athijayamani et al. 2009).

Images in Fig. 5.14a, b show a close-up view of crack propagation for dry and wet composites. In the case of dry composites, an extensive fibre breakage is observed
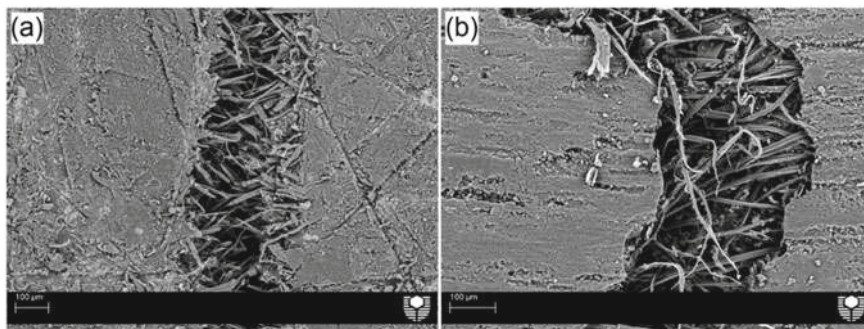
Fig. 5.14 SEM images of the crack propagation **a** dry RCF ecocomposites and **b** wet RCF ecocomposites

along the fibre propagation. Fibre breakage normally involves high energy to dissipate, which increases composite facture toughness properties. Fibre fracture can be an indicator of good fibre–matrix interaction (Kim and Seo 2006).

However, in the case of wet composites, there is less fibre fracture, which indicates lower energy is involved for crack to propagate through the wet composites compared to dry composites. Moreover, a great number of smooth fibre pull-out, not broken is observed along the crack propagation. This confirms the poor adhesion between the fibre and the matrix, which results in low fracture toughness.

5.4   Nano-SiC/Cellulose Fibre/Epoxy Eco-Nanocomposites

(a)   Role of Water Absorption

The effect of water absorption on the mechanical properties of RCF/epoxy composites filled with n-SiC particles is investigated after water treatment for 6 months period at room temperature and compared with the same composites in dry conditions. The data of the composites in dry condition have been demonstrated here only for the purpose of benchmarking. More details about the mechanical and thermal properties of n-SiC-filled RCF/epoxy eco-nanocomposites in dry condition can be found in Alamri and Low (2012).

(i)   *Stress–strain behaviour*

Figure 5.15 illustrates the typical flexural stress–strain curves for unfilled RCF/epoxy and 5 wt% n-SiC-filled RCF/epoxy composites before and after placing in water. It can be seen that the addition of n-SiC particles decreases the maximum stress of RCF/epoxy composites in dry condition. However, the presence of n-SiC leads to increase in maximum stress after water treatment. It also can be seen that flexural properties for both types of composites severely decrease due to the water absorption. The significant drop in maximum stress after water treatment can be attributed to

Fig. 5.15 Typical stress–strain curves of RCF/epoxy samples filled with 0 and 5wt% n-SiC in dry and wet conditions
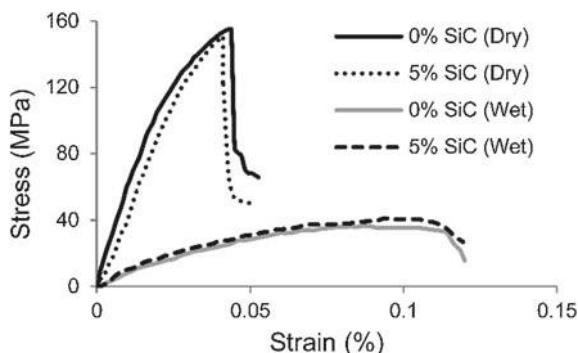
the fibre damage and degradation in fibre–matrix interfacial bonding due to the absorbed water (Kim and Seo 2006). Maximum bending strain of the composites is found to increase significantly due to the water absorption. Water molecules act as a plasticizer agent in fibre reinforced composites leading to an increase in materials ductility, which results in increase in maximum strain (Jodatnia and Rash-Ahmadi 2022).

(ii) *Flexural strength*

Figure 5.16 illustrates the effect of water absorption on the flexural strength of n-SiC-filled RCF/epoxy eco-nanocomposites. It can be clearly seen that flexural strength significantly dropped due to the water absorption for all composites. In comparison to dry composites, flexural strength of composites filled with 1 and 5 wt% n-SiC decreased by 77.4 and 73.3%, respectively, after immersing in water for 6 months. This significant reduction in flexural strength is attributed to the severe damage in the bonding at the fibre–matrix interface due to the water absorption, which leads to reduction in stress transferring between matrix and fibre, thus resulting in low flexural strength (Alamri and Low 2012). Similar reduction in flexural strength due to water absorption was observed by Athijayamani et al. (2009) which they reported a reduction in flexural strength ranged from 5.7% to 21.7% for polyester matrix

Fig. 5.16 Flexural strength of n-SiC-filled RCF/epoxy samples in dry and wet conditions
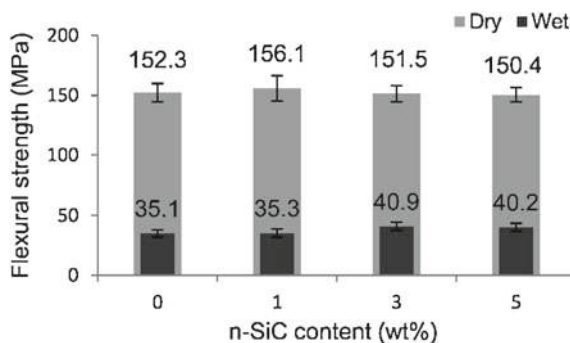
reinforced with different loading (10, 20, and 30 wt%) and length (50, 100, and 150 mm) of roselle and sisal fibres. In a previous study (Alamri and Low 2012), we investigated the effect of water absorption for 2 weeks on the flexural strength of RCF/epoxy composites as a function of fibre content. Results indicated that flexural strength decreased as fibre content increased due to the water absorption.

The role of n-SiC on enhancing flexural strength of RCF/epoxy composites in wet condition is investigated and shown in Fig. 5.16 (dark bars). It can be observed that the presence of n-SiC particles leads to a slight enhancement in flexural strength. Composites filled with 3 and 5 wt% n-SiC display an increase in flexural strength by 16.4 and 14.4% over unfilled RCF/epoxy composites. This enhancement in flexural strength is attributed to the presence of the nanoparticle which enhances the interfacial bonding between the fibre and matrix. Besides, the addition of n-SiC reduces the effect of water absorption on the mechanical properties of the composites by increasing the water absorption resistance. Interestingly, in dry condition, the flexural strength was found to decrease as n-SiC content (Alamri and Low 2012). However, in wet condition, it is found to increase as n-SiC content increases.

(iii) *Flexural modulus*

Figure 5.17 displays the flexural modulus of n-SiC-filled RCF/epoxy eco-nanocomposites as a function of n-SiC content in dry and wet conditions. All wet composites display very low flexural modulus when compared to same composites in dry condition. Flexural modulus of RCF/epoxy composites filled with 0, 1, 3, and 5 wt% n-SiC significantly decrease by 82.7, 81.7, 81.4 and 81.5%, respectively, compared to dry composites. This drop in modulus values could be attributed to the increase in composites ductility due to plasticization effect of absorbed water as reported by Jodatnia and Rash-Ahmadi (2022) and Dhakal et al. (2007). In our previous work (Alamri and Low 2012), we reported a reduction in flexural strength of RCF/epoxy composites reinforced with 46 wt% RCF by 17.1 after immersing in water for 2 weeks compared to dry composites.

The role of n-SiC on the flexural modulus of wet n-SiC-filled RCF/epoxy eco-nanocomposites is displayed in Fig. 5.17 (dark bars). The addition of n-SiC has a positive influence on the flexural modulus. This result is expected due to the fact that

Fig. 5.17 Flexural modulus of n-SiC-filled RCF/epoxy samples in dry and wet conditions
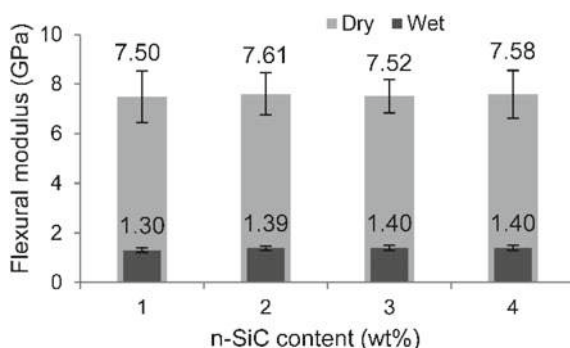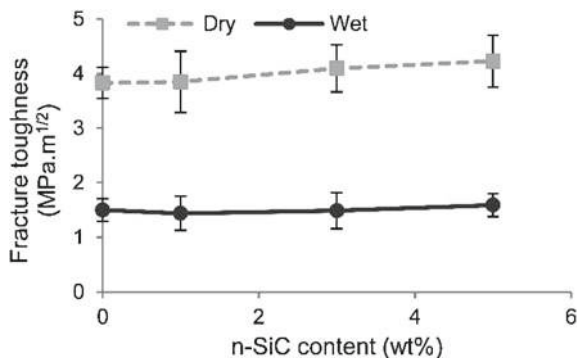
Fig. 5.18 Fracture
toughness of n-SiC-filled
RCF/epoxy samples in dry
and wet conditions

the presence of rigid nanoparticle in the matrix can reduce the ductility of the matrix
by restricting the mobility of polymer chains under loading resulting in enhancement
in n-SiC-filled composites modulus (Mohan and Kanny 2011). The enhancement in
flexural modulus of n-SiC-filled composites can be considered insignificant when
compared to unfilled composites. For instance, the addition of 5 wt% n-SiC increases
flexural modulus by maximum 7.5% over unfilled composites.

(iv)   *Fracture toughness*

The role of water absorption on the fracture toughness of n-SiC-filled RCF/epoxy eco-
nanocomposites is plotted in Fig. 5.18 as a function of n-SiC content and compared
to same composites in dry condition. Due to the water absorption, fracture toughness
of all types of composites considerably decreases compared to dry composites. The
percentage of reduction in fracture toughness of unfilled RCF/epoxy and 5 wt%
n-SiC-filled RCF/epoxy composites is 62.1 and 62.4%, respectively, compared to
same composites in dry condition. The reason behind this significant drop in fracture
toughness is due to the severe damage in fibre structure and interfacial bonding
between fibre and matrix resulting from absorbed water. Water absorption causes
swelling of fibres, which could create micro-cracks in the sample and eventually
could lead to failure in fracture toughness (Athijayamani et al. 2009). Moreover, water
molecules can diffuse into the fibre–matrix interfaces through these micro-cracks,
which result in debonding and weakening at the fibre–matrix interface (Kim and Seo
2006; Mohan and Kanny 2011). Kim and Seo (2006) reported a decrease in fracture
toughness of sisal fibre/epoxy composites as a function of increasing water treatment.
Likewise, in our previous study we reported a decrease in fracture toughness of
water-treated RCF/epoxy composites with increasing fibre content (Alamri and Low
2012).

   The role of n-SiC on the fracture toughness of RCF/composites in wet condi-
tion is shown in Fig. 5.18. In general, it can be observed that fracture toughness
of n-SiC-filled composites increases gradually as filler content increases. At low
filler content (i.e. 1 wt%) fracture toughness decreases by about 4% compared to
unfilled RCF/epoxy composites. However, the addition of 5 wt% n-SiC increases
fracture toughness by 6.1% compared to unfilled composites. This enhancement in

Fig. 5.19 Impact strength of
n-SiC-filled RCF/epoxy
samples in dry and wet
conditions
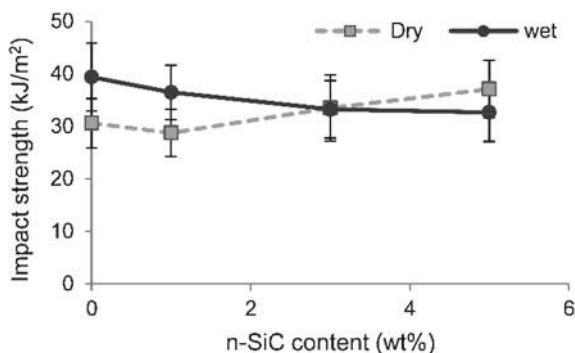
fracture toughness can be attributed to the increased resistance to crack propaga-
tion via number of possible toughness mechanisms such as crack pinning, particle-
debonding, plastic void growth, plastic deformation, and particle pull-out (Alamri
and Low 2012).

(v)   *Impact strength*

Figure 5.19 illustrates the effect of n-SiC particles on the impact strength of
RCF/epoxy composites under wet condition. Due to the water absorption, unfilled
and 1 wt% n-SiC-filled RCF/epoxy composites unexpectedly display better impact
strength than same composites at dry condition. Compared to dry composites, it was
observed that all composites exhibited partial fractures during Charpy tests. This non-
brittle fracture implies an increase in the ductility of the matrix. Nassar et al. (2021)
observed an increase in impact strength of PVC/wood sawdust composites due to
water absorption. Authors reported that the absorption of water led to the forma-
tion of hydrogen bonding between water molecules and fibres resulted in reduction
in the dipole–dipole interaction between fibre and matrix molecules, which in turn
increased the flexibility of matrix chain resulting in increase in impact strength. More-
over, water absorption can cause fibre swelling, which in turn increases fibre resis-
tance to impact energy (Dhakal et al. 2007). In our previous work (Alamri and Low
2012), we reported an increase in impact strength of cellulose fibre/epoxy compos-
ites as fibre content increased after water treatment for 2 weeks. Similarly, Chandel
et al. (2022) observed an enhancement in impact strength of jute fibre-reinforced
polypropylene composites after immersing in water for 2 weeks.

The addition of n-SiC is found to reduce the impact strength of n-SiC-filled
composites compared to unfilled composites. This result indicates that the ability of
n-SiC-filled composites to absorb impact energy decreases with increasing nano-filler
content. In wet condition, the impact strength of 5 wt% n-SiC-filled epoxy composites
decreases by 17% compared to unfilled RCF/epoxy composites. This reduction in
impact strength could be attributed to decrease in polymer chain mobility due to the
presence of nano-filler (Mohan and Kanny 2011). It is interesting to observe that
the effect of n-SiC on the impact properties of n-SiC-filled RCF/epoxy composites

in wet condition is completely different from the dry condition as can be seen in Fig. 5.19.

(b)   SEM Observations

The SEM images in Fig. 5.20a, b show the fracture surfaces of dry and wet 5 wt% n-SiC-filled RCF/epoxy eco-nanocomposites, respectively. Dry specimen displays rougher fracture surface with clear features, while wet specimen displays smoother fracture with damaged and overlapped fibres. This means that water absorption reduces the strength of the fibres in wet composites and eventually could lead to failure in mechanical properties of wet composites. Moreover, fibre fracture can be easily seen in dry specimen, while it is hard to be seen in wet composites. However, the presence of unbroken fibres in wet composites after fracture test reveals that fibres were easily pulled out from the matrix, which implies the lack of adhesion between fibre and matrix.

SEM images of unfilled RCF/epoxy composite and 5 wt% n-SiC-filled RCF/epoxy eco-nanocomposite after water treatment are shown in Fig. 5.20c, d. It is can be seen
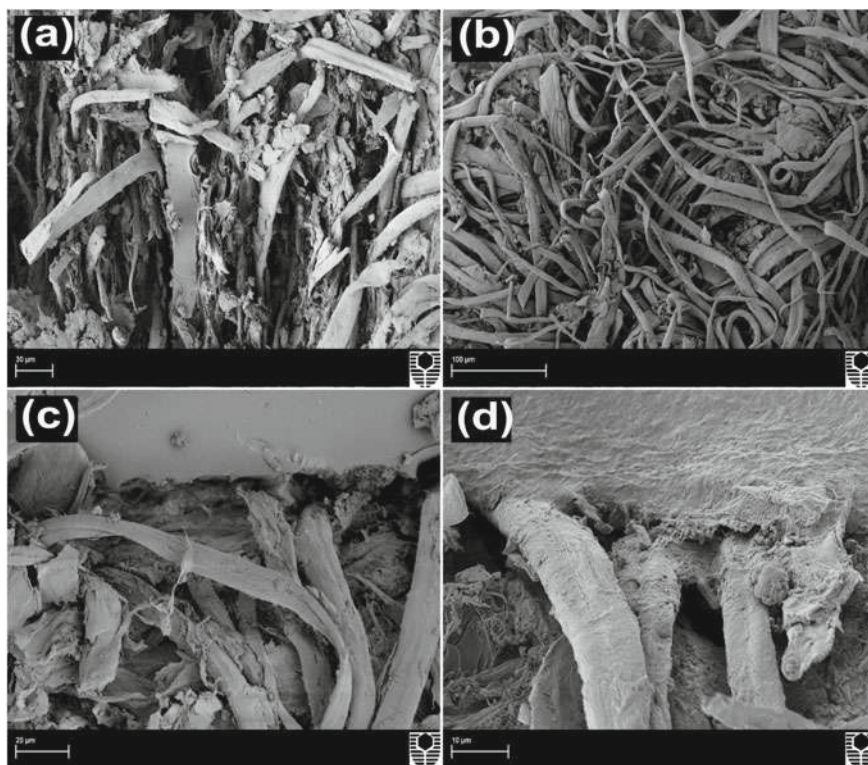

Fig. 5.20   SEM images showing the details of fracture surface for **a** 5 wt% n-SiC-filled RCF/epoxy in dry condition, **b** 5 wt% n-SiC-filled RCF/epoxy in wet condition, **c** RCF/epoxy in wet condition, and **d** 5 wt% n-SiC-filled RCF/epoxy in wet condition

that water absorption severely degrade the interfacial adhesion between the fibres and the matrix by substituting the strong covalent bonds with weaker hydrogen bonds (Kim and Seo 2006). As a result, fibre debonding (characterized by the appearance of gap between fibre and matrix) is a clear evidence of weak fibre–matrix interfacial adhesion in the structure of wet composites. However, the presence of n-SiC particles leads to enhancement in the interfacial bonding between the fibre and matrix as can be seen in Fig. 5.16d. Therefore, the presence of nano-filler plays an important role in improving the adhesion between fibre and matrix and hence enhances the mechanical properties of the composites.

5.5 Cellulose Fibre/Vinyl-Ester Ecocomposites

(a)   Density and Void Content

Table 5.6 provides results for the density, fibre volume fraction, and void content of the samples. As the weight fraction of the fibre increased, the theoretical and experimental composite densities also rose. This was due to the presence of fibrous material (1.54 gm/cm^3) within the composites, which was denser than the matrix (1.14 gm/cm^3). A plausible explanation for the increase in densities in these composites may be the efficient packing of fibres and favourable fibre–matrix adhesion (Sivaperumal and Jancirani 2021).

The experimental density values of the composites were lower than the theoretically predicted values (Table 5.6). This discrepancy suggests some void formation in the composites of this study (Alhuthali and Low 2021). Despite this, as the weight fraction of the fibre increased, there was a clear reduction in void content. This reduction could be linked to the preparation method. First, soaking the thin RCF sheets allowed for more contact of the fibre–matrix surfaces, thus leading to better adhesion. Second, formation of the composite using compression moulding forced the air to be expelled from specimens more readily during the composite processing. Thus,

Table 5.6 Fibre volume fraction and void content of VER/RCF samples

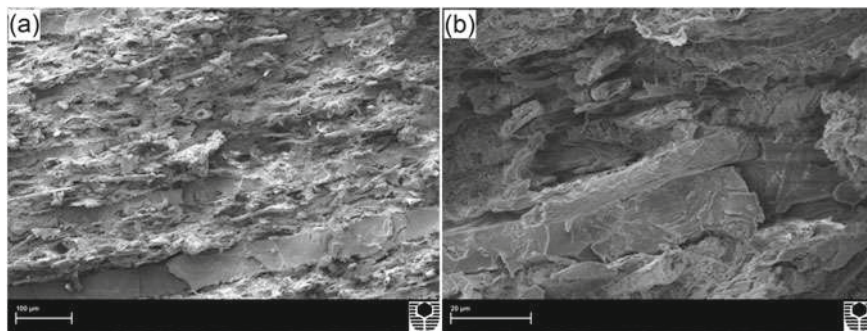| sample	Fibres weight fraction (wt%)	Fibres volume fraction (%)	Theoretical density (gm/cm^3)	Experimental density (gm/cm^3)	Void content (%)
VER/20% RCF	20	0.16	1.21	1.18 ± 0.03	5.55
VER/30% RCF	30	0.24	1.24	1.21 ± 0.02	4.75
VER/40% RCF	40	0.33	1.27	1.24 ± 0.05	3.28
VER/50% RCF	50	0.43	1.31	1.27 ± 0.02	2.74

Fig. 5.21 a Low- and **b** high-magnification SEM micrographs of fracture surfaces for 40 wt% RCF-reinforced VER

these processes minimize void content and increase the densities of the resultant composites.

These results agree with other earlier studies. For instance, Sivaperumal and Jancirani (2021) found that, as oil palm fibre volume fraction increased from 0.24 to 0.40 in phenol formaldehyde/glass fibre composites reinforced by oil palm fibres, the void content in these composites decreased from 3.33 to 2.83%. In another study, Facca et al. (2006) used a range of fibres to reinforce high-density polyethylene (HDP) composites. They found that void content reduced, in most cases, as the weight fraction of the fibre increased. In their study, as the weight fraction of hemp fibre was increased from 10 wt% to 50 wt%, the void content dropped from 9 to 3%. The fracture surfaces of composites with 40 wt% RCF at low and high magnifications are shown in Fig. 5.21. From these images, no noticeable voids can be detected within the composites and the appearance of good adhesion between the fibre and matrix is clearly observed.

(b)   Water Absorption Behaviour

Figure 5.22 shows the percentage of water uptake as a function of the square root of time for pure VER- and RCF-reinforced samples at 20, 30, 40, and 50 wt% addition, immersed in tap water at room temperature. The maximum water uptake for VER and the composites immersed for 2,500 h at room temperature was 0.76, 6.52, 9.56, 12.37, and 14.62%, respectively.

All the composites that were immersed in water for a prolonged period demonstrated Fickian diffusion behaviour. When first exposed to water, absorption occurred rapidly. However, the rate of moisture absorption slowed as time progressed, until reaching the point of equilibrium (Assarar et al. 2011). An increase in content of cellulose fibres led to an increase in water uptake, as would be expected (Wang et al. 2006). It is worth noting that, for the composites, in the first 250 h, the rate of water uptake was rapid, and thereafter steadied. In natural fibres, the mechanism of water absorption is well understood. When exposed to moisture, the first molecules of water are absorbed by the hydrophilic groups of the natural fibres. After this, a
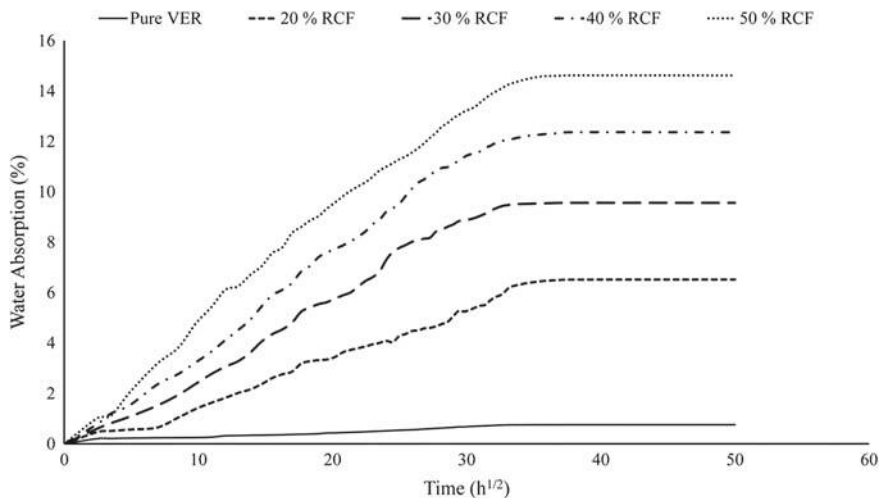
Fig. 5.22   Water absorption curves of VER and VER/RCF samples

second group of water molecules is attracted to the other hydrophilic groups present. A third group of water molecules may also be attracted to the top molecules already absorbed. When humidity is high, surface tension forces may hold liquid water in capillary spaces (Dhakal et al. 2007; Chen et al. 2009). The presence of hydroxyl groups on natural fibres gives the fibres a hydrophilic nature. This causes water molecules to be attracted and bound to the natural fibres by forming hydrogen bonds (Athijayamani et al. 2009; Gbadeyan et al. 2020). The addition of cellulose fibre to the polymer composites increases the size of the interfacial area, thereby allowing more water to be absorbed as a result of the capillary effect (Stamboulis et al. 2001; Chai et al. 2021). Hence, the higher the content of cellulose fibres in the composites, the higher the rate of water absorption (Kim and Seo 2006).

Moreover, when these composites are exposed to environments of extreme moisture, swelling of the cellulose fibres occurs. For brittle thermosetting resins, such as vinyl-ester, fibre swelling causes micro-cracking. These micro-cracks can create swelling stresses that lead to composite failure (Stamboulis et al. 2001; Bismarck et al. 2002). As the composite cracks, the damage facilitates capillarity and transport that uses micro-cracks. Capillarity is a mechanism that involves the flow of water molecules along fibre–matrix interfaces, and diffusion through the bulk matrix. The water molecules attack the interface, causing degradation of the fibre–matrix interface areas (Dhakal et al. 2007; Kim and Seo 2006; Athijayamani et al. 2009).

The microstructures of composites reinforced with 30 and 50 wt% RCF, after water absorption experiment are shown in Fig. 5.23. The loss of adhesion between fibre and matrix can be seen. The fibres appear degraded with absence of a covering matrix layer on them, and the microfibrils can be observed.

An increase in the fibre volume fraction of composites caused gradual increases in maximum water content and diffusion coefficient values (Table 5.7). As mentioned
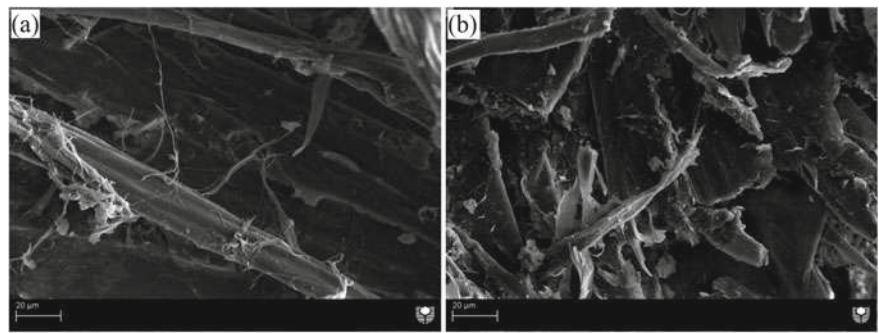
Fig. 5.23 SEM micrographs showing the degradation of the fibre–matrix interface due to moisture attacked samples with **a** 30 wt% RCF and **b** 50 wt % RCF

Table 5.7 Maximum water uptake, M_∞, and diffusion coefficients, D, of VER and VER/RCF samples

Sample	Fibres weight fraction (wt%)	Fibres volume fraction (%)	M_∞ (%)	D (mm^2/s)
VER	0	0	0.76	3.72×10^{-6}
VER/20% RCF	20	0.16	6.52	2.71×10^{-7}
VER/30% RCF	30	0.24	9.56	6.66×10^{-7}
VER/40% RCF	40	0.33	12.36	1.19×10^{-6}
VER/50% RCF	50	0.43	14.62	2.01×10^{-6}

earlier, composites with higher fibre loading contain a higher content of cellulose fibres and have greater interfacial area, each of which leads to greater diffusivity.

(c)   Elastic Modulus

Figure 5.24 shows the elastic modulus versus RCF volume fraction for VER/RCF composites in dry and wet conditions. For the dry samples, the elastic modulus increased as the fibre volume fraction increased. The addition of 20, 30, 40, and 50 wt% RCF, corresponding to 0.16, 0.24, 0.33, and 0.43 fibre volume fractions, increased the elastic modulus by 49.2 76.4, 113.8, and 143.4%, respectively, compared to pure VER (2.97 GPa). Thus, an increase in the fibre content of the composite material resulted in an increase in the elastic modulus. The improvement in elastic modulus is believed to be due to the higher initial modulus of the cellulose fibres acting as backbones in the composites (Kim and Seo 2006; Alhuthali and Low 2021). This is supported by earlier studies, which have reported significant increases in the elastic modulus of natural fibre-reinforced polymer composites. For example, Ma et al. (2005) investigated winceyette fibres reinforced thermoplastic starch composites with increasing fibres content from 0 to 20%. In this study, the elastic modulus increased from 45 GPa for neat resin to approximately 140 GPa as the fibre content increased. Hargitai et al. (2008) studied the elastic modulus for
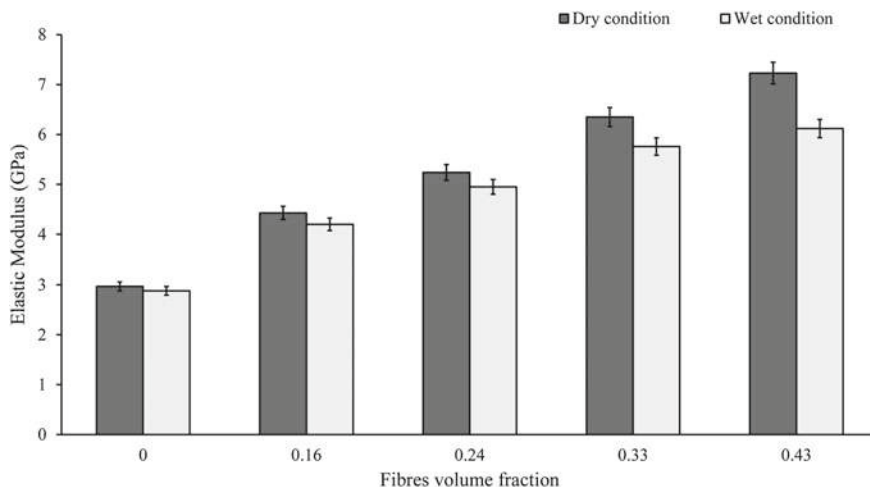
Fig. 5.24 Elastic modulus versus fibre volume fraction in dry and wet conditions

hemp fibre reinforced polypropylene with zero to 70 wt% fibre loading. Compared with an elastic modulus of 2.7 GPa for the matrix, at 50% fibre loading, the result was nearly 2.5 times greater. However, after the elastic modulus peaked at 50%, it was found to be lower at 70% fibre loading. Similarly, Khoathane et al. (2008) studied the effect of fibre contents on the elastic modulus of polypropylene copolymer composites reinforced with bleached hemp fibre. In this study, the elastic modulus for neat resin was 1.3 GPa, and it was found that increasing the amount of fibre to 30 wt% increased the elastic modulus to 4.4 GPa.

For wet samples, water absorption reduced elastic modulus (see Fig. 5.24). For example, RFC reinforced composites with 0.16 and 0.43 fibre volume fractions were found to show 5.2% and 15.4% reductions in elastic modulus when compared with the results for the dry samples with equivalent fibre volume fractions. A reduction in elastic modulus as a result of water absorption has also been found in earlier studies (Dhakal et al. 2007; Athijayamani et al. 2009). In the current study, the reduction in elastic modulus was found to be most noticeable for composites with high fibre content. The most likely reason for this is that moisture absorption reduces the integrity of bonding between the fibre and matrix, which degrades the interfacial stress transfer capability, thereby leading to reduced elastic modulus.

(d)   Analysis of Elastic Modulus

As there are no theoretical or experimental data available for the elastic modulus of RCF, as used in this study, the elastic modulus of RCF was assumed to be 39 GPa. This assumption was based on the earlier investigations of Lamy and Baley (2000) which found a close relationship between the diameter and elastic modulus for natural fibres. Lamy and Baley found that, where fibres were approximately 35 µm in diameter, elastic moduli were around 39 GPa, whereas a diameter of approximately 5 µm had elastic moduli at around 79 GPa. They attributed these variations in elastic moduli

Table 5.8 Material properties required for micromechanical models

Material property	Value
Poisson's ratio of VER	0.35[40]
VER density[a]	1.14
Elastic modulus of VER[a]	2.97
RCF density[a]	1.54 g/cm^3
RCF diameter and length[b]	30, 1500 μm

[a]This study's experimental data
[b]Measured based on 50 different fibres (SEM observation)

to changes in lumen size among fibres of different diameters. Another important parameter is the fibre orientation factor, β_{0E}. This value is determined by using fibre orientation distribution. The β_{0E} value for random in-plane orientation of the fibres is theoretically 0.375 (Chai et al. 2021; Garkhail et al. 2000). The value of 0.375 neglects the influence of transverse deformations. Nonetheless, it is expected that in-plane orientation would be approximately based on the arrangement of fibres in the RCF sheets.

Using the presumptions of the fibre's elastic modulus and orientation factor, the four models mentioned earlier could be applied to the data listed in Tables 5.6 and 5.8.

A plot of predicted elastic moduli against fibre volume fraction is shown in Fig. 5.25. All values of elastic modulus for both the prediction data and the experimental data fell between the upper bounds (ROM) and lower bounds (IROM). This finding could indicate that ROM–IROM models offer reasonable analytical solutions for validity in this study.
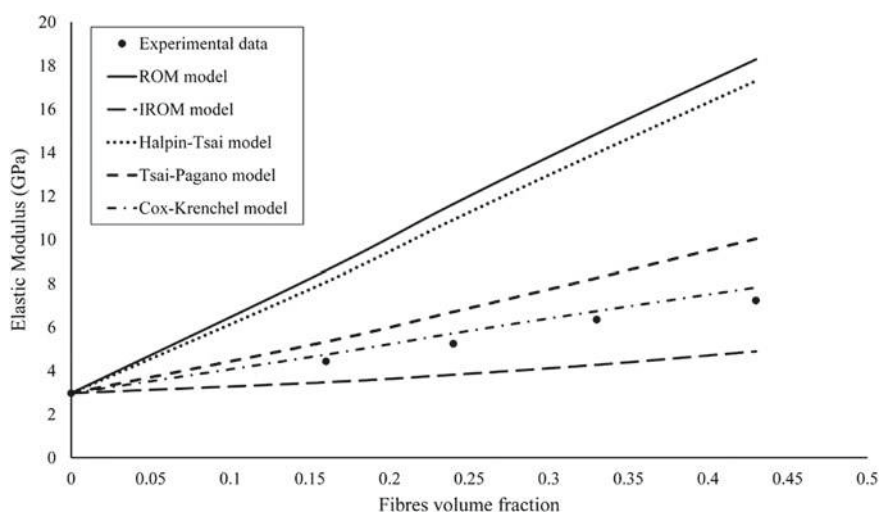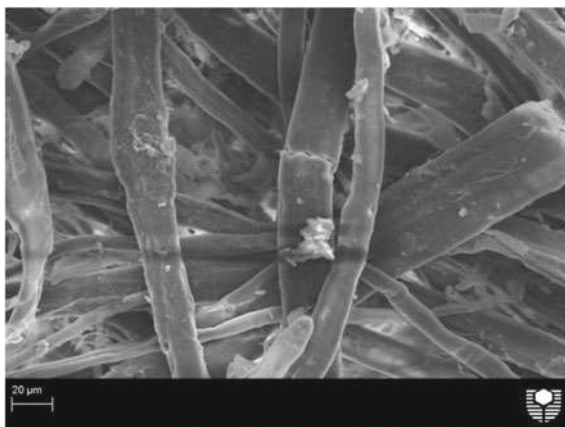

Fig. 5.25 Experimental and prediction data of elastic modulus against fibre volume fraction

Fig. 5.26 SEM micrograph showing irregularly shaped fibres

The Halpin–Tsai model greatly overestimated elastic modulus for composites. This is because this model relies upon the use of a fitting parameter, ξ which is determined using Eq. 2.20. This equation was based on observations of synthetic fibres primarily glass fibres. Synthetic fibres have lengths and cross sections that are well defined; thus, this model produces good prediction of the elastic modulus for composites reinforced with synthetic fibres. However, natural fibres do not possess the same uniformity of dimensions; they have complex, irregular lengths, and cross sections (see Fig. 5.26).

The initial overestimation of elastic modulus using the Halpin–Tsai model with values of ξ computed using Eq. 2.20 indicated large discrepancies between the values of ξ computed using Eq. 2.20 and the best-fit value of ξ. The calculations revealed that a value of ξ adjusted to 2.3 gave the best fit to the experimental data of this current study. The Tsai–Pagano model, similar to the Halpin–Tsai model, also overestimated the elastic modulus of experimental data. The explanation made earlier is also relevant here. The discrepancy between experimental data for the elastic modulus of natural fibre reinforced composites and prediction data based on the Halpin–Tsai model and the Tsai–Pagano model has been found in other studies (Alhuthali and Low 2021; Conzatti et al. 2012).

The Cox–Krenchel model prediction data gave the best agreement with the experimental data. The values obtained from the model were consistent with the experiment data, despite being slightly higher. A plausible explanation for the marginally greater elastic modulus results based on the prediction data is that the Cox–Krenchel model relies on an orientation factor (β_{0E}) of 0.375 a value based on two-dimensional random orientation synthetic fibre composites that is not necessary suitable for natural fibre composites.

Unlike glass fibres, which are stiff and remain straight, natural fibres exhibit curvature, and may readily bend or curl in the mat and after processing (Herrera-Franco and Valadez-González 2005). Thus, composites reinforced with natural fibres are more compliant than comparable composites reinforced with synthetic fibres

(Andersons et al. 2006). This highlights that the orientation factor (β_{0E}) of 0.375 that the Cox–Krenchel model relies on needs to be adjusted to provide a better fit with the experiment data for the elastic modulus of natural fibre reinforced composites.

The inaccuracy of predicted values obtained using elastic modulus modelling based on Cox–Krenchel has been reported in earlier studies by Bos et al. (2006) and Andersons et al. (2006). Bos et al. used an orientation factor (β_{0E}) of 0.62 to obtain best fit between the prediction and experimental data for polypropylene composites reinforced with short flax fibres. Andersons $_{et\ al}$. used an adjusted orientation factor (β_{0E}) of 0.2 to obtain best fit between the prediction and experimental data for polypropylene composites reinforced with extruded flax fibres.

Interestingly, for the present study, the best-fit orientation factor (β_{0E}) was found to be 0.333. This value is close to the theoretical orientation factor value of 0.375 that was taken to predict data with the Cox–Krenchel model. This may be due to the use of thin fibre sheets (mats) with fibre lengths (1500 μm) much greater than the thickness of the sheets (100 μm). It may also be because the fibres were expected to be mainly oriented in two directions.

(e)   Flexural Strength

Figure 5.27 provides the flexural strength results for dry and wet conditions as a function of fibre volume fraction. For the dry samples, increasing fibre content improved significantly flexural strength. Specifically, the addition of 20, 30, 40, and 50 wt% RCF led to 173.7, 216.5, 254.2, and 295.7% increases in flexural strength, respectively. These significant enhancements in strength were attributed to a reinforcing effect caused by cellulose fibres, which are of high strength and modulus (Alhuthali et al. 2012). Moreover, the ability of RCF to resist bending force is also believed to improve composite flexural strength as the fraction volume of fibre is increased in
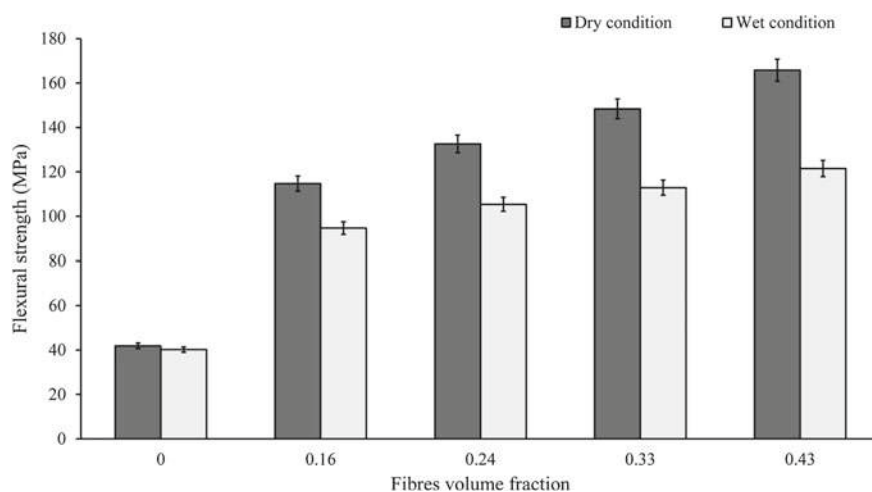

Fig. 5.27   Flexural strength versus fibre volume fraction in dry and wet conditions

composites (Ganesan et al. 2021). Increasing RCF content also provided increased resistance to shearing during the three-point flexure test (Sivaperumal and Jancirani 2021).

At lower RCF content, lower values of flexural strength were observed. This was attributed to a reduction in load transfer from matrix to fibre, resulting in lower load carrying by fibres. In general, the reinforcement provided by fibres in composites was not served where the volume fraction of fibre was insufficient (Ghosh et al. 2011). In contrast, at higher RCF content; there was an increase in flexural strength. This is believed to be due to the increase in stress transferred from matrix to fibres. The level of stress transfer from the matrix to the fibre is dependent on fibre–matrix interactions (Araújo et al. 2008). A good bond between the fibres and matrix is required in this process. Where good bonding is present, the fibres will provide uniform stress distribution from the continuous polymer matrix phase to the dispersed fibres phase, which gives the composite its strength. In this study, the enhancement of flexural strength with increasing fibre content suggests good bonding between the fibre and matrix. In general, blending higher fibre content (>40 wt%) with polymer matrix leads to poor fibre–matrix bonding, which promotes micro-crack formation (Yin and Zhang 2022). This poor bonding is due to limited wettability, in which the fibres are not completely surrounded by the matrix material (Bax and Müssig 2008). Limited wettability can increase fibre–fibre interaction, thereby reducing effective stress transfer from the matrix to the fibres and lowering the composite strength (Sivaperumal and Jancirani 2021).

The same figure (see Fig. 5.27) also reveals the effect of moisture absorption on flexural strength. The flexural strength for the samples decreased markedly after water absorption. Compared to the dry samples, the reductions in flexural strength of the samples reinforced with 20, 30, 40, and 50 wt% RCF were 17.4, 20.5, 23.9, and 26.7%, respectively. Gbadeyan et al. (2020) and Zamri et al. (2012) published similar reports that highlighted a negative effect of water uptake on the flexural strength of natural fibre composites. The reduction in flexural strength was due to the weakening of the fibre–matrix interface. As water content increased in the composite, the absorbed water formed intermolecular hydrogen bonding with the cellulose fibres. This occurrence reduced interfacial adhesion between the fibre and matrix, and the strength was subsequently reduced (Aquino et al. 2007; Bessadok et al. 2008). In environments with high percentages of hydroxyl groups, natural fibres exhibit low resistance to moisture (Nassar et al. 2021). This leads to dimensional variations of the composite products (the matrix and fibres) and poor bonding between the matrix and fibres. It also causes lower stress transfer from the matrix to the fibres. Again, these factors cause a decrease in the composite's mechanical properties (Mishra et al. 2003). Moreover, higher fibre content also leads to increased water absorption, which negatively affects the fibre–matrix bonding (Yin and Zhang 2022).

Figure 5.28 shows the adverse effects of water uptake on the fibre–matrix interface reinforced with 20 and 50 wt%. As the content of RCF increased, the effect of water uptake became more evident.
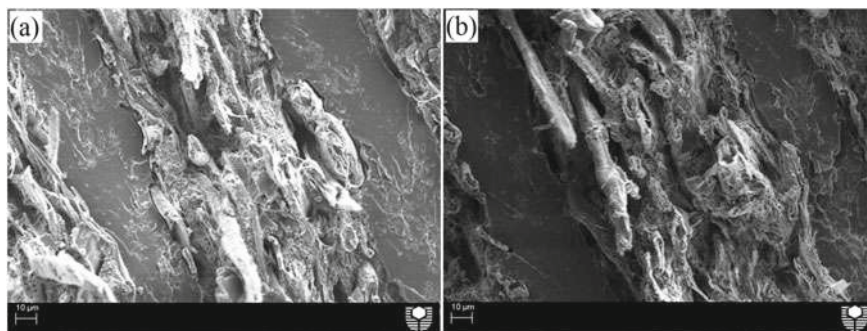
Fig. 5.28 Effect of water absorption on the fibre–matrix interface for samples reinforced with **a** 20 wt% RCF and **b** 50 wt% RCF

(f)   Impact Strength

Figure 5.29 shows the impact strength of VER/RCF composites in dry and wet conditions. For the dry samples, the addition of fibre content increased the impact strength markedly. Compared to the impact strength of pure VER (2.5 kJ/m^2), the addition of 20, 30, 40, and 50 wt% RCF increased impact strength to 10.3, 13.5, 18.9, and 28.7 kJ/m^2, respectively. Interestingly, the impact strength obtained in this study with 50 wt% RCF (28.7 kJ/m^2) was comparable to the impact strength of flax reinforced with polypropylene or maleated polypropylene, both of which have an impact strength of approximately 30 kJ/m^2. These are natural fibre reinforced composites commonly used in the automotive industry (Bos et al. 2006; Bax and Müssig 2008).
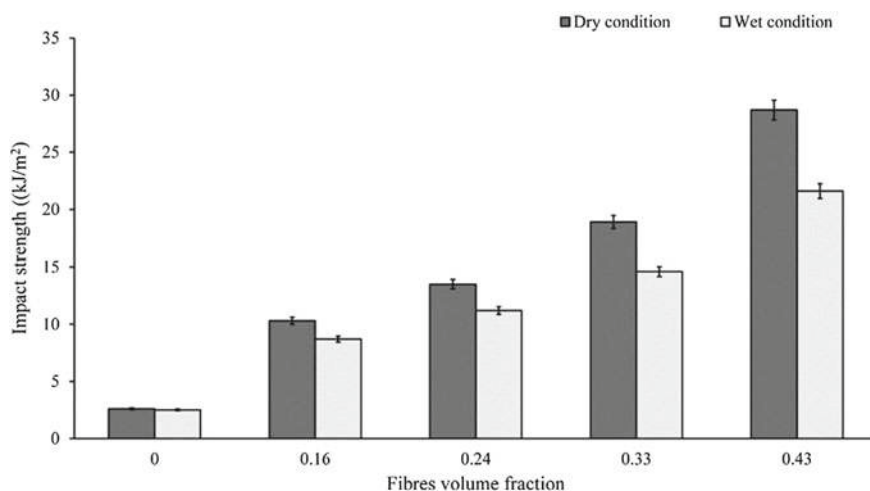
Fig. 5.29 Impact strength versus fibre volume fraction in dry and wet conditions

Impact strength is the ability of a material to resist fracture when experiencing high-speed stress. Fibres play an important role in impact resistance by transferring the stress of impact through energy dissipation mechanisms (Mishra et al. 2003; Wambua et al. 2003). Fibre pull-out, fibre fracture, and matrix deformation are believed to be important energy dissipation mechanisms that occur within fibre-reinforced composites during impact (Bax and Müssig 2008). By increasing the fibre content, fibre-reinforced composites with high impact strength can be fabricated.

Figure 5.29 also reveals a reduction in impact strength due to moisture absorption. Compared to the dry samples, the reductions of impact strength in the samples reinforced with 20, 30, 40, and 50 wt% RCF were 15.5, 17, 22.8, and 24.7%, respectively. Water absorption also reduced the impact strength of composites by compromising the fibre–matrix bonding. For un-notched samples, the impact strength depended on the quality of the fibre–matrix adhesion. During the impact tests, good fibre–matrix adhesion enhanced the resistance of the composite to the fracture (Kim and Seo 2006). Figure 5.30 shows the fracture surfaces of composites reinforced with 50wt% RCF in dry and wet conditions. For dry composite (see Fig. 5.30a), almost no fibre pull-out is observed, and the fibres can be seen to be broken off near the surface. This observation is a result of strong bonding between the fibres and the matrix materials. However, in wet condition (see Fig. 5.30b) more fibre pull-out clearly observed as a result of poor fibre–matrix bonding because of water absorption. This supports the notion that, when composites are exposed to water absorption, impact strength will decrease.

(g)   Fracture Toughness

Figure 5.31 shows fracture toughness results as a function of fibre volume fraction for both dry and wet samples. The addition of RCF leads to enhancement in fracture toughness properties. Compared to that of the pure sample (1.78 MPam$^{1/2}$), adding 20, 30, 40, and 50 wt% RCF improved fracture toughness to 2.4, 3.8, 4.5, and 5.9 MPam$^{1/2}$, respectively. Interaction between the cellulose fibres and the matrix
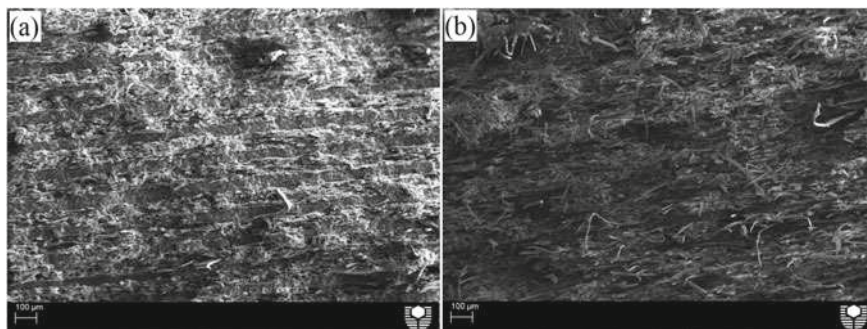
Fig. 5.30 SEM micrographs showing the fracture surfaces of samples with 50 wt% RCF are shown **a** before and **b** after water absorption
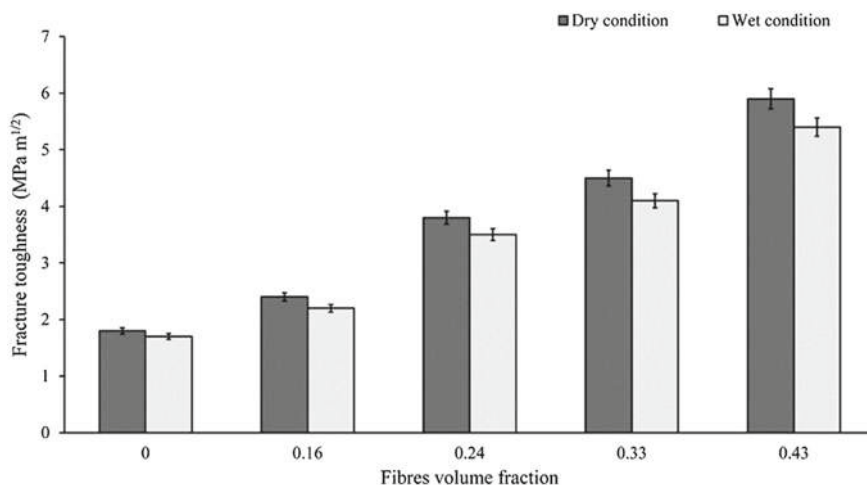
Fig. 5.31 Fracture toughness versus fibre volume fraction in dry and wet conditions

provided the composites with enhanced crack pinning, energy dissipation, and fracture resistance properties (Bax and Müssig 2008). Crack deflection, fibre–matrix debonding, fibre pull-out, and fibre-bridging are believed to contribute to the fracture toughness of natural fibre-reinforced polymer composites. In the case of neat polymers, plastic deformation is an important energy dissipation mechanism (Alhuthali et al. 2012); however, this mechanism is undermined by the addition of fibres. Nonetheless, overall material toughness is enhanced in composites by the mechanisms provided by natural fibre addition. High RCF content provided enhanced fracture toughness in the composites, which is believed to be a result of increased fibre pull-out, fibre fracture, and fibre-bridging mechanisms.

While composites can be prepared with high fracture toughness by adding natural fibre, this enhancement is dependent on interfacial adhesion. If the fibre–matrix adhesion is excessive, the composite will become brittle and exhibit poor toughness results. If the fibre–matrix adhesion is poor, fibre pull-out occurs readily and composites will again exhibit poor toughness results (Bax and Müssig 2008). Thus, achieving optimal fibre–matrix adhesion is paramount. The results of this study reveal a suitable level of fibre–matrix adhesion that is supported by enhanced fracture toughness and strength.

In this study, exposure to wet conditions caused a slight reduction in fracture toughness for the composite samples (see Fig. 5.31). Moisture absorption exposed the composites to water, which compromised the fibre–matrix interface. By weakening the fibre–matrix interface and causing poor fibre–matrix adhesion, fibre debonding, and pull-out occur without substantial resistance. Thus, insufficient amount of energy will be dissipated by these mechanisms during the fracture test, leading to lower toughness values (Alhuthali et al. 2012).

References

Abacha N, Kubouchi M, Tsuda K et al (2007) Performance of epoxy-nanocomposite under corrosive environment. Exp Polym Lett 1(6):364–369

Alamri H, Low IM (2012) Mechanical properties and water absorption behaviour of recycled cellulose fibre reinforced epoxy composites. Polym Testing 31(5):620–628

Alamri H, Low IM (2012) Characterization of epoxy hybrid composites filled with cellulose fibres and nano-SiC. J Appl Polym Sci 126:E221–E231

Alhuthali A, Low IM, Dong C (2012) Characterisation of the water absorption, mechanical and thermal properties of recycled cellulose fibre reinforced vinyl-ester eco-nanocomposites. Compos B 43:2772–2781

Alhuthali A, Low IM (2021) Vinyl-ester composites reinforced with natural fibers and nanofillers (Chapter 9). In: Low I-M, Dong Y (eds) Composite materials. Elsevier, pp 227–244. ISBN 9780128205129

Andersons J, Spārniņs E, Joffe R (2006) Stiffness and strength of flax fiber/polymer matrix composites. Polym Compos 27:221–229

Aquino EMF, Sarmento LPS, Oliveira W et al (2007) Moisture effect on degradation of jute/glass hybrid composites. J Reinf Plast Compos 26:219–233

Araújo JR, Waldman WR, De Paoli MA (2008) Thermal properties of high density polyethylene composites with natural fibres: coupling agent effect. Polym Degrad Stab 93:1770–1775

Assarar M, Scida D, Mahi A et al (2011) Influence of water ageing on mechanical properties and damage events of two reinforced composite materials: Flax–fibres and glass–fibres. Mater Des 32:788–795

Athijayamani A, Thiruchitrambalam M, Natarajan U et al (2009) Effect of moisture absorption on the mechanical properties of randomly oriented natural fibers/polyester hybrid composite. Mater Sci Eng, A 517:344–353

Bax B, Müssig J (2008) Impact and tensile properties of PLA/Cordenka and PLA/flax composites. Compos Sci Technol 68:1601–1607

Bessadok A, Marais S, Roudesli S et al (2008) Influence of chemical modifications on water-sorption and mechanical properties of Agave fibres. Compos A 39:29–45

Bismarck A, Aranberri-Askargorta I, Springer J et al (2002) Surface characterization of flax, hemp and cellulose fibers; Surface properties and the water uptake behavior. Polym Compos 23:872–894

Bos HL, Müssig J, van den Oever MJA (2006) Mechanical properties of short-flax-fibre reinforced compounds. Compos A 37:1591–1604

Buehler FU, Seferis JC (2000) Effect of reinforcement and solvent content on moisture absorption in epoxy composite materials. Composites A 31:741–748

Chai H, Wang X, Rehman WU et al (2021) Study on water absorption and mechanical properties of CNF–Ti reinforced epoxy resin composites. Plast Rubber Compos. https://doi.org/10.1080/146 58011.2021.2017127

Chandel PS, Gupta NK, Tyagi YK et al (2022) Experimental investigation of water absorptions and Charpy test of epoxy composite immersed in different aqueous medium. In: Dubey AK, Sachdeva A, Mehta M (eds) Recent trends in industrial and production engineering. Lecture notes in mechanical engineering. Springer, Singapore. https://doi.org/10.1007/978-981-16-313 5-1_9

Chen H, Miao M, Ding X (2009) Influence of moisture absorption on the interfacial strength of bamboo/vinyl ester composites. Composites A 40:2013–2019

Conzatti L, Giunco F, Stagnaro P et al (2012) Polyester-based biocomposites containing wool fibres. Compos A 43:1113–1119

Deka BK, Maji TK (2011) Study on the properties of nanocomposite based on high density polyethylene, polypropylene, polyvinyl chloride and wood. Compos A 42:686–693

Dhakal HN, Zhang ZY, Richardson MOW (2007) Effect of water absorption on the mechanical properties of hemp fibre reinforced unsaturated polyester composites. Compos Sci Technol 67:1674–1683

Doan T, Brodowsky H, Mader E (2007) Jute fibre/polypropylene composites II. Thermal, hydrothermal and dynamic mechanical behaviour. Compos Sci Technol 67:2707–2714

Dorigato A, Pegoretti A, Quaresimin M (2011) Thermo-mechanical characterization of epoxy/clay nanocomposites as matrices for carbon/nanoclay/epoxy laminates. Mater Sci Eng, A 528:6324–6333

Facca AG, Kortschot MT, Yan N (2006) Predicting the elastic modulus of natural fibre reinforced thermoplastics. Compos A 37:1660–1671

Fraga AN, Frullloni E, de la Osa O et al (2006) Relationship between water absorption and dielectric behaviour of natural fibre composite materials. Polym Testing 25(2):181–187

Ganesan K, Kailasanathan C, Rajini N et al (2021) Assessment on hybrid jute/coir fibers reinforced polyester composite with hybrid fillers under different environmental conditions. Constr Build Mater 301:124117

Garkhail SK, Heijenrath RWH, Peijs T (2000) Mechanical properties of natural-fibre-mat-reinforced thermoplastics based on flax fibres and polypropylene. Appl Compos Mater 7:351–372

Gbadeyan OJ, Adali S, Bright G et al (2020) Studies on the mechanical and absorption properties of achatina fulica snail and eggshells reinforced composite materials. Compos Struct 239:112043

Ghosh RKA, Reena G, Raju BL (2011) Effect of fibre volume fraction on the tensile strength of banana fibre reinforced vinyl ester resin composites. Int J Adv Eng Sci Technol 4:89–91

Hargitai H, Rácz I, Anandjiwala RD (2008) Development of HEMP fiber reinforced polypropylene composites. J Thermoplast Compos Mater 21:165–174

Herrera-Franco PJ, Valadez-González A (2005) A study of the mechanical properties of short natural-fiber reinforced composites. Compos B 36:597–608

Hossain MK, Imran KA, Hosur MV et al (2011) Degradation of mechanical properties of conventional and nanophased carbon-epoxy composites in seawater. J Eng Mater Technol 133(4):41004

Jodatnia S, Rash-Ahmadi S (2022) Hygrothermal aging effect on the properties of PMMA nanocomposites reinforced by ceramic nanoparticles. J Compos Mater. https://doi.org/10.1177/0021998322 11053910

Khoathane MC, Vorster OC, Sadiku ER (2008) Hemp fiber-reinforced pentene/polypropylene copolymer: the effect of fiber loading on the mechanical and thermal characteristics of the composites. J Reinf Plast Compos 27:1533–1544

Kim HJ, Seo DW (2006) Effect of water absorption fatigue on mechanical properties of sisal textile-reinforced composites. Int J Fatigue 28:1307–1314

Kim JK, Hu C, Woo R et al (2005) Moisture barrier characteristics of organoclay–epoxy nanocomposites. Compos Sci Technol 65:805–813

Lamy B, Baley C (2000) Stiffness prediction of flax fibers-epoxy composite materials. J Mater Sci Lett 19:979–980

Limpadapun K, Sukmanee J (2021) A study of an effect on moisture from 3D printer filament drying processes. Key Eng Mater 902:101–106

Liu W, Hoa SV, Pugh M (2005) Fracture toughness and water uptake of high-performance epoxy/nanoclay nanocomposites. Compos Sci Technol 65:2364–2373

Low IM, McGrath M, Lawrence D et al (2007) Mechanical and fracture properties of cellulose fibre reinforced epoxy laminates. Compos A 38:963–974

Low IM, Somers J, Kho HS et al (2009) Fabrication and properties of recycled cellulose fibre-reinforced epoxy composites. Compos Interfaces 16:659–669

Ma X, Yu J, Kennedy JF (2005) Studies on the properties of natural fibers-reinforced thermoplastic starch composites. Carbohyd Polym 62:19–24

Mishra S, Mohanty AK, Drzal LT et al (2003) Studies on mechanical performance of biofibre/glass reinforced polyester hybrid composites. Compos Sci Technol 63:1377–1385

Mohan TP, Kanny K (2011) Water barrier properties of nanoclay filled sisal fibre reinforced epoxy composites. Compos A 42(4):385–393

Nassar MMA, Alzebdeh KI, Pervez T et al (2021) Progress and challenges in sustainability, compatibility, and production of eco-composites: a state-of-art review. J Appl Polym Sci 138:e51284. https://doi.org/10.1002/app.51284

Pradhan S, Prakash V, Acharya SK (2021) Effect of weathering on physical and mechanical characteristics of eulaliopsis binata fiber/epoxy composites. Trans Indian Inst Met. https://doi.org/10.1007/s12666-021-02422-3

Reddy CR, Sardashti AP, Simon LC (2010) Preparation and characterization of polypropylene–wheat straw–clay composites. Compos Sci Technol 70:1674–1680

Rizal S, Mistar EM, Rahman AA et al (2021) Bio-nanocarbon functional material characterisation and enhancement properties in nonwoven kenaf fibre nanocomposites. Polymers 13(14):2303

Sánchez-Soto M, Pagés P, Lacorte T et al (2007) Curing FTIR study and mechanical characterization of glass bead filled trifunctional epoxy composites. Compos Sci Technol 67:1974–1985

Sivaperumal R, Jancirani J (2021) Characterization of amino silane modified ramie fibre, OMMT nanoclay-reinforced epoxy resin composite. Silicon. https://doi.org/10.1007/s12633-021-01502-9

Stamboulis A, Baillie CA, Peijs T (2001) Effects of environmental conditions on mechanical and physical properties of flax fibers. Compos A 32:1105–1115

Tang Y, Deng S, Ye L et al (2011) Effects of unfolded and intercalated halloysites on mechanical properties of halloysite–epoxy nanocomposites. Compos A 42(4):345–354

Wambua P, Ivens J, Verpoest I (2003) Natural fibres: can they replace glass in fibre reinforced plastics? Compos Sci Technol 63:1259–1264

Wang L, Wang K, Chen L et al (2006) Hydrothermal effects on the thermomechanical properties of high-performance epoxy/clay nanocomposites. Polym Eng Sci 46(2):215–221

Wang W, Sain M, Cooper PA (2006) Study of moisture absorption in natural fiber plastic composites. Compos Sci Technol 66:379–386

Yin J, Zhang J (2022) Enhancing hygrothermal mechanical properties stability of polymer composite based on the concrete structure. Compos Struct 115224. https://doi.org/10.1016/j.compstruct.2022.115224

Zamri MH, Akil HM, Bakar AA et al (2012) Effect of water absorption on pultruded jute/glass fiber-reinforced unsaturated polyester hybrid composites. J Compos Mater 46:51–61

Chapter 6
Materials Properties: Thermal Stability and Flammability

Abstract Characteristics of thermal stability and flammability in epoxy and vinyl-etser ecocomposites and eco-nanocomposites were investigated. The effects of cellulose fibre and nano-filler dispersion on the thermal properties of these composites have been characterized. At high temperatures, thermal stability of neat resin increased due to the presence of either nano-filler or cellulose fibres. However, the presence of cellulose fibres accelerated the thermal degradation of neat resin. However, the addition of nano-filler to the ecocomposites imparted some resistance in thermal degradation.

Keywords Nanocomposites · Cellulose fibres · Nanoclay platelets · Halloysite nanotubes · n-SiC · Epoxy resin · Diffusivity · Water uptake · Moisture diffusion · Microstructure · Mechanical properties · Flexural strength · Flexural modulus · Impact strength · Fracture toughness · Impact toughness

6.1 Nano-SiC/Cellulose Fibre/Epoxy Eco-Nanocomposites

(a) Thermal Stability

The thermal stability of the samples was determined using thermo-gravimetric analysis (TGA). In this test, the thermal stability was studied in terms of the weight loss as a function of temperature in nitrogen atmosphere. The thermograms (TGA) and the derivatives thermograms (DTA) of neat epoxy, epoxy/RCF, epoxy/n-SiC, and epoxy/n-SiC/RCF nanocomposites filled with 5 wt% n-SiC are shown in Figs. 6.1 and 6.2. The maximum decomposition temperature (T_{max}) and the char yields at different temperatures for all sample types are summarized in Table 6.1.

In the case of epoxy resin and its nanocomposites, it can be seen from Table 6.1 that, at low temperatures (<400 °C), pure epoxy displays better thermal stability than those filled with n-SiC particles. This means that the presence of n-SiC accelerates the degradation of epoxy nanocomposites compared to epoxy resin. This observation has been reported as the Hofmann elimination reaction, where nanoparticles act as a catalyser towards the degradation of the polymer matrix (Madaleno et al. 2010; Ismail et al. 2008; Zhao et al. 2005). The maximum decomposition temperature (T_{max}) of the nanocomposites slightly decreases by 2 °C after the addition of (3 and 5) wt%
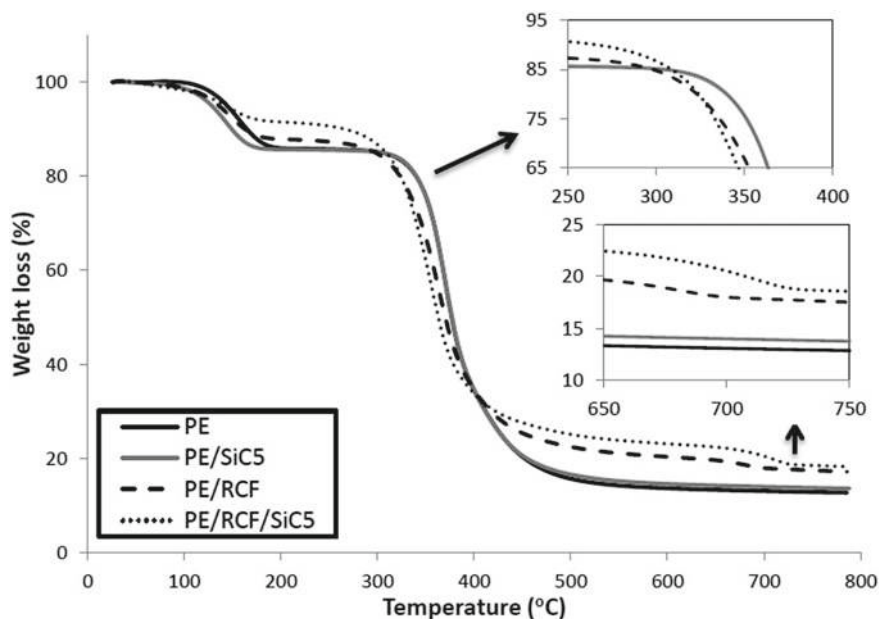
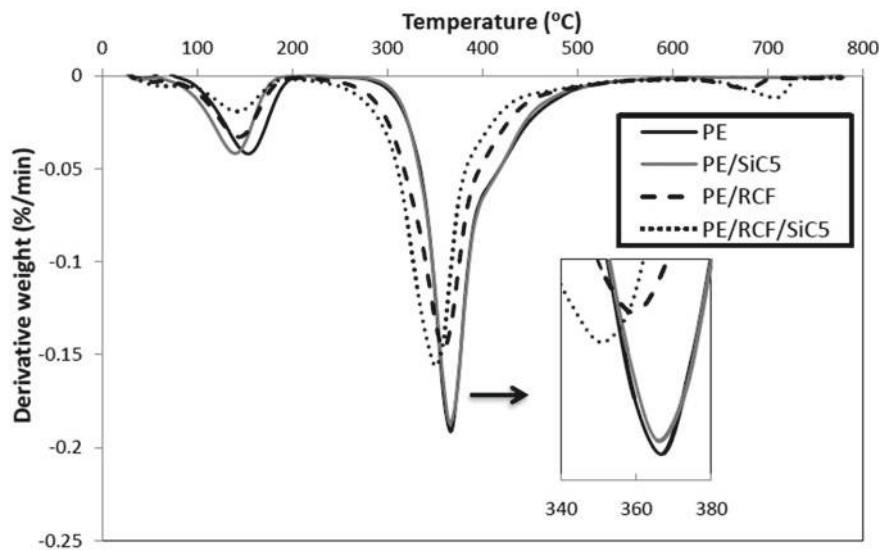**Fig. 6.1**   TGA curves of PE, PE/SiC5, PE/RCF and PE/RCF/SiC5

Fig. 6.2   DTG curves of PE, PE/SiC5, PE/RCF, and PE/RCF/SiC5

Table 6.1 Thermal properties of epoxy, epoxy/RCF composites, epoxy/n-SiC, and epoxy/RCF/n-SiC samples

Sample	Char yield at different temperature (%)							T_{max} (°C)
	100 °C	200 °C	300 °C	400 °C	500 °C	600 °C	700 °C	
PE	99.86	86.10	85.24	35.26	15.69	13.69	13.08	367.29
PE/SiC1	99.09	83.19	82.44	32.25	14.45	12.43	11.85	367.25
PE/SiC3	98.29	84.55	83.96	34.54	15.85	13.82	13.20	365.47
PE/SiC5	98.62	85.68	85.09	34.70	16.60	14.60	14.00	365.53
PE/RCF	98.65	87.88	85.01	34.58	22.49	20.37	17.96	359.62
PE/RCF/SiC1	97.34	94.30	88.48	33.72	26.90	25.15	21.66	351.43
PE/RCF/SiC3	97.96	92.74	87.65	33.83	25.84	23.92	20.87	351.37
PE/RCF/SiC5	98.22	91.51	86.65	33.84	25.15	23.14	20.50	350.87

n-SiC compared to pure epoxy. However, at high temperatures (>400 °C), epoxy reinforced with 3 and 5 wt% n-SiC show better thermal stability than neat epoxy. The char residue at 700 °C of neat epoxy increased from 13.1% to 13.2 and 14.0% after the addition of 3 and 5 wt% n-SiC, respectively. It was reported in previous studies that the addition of nanoparticles would efficiently raise the char residue of polymers at high temperature (Madaleno et al. 2010; Ismail et al. 2008).

The presence of RCF layers increases the amount of residue at temperatures range from 180 to 250 °C. At the second decomposition where the major degradation occurs, the addition of RCF clearly decreases the maximum decomposition temperature (T_{max}) by 7.7 °C compared to neat epoxy. Figure 6.2 shows that the peak of the maximum decomposition of RCF/epoxy composites shifted to lower temperature compared to neat epoxy, which indicates that the addition of RCF increases the rate of the sample major degradation. However, at high temperature (>400 °C), where samples lose (>70%) of their initial weight, the presence of RCF leads to significant enhancement in thermal stability by increasing the char yield at 500, 600, and 700 °C compared to epoxy system. The char yield at 700 °C of neat epoxy increase from 13.1 to 18.0 wt% after the addition of RCF. Similar results were obtained by Shih (2007) and De Rosa et al. (2011). They reported an improvement in thermal stability of plant fibre/epoxy composites by increasing char yield at high temperatures. Shih (2007) cited that the increasing in char yield is an indication of the potency of flame retardation of polymers. Thus, the addition of plant fibre enhanced the flame retardation of epoxy.

The addition of n-SiC to RCF/epoxy increases the thermal stability by increasing the amount of the residue at temperatures 200 and 300 °C. However, at the region of major degradation, the unfilled RCF/epoxy shows better thermal stability than samples filled with n-SiC. The maximum decomposition temperature (T_{max}) of RCF/epoxy nanocomposites decreased by ~8 °C compared to unfilled RCF/epoxy composite. Figure 6.2 shows that the peak of the major decomposition of RCF/epoxy filled with 5 wt% n-SiC moved to a lower temperature compared to unfilled RCF/epoxy composites. This is due to the catalytic effect of n-SiC particles on

RCF/epoxy nanocomposites. But, at high temperatures (>400 °C), n-SiC-filled RCF/epoxy nanocomposites show better thermal stability than unfilled RCF/epoxy composite by increasing the char residues at temperatures 500, 600, and 700 °C. This means that, at high temperature, the addition of n-SiC particles significantly enhances the thermal stability of epoxy/RCF nanocomposites. This enhancement on thermal properties is due to the presence of n-SiC, which acted as barriers and hindered the diffusion of volatile decomposition products out from the nanocomposites (Madaleno et al. 2010; Ismail et al. 2008; Yeh et al. 2006).

6.2 Halloysite/Cellulose Fibre/Epoxy Eco-Nanocomposites

(a)   Thermal Stability

The thermal stability of the samples was determined using thermo-gravimetric analysis (TGA). In this test, the thermal stability was studied in terms of the weight loss as a function of temperature in nitrogen atmosphere. The thermograms (TGA) of the epoxy/HNT and epoxy/HNT/RCF nanocomposites are shown in Fig. 6.3(a–b), respectively. The temperature at different weight loss %, the maximum decomposition temperature (T_{max}), and the char yield at 700 °C are all summarized in Table 6.2. In general, it can be seen from TGA curves that epoxy and its nanocomposites expose two similar distinct stages of decomposition. The first decomposition, which is in the region of 80–180 °C, may be related to the vaporization of water in the composites. The second decomposition may be related to epoxy degradation and its additives. It also can be seen that the major degradation for all samples occurs in the range of ~300–400 °C.

Table 6.2 shows that the temperature at 10% weight loss ($T_{10\%}$) of neat epoxy decreases because of the presence of HNTs. The ($T_{10\%}$) of neat epoxy and epoxy filled with 1, 3 and 5 wt% HNTs are 165.0, 148.7, 154.7, and 156.5 °C, respectively. However, as HNT content increases, ($T_{10\%}$) increases, which reveals that the addition of more halloysite decreases the moisture access to the sample. Then epoxy and its nanocomposites remained stable without significant degradation from 200 to around 300 °C just before the major degradation get started as seen in Fig. 6.3(a). In this study, the temperature at 20% weight loss ($T_{20\%}$) is considered as the onset temperature of the major degradation. The presence of 1 and 3 wt% HNTs decreases the ($T_{20\%}$) for epoxy from 339.4 to 331.8 and 335.9 °C, respectively, while the addition of 5 wt% HNT increases ($T_{20\%}$) slightly to 339.6 °C. This indicates that thermal stability enhances as HNTs content increases for nanocomposites samples. However, the maximum decomposition temperatures (T_{max}) of the composites remain not change after the addition of HNTs. The maximum decomposition temperatures of neat epoxy and epoxy filled with 1, 3, and 5 wt% HNTs are 367.3, 367.1, 367.6, and 367.3 °C, respectively. At high temperature (when samples lose 80% of their initial weight), epoxy reinforced with 3 and 5 wt% HNTs show better thermal stability than neat epoxy. ($T_{80\%}$) of neat epoxy (PE), PE/HNT1, PE/HNT3, and PE/HNT5 are 452.6,
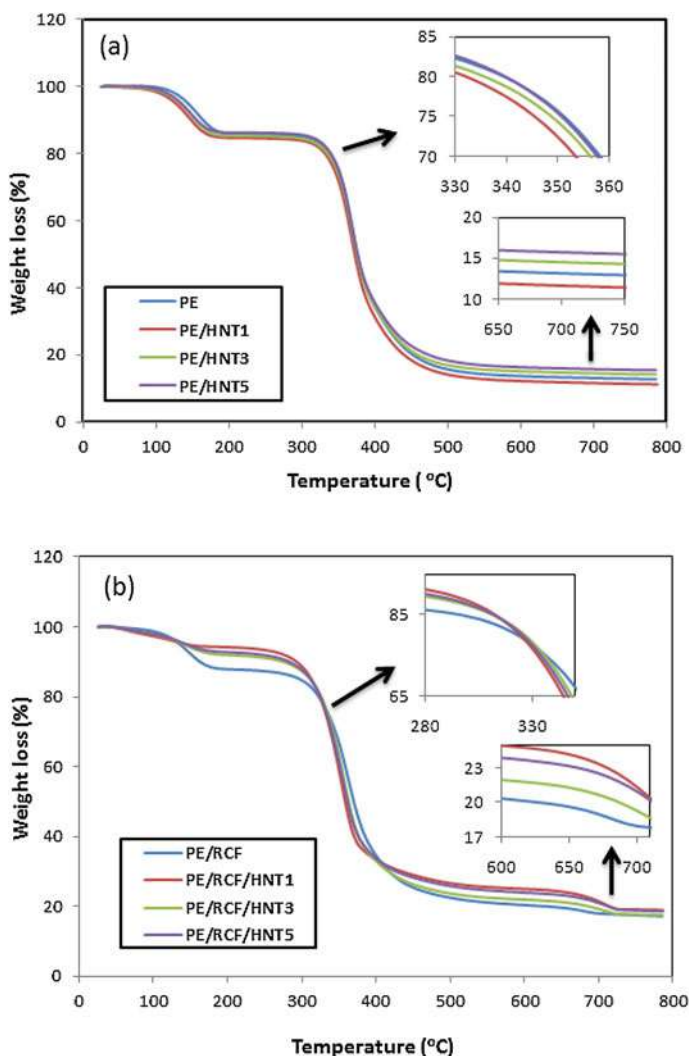
Fig. 6.3 TGA curves of epoxy and epoxy/HNT samples: **a** without RCF, **b** with RCF

440.4, 459.3, and 474.3 °C, respectively. As a result of this enhancement in thermal stability at high temperature, the char residue at 700 °C of neat epoxy increases from 13.0 to 14.5 and 15.8% after the addition of 3 and 5 wt% HNTs respectively. It was reported in previous studies that the addition of nanoparticles would efficiently raise the char residue of polymers at high temperatures (Madaleno et al. 2010; Chatterjee and Islam 2008).

The presence of RCF into epoxy system accelerates the degradation at low temperature (<400 °C). The temperature at 20% weight loss of pure epoxy is significantly

Table 6.2 Thermal properties of pure epoxy and epoxy composite samples

Sample	$T_{10\%}$ (°C)	$T_{20\%}$ (°C)	$T_{50\%}$ (°C)	$T_{80\%}$ (°C)	T_{max} (°C)	Char yield at 700 °C (wt%)
PE	165.0	339.4	376.9	452.6	367.3	13.1
PE/HNT1	148.7	331.8	372.8	440.4	367.1	11.6
PE/HNT3	154.7	335.9	375.7	459.3	367.6	14.5
PE/HNT5	156.5	339.6	376.9	474.3	367.3	15.8
PE/RCF	162.9	322.8	370.3	629.3	359.6	18.0
PE/RCF/HNT1	292.9	324.2	358.5	714.9	351.5	21.6
PE/RCF/HNT3	275.0	326.1	363.4	686.8	351.2	19.3
PE/RCF/HNT5	282.8	324.8	361.7	712.8	351.2	21.0
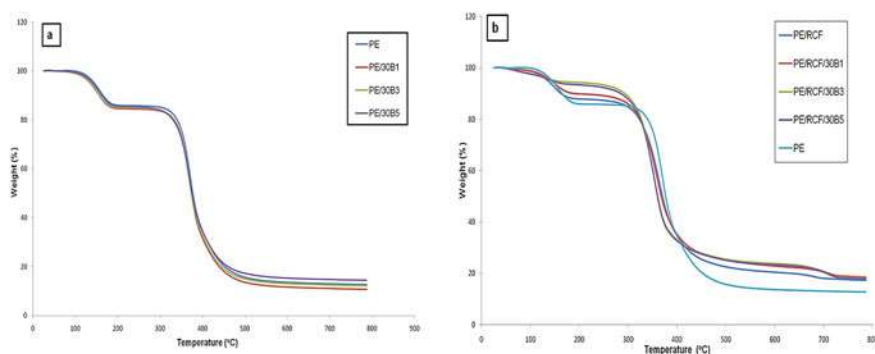
Fig. 6.4 TGA curves of epoxy and epoxy/clay samples: **a** without RCF, **b** with RCF

reduced from 339.4 to 322.8 °C and the maximum decomposition temperature (T_{max}) of epoxy is reduced from 367.3 to 359.6 °C as a result of the inclusion of RCF sheets. However, at temperature higher than 400 °C, the presence of RCF leads to an enhancement in thermal stability by increasing the char yield at 700 °C of epoxy system from 13.1 to 18.0 wt%. Shih (2007) carried out the thermal stability of epoxy reinforced with bamboo husk fibre and powder. It was found that the char yield of epoxy at 700 °C increased by 13.5–52.8% due the addition of 10 wt% of bamboo fibre or powder. Author cited that the increasing in char yield could be an indication of the potency of flame retardation of polymers. Thus, the addition of bamboo fibre or powder enhanced the flame retardation of epoxy. Similar results were obtained by De Rosa et al. (2010). They found an improvement in thermal stability of untreated phormium Tenax fibres/epoxy composites. The presence of plant fibre increased the maximum degradation temperature and the char yield of epoxy resin.

The addition of HNTs to RCF/epoxy composites and its influence on thermal stability can be seen in Fig. 6.3(b) and Table 6.2. The presence of HNTs into RCF/epoxy nanocomposites increases the temperature at (10% and 20%) weight

loss compared to unfilled RCF/epoxy composites. However, at the major degradation, unfilled RCF/epoxy shows better thermal stability that those samples filled with HNTs. The maximum decomposition temperature (T_{max}) of RCF/epoxy nanocomposites is decreased by 8 $_{°C}$ compared to unfilled RCF/epoxy composite. This is due to the catalytic role of HNT tubes on RCF/epoxy nanocomposites. This redaction in thermal stability is also confirmed by measuring the temperature at 50% weight loss ($T_{50\%}$). The addition of HNTs into RCF/epoxy composites reduce the ($T_{50\%}$) by 7–12 °C compared to unfilled RCF/epoxy sample. However, at high temperatures (>400 °C), the presence of HNTs increases the thermal stability of epoxy/RCF nanocomposites by increasing the char yield. The char yields at 700 °C of epoxy/RCF composites reinforced with (0, 1, 3, and 5) wt% HNT are 18.0, 21.6, 19.3, and 21.0%, respectively. This enhancement on thermal properties is due to the presence of HNT nanotubes, which act as barriers and hinder the diffusion of volatile decomposition products out from the nanocomposites (Madaleno et al. 2010; Zhao et al. 2005).

6.3 Organoclay/Cellulose Fibre/Epoxy Eco-Nanocomposites

(a) Thermal stability

The thermal stability of samples was determined using TGA. In this test, the thermal stability was studied in terms of the weight loss as a function of temperature in nitrogen atmosphere. The thermograms of the epoxy/nanoclay and epoxy/nanoclay/RCF nanocomposites are shown in Fig. 6.4a, b, respectively. The char yields at different temperatures are summarized in Table 6.3. It can be seen from TGA curves that epoxy and its nanocomposites exhibit two distinct stages of decomposition. The first stage of decomposition may be related to the vaporization of moisture in the composites. The second stage of decomposition may be related to

Table 6.3 Thermal properties of epoxy, epoxy/RCF, epoxy/clay, and epoxy/RCF/clay samples

Sample	Char yield at different temperature (%)							T_{max} (°C)
	100 °C	200 °C	300 °C	400 °C	500 °C	600 °C	700 °C	
PE	99.86	86.10	85.24	35.26	15.69	13.69	13.08	367.29
PE/30B1	99.01	84.66	83.70	31.89	13.68	11.72	11.16	367.13
PE/30B3	99.13	85.13	83.94	33.02	14.92	13.05	12.49	367.47
PE/30B5	99.40	85.56	84.16	34.58	17.2	15.30	14.72	367.35
PE/RCF	98.65	87.88	85.01	34.58	22.49	20.37	17.96	359.62
PE/RCF/30B1	98.79	89.90	86.04	35.45	25.22	22.93	20.56	352.23
PE/RCF/30B3	97.70	94.29	89.12	32.63	25.51	23.85	20.46	350.97
PE/RCF/30B5	97.42	93.39	87.91	32.92	25.17	23.45	20.71	351.32

degradation of epoxy and its additives. It also can be seen that the major degradation for all samples occurred in range of ~300–400 °C.

From the amounts of residue at low temperature from 100 to 300 °C, the presence of nanoclay slightly increased the rate of sample degradation compared to pure epoxy. But, the maximum decomposition temperature (T_{max}) of the composites remained unchanged after the addition of nanoclay. The maximum decomposition temperature of neat epoxy and epoxy filled with 1, 3, and 5 wt% nanoclay were 367.3, 367.1, 367.5, and 367.4 °C, respectively. However, at higher temperature, nanocomposite with 5 wt% clay loading performed better in thermal stability than neat epoxy with higher char residue of 14.7 wt% at 700 °C. It was reported in previous studies that the addition of nanoclay platelets would efficiently raise the char residue of polymers at high temperature (Madaleno et al. 2010; Ismail et al. 2008; Chatterjee and Islam 2008).

The presence of RCF in epoxy system also accelerates the degradation at low temperature. But at temperature higher than 400 °C, the inclusion of RCF leads to an enhancement in thermal stability by increasing the char yield of epoxy at 700 °C from 13.1 wt% to 18.0 wt%. Shih (2007) carried out the thermal stability of epoxy reinforced with wastewater bamboo husk fibre and found that the char yield of epoxy at 700 °C increased by 13.5–52.8% due the addition of 10 wt% of bamboo fibre. The increase in char yield is an indication of the potency of flame retardation of polymers. Thus, the addition of bamboo fibre enhanced the flame retardation of epoxy. Similar results were obtained by De Rosa and co-workers (Rosa et al. 2010) where they found an improvement in thermal stability of untreated phormium Tenax fibres/epoxy composites. The presence of plant fibre increased the maximum degradation temperature and the char yield of epoxy resin.

The addition of nanoclay to RCF/epoxy composites reduced the maximum decomposition temperature of the composites, which means that the decomposition was accelerated when compared to neat epoxy. This reduction in thermal stability at low temperature is due to the Hofmann elimination reaction, where clay acts as a catalyser towards the degradation of the polymer matrix (Madaleno et al. 2010; Zhao et al. 2005). However, at 600 and 700 °C, the char residues of the RCF filled epoxy nanocomposites are significantly higher than that for pure epoxy and RCF reinforced epoxy composites. This means that, at high temperature, the addition of nanoclay significantly enhances the thermal stability of epoxy/RCF composites. This enhancement on thermal properties is due to the presence of nanoclay, which acted as barriers and hindered the diffusion of volatile decomposition products out from the nanocomposites (Madaleno et al. 2010; Ismail et al. 2008; Yeh et al. 2006).

6.4 Nanoclay/Cellulose Fibre/Vinyl-Ester Eco-Nanocomposites

(a) Thermal Stability and Flammability

Figure 6.5 shows the TGA curves for vinyl-ester, ecocomposites, and eco-nanocomposites. The temperature range used for the analysis was room temperature to 800 °C. For vinyl-ester thermal degradation occurred in a single stage at around 370 °C. Compared with the pure samples, the samples reinforced with RCF sheets showed a slightly higher thermal stability. This is due to the higher and longer thermal resistance of the cellulose fibres. In all composites, the release of moisture led to a slight weight loss between 60 °C and 100 °C. At approximately 230–260 °C, the degradation profile of the composites started according to TGA. Between 270 °C and 480 °C, degradation of the ecocomposites followed relating to constituent decomposition. Continued decomposition was evident from 380 °C until the temperature reached near 500 °C at which point a constant mass was achieved. Eco-nanocomposite thermal stability results followed a similar trend however the temperature required for decomposition were slightly higher (Fig. 10.13). Eco-nanocomposites with 1 wt.%, 3 wt.%, and 5wt% of nanoclay required 387.1 °C, 399.76 °C, and 404.3 °C temperatures, respectively, to start constituent decomposition.

In terms of weight loss, from 60 to 250 °C, ecocomposites gave a percentage mass drop of 1.85% according to TGA analysis. At 350 °C, a 23.3% drop in mass was recorded. However, at the same temperature, the eco-nanocomposites gave about 22.9%, 21.9%, and 18.9% degradation for composites with 1%NC, 3%NC, and
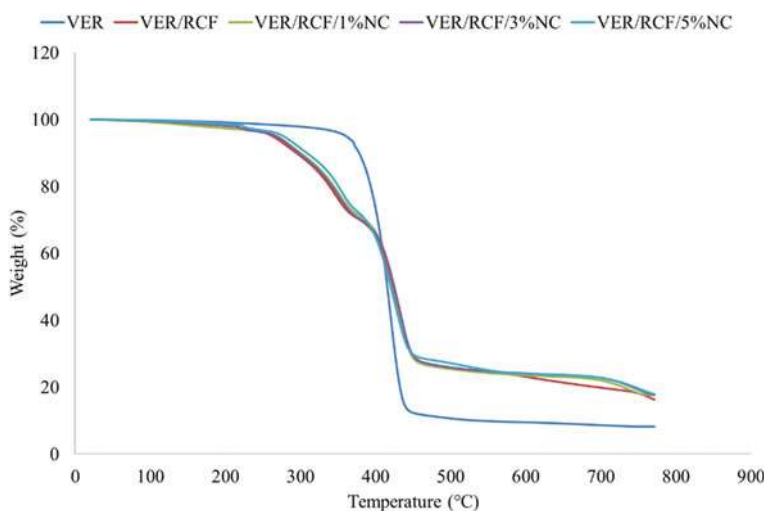

Fig. 6.5 TGA curves of ecocomposite and eco-nanocomposite samples

Table 6.4 Flammability properties of vinyl-ester resin and its composite samples

Sample	Burning out time (s)	Ignition time (s)	fire spreading speed (mm/s)
VER	92	3.2	0.109
VER/RCF	98	3.53	0.097
VER/RCF/1%NC	102	4.03	0.102
VER/RCF/3%NC	104	4.24	0.098
VER/RCF/5%NC	110	4.6	0.091

5% NC, respectively. Above 700 °C, the residual weight of ecocomposites was 16.3% of the original. While the pure samples, only 8.3% remained. For the eco-nanocomposites at 1%NC, 3%NC, and 5% NC, 17.6%, 17.8%, and 18% of the starting weight remained, respectively. The quantities of residual weights were only slightly higher due the addition of the nanoclay silicate.

Flammability tests simulate the realistic fire action and therefore were conducted at ambient conditions. Time of burning out and ignition time were determined and the fire spreading speed was calculated. Pure samples were found to burn out and ignite faster than ecocomposites and eco-nanocomposites as seen in Table 6.4.

As previously described in terms of thermal stability, cellulose fibres provide more favourable thermal properties. Nanoclay addition was found to further reduce the flammability of the composites due to its insulating mechanism and action as a mass transport barrier for volatile products of decomposition (Paul et al. 2003; Vyazovkin et al. 2004). Nanoclay addition also promotes the formation of char which acts as a fire-retardant (Pavlidou and Papaspyrides 2008).

6.5 Halloysite/Cellulose Fibre/Vinyl-Ester Eco-Nanocomposites

(a)   Thermal Stability and Flammability

The TGA curves for vinyl-ester, ecocomposites and eco-nanocomposites are shown in Fig. 6.6 and summarized in Table 6.5. Here, the temperature range used was from room temperature to 800 °C. Thermal degradation, for vinyl-ester, occurred in a single stage at around 430 °C. Across all composites, the release of moisture led to slight weight loss between 60 °C and 100 °C. In ecocomposites, decomposition occurred in two stages with complete degradation occurring at approximately 445 °C. These results also support that the ecocomposites, fibre-filled polymer matrix, decompose at higher temperatures compared to pure samples. The present results agree with previous studies on the thermal properties of lingo-cellulosic fibre composites. The thermal resistance of the cellulose fibres, and the ability of these natural fibres to increase char formation are responsible for the improved thermal stability (Curvelo et al. 2001).

Fig. 6.6 TGA curves of VER, VER/RCF, VER/RCF/1%HNTs, VER/RCF/3HNTs, and VER/RCF/5%HNT samples

Table 6.5 TGA data of pure VER, VER/RCF, and VER/RCF/HNT samples

Sample	Temperature at 50% weight loss (°C)	Temperature at maximum weight loss (°C)	Residual weight (%)
VER	418	430	8.7
VER/RCF	409	445	19.7
VER/RCF/1%HNTs	423	448	23.1
VER/RCF/3%HNTs	429	453	23.6
VER/RCF/5%HNTs	431	460	24.7

For eco-nanocomposites the thermal stability followed a similar trend albeit requiring a marginally higher temperature whereby eco-nanocomposites of 1, 3, and 5 wt% HNTs required 392 °C, 394 °C, and 395 °C, respectively. In terms of weight loss, from 100 to 200 °C, ecocomposites and eco-nanocomposites gave a weight loss of about 2% according to TGA analysis. At 300 °C, in ecocomposites a weight loss of 11.7% was recorded. However, at the same temperature, the eco-nanocomposites gave a weight loss of 11.7, 10.1, and 9.2% for loading of 1, 3, and 5 wt% HNTs, respectively. Above 700 °C, the residual weight of ecocomposites was 19.7% of the original. In contrast, only 8.7% remained in the control sample. For the eco-nanocomposites with 1%, 3%, and 5% HNTs, the residual weight was 23.1%, 23.6%, and 24.7%, respectively.

The improvement of interfacial adhesion between RCF and VER as a result of HNTs addition can lead to the enhancement of thermal stability (Rosa et al. 2011). Nano-fillers such as HNTs are believed to provide, firstly, a thermal barrier which prevents heat transfer inside the polymer matrix, and secondly a mass transport barrier

Table 6.6 Flammability properties of vinyl-ester resin and its composites

Sample	Burning out rate (g/min)	Ignition time (s)	Fire velocity (mm/min)
VER	0.67 ± 0.06	10.8 ± 1.6	31.5 ± 1.7
VER/RCF	0.54 ± 0.03	17.2 ± 1.5	25.7 ± 1.6
VER/RCF/1%HNTs	0.49 ± 0.02	18.7 ± 1.4	23.2 ± 1.2
VER/RCF/3%HNTs	0.46 ± 0.04	22.8 ± 1.2	19.1 ± 1.8
VER/RCF/5%HNTs	0.41 ± 0.05	25.4 ± 1.8	17.5 ± 1.4

which during the process of degradation forms a char which hinders the escape of the volatile products (Du et al. 2006; Rahman et al. 2012). The hollow tubular structure of HNTs is also reported to be another factor that leads to enhanced thermal stability. The hollow tubular structure of HNTs enables the entrapment of degradation products inside the lumens, causing effective delay in mass transfer which leads to improved thermal stability (Ismail et al. 2008; Lecouvet et al. 2011). The presence of iron oxides, Fe_2O_3, in silicate fillers is also a possible flame retardant which serve to enhance the thermal stability of composites by trapping radicals during the process of degradation (Rahman et al. 2012).

Flammability tests conducted at ambient conditions included time of burning out, ignition time, and fire velocity determinations. Pure VER samples were found to burn out and ignite faster than VER/HNT composites as indicated in Table 6.6. Calculations imply that fire spreads through pure VER at nearly twice the rate of 5 wt% VER/HNT composite, thus highlighting the favourable flammability resistance of the composites. Tthe presence of HNTs within composites provides a mechanism of insulation which protects the composites from contacting with fire. Furthermore, char formation of HNTs acts as a heat and fire-retardant.

6.6   Nano-SiC/Cellulose Fibre/Viny-Ester Eco-Nanocomposites

(a)   Thermal Stability and Flammability

The thermal degradation behaviour of VER, ecocomposites, and eco-nanocomposites was investigated using TGA and the results are shown in Fig. 6.7 and summarized in Table 6.7. The results show that thermal degradation of pure VER occurred in a single stage starting at ~260 °C with complete degradation at ~430 °C. However, in all composite samples, the release of moisture has led to a slight weight loss at 60–100 °C. In eco-composite samples, decomposition occurred in two stages with complete degradation occurring at ~445 °C. These results further support that ecocomposites decompose at higher temperatures compared to pure VER. This is due to the thermal resistance of cellulose fibres, and the ability of these natural fibres to increase char formation leading to improved thermal stability (Curvelo
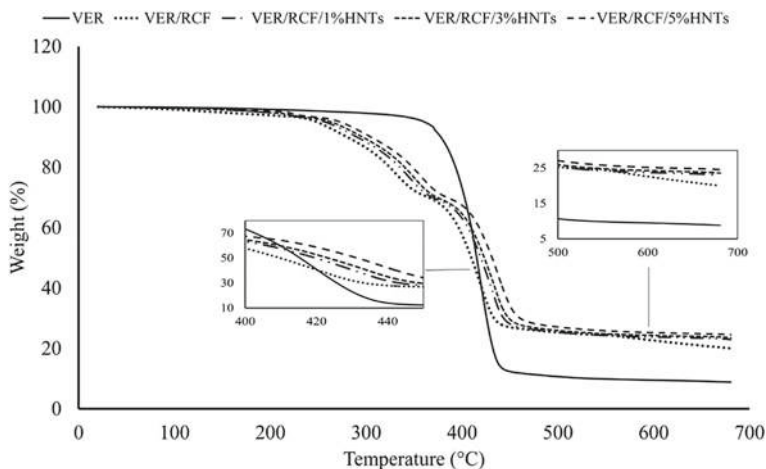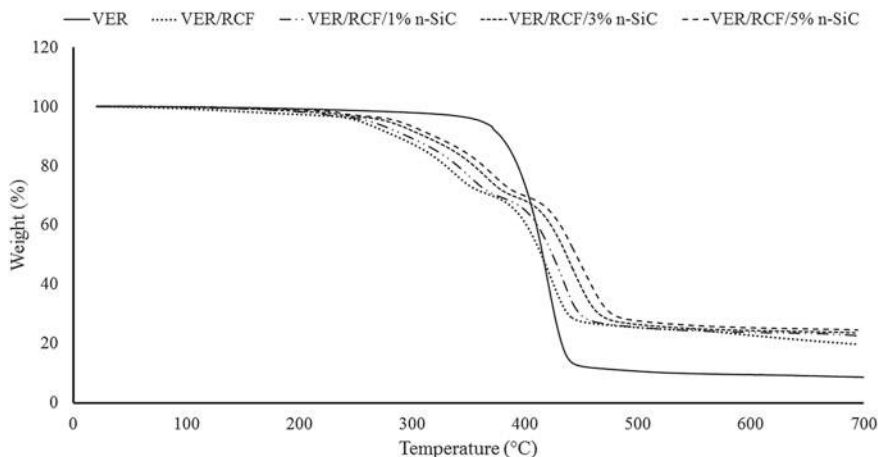
Fig. 6.7 TGA curves of pure VER, VER/RCF, and VER/RCF/n-SiC samples

Table 6.7 TGA data of pure VER, VER/RCF, and VER/RCF/n-SiC samples

Sample	Temperature at 50% weight loss (°C)	Temperature at maximum weight loss (°C)	Residual weight (%)
VER	418	430	8.7
VER/RCF	420	445	19.8
VER/RCF/1%n-SiC	429	456	22.8
VER/RCF/3%n-SiC	441	471	23.7
VER/RCF/5%n-SiC	451	484	24.6

et al. 2001; Alhuthali and Low 2021; Manfredi et al. 2006). These results agree with previous studies on thermal properties of lingo-cellulosic fibre composites (Nassar et al. 2021; Liu et al. 2004). In all ecocomposite samples, thermal depolymerization of hemicellulose, pectin, and cleavage of glycosidic linkages of cellulose are believed to occur at 200–300 °C, and the decomposition of cellulose occurs at 300–370 °C. The decomposition of lignin occurs over a wide range of temperatures, i.e. 200–700 °C because of the aromatic and highly branched structure of lignin (Araújo et al. 2008; Yang et al. 2007).

In a similar manner to ecocomposites, the decomposition of eco-nanocomposites followed the same trend albeit the temperatures required for complete decomposition of the eco-nanocomposites were slightly higher, with 1, 3, and 5 wt% loading of n-SiC showing complete decomposition at 456, 471, and 484 °C, respectively. While the residual weight of the pure sample was only 8.7% of the original, the residual weights of ecocomposites and eco-nanocomposites with 1, 3, and 5 wt% loading of n-SiC were found to be greater with 19.8, 22.8, 23.7, and 24.6% of the starting weight remaining, respectively. Nano-fillers (n-SiC) provide a thermal barrier which

Table 6.8 Flammability characteristics of pure VER, VER/RCF, and VER/RCF/n-SiC samples

Sample	Burning out rate (g/min)	Ignition time (s)	Fire velocity (mm/min)
VER	0.67 ± 0.06	10.8 ± 1.6	31.5 ± 1.7
VER/RCF	0.54 ± 0.02	17.2 ± 1.5	19.7 ± 1.3
VER/RCF/1%n-SiC	0.49 ± 0.02	23.6 ± 1.4	16.3 ± 1.8
VER/RCF/3%n-SiC	0.42 ± 0.05	27.4 ± 1.2	15.2 ± 1.2
VER/RCF/5%n-SiC	0.29 ± 0.06	37.7 ± 1.8	14.4 ± 1.6

prevents heat transfer inside the matrix and a barrier to mass transport by forming a char during the process of degradation. This char formation can hinder the escape of volatile products out of the composites (Leszczyńska et al. 2007). In addition, the improvement of the adhesion between RCF and VER due to the presence of n-SiC can lead to enhanced thermal stability (Curvelo et al. 2001; Yu et al. 2010).

Burning out rate, ignition time, and fire velocity were determined as part of an investigation into the flammability properties of the pure, ecocomposite, and eco-nanocomposite samples. Flammability tests were conducted at room temperature to simulate realistic fire action. Table 6.8 shows that pure VER samples burnt out and ignited faster than the ecocomposite and eco-nanocomposite samples. During flammability test the burning characteristics of the pure, ecocomposites and eco-nanocomposites were clearly different. When the test commenced, pure VER immediately started dripping and continued with fast burning rate, until total loss of material at the end of the test. In contrast, the ecocomposites showed a different behaviour; when the test commenced, the samples maintained a constant flame with much less burning rate, no dripping and at the end of the test became completely charred. The eco-nanocomposites also displayed similar burning characteristics with longer ignition time, no dripping, and slower burning rate.

As previous mentioned, cellulose fibres provide desirable thermal properties. The addition of n-SiC addition, due to its insulating and mass transport barrier capabilities, was found to further reduce the flammability of the composites. The further formation of a fire-retardant char due to addition of n-SiC serves to impart enhanced flammability (Vyazovkin et al. 2004). Char formation has been found to be directly correlated to the potency of flame retardation for polymer composites (Shih 2007). Hence, the use of both RCF and n-SiC has resulted in the observed improved thermal stability and reduced flammability. Similar observations have been reported elsewhere (Ramesh and Anand 2021; Kamble and Behera 2021; Salih 2021; Joshi et al. 2021).

References

Alhuthali A, Low IM (2021) Vinyl-ester composites reinforced with natural fibers and nanofillers. In: Low I-M, Dong Y (eds) Chapter 9 in composite materials. Elsevier, pp 227–244, ISBN 9780128205129

Araújo JR, Waldman WR, De Paoli MA (2008) Thermal properties of high density polyethylene composites with natural fibres: coupling agent effect. Polym Degrad Stab 93(10):1770–1775

Chatterjee A, Islam MA (2008) Fabrication and characterization of TiO_2–epoxy nanocomposite. Mater Sci Eng A 487:574–585

Curvelo AAS, de Carvalho AJF, Agnelli JAM (2001) Thermoplastic starch–cellulosic fibers composites: preliminary results. Carbohyd Polym 45(2):183–188

De Rosa IM, Santulli C, Sarasini F (2010) Mechanical and thermal characterization of epoxy composites reinforced with random and quasi-unidirectional untreated Phormium tenax leaf fibres. Mater Design 31:2397–2405

De Rosa IM, Kenny JM, Maniruzzaman M et al (2011) Effect of chemical treatments on the mechanical and thermal behaviour of okra (Abelmoschus esculentus) fibres. Compos Sci Technol 71(2):246–254

Du M, Guo B, Jia D (2006) Thermal stability and flame retardant effects of halloysite nanotubes on poly(propylene). Eur Polym J 42(6):1362–1369

Ismail H, Pasbakhsh P, Fauzi MNA et al (2008) Morphological, thermal and tensile properties of halloysite nanotubes filled ethylene propylene diene monomer (EPDM) nanocomposites. Polym Testing 27(7):841–850

Joshi A, Mangal SSPR, Bhojak N (2021) Thermal kinetics of ber-phenol formaldehyde composite. AIP Conf Proc 2369:020180. https://doi.org/10.1063/5.0061647

Kamble Z, Behera BK (2021) Mechanical and Thermogravimetric Properties of polypropylene based thermoplastic composites reinforced with cotton and polyester waste under dry and wet conditions. J Nat Fibers. https://doi.org/10.1080/15440478.2021.2002775

Lecouvet B, Gutierrez JG, Sclavons M et al (2011) Structure–property relationships in polyamide 12/halloysite nanotube nanocomposites. Polym Degrad Stab 96(2):226–235

Leszczyńska A, Njuguna J, Pielichowski K et al (2007) Polymer/montmorillonite nanocomposites with improved thermal properties: Part I. Factors influencing thermal stability and mechanisms of thermal stability improvement. Thermochimica Acta 453(2):75–96

Liu W, Mohanty AK, Drzal LT et al (2004) Effects of alkali treatment on the structure, morphology and thermal properties of native grass fibers as reinforcements for polymer matrix composites. J Mater Sci 39(3):1051–1054

Madaleno L, Schjødt-Thomsen J, Pinto JC (2010) Morphology, thermal and mechanical properties of PVC/MMT nanocomposites prepared by solution blending and solution blending + melt compounding. Compos Sci Technol 70:804–814

Manfredi LB, Rodríguez ES, Wladyka-Przybylak M et al (2006) Thermal degradation and fire resistance of unsaturated polyester, modified acrylic resins and their composites with natural fibres. Polym Degrad Stab 91(2):255–261

Nassar MMA, Alzebdeh KI, Pervez T et al (2021) Progress and challenges in sustainability, compatibility, and production of eco-composites: a state-of-art review. J Appl Polym Sci 138:e51284. https://doi.org/10.1002/app.51284

Paul MA, Alexandre M, Degee P et al (2003) New nanocomposite materials based on plasticized poly (L-lactide) and organo-modified montmorillonites: thermal and morphological study. Polymer 44:443–450

Pavlidou S, Papaspyrides CD (2008) A review on polymer–layered silicate nanocomposites. Prog Polym Sci 33:119–1198

Rahman NA, Hassan A, Yahya R et al (2012) Microstructural, thermal, and mechanical properties of injection-molded glass fiber/nanoclay/polypropylene composites. J Reinf Plast Compos 31(4):269–281

Ramesh V, Anand P (2021) Thermal analysis of Kevlar/basalt reinforced hybrid polymer composite. Mater Res Express 8:115302

Salih R (2021) Study of heat and sound insulation for polymeric composites reinforced with nano clay. Polym Polym Compos 29(2):096739112110511

Shih YF (2007) Mechanical and thermal properties of waste water bamboo husk fiber reinforced epoxy composites. Mater Sci Eng, A 445–446:289–295

Vyazovkin S, Dranca I, Fan X et al (2004) Kinetics of the thermal and thermo-oxidative degradation of a polystyrene–clay nanocomposite. Macromol Rapid Commun 25(3):498–503

Yang H, Yan R, Chen H et al (2007) Characteristics of hemicellulose, cellulose and lignin pyrolysis. Fuel 86(12–13):1781–1788

Yeh JM, Huang HY, Chena CL et al (2006) Siloxane-modified epoxy resin–clay nanocomposite coatings with advanced anticorrosive properties prepared by a solution dispersion approach. Surf Coat Technol 200:2753–2763

Yu T, Ren J, Li S et al (2010) Effect of fiber surface-treatments on the properties of poly(lactic acid)/ramie composites. Composites A 41(4):499–505

Zhao C, Qin H, Gong F et al (2005) Mechanical, thermal and flammability properties of polyethylene/clay nanocomposites. Polym Degrad Stab 87:183–189

Chapter 7
Conclusions: Summary and Directions for Future Work

Abstract This chapter provides a summary of the work described in this book and some future work recommendations for this emerging research field on ecocomposites and eco-nanocomposites. Potential applications, challenges, and future directions of these sustainable composites are highlighted and addressed.

Keywords Ecocomposites · Eco-nanocomposites · Cellulose fibres · Nanoclay particles · Nanoclay platelets · Halloysite nanotubes · Nano-SiC · Epoxy resin · Vinyl-ester resin · Microstructure · Water absorption · Water permeability · Mechanical properties · Flexural strength · Porosity · Fracture toughness · Crack-tip · Fibre–matrix adhesion · Thermal stability · Fibre debonding · Fibre pull-outs · Toughening mechanisms and crack-tip failure processes · Cellulose fibres · Nanoclay platelets · Epoxy resin · Vinyl-ester resin · Water uptake · Diffusion · Microstructure · Composites · Mechanical properties · Flexural strength · Impact strength · Fracture toughness · Impact toughness · Thermal stability · Flammability

7.1 Summary on Cellulose Fibre/Epoxy Ecocomposites and Eco-Nanocomposites

(a) Recycled Cellulose Fibre/Epoxy Ecocomposites

- RCF-reinforced epoxy composites with different fibre loadings have been prepared. The mechanical properties and water absorption were investigated as a function of fibre content. In addition, the effect of moisture absorption on the mechanical properties was studied. Results indicated that water absorption of RCF/epoxy composites increased as fibre content increased. The presence of RCF dramatically increased the water content of RCF/epoxy composites when compared to neat epoxy. The increase in water absorption was attributed to the hydrophilic nature of cellulose fibres. The mechanical properties (i.e. flexural strength, flexural modulus, fracture toughness, and impact toughness) also increased as the fibre content increased. In comparison to neat epoxy, addition of about 52 wt% RCF increased flexural strength

(by 160%), flexural modulus (by 760%), impact strength (by 444%), fracture toughness (by 350%), and impact toughness (by 263%). This significant increase in mechanical properties is attributed to the unique properties of cellulose fibres such as ability to withstand bending force and resist fracture force via number of energy absorbing events which include fibre pull-out, fibre fracture, fibre-debonding, crack deflection, and fibre-bridging. These micromechanisms of toughening were clearly observed by SEM on the fracture surface of RCF composites. These toughening mechanisms of RCF were the major factors of increasing fracture properties of samples reinforced with RCF when compared to neat epoxy. In addition, SEM results indicated an increase in energy dissipation events for composites filled with higher fibre content compared to their lower fibre content counterparts. In the case of thermal properties, the presence of RCF sheets accelerated the major degradation of epoxy filled with RCF compared to neat epoxy. This was as a result of reduction in the maximum decomposition temperature (T_{max}) by about 7.7 °C in epoxy filled with RCF as compared to neat epoxy. However, composites reinforced with RCF sheets showed better thermal stability than unfilled epoxy at elevated temperatures ($\geq$600 °C).

- The effect of water absorption on the mechanical properties of RCF-reinforced epoxy composites was investigated and compared to dry composites for a short period (i.e. two weeks) and for a long period (i.e. six months). Exposure to moisture for 2 weeks caused a reduction in flexural strength (by 34.9%), flexural modulus (by 17.1%), and fracture toughness (by 23.9%) in epoxy reinforced with 46 wt% RCF. On the other hand, exposure to moisture for a long time resulted in severe reduction in flexural strength (by 77%), flexural modulus (by 82.7%), and fracture toughness (by 60.8%) for epoxy reinforced with 52 wt% RCF. This significant drop in mechanical properties was attributed to the degradation of bonding at the fibre–matrix interfaces as a result of water absorption. However, impact strength and impact toughness were found to increase after water absorption. The effect of water absorption on the mechanical properties was more pronounced at high fibre content as compared to low fibre content. SEM results showed that water absorption severely damaged the cellulose fibres and degraded the bonding along the fibres–matrix interfaces in wet composites.

(b)   Nano-Filler/Epoxy Nanocomposites

Epoxy nanocomposites reinforced with organoclay platelets (Cloisite 30B), halloysite nanotubes (HNT), and nano-silicon carbide (n-SiC) were fabricated. The effect of nano-filler contents on the morphology, structure, mechanical, thermal, and moisture barrier properties of epoxy nanocomposites was investigated. The effect of moisture absorption on the mechanical properties of these nanocomposites was also studied.

- *Nanoclay/Epoxy Nanocomposites*

A series of nanoclay/epoxy nanocomposites were fabricated with 1, 3, and 5 wt% of organoclay (Cloisite 30B). WAXS results showed an increase in the inter-layer distance between the clay platelets from 1.85 to 3.4 nm indicating that clay/epoxy nanocomposites with intercalated structure had been formed. Based on TEM results, the dispersion of nanoclay was uniform with some particle agglomerations. These particle clusters were found to increase as clay contents increased. Furthermore, TEM results confirmed that the major structure of nanoclay in the epoxy matrix was intercalated with some exfoliated regions. The measured d-spacing ranged from 2.65 to 7.98 nm compared to 1.8 nm of nanoclay platelet.

The presence of nanoclay platelet was found to enhance the mechanical properties (i.e. flexural strength, flexural modulus impact strength, fracture toughness, and impact toughness) of the epoxy resin. For example, the addition of 1 wt% nanoclay increased flexural strength (by 45.6%), flexural modulus (by 87.6%) fracture toughness (by 30%), and impact toughness (by 50%) compared to neat epoxy. However, the addition of more clay did not cause any further increase in these properties. This was attributed to the increase in matrix viscosity and formation of voids as well as poor dispersion of particles at higher clay contents.

With regard to thermal stability, the presence of nanoclay showed no effect on the thermal stability of epoxy resin at low temperatures ($\leq$400 °C). The maximum decomposition temperatures of neat epoxy and its nanocomposites were found to be unchanged. However, the addition of only 5 wt% nanoclay slightly increased the char residue of epoxy at 700 °C.

The fracture surface of neat epoxy and clay/epoxy nanocomposites were investigated by SEM. The fracture surface of epoxy was found to be smooth and featureless, while epoxy filled with nanoclay displayed rougher fracture surface. This indicated the presence of crack pinning mechanisms which increase fracture toughness by increasing crack propagation length during deformation. Other fracture mechanisms such as crack pinning, particle debonding, plastic void growth, plastic deformation, and particle pull-outs were also observed for all types of nano-filler-reinforced epoxy nanocomposites. Such toughness mechanisms can increase the energy dissipated by resisting crack propagation during deformation, which lead to an increase in fracture toughness values. Close observation on SEM images indicated that crack pinning and plastic deformation due to the presence of clay clusters were the dominant toughening mechanisms for nanocomposites filled with nanoclay.

- *HNT/Epoxy Nanocomposites*

A series of epoxy/HNTs nanocomposites were fabricated with different HNT contents (i.e. 1, 3, and 5 wt%). Based on TEM observations, homogeneous dispersion of HNTs with some agglomerations was achieved by mixing the HNTs with the epoxy resin. Particle agglomerations increased as the HNT content increased.

The presence of only 1 wt% HNTs increased flexural strength (by 20.8%), flexural modulus (by 72.8%), fracture toughness (by 56.5%), and impact toughness (by 25.0%) over unmodified epoxy. However, adding more HNTs showed no further

increase in flexural strength and fracture toughness properties due to the poor dispersion of HNTs at higher content. Impact strength and impact toughness were however found to increase as HNTs loading increased to 5 w%. As in the case of nanoclay thermal results, addition of HNTs into epoxy did not influence the maximum decomposition temperatures of epoxy matrix. However, epoxy modified with 3 and 5 wt% HNT loading showed better thermal stability than unmodified epoxy at high temperatures. SEM results showed that epoxy/HNT nanocomposites had a rougher fracture surface as compared to that of neat resin due to the presence of HNTs. Crack pinning and crack bowing were the main toughening mechanisms for nanocomposites filled with HNT.

- *n-SiC/Epoxy Nanocomposites*

Silicon carbide nanoparticles (n-SiC) have been used as reinforcing filler for epoxy matrix. A series of n-SiC/epoxy nanocomposites were made with 1, 3, and 5 wt% of n-SiC. The synchrotron radiation diffraction (SRD) results showed the formation of five sharp narrow diffraction peaks in the epoxy/n-SiC nanocomposites due to the presence of n-SiC particles. TEM results indicated that n-SiC particles were homogeneously dispersed inside the epoxy matrix except for some particle agglomerations, which were clearly seen at higher n-SiC loading due to the increase in matrix viscosity. In general, the inclusion of n-SiC particles led to an increase in most of the mechanical properties. For instance, the incorporation of only 1 wt% n-SiC increased flexural strength (by 21.5%), flexural modulus (by 83.9%), impact strength (by 33.2%), impact toughness (by 25.0%), and fracture toughness (by 89.4%). Impact strength and impact toughness reached their maximum value at 5 wt% n-SiC. Thermal stability of n-SiC/epoxy nanocomposites was determined using TGA and DTA. Results indicated that the addition of 3 and 5 wt% n-SiC accelerated the major degradation of epoxy nanocomposites compared to unfilled epoxy since nanoparticles act as a catalyser in the degradation of polymer matrix. In contrast, epoxy filled with 3 and 5 wt% n-SiC displayed better thermal properties than neat epoxy at temperatures above 500 °C.

SEM observation indicated that the presence of n-SiC particles increased the roughness of the fracture surface of epoxy nanocomposites compared to neat epoxy. Particle agglomerations and voids in micro-scale were observed for epoxy/n-SiC nanocomposites. Samples filled with 5 wt% n-SiC showed an increase in particle agglomerates and voids as compared to samples filled with 1 wt% n-SiC. The existence of micro-voids revealed that plastic deformation of the matrix around the voids and crack pinning due to the presence of these voids were primary toughening mechanisms.

- Role of Water Absorption on Mechanical Properties of Nano-filler/Epoxy Nanocomposites

The role of water absorption on the mechanical properties of nano-filler-reinforced epoxy nanocomposites was investigated and compared to dry nanocomposites. Results indicated that, compared to dry nanocomposites, flexural strength, and

modulus of all types of nanocomposites decreased due to the plasticization effect of the water uptake. However, fracture toughness and impact strength were found to increase after water absorption due to increased ductility of the epoxy matrix.

The influence of the nano-fillers such as nanoclay platelets, HNTs, and n-SiC on enhancing the mechanical and barrier properties of epoxy-based nanocomposites in wet condition was investigated in terms of water absorption behaviour, flexural strength, flexural modulus, fracture toughness, and impact strength. Results indicated that, as compared to unfilled epoxy, the incorporation of nano-fillers into epoxy matrix led to significant reduction in both water uptake and diffusion coefficients (D). This reduction was attributed to the tortuosity path created by the addition of the nano-fillers. Addition of nanoclay, HNT, and n-SiC particles improved the mechanical properties of the nanocomposites after being exposed to water compared to neat epoxy under similar condition. Reinforcement with 1 wt% nano-filler showed better mechanical properties than other filler content. Enhanced barrier and mechanical properties of nanocomposites were more pronounced for composites filled with n-SiC as compared to those filled with nanoclay platelets and HNTs.

(c)   **Nano-Filler/RCF/Epoxy Eco-Nanocomposites**

A new class of epoxy eco-nanocomposites reinforced with nano-sized particles (i.e. nanoclay platelets, HNTs or n-SiC) and recycled cellulose-fibre sheets were successfully fabricated and investigated. The effects of these nano-fillers on the mechanical and thermal properties are summarized below.

• **Nanoclay/RCF/Epoxy Eco-Nanocomposites**

The addition of nanoclay to RCF/epoxy composites showed no significant increase in flexural strength, flexural modulus, and fracture toughness. In fact, addition of more than 1 wt% of clay led to a reduction in flexural strength as compared to unfilled RCF/epoxy composites. Flexural modulus and fracture toughness showed maximum values at 5 wt% nanoclay loading. For impact properties, the presence of 1% nanoclay significantly increased impact strength and impact toughness by 14.5% and 48.3%, respectively, compared to RCF/epoxy composites. Adding more clay led to reduction in both impact strength and toughness.

Based on TGA results, the addition of nanoclay to RCF/epoxy composites increased the rate of decomposition by decreasing (T_{max}) by about 9 °C as compared to unfilled RCF/epoxy composites. However, the char residues at 700 °C of the RCF filled epoxy increased by 3.0% due to the presence of nanoclay.

• **HNT/RCF/Epoxy Eco-Nanocomposites**

The addition of HNTs to RCF/epoxy composites was found to slightly increase flexural strength, flexural modulus and fracture toughness. The optimum values of flexural strength and fracture toughness were obtained at 1 wt% HNTs, while the optimum of flexural modulus was obtained at 5 wt% HNTs. On the other hand, the addition of HNTs to RCF/epoxy composites led to a reduction in impact strength.

However, the presence of HNTs gradually increased impact toughness of RCF/epoxy composites with maximum enhancement reaching up to 27.6% at 5 wt% filler content.

TGA results showed that the addition of HNTs increased the thermal stability of RCF/epoxy composites at temperatures between 200 and 300 °C and between 500 and 700 °C. However, the presence of HNTs led to reduction in thermal stability at temperatures between 300 and 400 °C, where the major decomposition occurred.

- Nano-SiC/RCF/Epoxy Eco-Nanocomposites

The incorporation of n-SiC to RCF/epoxy composites were found to increase flexural modulus, impact strength, fracture toughness, and impact toughness compared to unfilled RCF/epoxy samples. Flexural strength increased after the addition of only 1 wt% n-SiC. However, increased addition of SiC caused a reduction in flexural strength. In comparison to unfilled RCF/epoxy composites, the addition of 5 wt% n-SiC displayed optimum increase in facture toughness (by 10.4%), impact strength (by 21.2%), and impact toughness (by 41.4%). In general, RCF/epoxy eco-nanocomposites filled with n-SiC displayed better mechanical properties than same composites filled with either HNTs or nanoclay.

The addition of n-SiC to RCF/epoxy composites was found to increase the thermal stability by increasing the char yield of composites at high temperatures. However, the rate of degradation increased after adding n-SiC to RCF/epoxy composites due to decreased maximum decomposition temperatures by about 8 °C. The reduction in thermal stability at low temperatures is due to the Hofmann elimination reaction, where nano-fillers act as a catalyser toward the degradation of the polymer matrix. However, at high temperatures, nano-fillers acted as insulators to the heat as well as barriers and hindered the diffusion of volatile decomposition products out from the nanocomposites resulting in an increase in thermal stability.

- Water Absorption Behaviour of n-SiC/RCF/Epoxy Eco-Nanocomposites

The role of water absorption on the mechanical properties of n-SiC filled RCF/epoxy eco-nanocomposites was studied. The influence of n-SiC particles on enhancing the mechanical and barrier properties of RCF/epoxy composites in wet condition was investigated. Results indicated that maximum water uptake of n-SiC filled RCF/epoxy eco-nanocomposites decreased with increasing n-SiC contents due to enhancement in composite barrier properties. Maximum reduction in water uptake and diffusivity occurred at 5 wt% n-SiC loading.

In comparison to dry eco-nanocomposites, exposing to water for 6 months was found to severely reduce flexural strength, flexural modulus, and fracture toughness of n-SiC filled RCF/epoxy eco-nanocomposites. For example, significant drop in flexural strength by 73.3%, flexural modulus by 81.5%, and fracture toughness by 62.41% for composites filled with 5 wt% n-SiC compared to same composites in dry condition. This reduction was attributed to the degradation of bonding at the fibre–matrix interfaces and to the damage in the fibre strength and structure.

The role of n-SiC on enhancing the mechanical properties of RCF/epoxy composites in wet condition was investigated. In general, the addition of n-SiC was found

to increase the flexural strength, modulus, and fracture toughness of RCF/epoxy composites after water treatment. The addition of only 5 wt% n-SiC increased flexural strength by 14.4 %, flexural modulus by 7.5%, and fracture toughness by 6.1% over unfilled RCF/epoxy composites. The increase in these mechanical properties is due to the ability of n-SiC in enhancing the fibre–matrix interfacial bonding and increasing the crack propagation resistance by introducing toughness mechanisms such as crack pinning, crack bridging, and particle debonding. On the other hand, the presence of n-SiC particles was found to decrease the impact strength of water-treated composites. SEM results showed clean pull out of cellulose fibres as a result of degradation in fibre–matrix interfacial bonding by water absorption. The presence of nano-filler was found to enhance the adhesion between the fibre and the matrix.

Finally, it can be concluded that epoxy matrix modified with n-SiC particles displayed better mechanical, thermal, and barrier properties than those filled with nanoclay platelets and HNTs.

7.2   Summary on Cellulose Fibre/Vinyl-Ester Ecocomposites and Eco-Nanocomposites

RCF-reinforced polymer composites were prepared with a range of fibre contents (0–50 wt.%). A new infiltration method was used for the development of natural fibre-reinforced polymer composites, which involved very thin sheets of RCF being fully soaked in vinyl-ester resin. This method led to the development of composite materials with lower voids content and good fibre–matrix adhesion. The composites produced were investigated to identify and assess the effect of fibre reinforcement and water uptake on elastic modulus, flexural strength, impact strength, and fracture toughness of the VER/RCF composites. The effect of varying fibre content on water absorption behaviours was also investigated, and it was found that moisture uptake increased with fibre volume fraction. This positive relationship was attributed to the increased cellulose-fibre content and specifically the presence of hydroxyl groups on the natural fibres causing the fibres to be hydrophilic. At room temperature, maximum water uptake for VER, and its composites, immersed for 2,500 h was 0.76, 6.52, 9.56, 12.37, and 14.62%, respectively.

The elastic modulus was found to increase with fibre volume fraction with the addition of 20, 30, 40, and 50 wt.% RCF corresponding to 0.16, 0.24, 0.33, and 0.43 fibre volume fractions, increased elastic modulus by 49, 76, 114, and 143%, respectively. Elastic modulus improvement is attributed to the higher initial modulus of the cellulose fibres acting as backbones in the composites. Typical mathematical models for prediction were used to model composite elastic modulus, and results revealed consistency between experimental data and prediction data obtained using the Cox–Krenchel model.

Flexural strength increased with fibre content with the addition of 20, 30, 40, and 50 wt.% RCF leading to 173.7, 216.5, 254.2, and 295.7% increases, respectively. These enhancements were attributed to a reinforcing effect caused by the high strength and modulus cellulose fibres as well as the ability of the fibres to resist bending force. Impact strength increased significantly with fibre content with the addition of 20, 30, 40, and 50 wt.% RCF increasing impact strength by 312, 440, 656, and 1048%, respectively. This enhancement in impact strength is believed to be due to the ability of the cellulose fibres to transfer impact stress using energy dissipation mechanisms, primarily fibre pull-out, fibre fracture, and matrix deformation.

Fracture toughness increased with fibre content with 20, 30, 40, and 50 wt.% RCF increasing fracture toughness by 35, 113, 153, and 231%, respectively. This improvement in fracture toughness was attributed to enhanced crack deflection, energy dissipation, and fracture resistance properties provided when cellulose fibres interact with the VER matrix. High RCF content provided enhanced fracture toughness attributable to the energy dissipation mechanisms of increased fibre pull-out, fibre fracture, and fibre-bridging. Concerning thermal properties, ecocomposites were found to decompose at higher temperatures than pure samples. TGA data revealed that above 700 °C, the residual weight of ecocomposites was 19.7% of the original, whereas for pure VER only 8.7% remained. The thermal resistance of the cellulose fibres and the ability of these natural fibres to increase char formation are believed to be principal factors leading to enhanced thermal stability.

On exposure to water (2500 h), the elastic modulus, flexural strength, impact strength and toughness of all composites were dramatically reduced. For example, composites reinforced with 50 wt% RCF, exposure to moisture resulted in a 15% reduction in elastic modulus, a 27% reduction in flexural strength, a 25% reduction in impact strength, and a 9% reduction in fracture toughness compared to the corresponding dry samples. This drop in mechanical properties was attributed to the degradation of bonding at the fibre–matrix interfaces due to the effect of water absorption. At high fibre content, the adverse effect of water absorption on mechanical properties was more pronounced. SEM micrographs evidenced severe damage of cellulose fibres and degradation of bonding along fibre–matrix interfaces in wet composites. In addition, prior to exposure to water, SEM micrographs indicated almost no fibre pull-out and that fibres had broken off near surfaces. The observation is indicative of strong bonding between the fibres and the matrix materials. In contrast, after exposure to water, increased fibre pull-out was clearly observable, in SEM micrographs, suggestive of poor fibre/matrix bonding due to the effect of water absorption.

- Vinyl-Ester Nanocomposites

Vinyl-ester nanocomposites reinforced with HNTs and n-SiC were fabricated. The effect of nano-filler addition on the morphology, structure, water absorption, fracture, mechanical, thermal, and flammability properties of vinyl-ester nanocomposites was investigated.

- HNT/Vinyl-Ester Nanocomposites

Pure VER and VER/HNTs composites were fabricated. The latter were prepared by dispersion of HNTs at 1%, 3%, and 5wt.%. To remove pre-existing moisture, the HNTs were dried for 60 min at 150 °C. The HNTs were then mixed with the VER by high-speed electrical mixer (1200 rpm) for 30 min.

Despite polymeric nanocomposite development and characterization often featuring in scientific publications, the field of study on HNT nanocomposites is yet to contain an in-depth repository concerning the addition of HNTs in vinyl-ester. Therefore, an aim of study was to gather and present information concerning vinyl-ester/HNT nanocomposite development and characterisation, and specifically, the effect of HNT addition on water absorption, fracture, mechanical, thermal, and flammability properties of vinyl-ester filled by HNTs.

XRD results confirmed intercalation of the HNTs by chains of VER. For example, the d-space of the peak (001) of pure HNT increased from 0.721 to 0.745 nm for the 1wt.% VER/HNT. This result was believed to a confirmation of the successful formation of nanocomposites. TEM micrographs suggest HNTs have a length ranging from 500 nm to 3 μm with averages for HNTs outer diameters ranging from 100 to 300 nm and averages for inner diameters ranging between 50 and 150 nm. The aspect ratio of HNTs varies between 3 and 15. Though different-sized HNTs particle clusters can be found, the extent of dispersion is acceptable. HNTs were generally well dispersed in the matrix with short inter-tube distances resulting in the formation of HNT-rich regions, and in contrast, long inter-tube distances resulting in the formation of VER-rich regions.

Concerning water uptake, the most favourable reduction was demonstrated by the 5 wt.% VER/HNTs composites. Compared to pure VER, 1 wt.%, and 3 wt.%, the 5wt.% composites, on weight gain and FTIR tests, gave the best results. The high aspect ratio of the HNTs is believed to underpin the favourable reduction in water uptake demonstrated by these composites. The presence of HNTs forces water molecules to alter their path from direct-fast polymer matrix diffusion to a tortuous path. This maze-like path effectively decreases the overall uptake of water molecules.

The addition of HNTs also improved toughness. Enhanced toughness values for all VER/HNT composites samples were observed on the addition of HNTs. From 1.81 MPa.m$^{1/2}$ for pure VER, fracture toughness increased to 2.12 MPa.m$^{1/2}$, 2.43 MPa.m$^{1/2}$, and 2.64 MPa.m$^{1/2}$ for 1wt.%, 3wt.%, and 5wt.% VER/HNTs, respectively. Similarly, from 1.52 kJ/m^2 for unfilled VER, the addition of HNTs at 1, 3, and 5 wt.% increased the impact toughness to 2.93, 3.34, and 4.14 kJ/m^2, respectively. Crack bridging and plastic deformation around HNTs clusters were believed to be the mechanisms underpinning enhancement in toughness. An increase in fracture toughness was also attributed to the interaction of clusters of HNTs and cracks. This interaction was believed to effectively resisting crack advancement.

SEM micrographs of pure VER surfaces revealed flatness and smoothness notwithstanding this presence of river line markings near crack initiation sites. These river line markings suggested typical brittle fracture behaviour and thereby provided an explanation for the low fracture toughness of VER. This roughness at the surface

is believed to be an indicator of the quantity of energy dissipated during fracture. VER/HNT composite micrographs depicted increasing fracture surface roughness with increasing HNTs content. The fracture surfaces are rougher and the crack bifurcation more evident among the samples with greater HNTs content. These visual features suggest crack path pinning due to the rigid HNTs which are believed to hinder crack propagation.

HNTs addition enhanced flexural modulus. After increasing the HNTs content to 1, 3, and 5 wt%, flexural modulus increased from 2.90 GPa for pure VER, to 3.11, 3.31, and 3.46 GPa, respectively. HNTs addition also increased both flexural strength and impact strength albeit moderately. From 42 MPa for pure VER, reinforcement with 1, 3, and 5 wt% HNTs, increased flexural strength to 45.9, 51.1, and 56.5 MPa, respectively. Similarly, the addition of HNTs at 1, 3, and 5 wt% increased impact strength, from 2.60 kJ/m^2 for pure VER, to 3.32, 4.15. and 4.45 kJ/m^2, respectively.

The significant enhancements in flexural modulus of the VER/HNT nanocomposites, compared to the pure VER samples, are believed to be due the higher initial elastic modulus of HNTs (30 GPa) compared to the VER (2.90 GPa). By virtue of the rule-of-mixtures, VER/HNT composites thereby demonstrated improved elastic modulus. Strength property enhancements for the VER/HNTs composites are believed to be due to the HNT particles large aspect ratio, good adhesion between HNTs particles and VER, good degree of dispersion, and suitable extent of inter-tubular interaction in composites as supported by SEM, TEM, and XRD investigations.

The aspect ratio of particles, dispersion of particles within the matrix, and state of adhesion between particles and matrix were found to be each influential to the elastic modulus of the particulate reinforced composites fabricated in this study. This conclusion was supported by agreement of the experimental data with Paul model and Guth model.

A positive relationship existed between HNT additions and enhanced thermal properties. TGA curve data reveals that for a temperature range from room temperature to 800 °C, the VER, and all composites demonstrated single-stage thermal degradation. Pure VER displayed degradation at approximately 385 °C. Samples with 1 wt.%, 3 wt.%, and 5 wt.% HNTs started degradation at ~406 °C, 418 °C, and 422 °C, respectively, thus demonstrating slightly higher thermal stability. Sample decomposition continued until temperatures rose above 500 °C at which point a constant mass was achieved. Above 700 °C, the residual weight for pure VER was 8.2 wt.% whereas samples modified with 1 wt.%, 3 wt%, and 5 wt.% HNTs, at the same temperature, had residual weights of 10 wt%, 10.8 wt%, and 12.8 wt.%, respectively. Calculations imply that the burning rate of pure VER at nearly twice the rate of 5 wt.% VER/HNTs composite, thus highlighting the favourable flammability resistance properties of the composites. The good thermal stability and flame-retardant effects of HNTs are resulted from the HNTs hollow tubular structure, provision of thermal and mass transport barriers and presence of iron in HNTs.

- Nano-SiC/Vinyl-Ester Nanocomposites

VER/n-SiC composites were prepared at 1, 3, 5, and 10 wt. % using high-speed mechanical stirring. In particular, particle dispersion and particle/matrix interaction were investigated concerning their effects on the resulting mechanical and fracture properties of these nanocomposites.

The addition of n-SiC increased the elastic modulus and strength of the resulting materials. For example, compared with pure VER (2.9 GPa and 42.4 MPa), the elastic modulus and strength of VER/1 wt.% n-SiC were greater (3.05 GPa and 54.9 MPa), respectively. Similarly, the nanocomposites reinforced with 3 wt% n-SiC particles had favourable elastic modulus and strength (3.11 GPa and 59.1 MPa), respectively. The greatest increase in elastic modulus and strength was observed at 5 wt.% n-SiC (3.17 GPa and 67.2 MPa), respectively. At 10 wt.%, no further improvement in elastic modulus was observed (3.2 GPa) and the strength decreased at this concentration (63.2 MPa). Concerning impact strength, the results were similar. For neat VER, impact strength was 2.6 kJ/m2. While increasing n-SiC content increase impact strength to a point, (at 5 wt.% impact strength was 3.9 kJ/m^2), there was no further improvement in impact strength at 10 wt% (3.67 kJ/m^2).

By virtue of the rule of mixtures, the higher initial elastic modulus of n-SiC, compared to VER, meant that an improved elastic modulus was obtained for the resulting nanocomposites. Good interfacial adhesion and a good degree of dispersion enhanced the strength of the nanocomposites content 1, 3, and 5 wt. %, whereas agglomeration of nanoparticles at 10 wt.% forming clusters of n-SiC (as confirmed with SEM and TEM micrographs) decreased elastic modulus and strength. SEM micrographs of the VER/n-SiC fracture surfaces revealed no obvious voids at the particle/matrix interface. This is indicative of an absence of n-SiC pull-out from the polymer matrix supporting strong interaction between the n-SiC and VER matrix. Also supportive of generally uniform dispersion of n-SiC throughout the matrix is the absence of n-SiC agglomeration throughout the nanocomposite.

Concerning toughness, n-SiC addition led to lower fracture toughness and lower impact toughness. For example, while fracture toughness for pure VER was 1.81 MPa.m$^{1/2}$, addition of 1 wt.% reduced it to 1.62, and addition of 10 wt.% of n-SiC reduced it even more dramatically to 1.15 MPa.m$^{1/2}$. Similarly, while impact toughness for pure VER was 1.52 kJ/m^2, addition of 1 and 10 wt.% of n-SiC reduced to impact toughness to 1.33–1.13 kJ/m^2, respectively. Addition of stiff n-SiC is believed to hinder the mobility of surrounding chains in the polymer, consequently limiting the stress relief provided by plastic deformations. Strong filler/matrix interaction further hinders matrix component mobility. Strong fibre/matrix adhesion may also have prevented effective debonding of n-SiC particles from the VER matrix, thus reducing energy dissipation. Therefore, the reduction of toughness is most likely attributed to reduced plastic deformation and the prevention of particle debonding.

The experimental data consistent with that of both the Guth and the Kerner model suggested good dispersion within the matrix and good interfacial adhesion were both relevant to the prediction of elastic modulus of particulate reinforced composites.

- Vinyl-Ester Eco-Nanocomposites

A novel two-step approach was used to synthesize eco-nanocomposites. The first step was the dispersion of nano-fillers such as nanoclay platelets, HNTs and silicon carbide (n-SiC) into VER matrices to prepare nano-mixtures. The second step was the reinforcement of these nano-mixtures with sheets of RCF. The effects of these RCF/nano-fillers on the physical, water absorption, mechanical, thermal, and flammability properties are investigated.

- **Vinyl-Ester/RCF/Nanoclay Eco-Nanocomposites**

Nanoclay effectively decreased the water uptake in eco-nanocomposites. The addition of 5wt.% nanoclay provided substantial water absorption resistance to composites as evidenced by weight gain study and FTIR analysis.

Strength properties were also enhanced. The addition of 1 wt.%, 3 wt.% nanoclay showed 38.43% and 41.42% respective increase in flexural strength. The addition of 1 wt.% and 3 wt.% nanoclay gave impact strength results of 17.9 kJ/m^2 and 20.0 kJ/m^2, respectively. The addition of 5 wt.% nanoclay did not give further enhancement in flexural and impact strength properties. The reinforcing effect of RCF and nanoclay, and the improvement of fibre–matrix adhesion on nanoclay addition give greater strength properties to eco-nanocomposites. The SEM micrographs displayed fibres pull-outs from the matrix. The disparity in the length of fibres, the fibre surfaces, and matrix–fibre gaps is apparent in each of the composites. The pull-out lengths were greater for in the unfilled composites when compared to those of the filled composites. The number of fibres pulled out was also greater in the unmodified sample. This phenomenon is a result of poor fibre/matrix adhesion. The fibre surfaces in unmodified ecocomposite appear clean. This suggests poor adhesion with matrix materials failing to adhere to fibres. In contrast, the modified eco-nanocomposite fibres surfaces are rough indicating better adhesion between the fibres and the matrix materials. Finally, the matrix–fibre gaps appear larger in the unmodified composites compared to the small gaps of the modified composites. The fracture surface images are indicative of nanoclay addition's positive effect on matrix–fibre adhesion.

Processing events are believed to underpin the failure of 5 wt.% nanoclay addition further enhancing strength properties. At higher clay content, viscosity increases during mixing of resin. This renders degassing insufficient before curing leading to void formation. Ultimately, specimen failure occurs at even on exposure to very low strains. Moreover, highly viscous mixtures can cause reduction in wettability, interfacial adhesion between matrix and fibres are more likely further reducing the material strength.

Concerning flexural modulus, there was good agreement between the experimental data and predictive calculations. Flexural modulus was found to increase with the weight content of nanoclay up to a point. The 5% nanoclay specimens with high void content featured reduced flexural modulus.

The presence of cellulose fibre was found to increase the toughness properties of all composites compared to pure VER. However, nanoclay addition resulted in samples which were brittle due to the nanoclay's effect on the fibre–matrix adhesion limiting

the mechanisms of fibre pull-out and fibre debonding. Therefore, the toughness properties of the eco-nanocomposites were lower than those of the ecocomposites.

The eco-nanocomposites were found to have superior thermal properties. Both thermal stability and flammability results for the eco-nanocomposites were preferable to those of the ecocomposites or pure samples. The temperature required for decomposition for eco-nanocomposites with 1 wt.%, 3 wt.%, and 5wt% of nanoclay was 387.1 °C, 399.76 °C, and 404.3 °C temperatures, respectively. For the ecocomposites, constituent decomposition started at a lower temperature (380 °C). The superior thermal properties are believed to arise from the insulating mechanism of nanoclay and the fact that the nanoclay acts as a mass transport barrier for volatile products of decomposition features. Nanoclay addition also promotes the formation of char which acts as a fire-retardant.

- Vinyl-Ester/RCF/HNT Eco-Nanocomposites

The greatest resistance to water absorption was achieved in the 5 wt.% HNTs samples. The addition of 5 wt% HNTs reduced water absorption of unfiled ecocomposites from 12.83% to 9.58%. It is believed that HNTs, as nano-fillers, interfere with the transfer paths of the water molecules transforming the original path of direct-fast polymer matrix diffusion into a torturous path reducing overall uptake of water.

Compared unfilled ecocomposites (4.82 GPa), eco-nanocomposites reinforced with 1, 3, and 5wt% of HNTs exhibited enhancements in elastic moduli of 5.11, 5.75, and 5.24 GPa, respectively. A moderate increase in flexural strength and impact strength was demonstrated on HNT addition. Reinforcement with 1, 3, and 5 wt.% HNTs, increased flexural strength from 148.4 MPa for unfilled ecocomposites, to 156.1, 161.2, and 150.2 MPa, respectively. Similarly, impact strength increased to 16.8, 18.9, and 16.1 kJ/m^2, respectively, for 1, 3, and 5 wt.% eco-nanocomposites. The reinforcing effect of RCF and HNTs as well as HNT addition improved fibre-matrix adhesion in eco-nanocomposites are believed to the determinants underpinning the observed enhancements in elastic modulus and strengths properties.

The presence of cellulose fibres increased the fracture toughness of all composites. This enhancement in fracture toughness is attributed to the toughness mechanism provided by cellulose fibres. While HNTs addition improves in fibre–matrix adhesion leading to increased eco-nanocomposites strength properties, as previously described, these improvements in fibre–matrix adhesion make the eco-nanocomposites brittle and prevent fibre pull-outs and fibre de-bonding. As these are major energy absorption mechanisms of the material, prevention of their action causes the composite to become brittle, and thereby, without mechanisms to absorb energy, the toughness properties of the eco-nanocomposites are reduced.

HNT addition increased thermal stability and fire-resisting properties of the eco-nanocomposites. Nano-fillers such as HNTs are believed to provide, firstly, a thermal barrier which prevents heat transfer inside the polymer matrix, and, secondly, a mass transport barrier which during the process of degradation forms a char which hinders the escape of the volatile products. The hollow tubular structure of HNTs is also reported to lead to enhanced thermal stability by enabling the entrapment

of degradation products inside the lumens, causing effective delay in mass transfer leading to improved thermal stability. The presence of iron oxides, Fe_2O_3, in silicate fillers is believed to be flame-retardant enhancing thermal stability of composites by trapping radicals during the process of degradation. The dominant reasons for the reduction in flammability of VER/HNT composites are believed to the barrier effects of HNTs and the char formation caused by HNTs. These mechanisms each provide insulation for the composites and act as heat and fire-retardants.

- Vinyl-Ester/RCF/n-SiC Eco-Nanocomposites

The addition of n-SiC reduced the porosity and the water uptake. The presence of n-SiC was found to enhance the elastic moduli of the samples. While the elastic modulus of the unfilled ecocomposites was 4.8 GPa, the addition of 1, 3, and 5 wt% of n-SiC increased elastic moduli to 5.8, 6.2, and 6.9 GPa, respectively. The n-SiC used in this study, as other nano-fillers, has a high specific surface area, which is believed to provide dense interfacial interaction with polymer matrix. The presence of n-SiC is believed to affect the mobility of surrounding chains in the polymer matrix which leads to increased matrix stiffness. Another reason believed to lead to increased matrix stiffness is the very high initial elastic modulus of the n-SiC (470 GPa) compared to that of pure VER (2.9 GPa) and the VER/RCF ecocomposites (4.8 GPa). By virtue of the rule of mixtures, this high initial elastic modulus is believed to also contribute to the increased elastic modulus of each the eco-nanocomposites observed in this study. These two effects of n-SiC are believed to contribute to the overall stiffness of the composite.

Flexural strength and impact strength of the samples was also increased on the addition of n-SiC. While the flexural strength of unfilled ecocomposites was 148.4 MPa, 1, 3, and 5 wt.% n-SiC addition gave eco-nanocomposites with flexural strengths of 173.1, 176.1, and 179.4 MPa, respectively. The addition of 1, 3, and 5 wt% of n-SiC also increased the impact strength of the samples from 15.9 kJ/m^2 for unfilled ecocomposite to 21.8, 24.6, and 27.4 kJ/m^2, respectively, for the eco-nanocomposites. These results support the belief that fibre–matrix adhesion is an important determinant of composite quality.

Improvement of fibre–matrix adhesion is confirmed by SEM micrographs. The pull-out lengths and the number of pull-outs appear notably greater in the ecocomposites when compared to eco-nanocomposites. This supports the notion that the strength of interfacial adhesion is stronger in eco-nanocomposites compared to ecocomposites. The improvements in interfacial adhesion for eco-nanocomposites may be explained by the notion of thermal expansion mismatch. Stress can develop at the interface between matrix and filler of composite materials as a result of thermal expansion mismatch. Due to the presence of lower thermal expansion fillers (RCF and n-SiC) extra compressive stresses can be induced at the filler/VER interfaces which serve to improve the interfacial adhesion.

In addition, the high specific surface area and high surface energy of n-SiC due to its nano-sized dimension can facilitate rapid phase interactions within the polymer matrix. Therefore, RCF–VER interfacial adhesion can be improved. Furthermore,

n-SiC provides strong electrostatic attractive forces at the fibre–matrix interfaces serving to impart additional adhesion between the fibres and the matrix.

The fracture toughness and impact toughness of ecocomposites and eco-nanocomposites were significantly enhanced when compared to the control. The favourable toughness mechanisms that natural fibre–polymer composites provide such as crack deflection, debonding between fibre and matrix, the pull-out effect, and a fibre-bridging are believed to underpin these significant improvements. However, n-SiC addition resulted in reduced fracture toughness. The addition of 5 wt% n-SiC reduced the fracture toughness from 4.4 to 2.5 MPa.m$^{1/2}$ and the impact toughness from 42.3 to 23.1 kJ/m^2. The addition of n-SiC, as mentioned, resulted in strength improvements by virtue of enhanced interfacial adhesion. However, fibre–matrix adhesion enhancement causes the eco-nanocomposites to become more brittle inhibiting fibre debonding and fibre pull-out and ultimately leading to lower fracture toughness.

The fracture toughness of eco-nanocomposites was lower than ecocomposites. Notwithstanding this, the eco-nanocomposites showed better thermal stability and flammability by virtue of improved mass and heat barriers and the enhanced fibre–matrix interfacial adhesion provided by *n*-SiC.

7.3   Future Work Recommendations and Future Directions

The development of eco-friendly environmental and sustainable materials having high mechanical and fracture performances is imperative in the global quest for the minimization of greenhouse gas emission. In this regard, the recommendations for future work in these ecocomposites and eco-nanocomposites are detailed below.

(a)   RCF/Epoxy Ecocomposites and Eco-Nanocomposites

The role of recycled cellulose-fibre sheets, nano-fillers (i.e. nanoclay platelets, HNTs, and n-SiC) and both recycled cellulose-fibre and nano-fillers dispersion on the microstructure, mechanical, thermal, and barrier properties of epoxy resin was investigated and discussed. The research results provided a fundamental knowledge on the mechanism and performance of a new class of polymer eco-nanocomposites reinforced with nano-fillers and recycled cellulose fibres. Despite the significant improvement in mechanical properties for both RCF/epoxy composites and nano-filler reinforced epoxy nanocomposites, a very limited and slight improvement was achieved for nano-fillers filled RCF/epoxy eco-nanocomposites when compared to unfilled RCF/epoxy composites. This leaves a wide scope for future investigators to make further advances in new materials design and processing. Thus, some recommendations for further research are as follows:

1.   In this work no chemical or physical treatment has been used for cellulose fibres. Therefore, the use of coupling agents to improve fibre/epoxy interfacial bonding could be considered.

2. The dispersion of the nano-fillers in this work was homogenous with some particle agglomerations with the use of only high-speed mixture for 10 min. However, to get perfect dispersion for nano-fillers in polymer matrices is still challenge. Therefore, different methods and techniques as well as treatments are required to be investigated deeply to improve the nano-filler dispersion.

3. Advanced models are required to investigate the influence of nanostructures, such as shape and size distribution, orientation, aspect ratio, degree of spatial, and interfaces on the physico-mechanical properties of eco-nanocomposites. Multi-scale mechanics models and numerical methods should be developed for better understanding of the enhanced mechanisms of eco-nanocomposites materials.

4. The effect of water absorption on the mechanical properties of nano-fillers reinforced polymer nanocomposites has received very limited attention in previous studies. This work has presented several interesting findings regarding to the effect of nano-fillers in enhancing the mechanical properties of epoxy resin and RCF/epoxy composites immersed in water for long period. However, more investigations are needed. Particularly, it would be interesting to study the effect of water absorption on the mechanical properties of the composites as a function of time. This might provide essential information on the role of water diffusion in influencing the mechanical properties of nanocomposites and eco-nanocomposites.

5. The mechanical properties of RCF/epoxy composites, nano-filler-reinforced epoxy nanocomposites, and nano-filler-reinforced RCF/epoxy eco-nanocomposites were investigated and discussed in room temperature. Therefore, it is recommended to study the role of temperature on the mechanical and fracture properties of these composites.

6. This work aimed to synthesize environmentally friendly eco-nanocomposites reinforced with nano-fillers and recycled cellulose fibres. However, the use of epoxy as a matrix makes the resulted composites not fully green composites. Therefore, it is recommended to use biopolymer as a matrix to synthesize fully green nanocomposites reinforced with nanoclay and cellulose fibre.

(b)   RCF/Vinyl-Ester Ecocomposites and Eco-Nanocomposites

The role of recycled cellulose-fibre sheets, nano-fillers, and multi-scale reinforcement (RCF/nano-fillers) dispersion on the microstructure, water absorption, fracture, mechanical, thermal, and flammability properties of vinyl-ester resin was investigated and discussed.

This work has provided fundamental knowledge on the mechanism and performance of a new class of polymer eco-nanocomposites reinforced with nano-fillers and recycled cellulose fibres. Significant improvements in mechanical properties for RCF/vinyl-ester composites because of the new infiltration method, noticeable improvement in all properties of nano-filler-reinforced vinyl-ester nanocomposites, and interesting improvement in all properties for nano-filler-filled RCF/vinyl-ester eco-nanocomposites compared to unfilled RCF/vinyl-ester composites successfully

were achieved. For the future, there is a need to continue research and development in this field of materials science. Thus, the following recommendations have been formulated to help guide future study:

1. The new infiltration method introduced in this work produced successfully ecocomposites with high fibre content and good fibres/matrix adhesion which both are challenges without treatment. This method significantly improves the mechanical properties (elastic modulus by 150%), (flexural strength by 300%), (impact strength by 1048%), and (fracture toughness by %) of VER as result of 5 wt. % RCF addition. Therefore, adopting this method with increase the number of RCF sheets could increase the fibre content (>50 wt.%) and provide greater reinforcement effect.

2. In this work, matrix reinforced with fixed concentrations of nano-fillers (1, 3, 5 wt.%) and fixed fibres content (40 wt. %) clearly displayed improved interfacial adhesion between fibre and the matrix which results to noticeable mechanical and thermal properties. Therefore, further research into with different nano-fillers, fibres, and at different concentrations is required to obtain the optimum level of addition and reinforcements.

3. Nano-filler dispersion in this work was homogenous with some particle agglomerations with the use of only high-speed mixture for 30 min. Notwithstanding this to achieve optimal perfect dispersion for nano-fillers in polymer matrices further work is required. Therefore, different methods and techniques as well as treatments are required to be investigated deeply to improve the nano-filler dispersion.

4. Advanced models are required to investigate the influence of nanostructures, such as shape and size distribution, orientation, aspect ratio, degree of spatial, and interfaces on the physico-mechanical properties of eco-nanocomposites. Multi-scale mechanics models and numerical methods should be developed for better understanding of the enhanced mechanisms of eco-nanocomposites materials.

5. Here, interesting results concerning the effect of nano-filler addition in enhancing water absorption resistance in RCF/vinyl-ester composites immersed in water. This work, however, did not investigate the effect of water absorption on the mechanical properties of the eco-nanocomposites. Thus, experiments are required to study the role of water diffusion on the mechanical properties of these eco-nanocomposites.

6. The primary aim of this work was to synthesize sustainable eco-nanocomposites reinforced with nano-fillers and recycled cellulose fibres. It must be conceded, however, that the use of vinyl-ester as a matrix means that the resulting composites is not entirely environmentally friendly. Instead of 100% biodegradability, the biodegradability for the resulting ecocomposites in this study was estimated at 50% and even less for the eco-nanocomposites (~40%). Thus, there is a need to study the properties of non-petroleum-based 100% biodegradable resins reinforced with cellulose fibres and eco-nano-fillers.

7.4   Recommended Readings

There have been a steady but significant progress or advances in the research on ecocomposites and eco-nanocomposites in the past 10 years. In order to keep up with the latest advances in this emerging research field, the following articles and books are highly recommended for those wishing to keep abreast of the latest new developments or breakthroughs.

References

Chand N, Fahim M (2020) Tribology of natural fiber polymer composites, 2nd edn. Woodhead Publishing, London

Ganesan K, Kailasanathan C, Rajini, N et al (2021) Assessment on hybrid jute/coir fibers reinforced polyester composite with hybrid fillers under different environmental conditions. Constr Build Mater 301:124117

Gowda TGY, Sanjay MR, Jyotishkumar P et al (2019) Natural fibers as sustainable and renewable resource for development of eco-friendly composites: a comprehensive review. Front Mater 6:226

Jariwala H, Jain P (2019) A review on mechanical behavior of natural fiber reinforced polymer composites and its applications. J Reinf Plast Compos 38(10):441–453

Jawaid M, Hamdan A, Hameed Sultan MT (eds) (2021) Structural health monitoring system for synthetic, hybrid and natural fiber composites. Springer, Singapore

Jawaid M, Sapuan SM, Alothman OY (eds) (2017) Green biocomposites. Springer

Johnson RDJ, Arumugaprabu V, Ko TJ (2019) Mechanical property, wear characteristics, machining and moisture absorption studies on vinyl ester composites—a review. SILICON 11(5):2455–2470

Khan A, Rangappa SM, Siengchin S et al (eds) (2021) Hybrid natural fiber composites. Woodhead Publishing, London

Krishnasamy S, Thiagamani SMK, Muthukumar C et al (eds) (2022) Natural fiber-reinforced composites. Wiley-VCH

Kozlowski R, Mackiewicz-Talarczyk M (2020) Handbook of natural fibres. Woodhead Publishing, London

Mohammed L, Ansari MNM, Pua G et al (2015) A review on natural fiber reinforced polymer composite and its applications. Int J Polymer Sci 2015:243947

Nassar MMA, Alzebdeh KI, Pervez T et al (2021) Progress and challenges in sustainability, compatibility, and production of eco-composites: a state-of-art review. J Appl Polym Sci 138:e51284. https://doi.org/10.1002/app.51284

Nurazzi NM, Asyraf MRM, Khalina A et al (2021) A review on natural fiber reinforced polymer composite for bullet proof and ballistic applications. Polymers 13(4):646

Rangappa SM, Rajak DK, Siengchin S (eds) (2022) Natural and synthetic fiber reinforced composites: synthesis, properties and applications. Wiley

Sapuan SM, Ismail H, Zainudin ES (eds) (2018) Natural fiber reinforced vinyl ester and vinyl polymer composites. Woodhead Publishing, London

Sapuan SM, Razali N, Radzi AM et al (eds) (2021) Roselle: production, processing, products and biocomposites. Academic Press

Shah AUR, Prabhakar MN, Song JI (2017) Current advances in the fire retardancy of natural fiber and bio-based composites - a review. Int J Precis Eng Manuf-Green Technol 4(2):247–262

Thakur VK, Thakur MK, Kessler MR (2017a) Handbook of composites from renewable materials: structure and chemistry. Wiley, New Jersey

Thakur MK, Kessler MR, Thakur VK (2017b) Handbook of composites from renewable materials: physico-chemical and mechanical characterization. Wiley, New Jersey

Vijayan R, Krishnamoorthy A (2019) Review on natural fiber reinforced composites. Mater Today: Proc 16(2):897–906